

Polarising Poison – Synthesis,
characterization and development of
rapid, sensitive methods for the
detection of potent synthetic opiates.

NICOLAS GILBERT

PhD 2020

Polarising Poison – Synthesis,
characterization and development of rapid,
sensitive methods for the detection of potent
synthetic opiates.

NICOLAS GILBERT

A thesis submitted in partial fulfilment of the
requirements of

Manchester Metropolitan University
for the degree of Doctor of Philosophy

Department of Natural Sciences
Manchester Metropolitan University

2020

ACKNOWLEDGEMENTS

I first wish to thank Dr. Oliver Sutcliffe for his supervision, his constant support and his guidance throughout this project. Dr. Ryan Mewis has been equally important in the realisation of this thesis, through his invaluable advice and continued involvement. Both of them contributed to make this doctorate a successful experience and made me a better researcher.

I also want to thank the other members of the Sutcliffe group, especially Matt and Lysbeth, who have been great colleagues, teachers and friends. Thanks also to the other Ph.D. students met at MMU, but especially Jade, Mike, Olly, Antoine, Isabella and Matthieu, who made these three years enjoyable. Their friendship and understanding were, at times, all I needed to keep going.

Je veux aussi remercier mes parents, ma sœur, et toute ma famille, de m'avoir supporté depuis tout petit à poursuivre mon éducation. Dans tout ce que je fais, vous êtes au creux de moi. Thanks to Chris for putting up with me for three years now, and hopefully more.

Finally, I must thank the Fonds de Recherche du Québec – Nature et Technologies and the National Research Council of Canada for their doctorate funding, without which none of this would have been possible.

ABSTRACT

The occurrence of synthetic opioid fentanyl and its derivatives has grown significantly in forensic casework in recent years. This poses a threat for public health, as it has been reported that minute quantities of fentanyl are enough to induce an overdose. Approximately 32,400 people died because of synthetic opioids in the United States in 2018, and the current situation has been described as an “opioid epidemic”.

The increase in fentanyl abuse has been associated with the emergence of a large variety of fentanyl analogues. These novel compounds are more difficult to identify by forensic chemists and may not be detected when they emerge, because they have yet to be characterised and added to mass spectral databases. Another insidious phenomenon has been contributing to the increase in overdoses: fentanyl and its analogues have often been mixed into or sold as other illicit drugs. Most commonly, fentanyl has been found in heroin samples, a practice which may occur unbeknown to drug users and increase the risk of overdose.

This thesis aimed to solve these challenges associated with fentanyl detection, to aid in forensic casework and harm reduction. In Chapter II, eighteen common fentanyl analogues were synthesised, fully characterised, and submitted to presumptive colour tests, TLC and FT-IR analysis. A GC-MS method was developed to separate target analogues and allow their detection and quantification in seized heroin samples. Chapter III focused on fluorofentanyl regioisomers, which could not be separated by GC-MS. An orthogonal benchtop ^{19}F NMR method was developed to differentiate and quantify these

analogues. Chapter IV focused on the eosin Y colour test, which can be used to detect fentanyl analogues. The mechanism of the reaction between eosin Y and heroin/fentanyl was investigated by NMR. UV-Vis spectrophotometry and RGB detection were used to develop a quantitative version of the test. Finally, in Chapter V, a principal component analysis (PCA) model based on MS data from fentanyl analogues was developed. The model was able to group analogues based on their structural class and identify structural modifications in novel compounds.

Table of Contents

ACKNOWLEDGEMENTS	2
ABSTRACT	3
LIST OF TABLES	9
LIST OF FIGURES	13
ABBREVIATIONS AND ACRONYMS.....	20
CHAPTER I.....	22
INTRODUCTION	22
1.1 Fentanyl.....	22
1.2 Fentanyl detection	32
1.3 Objectives.....	41
CHAPTER II.....	42
SYNTHESIS AND DETECTION OF AMIDE-CHAIN FENTANYL DERIVATIVES.....	42
2.1 Overview.....	42
2.2 Synthesis.....	46
2.3 Presumptive colour tests	50
2.4 Thin-layer chromatography (TLC).....	53
2.5 Infrared spectroscopy	56
2.6 Electron ionisation mass spectrometry	57
2.7 Qualitative GC-MS analysis.....	63
2.8 Quantitative GC-MS analysis.....	70
2.9 Analysis of seized heroin samples.....	77

2.10	Conclusion	91
CHAPTER III.....		93
SYNTHESIS AND DETECTION OF FLUORINATED FENTANYL REGIOISOMERS		93
3.1	Overview.....	93
3.2	Synthesis.....	95
3.3	Presumptive colour tests	101
3.4	Thin-layer chromatography (TLC).....	102
3.5	Infrared spectroscopy	103
3.6	Electron ionisation mass spectrometry	104
3.7	Qualitative GC-MS analysis.....	107
3.8	Quantitative GC-MS analysis.....	109
3.9	Qualitative NMR analysis.....	116
3.10	Quantitative low-field ¹⁹ F NMR analysis	120
3.11	Conclusion	124
CHAPTER IV		125
INVESTIGATION OF THE EOSIN Y COLORIMETRIC TEST		125
4.1	Overview.....	125
4.2	Detection of fentalogues	126
4.3	Investigation of the reaction mechanism	127
4.4	Standardisation of colorimetric tests.....	155
4.5	Conclusion.....	169
CHAPTER V		171

PRINCIPAL COMPONENT ANALYSIS MODEL FOR FENTANYL ANALOGUE CLASSIFICATION	171
5.1 Overview.....	171
5.2 Data handling	173
5.3 Hierarchical clustering	185
5.4 Model evaluation	215
5.5 Conclusion.....	220
CHAPTER VI	221
CONCLUSION AND FUTURE WORK.....	221
CHAPTER VII	225
EXPERIMENTAL SECTION	225
7.1 Presumptive colour tests	225
7.2 Thin-layer chromatography.....	226
7.3 Infrared spectroscopy	226
7.4 GC-MS analysis.....	226
7.5 Benchtop NMR analysis	229
7.6 UV-Vis Eosin Y fentanyl quantification	230
7.7 Solgel preparation an fentanyl detection	230
7.8 Solgel RGB detection	230
7.9 Lighting conditions for RGB evaluation (reference for Table 4.7).....	232
7.10 PCA and clustering analysis R code	233
7.11 Structures of compounds included in the PCA study.....	236
7.12 Synthesis and characterisation data.....	242

References.....	306
-----------------	-----

LIST OF TABLES

Table 1.1. Comparison of analytical methods for detection/quantification of fentanyl (2), its derivatives and other drugs studied herein.....	39
Table 2.1. A selection of literature references where target fentalogues 2a-r have been reported.....	45
Table 2.2. ¹ H NMR attribution of fentalogues 2a-r	48
Table 2.3. Reactions of fentalogues (2a-r) and other drugs studied herein with the Marquis, Scott, Nitric acid and Eosin Y tests. Note: A dash indicates the absence of a discernible colour change.....	52
Table 2.4. Results of presumptive colour tests for mixtures of fentanyl and heroin.....	53
Table 2.5. Thin-layer chromatography results for 4-ANPP (4), fentalogues 2a-r and heroin (1c).....	55
Table 2.6. Leave-one-out validation of the ATR-FTIR method with analogues 2a-r	57
Table 2.7. Retention time and resolution for target fentalogues, controlled drugs and adulterants (see Figure 2.9 for chromatogram).....	65
Table 2.8. Summary of GC-MS validation data (SIM mode) for the quantification of fentalogues (2a-r), controlled substances (4, 23, 27, 1a-c) and relevant/common adulterants (24a-b, 25 and 26). NB. tR (eicosane, IS) = 3.47 min (see Figure 2.10 for chromatogram).....	72
Table 2.9. Comparison of GC-MS limits of detection/quantification determined in scan mode and selective ion monitoring (SIM) mode for fentalogues (2a-r), controlled substances (4, 23, 27, 1a-c) and relevant/common adulterants (24a-b, 25 and 26).....	74

Table 2.10. GC-MS recovery results for fentalogues (2a-r), controlled substances (4, 23, 27, 1a-c) and relevant/common adulterants (24a-b, 25 and 26).....	75
Table 2.11. Summary of GC-MS repeatability (intraday precision) and intermediate precision (interday precision) for fentalogues (2a-r), controlled substances (4, 23, 27, 1a-c) and relevant/common adulterants (24a-b, 25 and 26).....	76
Table 2.12 Infrared match scores for seized heroin samples SS-1 to 7.....	79
Table 2.13. Comparison of EI-MS ion ratios of the fentanyl reference and the supposed fentanyl signal in seized heroin samples SS-1 and SS-2.	87
Table 2.14. Qualitative and quantitative analysis of seized samples (SS-1 – SS-7) obtained from Greater Manchester Police. Note: A dash indicates a compound was not detected.	90
Table 3.1. ¹ H NMR attribution of fentalogues 42a-c, 46a-c, 47, 48 and numbering reference for fentanyl (2b).....	100
Table 3.2. Reactions of fluorofentalogues (42a-c, 46a-c, 47, 48), fentanyl and heroin with the Marquis, nitric acid and Eosin Y tests. Note: A dash indicates the absence of a discernible colour change.	102
Table 3.3 Thin-layer chromatography results for fentalogues 42a-c, 46a-c, 47, 48 and fentanyl 2b	103
Table 3.4. Leave-one-out validation of the ATR-FTIR method with analogues 42a-c, 46a-c, 47, 48	104
Table 3.5. EI-MS ions used for identification of analytes via Selective Ion Monitoring (SIM), relative intensity of each ion (relative to base peak) and precision (%RSD) of the relative intensities.	109
Table 3.6. Summary of GC-MS validation data (SIM mode) for the quantification of fentalogues (2b, 42a-c, 46a-c, 47, 48), heroin (1c) and common adulterants (25, 26). NB. t _R (eicosane, IS) = 3.47 min (see Figure 3.7 for chromatogram).	112

Table 3.7. Comparison of GC-MS limits of detection/quantification determined in scan mode and selective ion monitoring (SIM) mode for fentalogues (2b , 42a-c , 46a-c , 47 , 48), heroin (1c) and common adulterants (25 , 26).....	113
Table 3.8. GC-MS recovery results for fentalogues (2b , 42a-c , 46a-c , 47 , 48), heroin (1c) and common adulterants (25 , 26).....	114
Table 3.9. Summary of GC-MS repeatability (intraday precision) and intermediate precision (interday precision) for fentalogues (2b , 42a-c , 46a-c , 47 , 48), heroin (1c) and common adulterants (25 , 26).....	115
Table 3.10. Low-field ¹⁹ F NMR validation data for the quantification of fluorofentanyl (42a-c , 46a-c , 47 , 48). See Figure 3.9 for representative spectra.....	121
Table 3.11. Low-field ¹⁹ F NMR recovery results for fentalogues (42a-c , 46a-c , 47 , 48).....	122
Table 4.1. Results of the eosin Y test with compounds investigated in Chapter II and III.....	126
Table 4.2. Identification of fentalogues and other drugs and adulterants made using the eosin Y test.....	126
Table 4.3. ¹ H NMR chemical shifts of heroin and the eosin Y – heroin mixture (DMSO-D ₆).....	131
Table 4.4. Determination coefficient (R ²) of the fentanyl calibration graph (0.1 – 1.0 mg reconstituted in 5 mL eosin Y 750 μM) at different detection wavelengths.....	159
Table 4.5. Calibration of fentanyl reconstituted in 5 mL eosin Y 750 μM. ...	161
Table 4.6. RGB values for solgels prepared with 1000 μM eosin Y mixed with increasing concentrations of fentanyl.....	162
Table 4.7. RGB values of solgel vials photographed side-by-side in different lighting conditions (see Section 7.9 for photographs).	165
Table 4.8. Comparison of RGB standardisation methods with eosin Y solgels.	166

Table 4.9. Test results of common drugs and adulterants and seized heroin samples SS-4 – 5.....	168
Table 5.1. List of fentanyl analogues included in this study.	174
Table 5.2. Relative intensities for five fentanyl analogues.	176
Table 5.3. Inter-cluster inertia gains.....	192
Table 5.4. Individuals in each cluster of Classifier 1.	199
Table 5.5. Description of clusters by the five most significant <i>m/z</i> values...	203
Table 5.6. Individuals in each cluster of Classifier 2.	209
Table 5.7. Description of Classifier 2 clusters by the five most significant <i>m/z</i> values.	214
Table 5.8. Comparison of the centroid and nearest neighbour classification criteria.	215
Table 5.9. Detailed model evaluation results obtained with the nearest neighbour method.	216
Table 7.1. Chemical structure of fentanyl analogues included in the PCA study (Chapter V).	236

LIST OF FIGURES

Figure 1.1. Chemical structure of common opiates and fentanyl.	23
Figure 1.2. Chemical structure of α -methylfentanyl (3).	24
Figure 1.3. Chemical structure of fentanyl precursors 4-ANPP (4) and NPP (5).	25
Figure 1.4. Major metabolic pathways of fentanyl.	27
Figure 1.5. Average positioning and intermolecular interactions of fentanyl and morphine in the MOR binding pocket (reported by Lipiński <i>et al.</i> [49]).....	28
Figure 1.6. Retrosynthetic analysis of fentanyl.....	30
Figure 1.7. Numbering of the fentanyl molecule and nomenclature of some methylated analogues.	30
Figure 1.8. Chemical structure of 4-substituted fentanyl derivatives.	31
Figure 1.9. Chemical structure of the coloured products formed by Marquis' reagent with morphine and amphetamine derivatives.....	34
Figure 1.10. Chemical structure of eosin Y.	34
Figure 2.1. Synthesis of fentanyl analogues 2a-r and structure of controlled drugs and adulterants (1a-c , 23-27) included in this study. <i>Reagents and conditions</i> : (a) RCOCl (2.0 eq.), <i>i</i> Pr ₂ NEt (2.0 eq.), DCM (0.1 M), 0°C to r.t., 2 h; (b) HCl (3 M in CPME, 1.0 eq.), Et ₂ O or acetone (0.1 M), r.t., 10 min (15-64%).	44
Figure 2.2. Numbering reference for fentanyl (2b).	47
Figure 2.3. Electron ionisation mass spectra of fentalogues 2a-i	58
Figure 2.4. Electron ionisation mass spectra of fentalogues 2g-j	59
Figure 2.5. EI-MS spectrum of fentanyl (2b) and structure of main fragments.	61

Figure 2.6. EI-MS fragmentation of fentanyl (2b) leading to the observed fragments.....	61
Figure 2.7. EI-MS spectrum of cyclopropylfentanyl (2f) and structure of fragments 36 and 37	62
Figure 2.8. Potential $m/z = 158$ fragments of fentalogues 2n-p	63
Figure 2.9. Exemplar chromatogram demonstrating GC-MS separation of 18 fentalogues (2a-r), MDMA (23), benzocaine (24a), acetaminophen (26), caffeine (25), eicosane (internal standard, E), procaine (24b), cocaine (27), codeine (1a), morphine (1b), 4-ANPP (4) and heroin (1c).	64
Figure 2.10. Exemplar chromatogram demonstrating the optimal GC-MS method of 18 fentalogues (2a-r), MDMA (23), benzocaine (24a), acetaminophen (26), caffeine (25), eicosane (internal standard, E), procaine (24b), cocaine (27), codeine (1a), morphine (1b), 4-ANPP (4) and heroin (1c).	66
Figure 2.11. SIM mode chromatogram of a mixture of 2f , 2h , 2n , 2o-p . a) Total ion chromatogram; b) Monitoring of $m/z = 261.1$ (2n); c) Monitoring of $m/z = 257.1$ (2f); d) Monitoring of $m/z = 285.1$ (2h); e) Monitoring of $m/z = 283.1$ (2o-p).	69
Figure 2.12. ATR-FTIR spectrum of fentanyl (2b).	80
Figure 2.13. ATR-FTIR spectrum of heroin (1c).	81
Figure 2.14. ATR-FTIR spectrum of seized heroin sample SS-1.	82
Figure 2.15. ATR-FTIR spectrum of seized heroin sample SS-2.	83
Figure 2.16. Qualitative scan mode GC-MS analysis of heroin samples SS-1 to SS-7 (0.1 mg/mL in methanol). Key: DAAP = N,O-diacetylamino-phenol; 6-MAM = 6-monacetylmorphine; E = eicosane (internal standard).	85
Figure 2.17. Chemical structure of compounds 40 and 41 , detected in seized heroin samples.....	86
Figure 2.18. Qualitative GC-MS analysis heroin samples SS-1 and SS-2 (0.1 mg/mL in methanol). a) SS-1 in scan mode; b) Total ion chromatogram of SS-	

1 in SIM mode ($m/z = 245.1, 189.0, 146.0$); c) SS-2 in scan mode; d) Total ion chromatogram of SS-1 in SIM mode ($m/z = 245.1, 189.0, 146.0$); e) SIM spectrum of peak ($t_R = 12.0$ min) corresponding to fentanyl (2b).....	88
Figure 3.1. Chemical structure of known and potential fluorinated fentalogues.	94
Figure 3.2. Synthesis of target fluorofentanyls (42a-c , 46a-c , 47 , 48) and structure of controlled drugs and adulterants included in this study. <i>Reagents and conditions</i> : (a) ArNH ₂ , AcOH, NaBH(OAc) ₃ , DCE, r.t., 48 h; (b) Propionyl chloride (2.0 eq.), iPr ₂ NEt (2.0 eq.), DCM (0.1 M), 0 °C to r.t., 2 h; (c) HCl (3 M in CPME, 1.0 eq.), Et ₂ O or acetone (0.1 M), r.t., 2 h; (d) 1. TFA/DCM (1:3) (0.3 M), 0 °C to r.t., 1 h, 2. Ar(CH ₂) ₂ Br, Cs ₂ CO ₃ , ACN, reflux, 5 h.....	96
Figure 3.3. Aromatic region (7.025 – 7.750 ppm) of the high-field ¹ H NMR spectra of fluorofentanyls 42a-c , 46a-c , 47 , 48 in DMSO-D ₆	99
Figure 3.4. Electron ionisation mass spectra of fentalogues 42a-c , 46a-c , 47 , 48	105
Figure 3.5. Initial EI-MS fragmentations of 2'-, 3'- and 4'-fluorofentanyl (46a-c).	106
Figure 3.6. EI-MS fragmentation of <i>ortho</i> -, <i>meta</i> -, <i>para</i> -fluoro fentanyl (42a-c).	107
Figure 3.7. Exemplar GC-MS chromatogram of target fluorofentanyls (42a-c , 46a-c , 47 , 48), fentanyl (2b), heroin (1c), acetaminophen (26), caffeine (25) and eicosane (internal standard, E).	108
Figure 3.8. (a) Overlay of high-field ¹⁹ F NMR spectra of target fluorofentanyls (42a-c , 46a-c , 48); (b) High-field ¹⁹ F NMR of compound 47	117
Figure 3.9. (a) Overlay of low-field ¹⁹ F NMR spectra of target fluorofentanyls (42a-c , 46a-c , 48); (b) Low-field ¹⁹ F NMR of compound 47	118
Figure 3.10. ¹⁹ F NMR signal ratio of a 46a and 42a mixture (integration of 46a /(46a + 42a)) against the concentration of 46a . The orange line marks the signal ratio observed in a pure solution of 47	120

Figure 3.11. (a) Low-field ^1H NMR spectrum of an <i>ortho</i> -fluorofentanyl (42a)/heroin (1c) mixture (2.4 %w/w); (b) Low-field ^{19}F NMR spectrum of an <i>ortho</i> -fluorofentanyl (42a)/heroin (1c) mixture (with TFA as reference).	123
Figure 4.1. ^1H NMR spectra (400 MHz, DMSO-D_6) of a) Eosin Y and caffeine; b) Caffeine; c) Eosin Y; d) Chemical structure of eosin Y.	129
Figure 4.2. ^1H NMR spectra (400 MHz, DMSO-D_6) of a) Heroin free-base; b) Heroin free-base and eosin Y; c) Heroin protonated with HCl (1.0 eq.); d) Chemical structure of heroin.	131
Figure 4.3. ^1H NMR spectra (400 MHz, DMSO-D_6) of a) Eosin Y deprotonated with NaOH (2 eq.); b) Eosin Y deprotonated with NaOH (1 eq.); c) Eosin Y; d) Eosin Y and heroin free-base.	132
Figure 4.4. ^1H NMR spectra (400 MHz, DMSO-D_6) of a) Fentanyl HCl and eosin Y; b) Fentanyl HCl; c) Eosin Y.	133
Figure 4.5. ^1H NMR spectra (400 MHz, DMSO-D_6) of a) Eosin Y deprotonated with NaOH (1 eq.); b) Eosin Y; c) Fentanyl free-base and eosin Y.	134
Figure 4.6. ^1H NMR spectra (400 MHz, DMSO-D_6) of a) Fentanyl HCl; b) Fentanyl free-base and eosin Y; c) Fentanyl free-base.	135
Figure 4.7. ^1H NMR spectra (400 MHz, D_2O) of a) Eosin Y and caffeine; b) Eosin Y; c) Caffeine; d) Eosin Y and caffeine (6.5-8.7 ppm region); e) Eosin Y (6.5-8.7 ppm region)	137
Figure 4.8. Acid-base equilibrium between caffeine and eosin Y.....	139
Figure 4.9. ^1H NMR spectra (400 MHz, D_2O) of a) Heroin free-base; b) Eosin Y; c) Heroin free-base and eosin Y.	140
Figure 4.10. Aromatic region of the ^1H NMR spectra (400 MHz, D_2O) of a) Eosin Y; b) Heroin free-base and eosin Y.....	141
Figure 4.11. ^1H NMR spectra (400 MHz, D_2O) of a) Fentanyl HCl; b) Eosin Y; c) The supernatant obtained from mixing fentanyl HCl and eosin Y.	142

Figure 4.12. ¹ H NMR spectra (400 MHz, DMSO-D ₆) of a) Fentanyl free-base; b) Fentanyl HCl; c) The precipitate obtained from mixing fentanyl HCl and eosin Y.	143
Figure 4.13. Chemical structure of fentanyl and ¹ H NMR spectra (400 MHz, DMSO-D ₆) of a) Fentanyl free-base; b) Fentanyl HCl; c) The precipitate obtained from mixing fentanyl HCl and eosin Y; d) Chemical structure of fentanyl.	144
Figure 4.14. ¹ H NMR spectra (400 MHz, DMSO-D ₆) of a) The precipitate obtained from mixing fentanyl HCl and eosin Y; b) Fentanyl free-base.	145
Figure 4.15. ATR-FTIR spectrum of the precipitate obtained from fentanyl and eosin Y.	146
Figure 4.16. ATR-FTIR spectrum of fentanyl hydrochloride.	147
Figure 4.17. ATR-FTIR spectrum of fentanyl free-base.	148
Figure 4.18. ¹ H- ¹ H COSY spectrum of the precipitate obtained from fentanyl and eosin Y (400 MHz, DMSO-D ₆).	150
Figure 4.19. Conformational equilibria of 4- <i>p</i> -chlorophenyl-1-ethylpiperidine and corresponding Δ <i>G</i> [°] values calculated by Jones <i>et al.</i> [166]	151
Figure 4.20. ¹ H NMR spectra (400 MHz, DMSO-D ₆) of the precipitate obtained from fentanyl and eosin Y, taken at 25, 40, 50 and 60°C.	153
Figure 4.21. a) Visible light absorption spectra of eosin Y (red) and a heroin/eosin Y mixture (blue); b) Visible light absorption spectrum of a fentanyl/eosin Y mixture.	156
Figure 4.22. Visible light absorption spectrum of 500 mg fentanyl reconstituted in 150 μM eosin Y (2 mL) after eosin Y subtraction.	157
Figure 4.23. Absorbance at λ = 568 nm of fentanyl reconstituted in eosin Y 750 μM (2 mL).	158
Figure 4.24. Absorbance at λ = 590 nm of fentanyl reconstituted in eosin Y 750 μM (5 mL).	160

Figure 4.25. Photographs of solgels taken in three different lighting conditions, reacted with blank methanol (left) and 1 mg/mL fentanyl (right). RGB values of the fentanyl-solgel mixture: a) R: 191, G: 62, B: 74; b) R: 215, G: 81, B: 71; c) R: 153, G: 49, B: 47	164
Figure 4.26. Calibration of fentanyl with eosin Y solgel RGB detection, a) 0.1 – 1.0 mg/mL concentration range; b) 0.5 – 1.0 mg/mL concentration range..	167
Figure 5.1. a) Projection of model fentanyl analogues on principal components PC1 and PC2; b) Correlation circle of m/z values projected on principal components PC1 and PC2, coloured according to \cos^2 values ($\cos^2 > 0.3$).	179
Figure 5.2. Scree plot of the eigenvalues for the first ten principal components.	180
Figure 5.3. a) Projection of model fentanyl analogues on principal components PC3 and PC4; b) Correlation circle of m/z values projected on principal components PC3 and PC4, coloured according to \cos^2 values ($\cos^2 > 0.3$).	183
Figure 5.4. a) Projection of model fentanyl analogues on principal components PC5 and PC6; b) Correlation circle of m/z values projected on principal components PC5 and PC6, coloured according to \cos^2 values ($\cos^2 > 0.3$).	184
Figure 5.5. Dissimilarity matrix of the 54 fentanyl derivatives PCA.	187
Figure 5.6. Initial hierarchical dendrogram of fentanyl analogues data.	190
Figure 5.7. Dendrograms created from the hierarchical clustering of fentanyl analogues. a) $k = 7$ clusters; b) $k = 11$ clusters.....	193
Figure 5.8. Gap statistic for each number of clusters ($k_{max} = 12$, $B = 1000$). Note: Error bars represent one standard deviation of $Gap(k)$ ($n = 1000$)....	195
Figure 5.9. Classifier 1 dendrogram created from the hierarchical clustering of fentanyl analogues. Note: The vertical axis represents the loss of inertia caused by each grouping.	197

Figure 5.10. Classifier 1 hierarchical clustering shown on the PC1-PC2 plane. <i>Note:</i> PCs 3-5 are not shown but also contribute to the clustering.....	198
Figure 5.11. Silhouette coefficients of individuals in classifier 1. <i>Note:</i> The dotted line represents the average silhouette coefficient.	207
Figure 5.12. Dendrogram created from the hierarchical clustering of fentanyl analogues (Classifier 2). <i>Note:</i> The vertical axis represents the loss of inertia caused by each grouping.....	210
Figure 5.13. Classifier 2 hierarchical clustering shown on the PC1-PC2 plane.	211
Figure 5.14. Classifier 2 hierarchical clustering shown on the PC3-PC4 plane.	212
Figure 5.15. Dendrogram created from the hierarchical clustering of aromatic amide analogues. <i>Note:</i> The vertical axis represents the loss of inertia caused by each grouping.	219
Figure 7.1. a) ^1H NMR spectrum of heroin (1c) free-base in DMSO-D_6 ; b) Detail of 7.1a, showing hidden proton signals.....	300
Figure 7.2. ^1H - ^1H COSY NMR spectrum of heroin (1c) free base in DMSO-D_6 (0.8-4.0 ppm)	301
Figure 7.3. ^1H - ^1H COSY NMR spectrum of heroin (1c) free base in DMSO-D_6 (2.5-7.0 ppm)	302
Figure 7.4. ^1H - ^{13}C HMQC NMR spectrum of heroin (1c) free base in DMSO-D_6 (0-100 ppm)	303
Figure 7.5. ^1H - ^{13}C HMQC NMR spectrum of heroin (1c) free base in DMSO-D_6 (105-150 ppm)	304
Figure 7.6. ^{13}C NMR spectrum of heroin (1c) free base in DMSO-D_6 (with partial attribution based on HMQC)	305

ABBREVIATIONS AND ACRONYMS

General abbreviations	
4-ANPP	4-Aminophenyl-1-phenethylpiperidine
6-MAM	6-Monoacetylmorphine
Ac	Acetyl-
ACN	Acetonitrile
Ar	Aromatic group
ATR-FTIR	Attenuated total reflectance – Fourier transform infrared spectroscopy
C _p	Plasma concentration
CPME	Cyclopentyl methyl ether
DAAP	Diacetyl- <i>p</i> -aminophenol (diacetamate)
DART-MS	Direct analysis in real time – Mass spectrometry
DCE	Dichloroethane
DCM	Dichloromethane
DEA	Drug Enforcement Administration
EI-MS	Electron ionisation – Mass spectrometry
Et	Ethyl-
GC-MS	Gas chromatography – Mass spectrometry
HCPC	Hierarchical clustering of principal components
HPLC	High performance liquid chromatography
HRMS	High-resolution mass spectrometry
i.v.	Intravenous
ICP-MS	Inductively coupled plasma – Mass spectrometry
IMS	Ion-mobility spectrometry
<i>i</i> Pr	Isopropyl-
IS	Internal standard
LC-MS	Liquid chromatography – Mass spectrometry
LC ₅₀	Median lethal concentration
LOD	Limit of detection
LOQ	Limit of quantification
MDMA	3,4-Methylenedioxymethamphetamine
MOR	μ-opioid receptor
MS	Mass spectrometry
NFEPP	<i>N</i> -(3-Fluoro-1-phenethylpiperidin-4-yl)- <i>N</i> -phenylpropionamide
NIST	National Institute of Standards and Technology

NMR	Nuclear magnetic resonance
NPP	<i>N</i> -Phenethyl-4-piperidone
NPS	New psychoactive substance
PC	Principal component
PCA	Principal component analysis
PLS-DA	Partial least squares – discriminant analysis
Pr	Propyl-
qNMR	Quantitative NMR
RGB	Red, green, blue
R _f	Retention factor
RR _f	Relative retention factor
RRT	Relative retention time
RSD	Relative standard deviation
S/N (or SNR)	Signal to noise (ratio)
SERS	Surface-enhanced Raman spectroscopy
SIM	Selected ion monitoring
SWGDRUG	Scientific Working Group for the Analysis of Seized Drugs
TFA	Trifluoroacetic acid
TLC	Thin-layer chromatography
t _R	Retention time
UNODC	United Nations Office on Drugs and Crime
UPLC-MS	Ultra-performance liquid chromatography – Mass spectrometry
UV-Vis	Ultraviolet-visible spectroscopy
WADA	World Anti-Doping Agency
NMR multiplicities	
s	Singlet
d	Doublet
t	Triplet
q	Quartet
quint	Quintet
sext	Sextet
dd	Doublet of doublets
tt	Triplet of triplets
m	Multiplet

CHAPTER I

INTRODUCTION

1.1 Fentanyl

1.1.1 Overview

The term “opiate” is generally used to designate alkaloids obtained from the opium poppy *Papaver somniferum*. They can be either completely natural, such as codeine (**1a**) and morphine (**1b**), or semi-synthetic, in the way that heroin (**1c**) is chemically derived from morphine through acetylation (Figure 1.1). Some entirely laboratory-made compounds, such as fentanyl (**2**), are called synthetic “opioids”; although its chemical structure is quite far from that of its natural counterparts, fentanyl exhibits similar effects due to its strong affinity towards the body’s opioid receptors. Activation of these receptors leads to analgesia and euphoria, but potentially to physical dependence, constipation and respiratory depression. [1, 2]

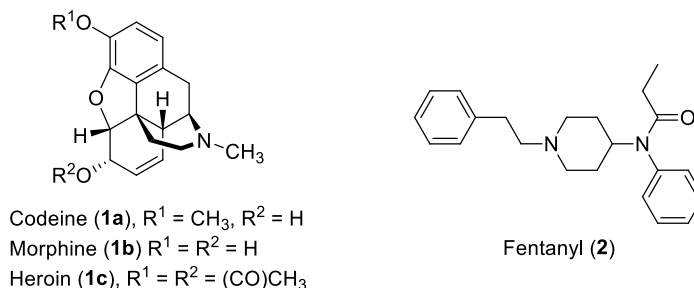


Figure 1.1. Chemical structure of common opiates and fentanyl.

Fentanyl was first patented as an analgesic by Janssen Pharmaceutical in 1965 and eventually reached widespread medical use, due to its very strong and fast action. [3, 4] Depending on the assay, it has been estimated around 100-300 times more potent than morphine. [5-7] Although it used to be administered as an intravenous injection, it is now available in many non-invasive, rapid-onset administration routes. [8] This includes transdermal patches, [9] nasal sprays, buccal or sublingual tablets and transmucosal lollipops. [10] It is commonly used as an analgesic during and after surgery, [11, 12] to manage acute pain, [11] chronic pain in cancer patients, [8] breakthrough pain (*i.e.* sudden pain flares linked to chronic conditions) [13] and even to control pain in children. [14]

Fentanyl use carries a high risk of side-effects and addiction, and it should not be prescribed indiscriminately. However, side-effects occur in less than 10% of patients who are already tolerant to opioids. [13] Davis also cautions that patients should be screened for abuse and addiction risk before fentanyl is administered. [13]

1.1.2 Recreational use and opioid epidemic

Because of their euphoria-inducing effects, resembling those of heroin, fentanyl and its analogues have been used recreationally. Certain analogues of fentanyl are used medicinally, but many non-medicinal analogues have been illegally synthesised and sold on drug markets. This poses a threat for public health, as it has been reported that minute quantities of fentanyl are enough to induce an overdose.

The first large outbreak of deaths happened in California between 1979 and 1988, where 112 deaths were related to α -methylfentanyl abuse (**3**, Figure 1.2). Frequent isolated outbreaks have been reported since then. [15] Since 2013, however, fentanyl abuse and overdose-related deaths have kept rising across North America (and Europe, to a lesser extent). [16-18] The current situation has been described as an “opioid epidemic”. [19, 20] In the United States alone, the Center for Disease Control reports that approximately 32,400 people died because of synthetic opioids in 2018. [21]

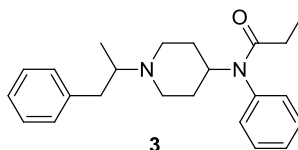


Figure 1.2. Chemical structure of α -methylfentanyl (**3**).

Illicit fentanyl comes mainly from two sources. Firstly, diversion of pharmaceutical supplies. This includes inappropriate or over-prescribing by medical practitioners, theft, collection from hospital waste, sale of unused prescription by patients, fraudulent prescriptions, as well as misuse and sale

by medical staff. [22] The problem is compounded by the drug's high potential for addiction, even during legitimate treatment. Fentanyl and its analogues are also produced clandestinely. Fentanyl entering the United States comes primarily from synthesis laboratories in China, where poor regulation allows precursors to be diverted from legitimate pharmaceutical uses. [23] A lower percentage comes from criminal organisations in Mexico, which synthesise fentanyl from precursors shipped from China. [24] Following the scheduling of precursors 4-ANPP and NPP (Figure 1.3, **4-5**) by Chinese authorities in 2017, India emerged as a precursor supplier for Mexican organisations. [24] It remains to be seen whether the scheduling of fentanyl and all its analogues by China, in May of 2019, will have a significant impact on the quantity and the sources of fentanyl supplied to North America.

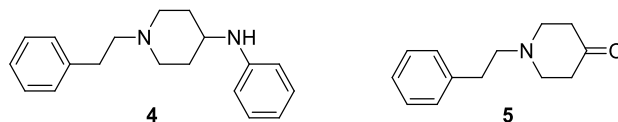


Figure 1.3. Chemical structure of fentanyl precursors 4-ANPP (**4**) and NPP (**5**).

An insidious phenomenon which has been contributing to the increase in synthetic opiates-related overdoses is the fact that fentanyl and its analogues have often been mixed into or sold as other illicit drugs. Since the 1980s, numerous cases have been reported where death was due to heroin contaminated with fentanyl. [25, 26] It has been surmised that this practice increased demand and profit margins, due to the increased high experienced by consumers and the much greater potency of fentanyl. [27] Fentanyl analogues have also been sold in combination with U-47700 as “fake Norco” (a formulation of acetaminophen and hydrocodone), and have been detected

in street samples of cocaine, and even purportedly sold as 3',4'-methylenedioxymethamphetamine (MDMA) – which potentially may have more serious implications to wider drug using communities. [28-35] These practises are likely to occur unbeknown to consumers [27] and, in the case of adulteration, the poor mixing techniques used by dealers can result in variable doses of fentanyl in illicit samples [36]. This combination of factors greatly increases the risk of fentanyl overdose. The development of simple, sensitive methods for the screening of fentanyl and its analogues at trace level in complex mixtures is therefore crucial for public health protection.

1.1.3 Pharmacology

Common fentanyl administration routes include intravenous, intramuscular and intrathecal injections, as well as an array of non-invasive routes (transdermal, intranasal, buccal or sublingual). [9, 10, 37] As opposed to other opiates, it is rarely administered as oral tablets. [37]

Pharmacokinetics depend on the administration route and high inter-individual variability has been reported. [8, 38, 39] Fentanyl has a large volume of distribution ($3.5 - 5.9 \text{ L kg}^{-1}$). [11] After intravenous injection, it diffuses rapidly from blood plasma: 80% of the injected dose leaves plasma in 5 min, [40] and 98.6% in 1 h. [41] This is due to extensive diffusion to highly vascularised tissues (brain, heart, lung, liver, kidney), then to muscle and fat. [42] The latter tissues act as storage sites and slowly release fentanyl back into the plasma, resulting in a relatively long elimination half-time (3.1 – 7.9 h). [11, 43]

With an octanol-water partition coefficient $\log P = 2.9$ at $\text{pH} = 7.4$, fentanyl is highly lipophilic in comparison to morphine ($\log P = 1.4$). Even though most of the fentanyl found in plasma (84%) is bound to erythrocytes, α_1 -acid

glycoprotein and albumin, its ability to cross the blood-brain barrier is still 133 times larger than that of morphine. [11, 44] This may be the main reason behind the high potency of fentanyl compared to morphine. Both compounds have similar μ -opioid receptor (MOR) agonist strength. [45]

In a study on healthy volunteers, in the 72 h following an i.v. dose, approximately 77% of fentanyl metabolites were recovered in urine and 8% in stool, while less than 8% of the dose was excreted intact. [41] Fentanyl is metabolised by cytochrome P450 3A4, predominantly in the liver but also in the duodenum. [46] The major metabolic pathways previously reported are shown in Figure 1.4. In liver microsome studies, more than 99% of fentanyl was metabolised as norfentanyl (**6**), an inactive metabolite resulting from *N*-dealkylation. [46] Minor metabolites resulted from amide hydrolysis, leading to **4**, or from hydroxylation of fentanyl or norfentanyl. [46, 47] In metabolite **2-OH**, the exact position of the hydroxyl group was not determined and hydroxylation may occur at different positions of the structure; detection of **7**, on the other hand, confirmed hydroxylation of norfentanyl of the propionyl moiety.

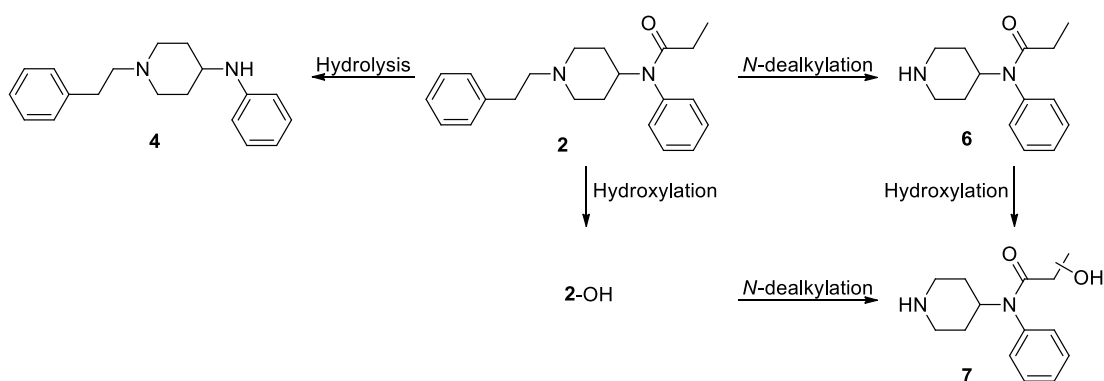


Figure 1.4. Major metabolic pathways of fentanyl.

Fentanyl is a strong agonist of the MOR, which is found across the central and peripheral nervous system as well as the intestinal tract. [48] It also has a weaker affinity for δ - and κ -opioid receptors. [48] Figure 1.5 shows the average positioning of fentanyl and morphine in the MOR binding pocket over molecular dynamics simulations performed by Lipiński *et al.* [49] There is little similarity in the positioning of the two ligands, although they both form an ionic interaction with Asp147. The piperidine ring of fentanyl also interacts with hydrophobic residues Gln124, Ile322 and Tyr326. The *N*-phenethyl chain interacts with Tyr326 and, depending on its rotation, with Ile322, Ile296 and Trp293. On the phenylpropanamide side, the amide group can interact with polar residues Gln124 or Thr218, while the ethyl and phenyl groups interact with a group of seven hydrophobic residues.

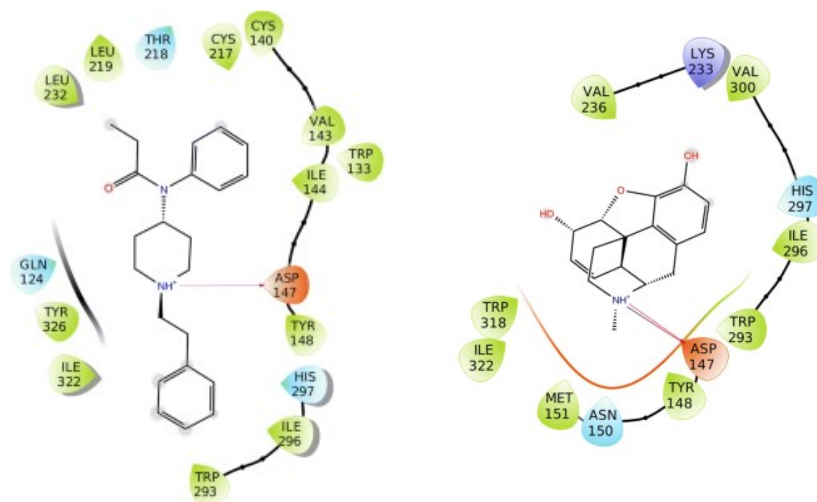


Figure 1.5. Average positioning and intermolecular interactions of fentanyl and morphine in the MOR binding pocket (reported by Lipiński *et al.* [49])

Fentanyl acts at the MOR located in the spinal cord and brain; the desired effect is analgesia (or euphoria, for illicit users), while the most dangerous side-effect is respiratory depression. [11] Opioid effects measured by

electroencephalography show only a 3 to 5 minute lag behind the increase in plasma concentration (C_p), indicating a rapid onset of effects. [50] Both the intensity of analgesia and respiratory depression are directly correlated to C_p , with a therapeutic window between 0.6 and 2.0 ng mL⁻¹. [11, 51] Higher concentrations may cause significant respiratory depression, and potentially overdose. It has been reported that quantities as low as 2 mg of fentanyl could induce an overdose, but this value is based on the LD₅₀ in monkeys, extrapolated to humans. [52]

1.1.4 Synthesis and analogues

The increase in fentanyl abuse has been associated with the emergence of a large variety of fentanyl analogues: between 2013 and 2019, the United Nations Office on Drugs and Crime (UNODC) reported more than 75 New Psychoactive Substances (NPS) with opioid effect (including fentanyl analogues) in its Early Warning Advisory and this number keeps growing. [53] This quick emergence of synthetic analogues of controlled drugs constitutes a challenge for their identification, because of the time it takes before extensive chemical characterisation of these analogues is disseminated in academic journals or specialised databases. [19, 28] This likely leads to an under-reporting of cases, as analytical methods remain limited and medical and forensic practitioners may not routinely test for new analogues [54, 55].

The retrosynthetic analysis of fentanyl (Figure 1.6) reveals a straightforward and flexible synthesis. Fentanyl comprises four major moieties: (i) phenethyl chain (red), (ii) piperidine ring (blue), (iii) aniline (green) and (iv) acyl chain (orange). Each part is added in a different step, using simple and easily accessible reagents. Alterations to the general structure are easily achieved by changing one (or more) of these reagents.

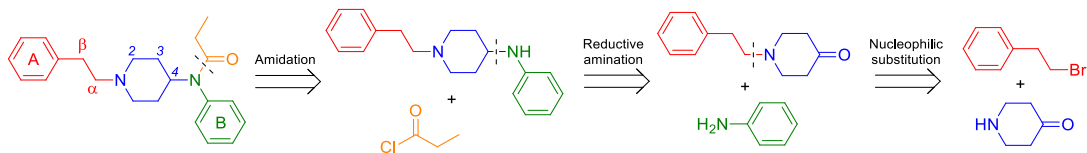


Figure 1.6. Retrosynthetic analysis of fentanyl.

Figure 1.7 illustrates the common nomenclature of fentanyl analogues, with prefixes indicating the position of substituents. One exception to this rule is the modification of the amide chain, which is typically denoted by adding the name of the new moiety in front of the compound name (like in *butyrfentanyl 11*).

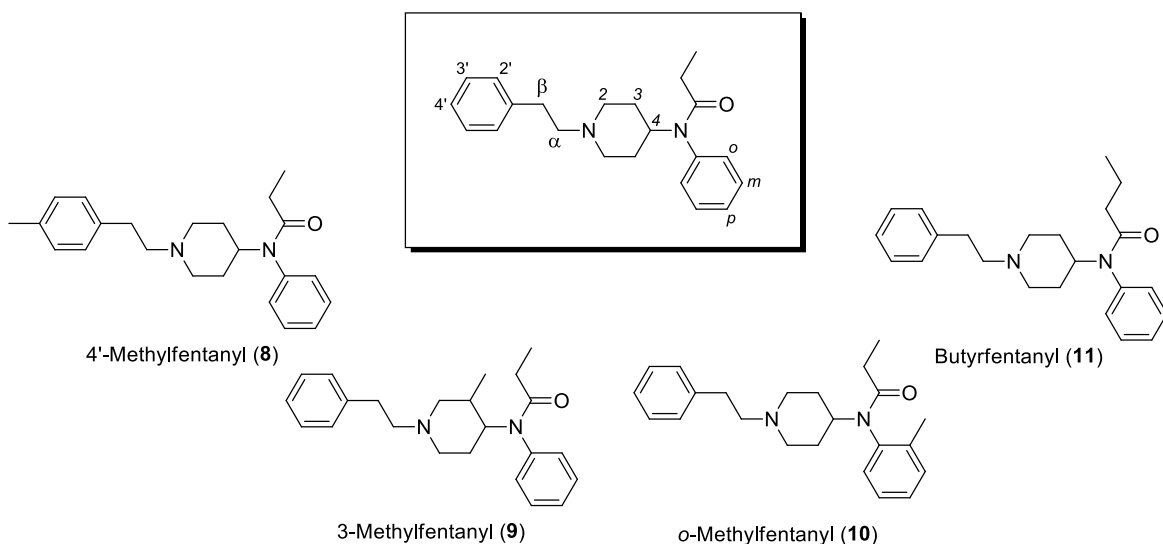


Figure 1.7. Numbering of the fentanyl molecule and nomenclature of some methylated analogues.

The most commonly modified part of the structure is the amide chain, which is often replaced with other alkyl, cycloalkyl, aryl and alkenyl groups. Substitution

of the *N*-phenyl ring with fluoro-, chloro-, methyl-, hydroxyl- or methoxy- groups is also common. [15, 22, 56-64] In fewer derivatives, substitution can also occur on the piperidine ring [65-67] and the phenethyl chain. [65, 68-70] The phenethyl chain can be replaced by a benzyl or methyl chain. Finally, both phenyl rings have been replaced with other aromatic rings (thiophene, ethyltetrazolone, furan, and a variety of nitrogen heterocycles). [65, 66, 71] Most derivatives combine more than one modification.

A common modification for analogues used in the medical field as analgesics is substitution at the 4-position (Figure 1.8), but synthesis of these compounds is much more complex. [66] Substituents include methoxymethyl- (sufentanil **12**/Sufenta[®], alfentanil **13**/Alfenta[®]/Rapifen[®]) or a methyl ester (carfentanil **14**/Wildnil[®], thiafentanil **15**/Thianil[®], remifentanil **16**/Ultiva[®]). [65, 66, 72] Carfentanil especially has been associated with a high number of overdoses following illicit use, and its potency is estimated to be 100 times stronger than that of fentanyl. [73, 74] Phenyl-bearing derivatives (4-phenylfentanyl, trefentanil), as well as their thiazolo- and thiophenyl- equivalents, have been prepared but do not have any medical use. [66]

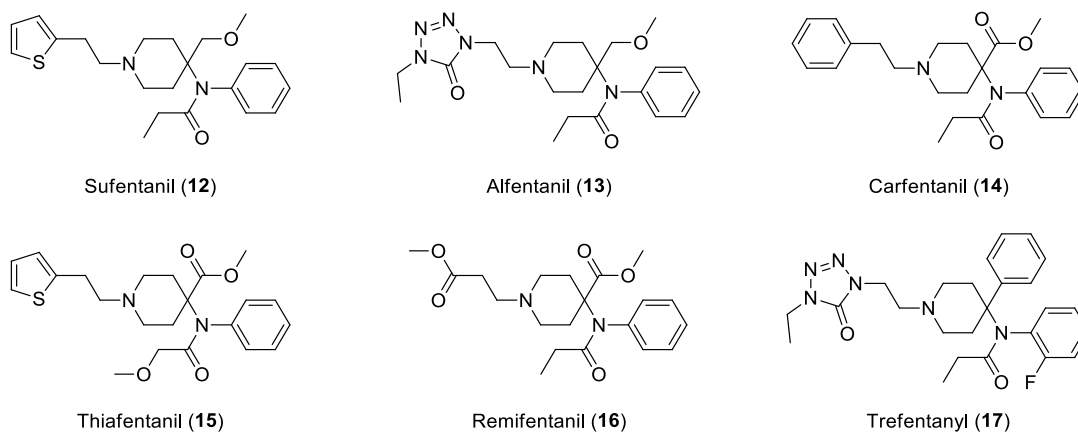


Figure 1.8. Chemical structure of 4-substituted fentanyl derivatives.

Drug manufacturers used to make new analogues in an attempt to avoid legislation. [28] Before legislation was introduced to cover possible analogues, most governmental and intergovernmental agencies had a reactive approach to scheduling new fentanyl derivatives. In Sweden, for instance, the scheduling of acetyl-, butyr- and *para*-fluorobutyrfentanyl in 2015 caused a wave of new analogues to emerge, which were banned only to be replaced again. [19] Manufacturers may also turn to analogues for their increased potency, to explore possible novel effects or because of changes in the supply of starting materials. [28]

1.2 Fentanyl detection

To summarise, the main challenges of fentanyl detection are: (i) the proper identification / discrimination of analogues and (ii) the detection of fentanyl and its analogues at low concentration in complex matrices, such as in heroin samples. Analytical techniques should aim to address these challenges. Although no one technique is perfectly suited to every situation, the ideal method would balance selectivity and sensitivity against instrument complexity and cost/accessibility. Techniques which have previously been used to detect fentanyl and its analogues, or which have been used for controlled drugs and could be applied to fentanyl, are described in order of complexity.

1.2.1 Presumptive tests

Colorimetric tests are used for the presumptive identification of illicit drugs, with the advantage of being portable and giving a very quick result. A number of colour tests could be used to detect fentanyl, or differentiate it from compounds it may be found in mixtures with (*i.e.* heroin, cocaine, MDMA and their adulterants). Of the following, only Marquis' and eosin Y are known to react with fentanyl, and they have not been tested on analogues.

Scott's reagent, cobalt(II) thiocyanate, is generally used to detect cocaine but is known to react positively with many other drugs. [75] It is suspected that cocaine acts as a bidentate *N,O*-ligand on the cobalt centre, resulting in a colour change from red to blue. [76]

The nitric acid test is known to react with various opiates, such as morphine, codeine and heroin. [77] It proceeds through nitration (electrophilic aromatic substitution) of the electron-rich phenyl ring found in these compounds. The resulting colour, different for all three opiates mentioned, depends on the nature of the substituents on the aromatic ring.

Marquis' reagent, a mixture of formaldehyde and sulfuric acid, reacts with various opiates to give a pink to violet colour, whereas fentanyl produces an orange to dark brown colour. [26] Amphetamine derivatives also react to produce various colours. Morphine reacts with two formaldehyde molecules, through consecutive aromatic substitutions and dehydrations, to produce dimer **19** (Figure 1.9). [77] Amphetamines (**20**) only react with one formaldehyde molecule, and the mechanism for fentanyl is likely similar, resulting in carbocation **21** (Figure 1.9).

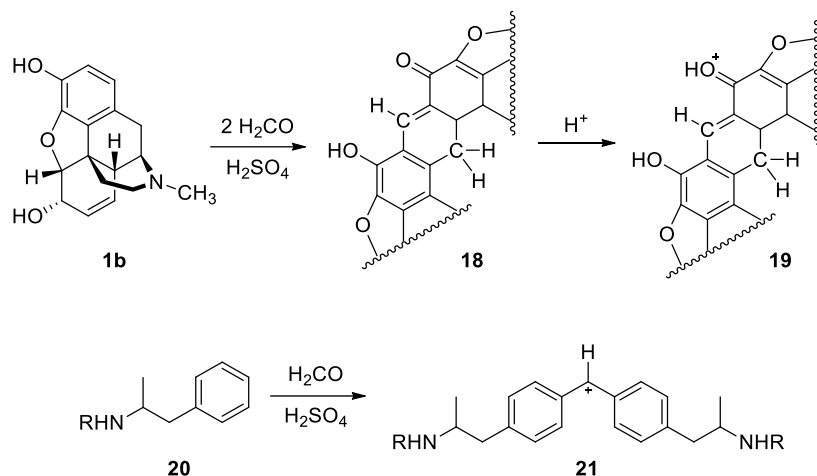


Figure 1.9. Chemical structure of the coloured products formed by Marquis' reagent with morphine and amphetamine derivatives.

Eosin Y (2', 4', 5', 7'-tetrabromofluorescein, see Figure 1.10) has been used in multi-dye sensors for the detection of controlled drugs. [78] It has recently been proposed as a colorimetric test to differentiate fentanyl from cocaine. [79] At pH 7, the reagent has a peach colour. It changes to light pink in the presence of various controlled drugs, but produces a much darker shade of pink when mixed with fentanyl. The mechanism of this reaction is not currently known.

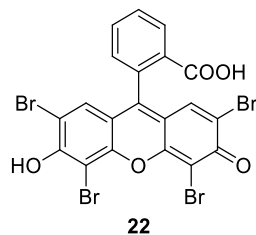


Figure 1.10. Chemical structure of eosin Y.

Although colour tests may have legitimate applications in an operational setting, their reliability tends to be limited. Analogues can cause misleading results, mixtures cannot be correctly identified, and results are strongly dependent on analyte concentration. Coupled with the subjective nature of colour-based results, these factors mean that this method should be carefully limited to presumptive testing and results confirmed using other analytical techniques.

Thin-layer chromatography (TLC), which has been used to analyse illicit drugs, could also be considered a presumptive technique. [80-82] It can provide useful separation for screening mixtures and has been used to discriminate fentanyl analogues. [83]

1.2.2 Spectroscopic methods

Spectroscopic techniques, such as Raman, FT-IR and NMR, are much more specific and sensitive than colour tests. They mostly give quick results, depending on acquisition settings, and portable versions are available for on-site analysis. However, their main drawback is the lack of separation, and mixture components producing overlapping signals can impede identification or quantification.

Portable Raman spectroscopy has been used for on-site identification of psychoactive drugs during music events. [84] The technique worked with only 73% accuracy (compared to GC-MS results) and mostly identified traditional drugs of abuse (*e.g.* MDMA, ketamine, cocaine and amphetamine). The authors noted that the technique only reports the major component in a mixture, [84] so it is unlikely to detect fentanyl in heroin. Surface-enhanced Raman spectroscopy (SERS), however, has been used for the detection and

quantification of fentanyl in heroin (as low as 1% w/w). [85] Fentanyl is detected by a C-C-C benzene trigonal stretch band which does not overlap heroin signals, though the specificity of this band is unclear. The technique also relies on the absence of other fillers in the mixture. In a more recent development, sensitivities as low as 0.0001 mol% fentanyl in heroin were reached by conducting SERS with a microfluidic octanol extraction chip. [86] Another study has shown that the Raman spectra of fentanyl and precursors 4-ANPP and NPP are very similar but may be distinguished using a partial least squares – discriminant analysis (PLS-DA) algorithm. [87] Similar approaches have shown that principal component analysis (PCA) applied to Raman spectroscopy data can differentiate fentanyl analogues from other classes of illicit drugs, but not from each other. [88, 89]

Infrared spectroscopy has also been used for on-site drug safety testing in UK city centres, although the agreement of the FT-IR results with MS analysis was not reported. [90] A recent study applied FT-IR to the detection of fentanyl in seized samples. [91] It showed that samples containing 10% or less fentanyl were more likely to give a negative result by FT-IR analysis. Infrared imaging has also been used to separately analyse mixture components, by relying on the poor mixing of drug samples, but this has yet to be applied to fentanyl detection. [92]

Like the previous techniques, benchtop ^1H NMR spectroscopy has been used to identify illicit drug samples, with 93% accuracy across 416 samples. [93] NMR analysis also provides structural information about unknown compounds: it can detect structural similarities between members of the same drug family and aid in the identification of novel drugs. [93, 94] Benchtop ^1H NMR has also been used to differentiate fentanyl analogues, including certain regioisomeric derivatives. [95] While high-field qNMR can be used to quantify fentanyl down

to 1% concentrations in mixtures, [91] benchtop instruments lack this kind of sensitivity.

1.2.3 Chromatographic methods

Chromatographic methods tend to be better suited to the analysis of real-world samples, because of their ability to separate mixtures. However, instruments can be more expensive than those required for the techniques previously described, are often not portable, and require specialised staff for maintenance and operation.

Multiple studies have reported the analysis of fentanyl and some of its analogues (see Table 1.1). Sisco *et al.* have reported very sensitive direct analysis in real-time mass spectrometry [DART-MS, Limit of Detection = 0.08 – 0.35 ng] and ion mobility spectrometry [IMS, Limit of Detection = 1.0 – 10.0 ng] screening methods, but neither of these techniques facilitated efficient separation of the eighteen analogues within the study. [96] High performance liquid chromatography (HPLC) has been applied in a number of studies [97-99] including one validated method, which has been developed and utilized to quantify fentanyl within bulk forensic samples of heroin. [98] Hyphenated techniques (LC-MS, LC-MS² and UPLC-MS²) have also been applied to detect fentalogues and their metabolites in blood [100-103], urine [101] and wastewater. [104] Although these methods are impressively quick, they were not optimized to chromatographically resolve the targeted analytes, which can lead to ion suppression when analyzing low-concentration, adulterated street samples. [105] More importantly, the published method(s) rely on equipment that is prohibitively expensive for smaller forensic laboratories, which normally rely on gas chromatography-mass spectrometry (GC-MS) as a primary method of analysis. [106] The United Nations Office on Drugs and Crime (UNODC)

have recently published guidelines for the identification and analysis of fentanyl and its analogues – primarily focused on their detection within in biological samples. [107] Bravo *et al.*, Strano-Rossi *et al.* and Misailidi *et al.* have also independently developed GC-MS methods for the determination of sufentanil [108], alfentanil [108], 2-furanylfentanyl [109] and ocfentanil [109] in toxicological/post-mortem samples. Abonamah *et al.* recently reported an especially interesting nano-LC-EI-MS, a semi-portable instrument which could be used for on-site detection of heroin, fentanyl, acetylfentanyl, butyrfentanyl and carfentanil, though it could not separate the later two. [110] Surprisingly, simple validated GC-MS methods with the ability to separate and quantify an array of fentalogues, for the routine analysis of bulk samples, both in their pure form and in the presence of other controlled substances or adulterants have not yet been reported in the literature.

Table 1.1. Comparison of analytical methods for detection/quantification of fentanyl (**2**), its derivatives and other drugs studied herein.

Technique	Matrix	Run Time (min)	LOD ^a (µg/mL unless stated)	LOQ ^b (µg/mL unless stated)	Linear Range (µg/mL unless stated)	Reference
TD-DART-MS ^c	- ^d	- ^d	8 – 0.22 ng (LOD ₉₀) ^e	- ^d	0 – 10 ng per wipe	[96]
IMS ^f	- ^d	- ^d	1 ng – 5 ng (LOD ₉₀) ^e	- ^d	1 – 100 ng per wipe	[96]
GC-MS ^g	Blood, Plasma	17	0.4 x 10 ⁻³ – 4.62 x 10 ⁻³	1.3 x 10 ⁻³ – 14 x 10 ⁻³	20 x 10 ⁻³ – 1.5	[111]
GC-MS ^g	Urine	23	0.08 x 10 ⁻³	0.5 x 10 ⁻³	0.5 x 10 ⁻³ – 50 x 10 ⁻³	[108]
GC-MS ^g	Blood	12	0.15 x 10 ⁻⁴ – 0.3 x 10 ⁻⁴	0.5 x 10 ⁻⁴ – 1 x 10 ⁻³	0.5 x 10 ⁻⁴ – 0.1	[109]
HPLC-UV ^h	Bulk powder	20	- ^d (qualitative)	- ^d (qualitative)	- ^d (qualitative)	[97]
HPLC-UV ^h	Bulk powder	30	16.2 x 10 ⁻² – 1.36	54.0 x 10 ⁻² – 4.55	5.0 – 120.0	[98]
HPLC-AD ⁱ	Serum	- ^d	1.0 x 10 ⁻³ – 7.5 x 10 ⁻¹	- ^d	- ^d	[99]
HPLC-AD ⁱ	Bulk powder	30	0.45 – 2.93	1.49 – 9.76	10.0 – 120.0	[98]
LC-MS ^j	Blood	- ^d	0.2 x 10 ⁻³ – 0.6 x 10 ⁻³	0.6 x 10 ⁻³ – 2.0 x 10 ⁻³	- ^d	[100]
LC-MS-MS ^k	Blood, Urine	20	8.0 x 10 ⁻⁵ – 2.0 x 10 ⁻³	1.0 x 10 ⁻⁴	1.0 x 10 ⁻⁴ – 0.76	[101]
LC-MS-MS ^k	Blood	13.5	17.0 x 10 ⁻³ – 56.0 x 10 ⁻³	0.1 x 10 ⁻³ – 0.5 x 10 ⁻³	0.1 x 10 ⁻³ – 50 x 10 ⁻³	[102]
LC-MS-MS ^k	Blood	5	- ^d	0.1 x 10 ⁻³ – 1.0 x 10 ⁻³	0.1 x 10 ⁻³ – 40 x 10 ⁻³	[103]
UPLC-MS-MS ^l	Wastewater	8	3.0 x 10 ⁻⁸ – 2.1 x 10 ⁻⁷	1.0 x 10 ⁻⁷ – 7.0 x 10 ⁻⁷	1.0 x 10 ⁻⁷ – 1.0 x 10 ⁻³	[104]
nLC-EI-MS ^m	Bulk powder	10-15	1.6 ng/mL	- ^d	5 – 20 ng	[110]

Key: ^aLimit of detection; ^bLimit of quantification; ^cThermal desorption-direct analysis in real-time-mass spectrometry; ^dNot disclosed; ^eLOD₉₀ is the lowest mass which can be detected per wipe with a 90% probability of true detection; ^fIon mobility spectrometry; ^gGas chromatography-mass spectrometry; ^hHigh performance liquid chromatography (utilising ultraviolet detection); ⁱHigh performance liquid chromatography (utilising amperometric detection); ^jLiquid chromatography-mass spectrometry; ^kLiquid chromatography-mass spectrometry-mass spectrometry (or LC-MS²); ^lUltra performance liquid chromatography-mass spectrometry-mass spectrometry (or UPLC-MS²); ^mNano-liquid chromatography-electron ionization-mass spectroscopy.

1.2.4 Statistical analysis and clustering algorithms

As discussed previously, novel drug analogues can be difficult to identify, because they have yet to be added to mass spectral databases. The development of detection methods aims to make the detection of known analogues more accessible, to help harm reduction and decrease under-reporting. However, it is inherently a reactive approach to the issue, and as long as new analogues keep appearing, new detection methods will have to be developed. Proactive solutions should therefore be considered to quickly identify future analogues. Efforts should focus on the development of predictive models which, when confronted with an unknown drug analogue, not present in their database, can still identify common features and discern how the analogue differs from the parent drug.

Multivariate analysis has previously been used to determine the synthetic route used to manufacture fentanyl samples based on an inventory of contaminants detected by GC-MS, LC-MS-MS and ICP-MS. [112] It also helped identify fentanyl analogues based on their Raman spectra. [88] Principal component analysis has been used to differentiate regioisomeric synthetic drugs, including regioisomers of fluorofentanyl, by highlighting differences in specific m/z ion ratios. [113-115] Recently, spectral similarity mapping was applied to group fentanyl analogue mass spectra based on their match factors. [116] Part of this thesis will focus on the development of a model using principal component analysis (PCA) and hierarchical clustering algorithms to group fentanyl analogues in structural families, based on their mass spectra. The model can automatically classify novel analogues to aid structural elucidation.

1.3 Objectives

This thesis aims to solve different challenges associated with the analysis of fentanyl analogues in a forensic context. In Chapter II, eighteen common fentanyl analogues will be synthesised, fully characterised, and submitted to presumptive colour tests, TLC and FT-IR analysis. A GC-MS method will be developed to separate target analogues and allow their detection and quantification in seized heroin samples. Chapter III will focus on fluorofentanyl regioisomers, which cannot be separated by GC-MS. An orthogonal benchtop ^{19}F NMR method will be developed to differentiate and quantify these analogues. Chapter IV will focus on the eosin Y colour test. The mechanism of the reaction between eosin Y and heroin/fentanyl will be investigated by NMR. UV-Vis spectrophotometry and RGB detection will be used to develop a quantitative version of the test. Finally, Chapter V will describe a principal component analysis (PCA) model based on MS data from fentanyl analogues. The model will be able to group analogues based on their structural class and identify structural modifications in novel compounds.

CHAPTER II

SYNTHESIS AND DETECTION OF AMIDE-CHAIN FENTANYL DERIVATIVES

2.1 Overview

By far the most commonly encountered modification of the fentanyl structure is the variation of the amide chain. It is the easiest portion to modify synthesis-wise, as the amide bond is formed in the last reaction step. In the case of fentanyl, this is done *via* the reaction between the drug precursor 4-anilino-*N*-phenethylpiperidine (4-ANPP, **4**) and propionyl chloride. Acyl chlorides bearing a variety of alkyl, alkenyl, aryl, heteroaryl groups are indeed widely available, which gives easy access to a variety of analogues. This is illustrated by the fact that acetylfentanyl (2015) and butyrylfentanyl (2016) were some of the first analogues to emerge in the current resurgence of the drug, and there is an ever-growing range of derivatives bearing new amide chains. [15]

Therefore, this study starts with the development of detection and quantification methods for amide-chain analogues of fentanyl. Eighteen target compounds were synthesised (see Figure 2.1; see section 2.2 for more details). Analogues were included mainly based on reports found in the scientific literature or made by official organisations (*e.g.* the Drug Enforcement Agency). A selection can

be found in Table 2.1 and includes reports of overdoses, identification by early warning systems, law enforcement seizures or scheduling as controlled drugs.

Selected analogues include alkyl (**2a-e**) and cycloalkyl (**2f-i**) derivatives. Although cyclohexylfentanyl (**2i**) was not found in the literature, it was included in this study as the logical continuation of the cycloalkyl series. Branched alkyl compounds **2j** and **2k** were also included to determine whether detection methods can discriminate regioisomers of **2c** and **2d**, respectively.

The reasoning behind the inclusion of fluorinated compounds **2l** and **2m** is two-fold. Firstly, the introduction of fluorine atoms, especially the use of a trifluoromethyl group as a bioisostere for a methyl group, has been observed in the design of various controlled drugs, such as phenethylamines and diphenidines. [117, 118] This is generally done to block potential metabolic oxidation sites, because fluorine atoms can replace hydrogen atoms without significantly altering the geometry of the molecule, thus preserving the biological activity but slowing down metabolism. The amide chain gets hydroxylated during the metabolism of fentanyl, meaning that such derivatives could potentially emerge. On the other hand, trifluoroacetylation has been reported as a useful GC derivatization for the analysis of amines, including amphetamines and fentanyl metabolites, to greatly improve their chromatographic properties. [119, 120] This type of derivatisation could be used for the analysis of fentanyl precursor (and metabolite) 4-ANPP.

The study also includes common fentalogues methoxyacetylfentanyl (**2n**), two furanylfentanyl isomers (**2o-p**), acrylfentanyl (**2q**) and phenylfentanyl (**2r**).

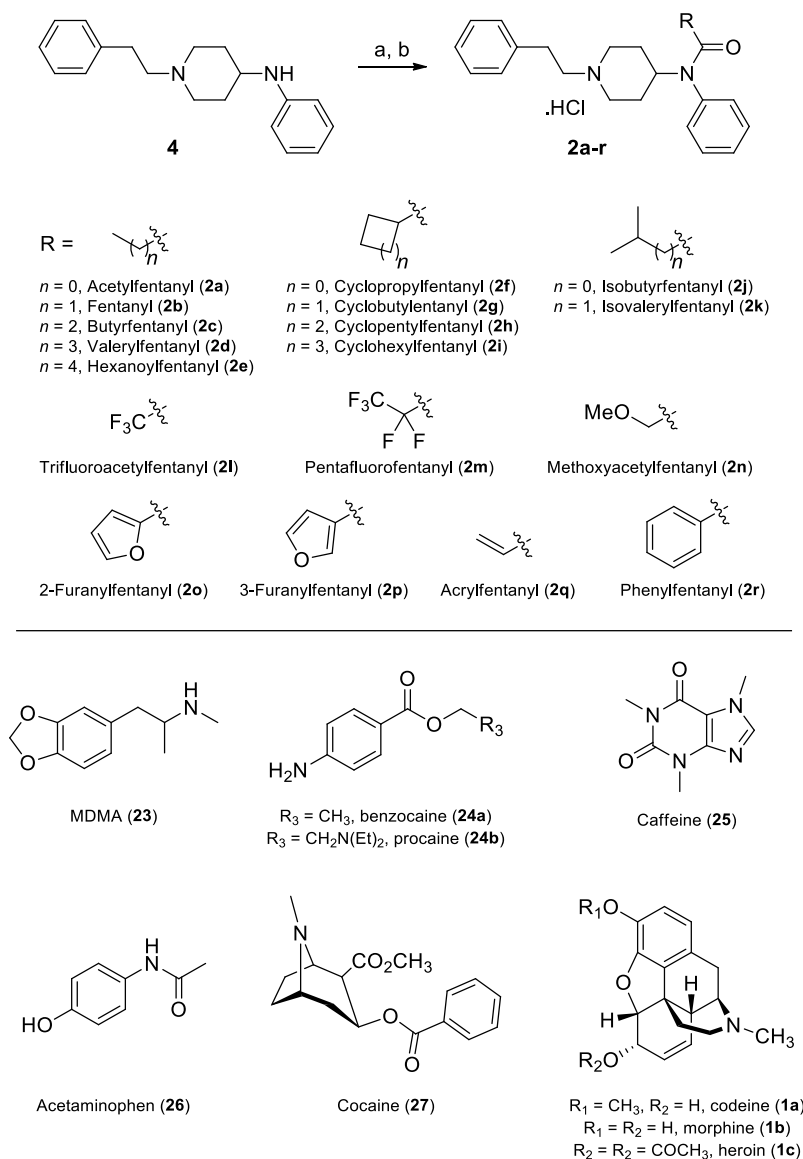


Figure 2.1. Synthesis of fentanyl analogues **2a-r** and structure of controlled drugs and adulterants (**1a-c**, **23-27**) included in this study. *Reagents and conditions:* (a) RCOCl (2.0 eq.), *i*Pr₂NEt (2.0 eq.), DCM (0.1 M), 0°C to r.t., 2 h; (b) HCl (3 M in CPME, 1.0 eq.), Et₂O or acetone (0.1 M), r.t., 10 min (15-64%).

Table 2.1. A selection of literature references where target fentalogues **2a-r** have been reported.

Compound	Common Name	References
2a	Acetylfentanyl	[28, 121-126]
2b	Fentanyl	[25, 35, 55, 124-127]
2c	Butyrylfentanyl	[62, 122-128]
2d	Valerylfentanyl	[123, 129, 130]
2e	Hexanoylfentanyl	[129, 131, 132]
2f	Cyclopropylfentanyl	[123, 124, 128, 133, 134]
2g	Cyclobutylfentanyl	[135]
2h	Cyclopentylfentanyl	[123, 130]
2i	Cyclohexylfentanyl	N/A
2j	Isobutyrylfentanyl	[124, 130]
2k	Isovalerylfentanyl	N/A
2l	Trifluoroacetylfentanyl	N/A
2m	Pentafluorofentanyl	N/A
2n	Methoxyacetylfentanyl	[123, 128, 129, 136]
2o	2-Furanylfentanyl	[32, 123-126, 129, 137]
2p	3-Furanylfentanyl	[138]
2q	Acrylfentanyl	[64, 123, 124, 126, 129, 139]
2r	Phenylfentanyl	[129, 132]

This chapter focuses on the testing and development of analytical methods to detect and/or quantify these 18 target fentalogues as well as common controlled drugs and adulterants with which they have been found in mixtures (see Figure 2.1). It will start with presumptive detection methods, *i.e.* colorimetric tests and thin-layer chromatography, which, though they do not allow confident identification and must be employed with caution, are rapid and can be used on the field. Reliable identification of the 18 fentalogues by mass spectrometry will then be discussed, along with a comparison of their electron ionisation (EI-MS) fragmentation patterns. A GC-MS method will then be developed for the separation of target analytes. This method will be adapted and fully validated for quantification. Finally, the methods previously discussed will be applied to screen seized heroin samples, provided by law enforcement, for the presence of fentalogues.

2.2 Synthesis

Synthesis was adapted from the procedure reported by Valdez *et al.*, starting from 4-ANPP (**4**, Figure 2.1). [4] Acylation with an acyl chloride, followed by reaction with hydrogen chloride, afforded 18 amide-chain fentalogues (**2a-r**) as their hydrochloride salt with 15-64% yield. Synthesised materials were fully characterised: ATR-FTIR and NMR (^1H , ^{13}C , ^{19}F) and high-resolution mass spectrometry (HRMS) data are reported in Section 7.12. ATR-FTIR and NMR (^1H , ^{13}C , ^{19}F) spectra are reported in the Appendix. EI-MS spectra are reported in section 2.6 (Figure 2.3 and Figure 2.4).

Although high-field NMR analysis is not routinely used in forensic casework, it may be useful to outline some similarities across fentanyl NMR spectra for characterisation purposes. This is also relevant for recently reported techniques which employ low-field ^1H NMR for NPS identification, and identify NPS classes based on common spectral features. [93] Table 2.2 summarises the ^1H NMR data for fentalogues **2a-r**. A numbering reference for this table can be found in Figure 2.2. Spectra are relatively consistent in the aromatic region, with deshielding of protons 17-19 compared to other aromatic protons. The latter usually appear as one multiplet, though they can be separated in some analogues (**2g**, **2k**, **2l** and **2m**).

Table 2.2 clearly highlights the consistency in piperidine and ethyl chain protons signals for all analogues. These signals are most indicative of the fentanyl backbone. Overlap with the amide chain occurs in some compounds (**2a**, **2g**, **2h**, **2l**, **2k**, and **2n**), but signals can easily be resolved using 2D correlation spectroscopy (^1H - ^1H or ^1H - ^{13}C).

Amide chain proton signals are specific to each fentanyl studied and thus allow their identification. **2l** and **2m** must be identified by ^{13}C and ^{19}F NMR, as their amide chains do not bear protons. The benzoyl signals of **2r** overlap the other aromatic protons in the molecule, but identification is possible by ^{13}C NMR.

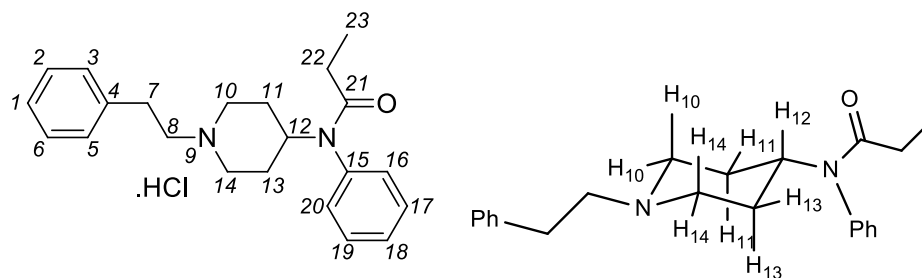


Figure 2.2. Numbering reference for fentanyl (**2b**).

Table 2.2. ¹H NMR attribution of fentalogues **2a-r**.

	Aromatic protons				Piperidine ring and ethyl chain protons ^a						Amide chain protons ^b					
	17-19	2, 6	3,5	1, 16, 20	12	10a/ 14a	8/10b/ 14b	7	11a/ 13a	11b/ 13b	22	23	24	25	26	27
2a	7.58-7.40 (m)	7.34-7.17 (m)			4.69 (t)	3.52 (d)	3.20-3.04 (m)	3.02-2.93 (m)	1.92 (d)	1.70-1.55 (m)	1.70-1.55 (m)	-	-	-	-	-
2b	7.50-7.42 (m)	7.33-7.21 (m)			4.71 (t)	3.51 (d)	3.26-3.02 (m)	2.99-2.95 (m)	1.92 (d)	1.62 (q)	1.82 (q)	0.87 (t)	-	-	-	-
2c	7.51-7.44 (m)	7.33-7.22 (m)			4.71 (t)	3.51 (d)	3.20-3.06 (m)	2.99-2.95 (m)	1.92 (d)	1.62 (q)	1.79 (t)	1.42 (sext)	0.71 (t)	-	-	-
2d	7.53-7.40 (m)	7.35-7.17 (m)			4.71 (t)	3.51 (d)	3.20-3.04 (m)	3.03-2.94 (m)	1.91 (d)	1.63 (q)	1.81 (t)	1.39 (quint)	1.1 (sext)	0.71 (td)	-	-
2e	7.51-7.43 (m)	7.33-7.22 (m)			4.71 (t)	3.52 (d)	3.21-3.02 (m)	3.02-2.87 (m)	1.92 (d)	1.61 (q)	1.81 (t)	1.41 (quint)	1.14-1.02 (m)		0.77 (t)	-
2f	7.53-7.43 (m)	7.33-7.21 (m)			4.69 (tt)	3.51 (d)	3.25-3.05 (m)	3.00-2.96 (m)	1.93 (d)	1.67 (q)	1.00 (bs)	0.75 (t) / 0.56-0.54 (m)		-	-	-
2g	7.49-7.41 (m)	7.32-7.29 (m)	7.24-7.16 (m)		4.67 (t)	3.51 (d)	3.19-3.05 (m)	2.99-2.95 (m)	1.91 (d)	1.66-1.51 (m)	2.73 (quint)	2.15-2.06 (m)	-	2.15-2.06 (m)	-	-
												1.66-1.51 (m)				
2h	7.48-7.44 (m)	7.32-7.21 (m)			4.69 (t)	3.51 (d)	3.20-3.03 (m)	3.02-2.94 (m)	1.91 (d)	1.70-1.39 (m)	2.23 (quint)	1.70-1.39 (m)				-
												1.29 (bs)				
2i	7.52-7.44 (m)	7.33-7.21 (m)			4.67 (t)	3.51 (d)	3.20-3.02 (m)	3.01-2.93 (m)	1.94-1.76 (m)	1.67-1.51 (m)	1.94-1.76 (m)	1.67-1.51 (m)	1.32 (q) / 0.78 (q)	1.46 (d) / 1.06 (q)	1.32 (q) / 0.78 (q)	1.67-1.51 (m)

Table 2.2. ¹H NMR attribution of fentalogues **2a-r**. (cont.)

	Aromatic protons				Piperidine ring and ethyl chain protons ^a						Amide chain protons ^b					
	17-19	2, 6	3,5	1, 16, 20	12	10a/ 14a	8/10b/ 14b	7	11a/ 13a	11b/ 13b	22	23	24	25	26	27
2j	7.52- 7.43 (m)	7.33-7.21 (m)			4.68 (t)	3.51 (d)	3.20- 3.03	3.02- 2.94 (m)	1.91 (d)	1.62 (q)	2.11 (sep)	0.88 (d)		-	-	-
2k	7.52- 7.41 (m)	7.31 (t)	7.26-7.17 (m)		4.72 (tt)	3.51 (d)	3.20- 3.03 (m)	3.01- 2.93 (m)	2.01- 1.87 (m)	1.63 (q)	1.71 (d)	2.01- 1.87 (m)	0.73 (d)		-	-
2l	7.53- 7.47 (m)	7.37 (t)	7.31 (t)	7.26- 7.18 (m)	4.67 (tt)	3.55 (d)	3.20- 3.09 (m)	3.01- 2.94 (m)	2.05 (d)	1.69 (q)	-	-	-	-	-	-
2m	7.61- 7.46 (m)	7.43- 7.36 (m)	7.35- 7.28 (m)	7.26- 7.20 (m)	4.68 (tt)	3.55 (d)	3.24- 3.07 (m)	3.03- 2.93 (m)	2.10- 2.00 (m)	1.89- 1.54 (m)	-	-	-	-	-	-
2n	7.52- 7.43 (m)	7.35-7.19 (m)			4.69 (t)	3.56- 3.49 (m)	3.20- 3.04 (m)	3.01- 2.94 (m)	1.93 (d)	1.64 (q)	3.56- 3.49 (m)	3.20- 3.04 (m)	-	-	-	-
2o	7.53- 7.46 (m)	7.35-7.19 (m)			4.83 (tt)	3.56 (d)	3.24- 3.09 (m)	3.05- 2.95 (m)	2.04 (d)	1.76 (q)	-	5.38 (s)	6.32 (dd)	7.66 (s)	-	-
2p	7.55- 7.46 (m)	7.43-7.14 (m)			4.83 (t)	3.55 (d)	3.25- 3.09 (m)	3.05- 2.96 (m)	2.02 (d)	1.76 (q)	-	5.98 (s)	6.75 (s)	7.55- 7.46 (m)	-	-
2q	7.53- 7.44 (m)	7.34-7.19 (m)			4.75 (t)	3.53 (d)	3.21- 3.06 (m)	3.02- 2.93 (m)	1.97 (d)	1.69 (dd)	5.71 (dd)	6.15 (dd) / 5.53 (dd)	-	-	-	-
2r	7.35-7.11 (m)				4.82 (bs)	3.58 (d)	3.24- 3.11 (m)	3.04- 2.97 (m)	2.11 (d)	1.8 (dq)	7.35-7.11 (m)					

Key: ^a a and b are axial and equatorial protons on the same carbon; ^b Amide chain protons are numbered moving away from the carbonyl.

2.3 Presumptive colour tests

Colorimetric tests were chosen strategically to differentiate fentanyl analogues from common drugs of abuse, with which they have been found in mixtures, and their adulterants. Tests were carried out according to the United Nations recommended guidelines, on pure powders. [77, 140] Results are reported in Table 2.3. Procedures to prepare the presumptive test solutions are reported in Section 7.1.

Scott's test did not prove specific enough to discriminate fentalogues from cocaine, or even heroin: it gave a positive (blue) result for cocaine (**27**), procaine (**24b**), all fentanyl analogues (**2a-r**) and heroin after 5 minutes (**1c**).

The nitric acid test gave positive results with MDMA and paracetamol. The only target compounds that reacted with the test were 4-ANPP, 2- and 3-furanylfentanyl (**2o-p**). The difference between 4-ANPP and most fentalogues can be explained by their reactivity towards electrophilic aromatic substitution; 4-ANPP is an aromatic amine rather than an amide, and an amine substituent activates the aromatic ring more than an amide because in the latter the carbonyl draws some of the electron density away from the nitrogen. In furanyl derivatives, the colour change may have resulted from nitration of the furan ring.

With Marquis' reagent, 4-ANPP (**4**) and fentanyl analogues (**2a-r**) all gave positive colour changes. A notable exception was 3-furanylfentanyl (**1p**), which turned into a brown precipitate in an orange solution. Marquis' reagent successfully discriminated fentalogues from cocaine and all adulterants tested (**24a-b**, **25**, **26**), none of which react to the test. It also differentiated fentalogues from MDMA (**23**), codeine, morphine and heroin (**1a-c**), though it is unclear how

the test would perform on mixtures, as the brown and purple colorations may interfere with each other. As will be discussed in section 2.9, matrix interference can also affect the outcome of the test.

Eosin Y changes to light pink in the presence of various controlled drugs, but produces a very specific, darker shade of pink when mixed with fentanyl. The mechanism of this reaction is currently not known, but it will be explored more in-depth in Chapter 4. Although most common drugs and adulterants tested gave a light pink colour, this result is significantly different from that obtained with fentalogues to allow successful discrimination. All fentanyl analogues tested produced the expected dark pink colour, except **2m** that gave a light pink result. This shows that Eosin Y can discriminate between most fentanyl analogues and common drugs of abuse.

A combination of the Marquis and Eosin Y seems most appropriate to differentiate fentalogues from common controlled drugs and adulterants. The nitric acid test provides only moderately useful results, as it does not react with most fentalogues, but can be used to identify traditional opiates (morphine, codeine, heroine) and to differentiate precursor 4-ANPP. Scott's reagent did not allow discrimination of cocaine from fentalogues.

Table 2.3. Reactions of fentalogues (**2a-r**) and other drugs studied herein with the Marquis, Scott, Nitric acid and Eosin Y tests. Note: A dash indicates the absence of a discernible colour change.

	Scott		Nitric Acid		Marquis		Eosin Y	
	Immediate colour	Colour after 5 min	Immediate colour	Colour after 5 min	Immediate colour	Colour after 5 min	Immediate colour	Colour after 5 min
4	Blue	Blue	Orange	Dark Yellow	Orange	Dark brown	Light pink	Light pink
2a	Blue	Blue	—	—	Orange	Dark brown	Dark pink	Dark pink
2b	Blue	Blue	—	—	Orange	Dark brown	Dark pink	Dark pink
2c	Blue	Blue	—	—	Orange	Dark brown	Dark pink	Dark pink
2d	Blue	Blue	—	—	Orange	Dark brown	Dark pink	Dark pink
2e	Blue	Blue	—	—	Orange	Dark brown	Dark pink	Dark pink
2f	Blue	Blue	—	—	Orange	Dark brown	Dark pink	Dark pink
2g	Blue	Blue	—	—	Orange	Dark brown	Dark pink	Dark pink
2h	Blue	Blue	—	—	Orange	Dark brown	Dark pink	Dark pink
2i	Blue	Blue	—	—	Orange	Dark brown	Dark pink	Dark pink
2j	Blue	Blue	—	—	Orange	Dark brown	Dark pink	Dark pink
2k	Blue	Blue	—	—	Orange	Dark brown	Dark pink	Dark pink
2l	Blue	Blue	—	—	Orange	Dark brown	Dark pink	Dark pink
2m	Blue	Blue	—	—	Orange	Dark brown	Light pink	Light pink
2n	Blue	Blue	—	—	Orange	Dark brown	Dark pink	Dark pink
2o	Blue	Blue	—	Light Yellow	Orange	Dark brown	Dark pink	Dark pink
2p	Blue	Blue	—	Light Yellow	Brown	Orange	Dark pink	Dark pink
2q	Blue	Blue	—	—	Orange ^a	Dark brown ^b	Dark pink	Dark pink
2r	Blue	Blue	—	—	Orange	Dark brown	Dark pink	Dark pink
23	—	—	Yellow	Yellow	Dark purple	Dark purple	Light pink	Light pink
24a	—	—	—	—	—	—	Peach	Peach
24b	Blue	Blue	—	—	—	—	Light pink	Light pink
25	—	—	—	—	—	—	Light pink	Light pink
26	—	—	Orange	Yellow-orange	—	—	Light pink	Light pink
27	Blue	Blue	—	—	—	—	Light pink	Light pink
1a	—	—	Brown-orange	Yellow	Violet	Violet	Light pink	Light pink
1b	—	—	Orange	Yellow-orange	Purple	Purple	Light pink	Light pink
1c	—	Blue	Yellow	Green	Violet	Violet	Light pink	Light pink

^aBrown precipitate forms; ^bBrown precipitate separates from orange solution.

An additional test was performed using a mixture of fentanyl and heroin at different concentrations in methanol (Table 2.4).

Table 2.4. Results of presumptive colour tests for mixtures of fentanyl and heroin.

Concentration (mg/mL)		Marquis		Eosin Y	
Heroin (1c)	Fentanyl (2b)	Immediate colour	Colour after 5 min	Immediate colour	Colour after 5 min
5	0	Purple	Purple	Peach	Light Pink
5	0.05 (1% w/w)	Purple	Purple	Peach	Light Pink
5	0.1 (2% w/w)	Purple	Purple	Peach	Light Pink
5	0.25 (5% w/w)	Purple	Purple	Peach	Light Pink
0	5	—	—	Peach	Dark pink
0	10	Brown	Brown	Peach	Dark pink

Positive controls were performed to show that both tests allow detection of the pure materials in methanolic solutions (at 10 mg/mL). Neither Marquis' nor the Eosin Y tests allowed detection of fentanyl in low concentration mixtures (up to 5% w/w), only producing a positive result for heroin. This is consistent with Marinetti's findings, which show that Marquis' test can only distinguish fentanyl from heroin when it is the major component of a mixture. [26] In fact, at a concentration as high as 5 mg/mL in methanol, a pure solution of fentanyl gave a negative result. This highlights a limitation of presumptive tests with mixtures that could prove problematic when analysing actual samples (see section 2.9).

2.4 Thin-layer chromatography (TLC)

TLC analysis of 25 fentalogues has been reported by Suzuki *et al.*, which included derivatives **2a-c** and **2j**. [141] Using a chloroform-benzene-methanol

(10:2:1) eluent, they were unable to fully separate these compounds (**2c** and **2j** co-eluted).

In the present study, TLC analysis of 4-ANPP (**4**), fentalogues **2a-r** and heroin (**1c**) was performed using a dichloromethane-methanol (9:1 v/v) eluent containing 1% triethylamine. TLC plates were developed using a modified Dragendorff-Ludy-Tenger reagent, producing orange spots for all analytes. Results are reported in Table 2.5. Fentanyl analogues could be separated with a varying degree of success. For alkyl derivatives **2a-e**, RR_f values increased with the length of the carbon chain (from $RR_f = 0.91$ to 1.10) and only **2b** and **2c** co-elute. Cycloalkyl derivatives **2f-i** exhibited the same trend but were fully separated from each other.

Separation was less evident for most isomeric compounds. Cyclobutylfentanyl (**2g**, $RR_f = 1.05$) eluted very close to valeryl fentanyl (**2d**, $RR_f = 1.06$), while isobutyrylfentanyl (**2j**, $RR_f = 1.00$) co-eluted with butyrylfentanyl (**2c**). TLC did, however, manage to separate isovaleryl fentanyl (**2k**, $RR_f = 1.09$) from its isomers **2g** and **2d**, as well as 2- and 3-furanylfentanyl from each other (**2o** and **2p**, $RR_f = 1.04$ and 1.09, respectively). Less polar fluorinated derivatives **2l** and **2m** clearly separated from others ($RR_f = 1.32$ and 1.40). All fentalogues were clearly separated from 4-ANPP (**4**, $RR_f = 0.76$) and heroin (**1c**, $RR_f = 0.43$).

Table 2.5. Thin-layer chromatography results for 4-ANPP (**4**), fentalogues **2a-r** and heroin (**1c**).

Compound	R _f ^a	RR _f ^b
4	0.36	0.76
2a	0.46 (0.63) ^c	0.91
2b	0.51 (0.67) ^c	1.00
2c	0.51 (0.70) ^c	1.00
2d	0.54	1.06
2e	0.58	1.10
2f	0.53	1.02
2g	0.55	1.05
2h	0.57	1.09
2i	0.59	1.13
2j	0.51 (0.70) ^c	1.00
2k	0.55	1.09
2l	0.69	1.32
2m	0.74	1.40
2n	0.42	0.88
2o	0.51	1.04
2p	0.54	1.09
2q	0.59	1.14
2r	0.54	1.10
1c	0.22	0.43

Key: ^aRetention factor (DCM-MeOH (9:1 v/v) with 1% Et₃N); ^bRelative Retention Factor (with respect to fentanyl, **2b**); ^cRetention factor reported by Suzuki *et al.* (CHCl₃-benzene-MeOH (10:2:1 v/v/v)).

These results indicate that separation of all eighteen analogues by TLC is difficult. Although this technique does offer a higher discrimination power than colorimetric tests, it should be reserved for presumptive purposes. Identification of controlled drugs must exclusively be conducted using more powerful techniques, such as GC-MS.

2.5 Infrared spectroscopy

ATR-FTIR spectra of fentalogues **2a-r** are reported in Section 7.13. All compounds are characterised by weak to medium aromatic and aliphatic C–H bands ($\sim 3050\text{-}2850\text{ cm}^{-1}$), weak to medium ammonium salt N–H bands ($\sim 2600\text{-}2400\text{ cm}^{-1}$) and a strong amide C=O stretching band ($\sim 1680\text{-}1620\text{ cm}^{-1}$ depending on the amide group).

To test the possibility to discriminate analogues by their infrared spectra, a library containing compounds **2a-r** was built on the PerkinElmer Spectrum software (version 10.5.3). An individual sample was then removed from the library, and a database search was performed to find the second closest match (leave-one-out validation). Match scores close to 100% would mean that the technique is not able to differentiate a compound from its most similar analogue. As shown in Table 2.6, all match scores are less than or equal to 82%, which indicates a good ability to discriminate compounds based on their infrared spectra.

Table 2.6. Leave-one-out validation of the ATR-FTIR method with analogues **2a-r**.

Compound	Closest match	Match score
2a	2h	76%
2b	2c	82%
2c	2b	82%
2d	2e	81%
2e	2k	82%
2f	2q	76%
2g	2e	74%
2h	2k	77%
2i	2d	68%
2j	2g	72%
2k	2e	82%
2l	2p	43%
2m	2r	37%
2n	2l	38%
2o	2p	37%
2p	2l	43%
2q	2f	76%
2r	2e	60%

Most likely, compounds are differentiated by infrared bands in the fingerprint region ($1500\text{-}500\text{ cm}^{-1}$), but problems are likely to arise when analysing mixtures. This will be discussed in section 2.9.

2.6 Electron ionisation mass spectrometry

Electron ionisation mass spectra of fentalogues **2a-r** were acquired and are reported in Figure 2.3 and Figure 2.4.

Figure 2.3. Electron ionisation mass spectra of fentalogues **2a-i**.

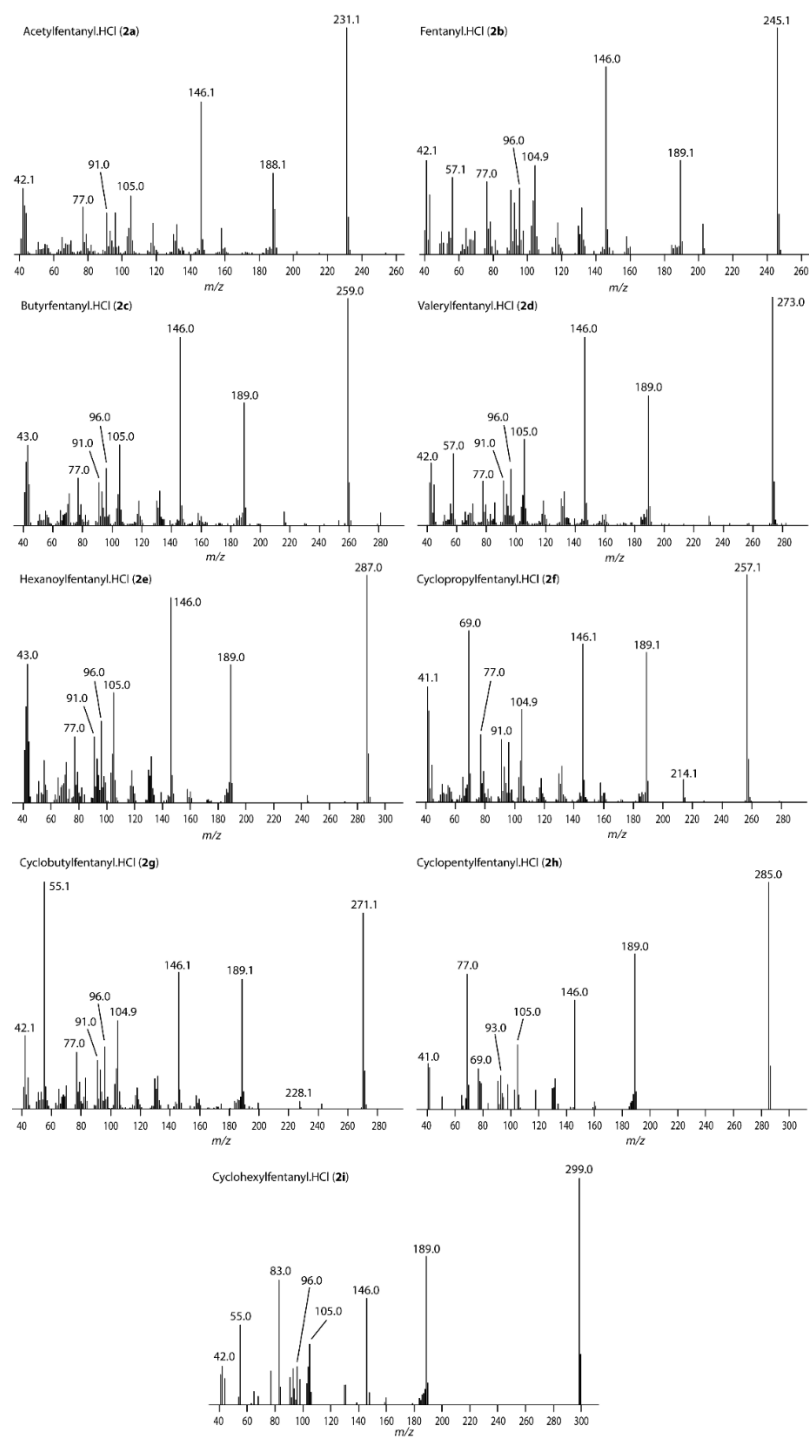
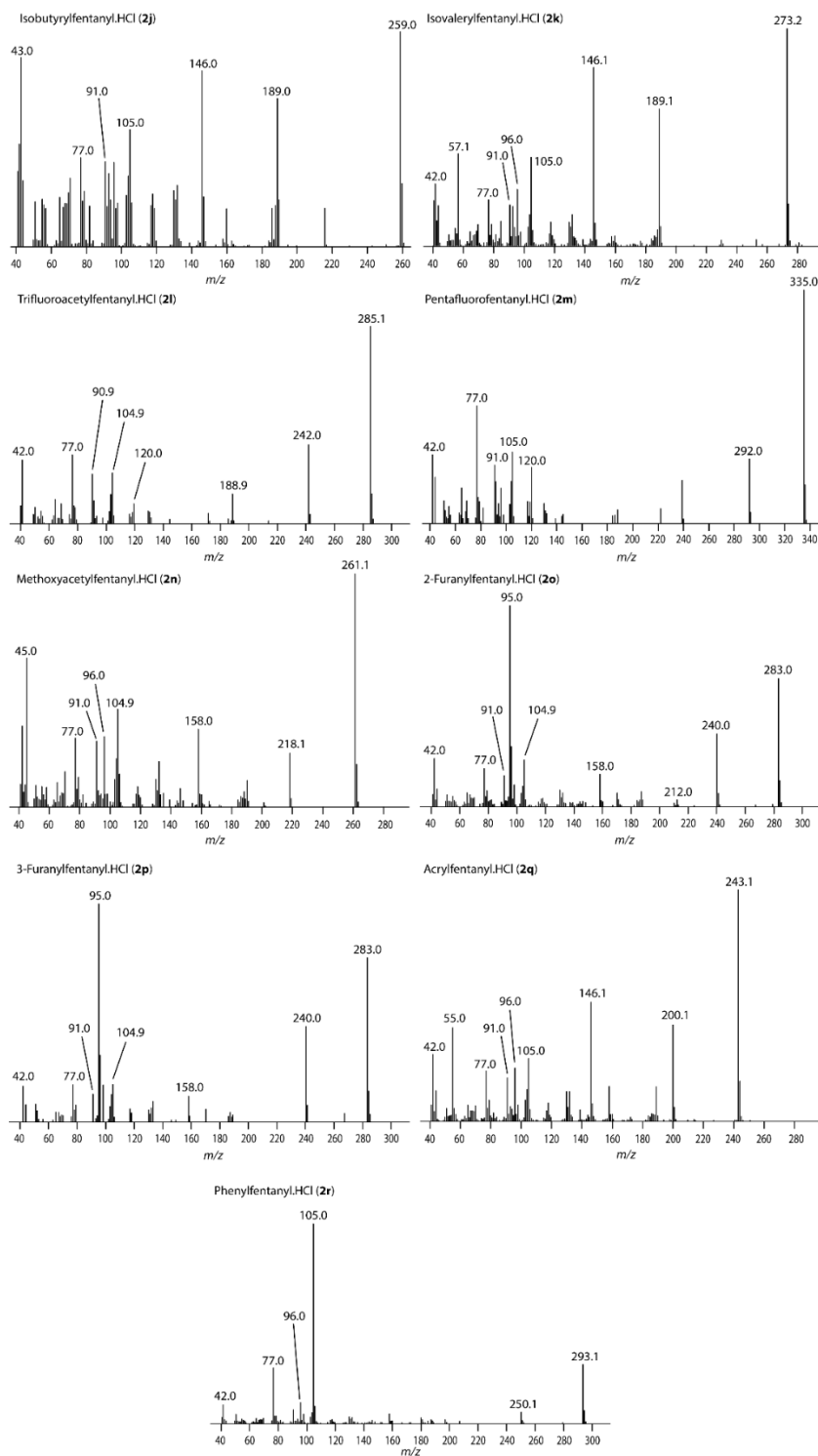


Figure 2.4. Electron ionisation mass spectra of fentalogues **2j-r**.



As EI-MS fragmentation patterns are generally specific to certain fentalogues, this technique is a powerful tool for identification. The mass spectrum of fentanyl, shown in Figure 2.5, serves as a typical example. Figure 2.6 shows the fragmentation pathways leading to the observed fragments. [141] Fragment **28** ($m/z = 245$) constitutes the base peak and arises through α,β cleavage of the phenylethyl chain; fragment **29** ($m/z = 202$) is formed through subsequent contraction of the piperidine ring. Fragments **28** and **29** are thus generally specific to each fentalogue, as their mass varies depending on the amide chain of the compound. This is not the case for the other fragments which are present, with the same mass, in most fentalogues studied. Cleavage of the C–N amide bond in **28** leads to fragment **30** ($m/z = 189$), while **31** ($m/z = 146$) can arise from **29** or **30** through previously described mechanisms. Fragments **30** and **31**, because they ultimately result from the loss of the amide chain, are common to most fentalogues studied (Figure 2.3).

Benzyl (**32**, $m/z = 105$) and tropylium (**33**, $m/z = 91$) cations come from the scission of the phenethyl chain. Phenyl cation **34** ($m/z = 77$), though it could come from further fragmentation of **33**, actually comes mostly from scission of the N–Ph bond, as will be explained in Chapter 3 (Section 3.6). Finally, acylium ion **35** has been attributed to the $m/z = 57$ peak.

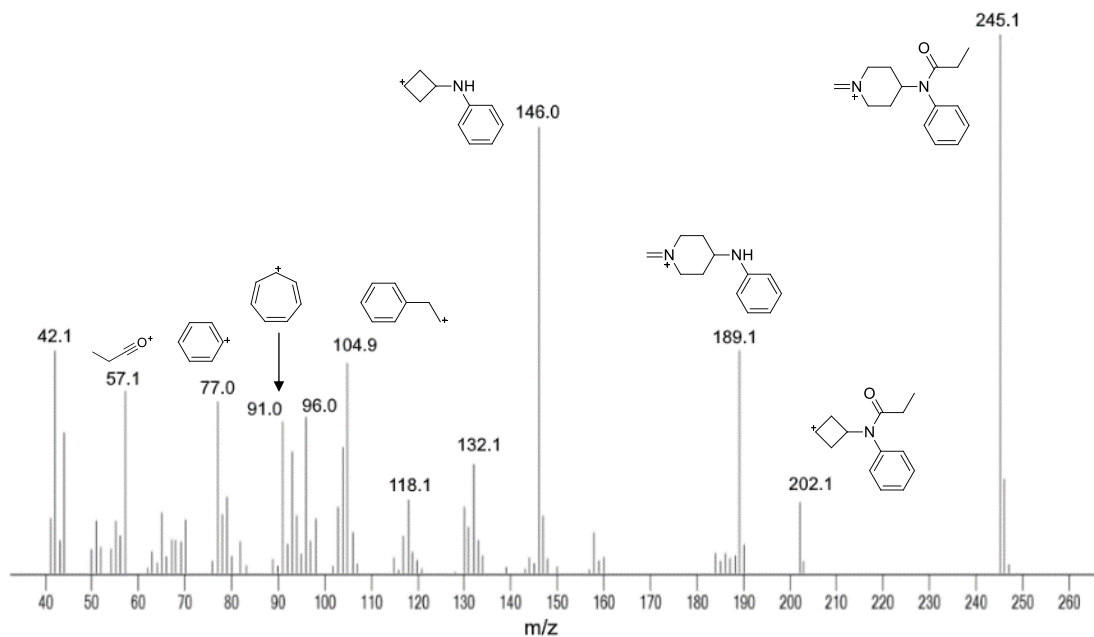


Figure 2.5. EI-MS spectrum of fentanyl (**2b**) and structure of main fragments.

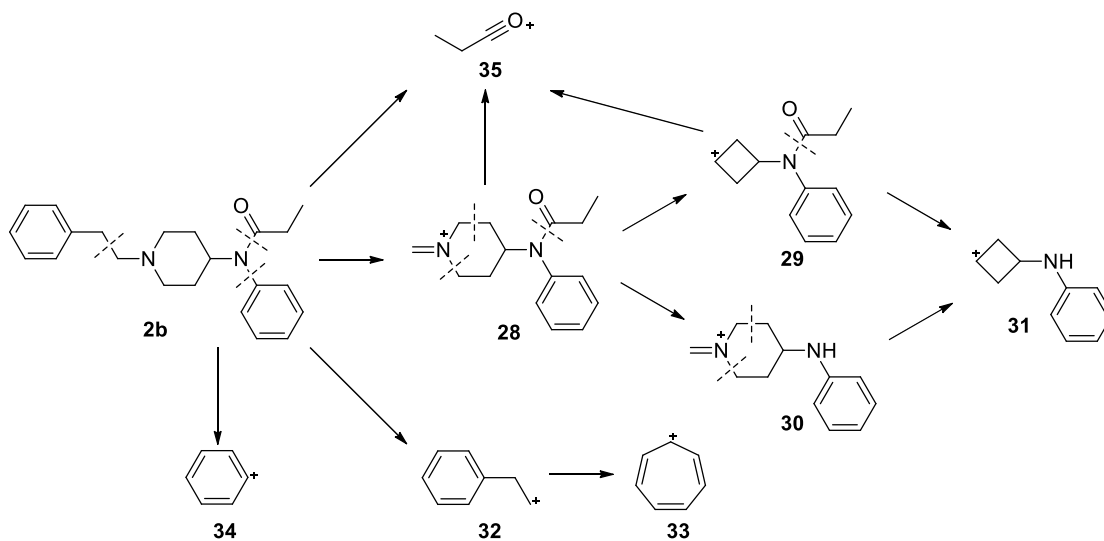


Figure 2.6. EI-MS fragmentation of fentanyl (**2b**) leading to the observed fragments.

Other fentanyl derivatives show analogous fragmentation patterns. Notable exceptions include cycloalkyl derivatives. Cyclopropylfentanyl (**2f**, Figure 2.7) produces a relatively abundant acylium ion **36** ($m/z = 69$), while cyclopropyl cation **37** ($m/z = 41$) is also observed. Compounds with larger rings (**2g-i**) only significantly produce fragments analogous to **37**. Unsaturated derivatives **2o-r** also produce abundant acylium cations akin to **36**.

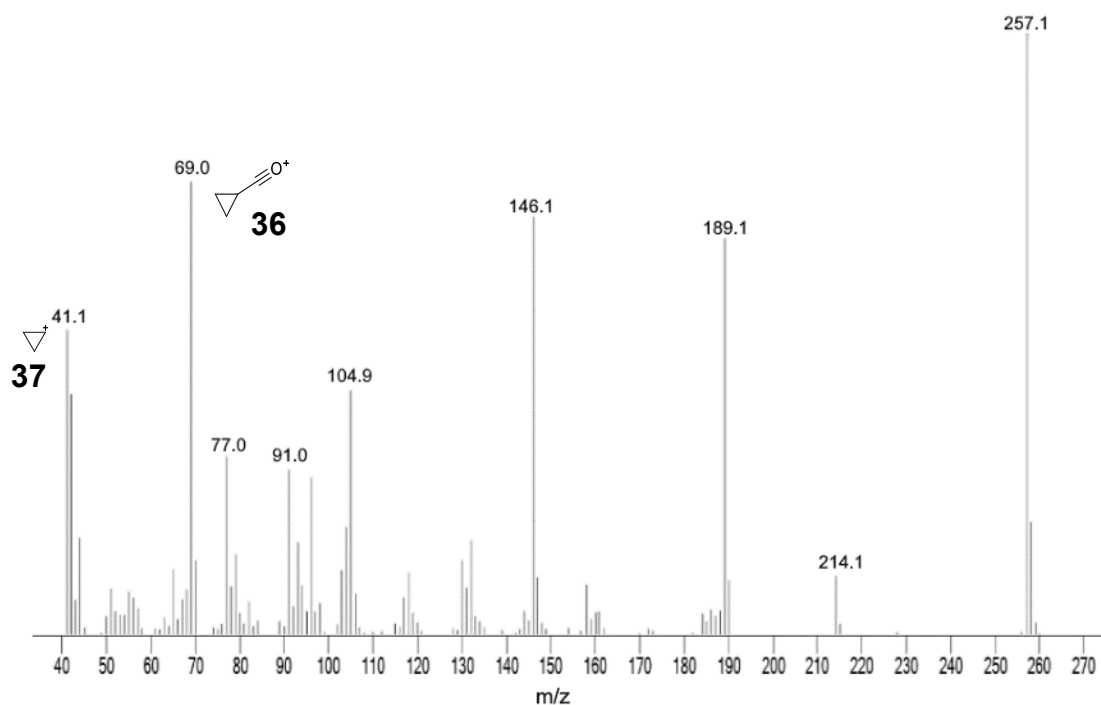


Figure 2.7. EI-MS spectrum of cyclopropylfentanyl (**2f**) and structure of fragments **36** and **37**.

All three oxygen-containing derivatives (**2n-p**) exhibit a relatively abundant fragment at $m/z = 158$. The fact that it has the same mass for all of them implies that it does not contain the amide moiety. This mass can only correspond to

piperidine-contraction fragments **38** or **39** (see Figure 2.8); the mechanism leading to their formation is not readily explained, but a rearrangement involving the oxygen-containing amide chain is likely.

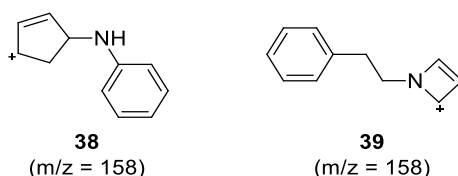


Figure 2.8. Potential $m/z = 158$ fragments of fentalogues **2n-p**.

2.7 Qualitative GC-MS analysis

The qualitative GC-MS method used in this study required straightforward solvation of the samples in methanol (0.1 mg/mL). No derivatization step was required. The complete GC-MS experimental procedure is reported in Section 7.4.

GC-MS methods have previously been reported by the Scientific Working Group for the Analysis of Seized Drugs (SWGDRUG) for fentalogue analysis. However, a representative SWGDRUG method (100 °C for 1.0 min, ramp to 280 °C at 12 °C/min and hold for 9.0 min) proved unsuitable for separating the 18 derivatives studied.

An initial optimisation of the temperature gradient was performed until the following conditions were reached: 100-200 °C at 30 °C/min, 200-235 °C at 10 °C/min, hold 6 min, 235-250 °C at 3 °C/min, hold 11 min, 250-260 °C/min at 1 °C/min, 260-280 °C at 10 °C/min, hold 1 min. A representative chromatogram

is shown in Figure 2.9. This very careful temperature gradient achieved separation of most fentalogues from each other, five controlled substances (cocaine, codeine, heroin, MDMA, morphine) and four adulterants (paracetamol, benzocaine, caffeine and procaine). Two pairs of compounds (**2f/2n** and **2h/2o**) still co-eluted, but they can be separated based on their mass spectra when using a Selected Ion Monitoring (SIM) method.

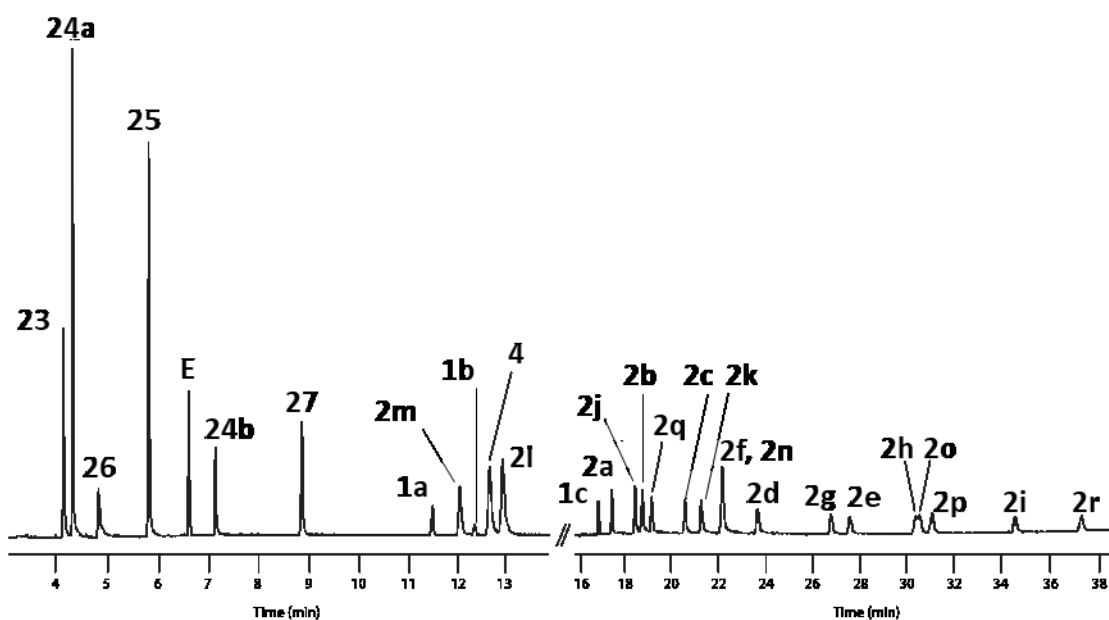


Figure 2.9. Exemplar chromatogram demonstrating GC-MS separation of 18 fentalogues (**2a-r**), MDMA (**23**), benzocaine (**24a**), acetaminophen (**26**), caffeine (**25**), eicosane (internal standard, E), procaine (**24b**), cocaine (**27**), codeine (**1a**), morphine (**1b**), 4-ANPP (**4**) and heroin (**1c**).

Before moving on to SIM analysis, however, further optimisation was necessary. Although the method provided satisfactory separation, the 38-minute runtime made it much too long for use in an operational context. Examination of the chromatogram (Figure 2.9) reveals sections where the

method could be shortened. This is corroborated when looking at the resolution data, a measure of how far a peak is from the one before it (see Table 2.7). A resolution of at least 2 indicates that two compounds are separated; resolutions higher than 10 (some even as high as 30) can be reduced to shorten the runtime. Additionally, time can be saved at the start of the run, as the first peak only elutes after 4.1 minutes.

Table 2.7. Retention time and resolution for target fentalogues, controlled drugs and adulterants (see Figure 2.9 for chromatogram).

	t_R (min)	Resolution		t_R (min)	Resolution
23	4.10	-	2b	18.77	2.1
24a	4.27	4.9	2q	19.18	2.9
26	4.79	9.4	2c	20.59	9.9
25	5.80	17	2k	21.27	3.4
24b	7.14	12	2f	22.16	3.9
27	8.87	31.7	2n	22.18	3.9
1a	11.48	38.7	2d	23.69	2.2
2m	12.03	6.3	2g	26.82	3.4
1b	12.34	3.3	2e	27.63	1.7
4	12.63	3.1	2h	30.43	10.4
2l	12.89	2.2	2o	30.60	0.7
1c	16.89	36.6	2p	31.13	1.9
2a	17.47	5.3	2i	34.70	8.4
2j	18.45	7.9	2r	37.54	8

Making the necessary modifications, a new temperature gradient was optimised: 175-235 °C at 30 °C/min, hold 7 min, 235-270 °C at 30 °C/min, hold 7.5 min, 270-290 °C at 30 °C/min, hold 2 min, reducing the total runtime to a much more acceptable 20.33 min (see Figure 2.10). Adequate separation of the analytes was retained (see Table 2.8 for resolution data).

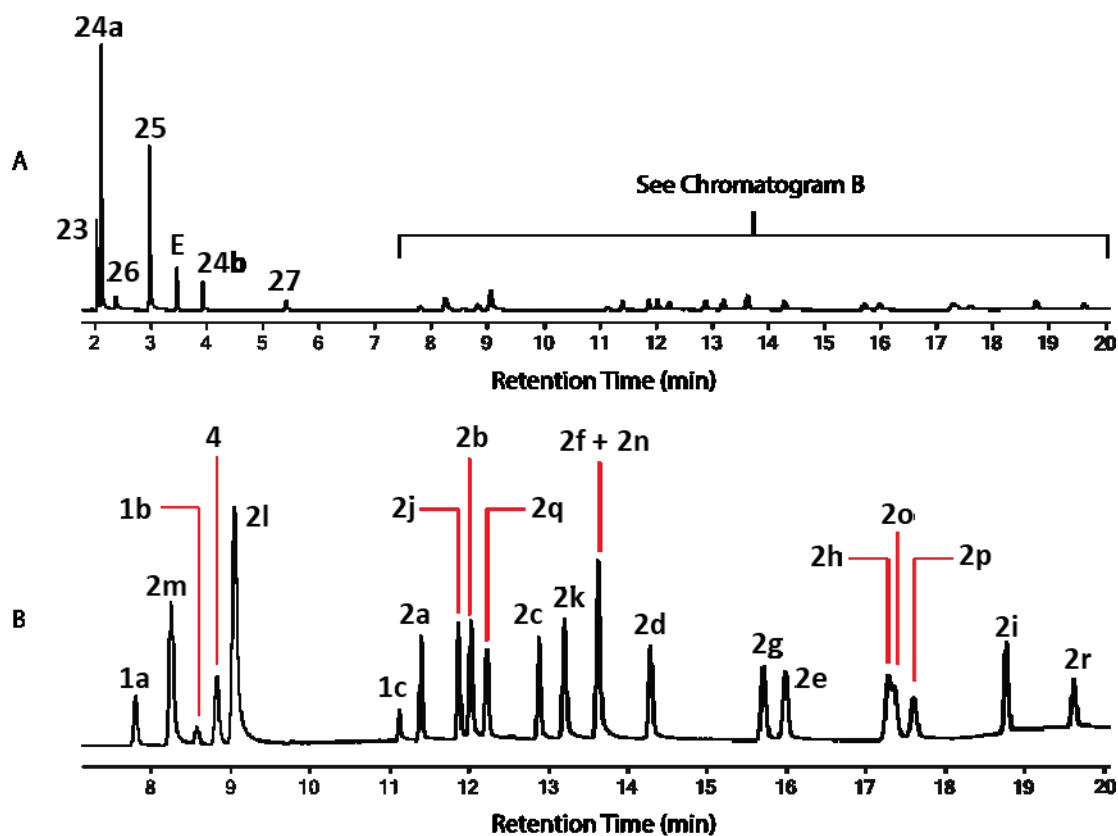


Figure 2.10. Exemplar chromatogram demonstrating the optimal GC-MS method of 18 fentalogues (**2a-r**), MDMA (**23**), benzocaine (**24a**), acetaminophen (**26**), caffeine (**25**), eicosane (internal standard, E), procaine (**24b**), cocaine (**27**), codeine (**1a**), morphine (**1b**), 4-ANPP (**4**) and heroin (**1c**).

The use of SIM-mode analysis solves the issue of co-eluting compounds and increases the sensitivity of the method. Instead of scanning for all possible ions, three ions per compound are monitored: one for quantification, usually the most abundant and specific, and two for confirmatory analysis (see Table 2.7). Because only a partial mass spectrum is obtained, SIM analysis is less specific than scan analysis. The two confirmatory ions can be used to remedy this: when analysing an unknown sample, ratios between the three monitored ions

are calculated and compared to those of a reference SIM spectrum. For conclusive identification, the difference between the unknown sample and the reference spectrum should fall within a pre-defined tolerance window, as prescribed by the World Anti-Doping Agency (WADA) in their published guidelines. [142] Ion ratios for each analyte are reported in Table 2.7 for reference purposes.

SIM analysis was thus used to separate co-eluting fentalogues **2f/2n** and **2h/2o**. Because these derivatives all bear different amide chains, their base peaks, analogous to fragment **28** in Figure 2.6, all have different masses. By monitoring only the base peak for quantification, methoxyacetylfentanyl **2n** ($m/z = 261.1$, Figure 2.11b) was separated from cyclopropylfentanyl **2f** ($m/z = 257.1$, Figure 2.11c) and cyclopentylfentanyl **2h** ($m/z = 285.1$, Figure 2.11d) from 2-furanylfentanyl **2o** ($m/z = 283.1$, Figure 2.11e).

Table 2.7. EI-MS ions used for identification of analytes via Selective Ion Monitoring (SIM), relative intensity of each ion (relative to base peak) and precision (%RSD) of the relative intensities (cont.)

1b	SIM ions	285.1	215.1	162.1
	Relative intensities (%)	100.0	33.0	45.4
	Precision (% RSD, n = 3)	-	4.8	6.0
4	SIM ions	189.0	146.1	93.0
	Relative intensities (%)	83.0	100.0	11.7
	Precision (% RSD, n = 3)	0.3	-	11.3
2i	SIM ions	285.1	242.0	189.1
	Relative intensities (%)	100.0	33.6	8.7
	Precision (% RSD, n = 3)	-	0.9	6.4
1c	SIM ions	369.0	327.2	268.1
	Relative intensities (%)	62.7	100.0	67.5
	Precision (% RSD, n = 3)	2.3	-	4.0
2a	SIM ions	231.1	189.1	146.0
	Relative intensities (%)	100.0	38.1	52.2
	Precision (% RSD, n = 3)	-	1.7	1.2
2j	SIM ions	259.1	189.1	146.0
	Relative intensities (%)	100.0	59.6	54.0
	Precision (% RSD, n = 3)	-	1.5	1.9
2e	SIM ions	287.2	189.1	146.0
	Relative intensities (%)	100.0	53.7	57.3
	Precision (% RSD, n = 3)	-	0.5	0.1
2h	SIM ions	285.1	189.1	146.0
	Relative intensities (%)	100.0	65.8	50.4
	Precision (% RSD, n = 3)	-	4.7	3.2
2o	SIM ions	283.1	240.0	95.0
	Relative intensities (%)	57.7	29.1	100.0
	Precision (% RSD, n = 3)	1.6	2.8	-
2p	SIM ions	283.1	240.0	95.0
	Relative intensities (%)	100.0	59.7	73.4
	Precision (% RSD, n = 3)	-	1.5	1.1
2i	SIM ions	299.1	189.1	146.0
	Relative intensities (%)	100.0	63.2	48.0
	Precision (% RSD, n = 3)	-	0.4	0.7
2r	SIM ions	293.1	250.0	105.0
	Relative intensities (%)	86.7	30.6	100.0
	Precision (% RSD, n = 3)	6.7	3.2	-

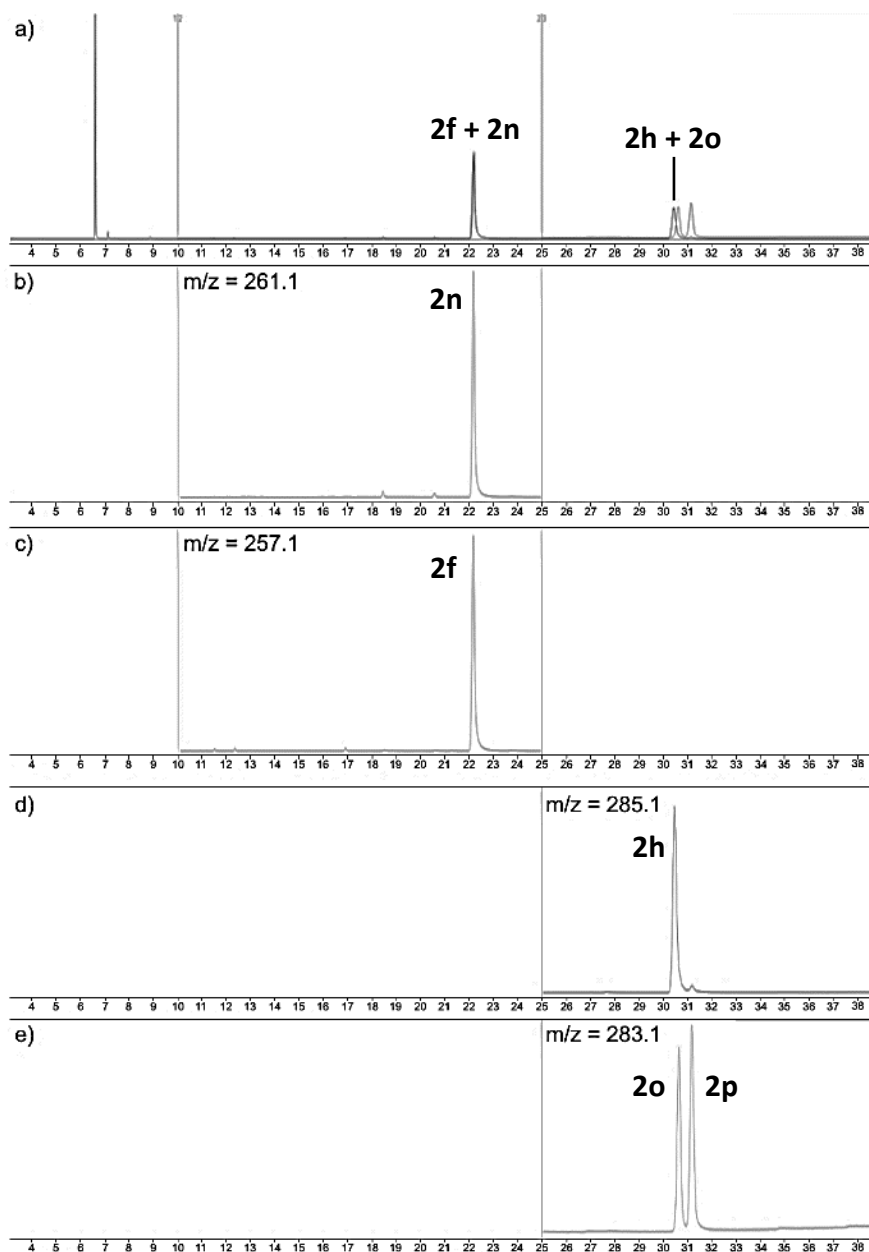


Figure 2.11. SIM mode chromatogram of a mixture of **2f**, **2h**, **2n**, **2o-p**. a) Total ion chromatogram; b) Monitoring of $m/z = 261.1$ (**2n**); c) Monitoring of $m/z = 257.1$ (**2f**); d) Monitoring of $m/z = 285.1$ (**2h**); e) Monitoring of $m/z = 283.1$ (**2o-p**).

2.8 Quantitative GC-MS analysis

The quantitative GC-MS method (SIM mode), was developed and validated in accordance with the ICH guidelines (see Section 7.4 for experimental procedure). [143] A summary of GC-MS validation data is reported in Table 2.8. As previously discussed, resolution was satisfactory except for compounds **2f/2n** and **2h/2o**. Most peaks proved relatively symmetrical (A_s value close to 1) except MDMA (**23**, $A_s = 2.4$), caffeine (**25**, $A_s = 2.4$) and paracetamol (**26**, $A_s = 5.6$) because of their amine or alcohol moieties. Paracetamol especially tailed a lot, due to its polar alcohol moiety, and though this could be resolved by prior derivatization it did not prevent validation in this case. Limits of detection and quantification were determined based on signal-to-noise (S/N) ratio. For fentalogues, these were 0.008 – 0.125 µg/mL (LOD) and 0.025 – 0.415 µg/mL (LOQ). For other controlled substances and adulterants they were 0.007 – 0.822 µg/mL (LOD) and 0.023 – 2.742 µg/mL (LOQ).

Due to the level of sensitivity required for the detection of fentanyl analogues as low-concentration adulterants in seized samples, the LOD/LOQs determined in SIM mode were compared to those in scan mode (Table 2.9). For fentalogues, SIM analysis proved 72 to 1280 times more sensitive than scan mode, confirming that it is more suitable for this application.

Calibration standards were prepared over a 2.5–25.0 µg/mL concentration range, using eicosane as an internal standard, to produce a calibration curve for each analyte (see calibration curve equations below Table 2.8). All eighteen substituted fentalogues demonstrated a linear response ($r^2 = 0.997$ – 0.999) with satisfactory repeatability (RSD = 0.3 – 4.5%, $n = 6$). The method was also suitable for quantification of the other controlled substances and adulterants,

demonstrating linear response ($r^2 = 0.992 - 0.999$) with reasonable repeatability (RSD = 0.7 – 6.9%, n = 6).

The accuracy of the method was determined using a percentage recovery study (see Table 2.10). Spiked samples were prepared in triplicates at three concentration levels over a range of 80–120% of a target concentration (15 µg/mL). The result of these injections is fed back into the calibration curve and the experimental concentration is compared with the theoretical concentration (assay recovery). The relative error shows how the mean assay recovery diverges from an expected 100%. Acceptable recoveries ($100 \pm 3\%$) were obtained for all analytes.

The precision (inter- and intraday precision) was calculated from six replicate injections of a spiked sample (10 µg/mL), analysed on two consecutive days (see Table 2.11). Most analytes showed acceptable precision, with intraday RSDs between 0.8 and 4.0% and interday RSDs between 0.7 and 2.4%, apart from two exceptions: paracetamol (**26**, intraday: 7.9%, interday: 6.2%) and morphine **1b** (intraday: 6.9%, interday: 8.0%). Both of these analytes have poor response factors and/or peak shape, and thus high standard deviations are observed around the target concentration.

The GC-MS method was deemed suitable for the analysis of seized heroin samples.

Table 2.8. Summary of GC-MS validation data (SIM mode) for the quantification of fentalogues (**2a-r**), controlled substances (**4**, **23**, **27**, **1a-c**) and relevant/common adulterants (**24a-b**, **25** and **26**). NB. tR (eicosane, IS) = 3.47 min (see Figure 2.10 for chromatogram).

	t _R (min)	RRT ^a	R _s ^b	A _s ^c	N ^d (plates)	H ^e (x10 ⁻⁴ mm)	LOD ^{ah} (µg/mL)	LOQ ^{ai} (µg/mL)	r ²	Precision (% RSD, n = 6)					
										2.5 µg/mL	5 µg/mL	10 µg/mL	15 µg/mL	20 µg/mL	25 µg/mL
23	2.04	0.17	-	2.4	136219	2.20	0.023	0.007	0.996 ^f	3.6	2.1	1.3	2.5	1.4	3.2
24a	2.11	0.18	3.9	1.6	228879	1.31	0.023	0.007	0.992 ^g	6.7	2.9	1.9	2.1	0.9	3.0
26	2.36	0.20	9.3	5.6	93224	3.22	0.793	0.238	0.992 ^h	5.8	6.4	4.0	3.5	1.7	3.4
25	3.0	0.25	18.2	2.4	200019	1.50	0.045	0.014	0.994 ⁱ	6.8	4.3	1.6	1.8	1.4	2.3
24b	3.91	0.33	14	1.2	196150	1.53	0.046	0.014	0.999 ^j	1.5	1.6	1.7	0.9	1.8	1.6
27	5.37	0.45	30.3	1.4	140356	2.14	0.030	0.009	0.999 ^k	2.2	1.2	2.0	0.8	1.7	1.0
1a	7.75	0.65	33.7	1.0	136584	2.20	0.073	0.022	0.998 ^l	1.7	1.6	2.0	0.8	1.9	1.8
2m	8.20	0.68	4.8	1.0	113948	2.63	0.025	0.007	0.999 ^m	1.6	1.1	2.2	1.0	1.8	1.7
1b	8.52	0.71	3.3	1.0	135096	2.22	2.742	0.822	0.999 ⁿ	- ^{aj}	6.9	3.8	3.3	2.7	2.0
4	8.77	0.73	2.7	1.3	119168	2.52	0.090	0.027	0.999 ^o	1.2	1.3	2.4	1.1	1.9	1.9
2l	8.99	0.75	2.0	1.6	105886	2.83	0.049	0.015	0.999 ^p	1.1	0.9	2.0	1.1	1.8	1.5
1c	11.09	0.92	24.5	1.0	515458	0.58	0.236	0.071	0.998 ^q	2.3	1.6	2.9	0.7	1.9	2.5
2a	11.36	0.95	4.5	1.0	540884	0.56	0.026	0.008	0.997 ^r	0.5	1.2	2.1	1.4	2.0	2.6
2j	11.84	0.99	7.3	1.4	510511	0.59	0.058	0.017	0.997 ^s	0.7	0.9	2.1	1.2	2.3	2.3

Table 2.8. Summary of GC-MS validation data (SIM mode) for the quantification of fentalogues (**2a-r**), controlled substances (**4**, **23**, **27**, **1a-c**) and relevant/common adulterants (**24a-b**, **25** and **26**). NB. t_R (eicosane, IS) = 3.47 min (see Figure 2.10 for chromatogram). (cont.)

	t _R (min)	RRT ^a	R _s ^b	A _s ^c	N ^d (plates)	H ^e (x10 ⁻⁴ mm)	LOD ^{ah} (µg/mL)	LOQ ^{ai} (µg/mL)	r ²	Precision (% RSD, n = 6)					
										2.5 µg/mL	5 µg/mL	10 µg/mL	15 µg/mL	20 µg/mL	25 µg/mL
2b	11.99	1.00	2.3	1.2	460776	0.65	0.034	0.010	0.998 ^t	0.5	1.0	2.2	1.4	2.2	2.3
2q	12.19	1.02	2.8	1.4	541711	0.55	0.044	0.013	0.997 ^u	1.1	1.1	2.4	1.5	2.1	2.5
2c	12.85	1.07	8.9	0.9	418336	0.72	0.047	0.014	0.997 ^v	0.7	1.1	2.4	1.5	2.3	2.4
2k	13.16	1.10	3.8	1.2	393893	0.76	0.044	0.013	0.997 ^w	1.1	0.7	2.2	1.5	2.3	2.3
2f	13.60	1.13	4.8	1.5	343508	0.87	0.082	0.025	0.998 ^x	0.8	1.4	2.4	1.3	2.1	2.2
2n	13.60	1.13	4.8	1.2	343508	0.87	0.043	0.013	0.998 ^y	1.2	1.3	2.1	1.4	2.2	2.5
2d	14.25	1.19	7.1	1.2	377429	0.80	0.052	0.016	0.997 ^z	0.8	1.1	2.3	1.3	2.1	2.5
2g	15.68	1.31	14	1.0	322327	0.93	0.077	0.023	0.997 ^{aa}	1.1	1.1	2.5	1.2	2.3	2.5
2e	15.95	1.33	2.5	1.1	333544	0.90	0.038	0.011	0.997 ^{ab}	0.4	1.0	2.2	1.3	2.2	2.3
2h	17.25	1.44	9.9	1.0	271035	1.11	0.138	0.042	0.997 ^{ac}	1.0	0.3	2.4	1.2	2.2	2.5
2o	17.31	1.44	0.5	1.1	273246	1.10	0.413	0.124	0.997 ^{ad}	3.2	1.1	4.5	1.4	2.7	2.8
2p	17.57	1.47	2.4	1.0	281061	1.07	0.415	0.125	0.998 ^{ae}	4.5	1.8	2.2	1.3	2.3	4.0
2i	18.77	1.61	12.4	1.3	249699	1.20	0.051	0.015	0.997 ^{af}	1.1	0.8	2.4	1.3	2.2	2.5
2r	19.62	1.74	9.7	1.1	247424	1.21	0.092	0.028	0.997 ^{ag}	0.9	1.2	2.5	1.1	2.3	2.6

Key: ^a Relative Retention Time (with respect to fentanyl, **2b**); ^b Resolution; ^c Asymmetry (or tailing) factor; ^d Number of theoretical plates; ^e Height of a theoretical plate; ^f $y=0.3731x-0.1005$; ^g $y=0.5935x-0.6021$; ^h $y=0.1037x-0.1519$; ⁱ $y=0.3539x-0.2284$; ^j $y=0.1587x+0.1199$; ^k $y=0.0742x+0.0602$; ^l $y=0.0488x+0.0531$; ^m $y=0.1322x+0.1305$; ⁿ $y=0.0129x-0.0235$; ^o $y=0.0904x+0.0401$; ^p $y=0.1642x+0.1149$; ^q $y=0.0208x+0.0295$; ^r $y=0.0926x+0.1140$; ^s $y=0.0846x+0.1060$; ^t $y=0.0930x+0.1058$; ^u $y=0.0924x+0.1122$; ^v $y=0.0926x+0.1140$; ^w $y=0.0936x+0.1139$; ^x $y=0.0963x+0.1098$; ^y $y=0.1004x+0.0963$; ^z $y=0.0911x+0.1138$; ^{aa} $y=0.0924x+0.1198$; ^{ab} $y=0.0943x+0.1206$; ^{ac} $y=0.0866x+0.1103$; ^{ad} $y=0.0904x+0.1040$; ^{ae} $y=0.0863x+0.1045$; ^{af} $y=0.0951x+0.1214$; ^{ag} $y=0.0852x+0.0906$; ^{ah} Limit of detection (calculated using a signal-to-noise ratio of 3:1); ^{ai} Limit of quantification (calculated using a signal-to-noise ratio of 10:1); ^{aj} Not determined as concentration is below the LOQ for morphine (**1b**).

Table 2.9. Comparison of GC-MS limits of detection/quantification determined in scan mode and selective ion monitoring (SIM) mode for fentalogues (**2a-r**), controlled substances (**4, 23, 27, 1a-c**) and relevant/common adulterants (**24a-b, 25** and **26**).

Ana lyte	t _R (min)	Scan Mode		Selective Ion Monitoring (SIM) Mode	
		LOD ^a (µg/mL)	LOQ ^b (µg/mL)	LOD ^a (µg/mL)	LOQ ^b (µg/mL)
23	2.04	2.2	0.6	0.023	0.007
24a	2.11	0.8	0.3	0.023	0.007
26	2.36	9.7	2.9	0.793	0.238
25	3.0	1.5	0.5	0.045	0.014
24b	3.91	7.4	2.2	0.046	0.014
27	5.37	6.7	2.0	0.030	0.009
1a	7.75	21.6	6.5	0.073	0.022
2m	8.20	13.9	4.2	0.025	0.007
1b	8.52	210.5	63.2	2.742	0.822
4	8.77	11.2	3.4	0.090	0.027
2l	8.99	9.8	2.9	0.049	0.015
1c	11.09	31.0	9.3	0.236	0.071
2a	11.36	33.3	10.0	0.026	0.008
2j	11.84	29.9	9.0	0.058	0.017
2b	11.99	28.5	8.6	0.034	0.010
2q	12.19	34.6	10.4	0.044	0.013
2c	12.85	35.3	10.6	0.047	0.014
2k	13.16	30.7	9.2	0.044	0.013
2f	13.60	25.1	7.5	0.082	0.025
2n	13.60	24.7	7.4	0.043	0.013
2d	14.25	29.3	8.8	0.052	0.016
2g	15.68	37.0	11.1	0.077	0.023
2e	15.95	37.4	11.2	0.038	0.011
2h	17.25	38.4	11.5	0.138	0.042
2o	17.31	29.8	8.9	0.413	0.124
2p	17.57	41.1	12.3	0.415	0.125
2i	18.77	40.2	12.1	0.051	0.015
2r	19.62	42.5	12.7	0.092	0.028

Key: ^aLimit of detection (calculated using a signal-to-noise ratio of 3:1); ^bLimit of quantification (calculated using a signal-to-noise ratio of 10:1).

Table 2.10. GC-MS recovery results for fentalogues (**2a-r**), controlled substances (**4, 23, 27, 1a-c**) and relevant/common adulterants (**24a-b, 25** and **26**).

Analyte	Assay recovery ^a			Mean recovery (%)	%RSD (n = 3)	Relative Error ^b (%)
	12 µg/mL (% , n = 3)	15 µg/mL (% , n = 3)	18 µg/mL (% , n = 3)			
23	98.8	100.2	99.4	99.5	0.7	-0.5
24a	97.3	99.1	99.8	98.7	1.3	-1.3
26	101.1	103.0	101.3	101.8	1.0	1.8
25	100.4	100.9	101.5	101.0	0.6	1.0
24b	99.1	100.5	98.4	99.3	1.1	-0.7
27	99.1	100.3	98.5	99.3	0.9	-0.7
1a	98.5	99.7	97.6	98.6	1.1	-1.4
2m	99.5	100.5	98.2	99.4	1.1	-0.6
1b	101.4	99.2	100.0	100.2	1.1	0.2
4	97.8	98.9	97.0	97.9	1.0	-2.1
2l	98.1	99.3	97.3	98.3	1.0	-1.7
1c	97.4	101.1	96.9	98.5	2.3	-1.5
2a	98.9	100.1	97.5	98.8	1.3	-1.2
2j	98.2	100.0	97.3	98.5	1.4	-1.5
2b	99.0	100.4	97.3	98.9	1.6	-1.1
2q	98.6	99.3	97.2	98.4	1.1	-1.6
2c	98.9	100.0	97.2	98.7	1.5	-1.3
2k	98.4	100.0	97.2	98.5	1.4	-1.5
2f	98.0	99.8	97.4	98.4	1.3	-1.6
2n	99.0	99.5	97.1	98.5	1.3	-1.5
2d	98.7	99.8	97.3	98.6	1.3	-1.4
2g	98.8	100.2	97.3	98.7	1.5	-1.3
2e	98.7	100.1	97.2	98.7	1.4	-1.3
2h	98.5	100.3	97.0	98.6	1.7	-1.4
2o	97.0	98.6	97.2	97.6	0.9	-2.4
2p	97.2	98.3	96.6	97.4	0.9	-2.6
2i	98.2	99.6	97.3	98.4	1.2	-1.6
2r	98.9	99.8	97.5	98.7	1.2	-1.3

Key: ^a Determined as a percentage ratio between the experimental concentration (calculated from the calibration curve) and the known concentration (12, 15 or 18 µg/mL); ^b Deviation between the average experimental recovery and a 100% recovery.

Table 2.11. Summary of GC-MS repeatability (intraday precision) and intermediate precision (interday precision) for fentalogues (**2a-r**), controlled substances (**4, 23, 27, 1a-c**) and relevant/common adulterants (**24a-b, 25** and **26**).

Analyte	Intraday precision ^a (%RSD, n = 12)	Interday precision ^b (%RSD, n = 12)
23	1.0	1.7
24a	2.6	2.1
26	7.9	6.2
25	4.0	2.2
24b	1.7	1.6
27	2.0	0.7
1a	0.8	0.9
2m	6.9	8.0
1b	1.0	0.7
4	0.8	1.1
2l	1.3	1.1
1c	0.9	0.9
2a	1.6	1.0
2j	1.5	0.9
2b	1.4	0.9
2q	1.6	1.1
2c	1.3	1.0
2k	3.7	2.4
2f	1.3	0.9
2n	1.1	1.4
2d	1.1	0.9
2g	1.3	1.2
2e	1.5	1.2
2h	1.1	0.8
2o	2.1	1.7
2p	1.8	1.8
2i	1.3	1.3
2r	1.2	1.1

Key: ^aRelative standard deviation of twelve injections (10 µg/mL) performed over a short time interval; ^bRelative standard deviation of twelve injections (10 µg/mL) performed over two consecutive days.

2.9 Analysis of seized heroin samples

Seven seized heroin samples, arbitrarily labeled SS-1 – SS-7, were obtained from Greater Manchester Police. Samples weighed between 0.07 – 1.04 g and were suspected to contain heroin (**1c**).

Samples were submitted to the analytical techniques previously reported in this chapter. Presumptive colour tests were first carried out. All seven samples gave positive reactions with Marquis' reagent, producing a brownish-purple colour. On the one hand, the purple tint potentially indicates the presence of heroin or another opioid. The brown colour, however, appeared to be caused by the inherent colour of the sample matrix, which dissolved in sulfuric acid. This highlights a weakness of Marquis' test, in that it may produce uncertain results with complex matrices and cannot lead to the confident identification of fentanyl in real-life samples. Additionally, previous studies have shown that Marquis' test can only detect fentanyl mixed with heroin when it is the major component of the mixture. [26] The Eosin Y test, however, is pH-neutral and does not dissolve the sample matrix. Only one of the samples (SS-1) gave a positive reaction with Eosin Y (deep pink) potentially indicating the presence of fentanyl (**2b**) or a structural analogue. The seven samples gave inconclusive results with both Scott's reagent and concentrated nitric acid.

Thin layer chromatographic (TLC) analysis was performed. All samples showed significant levels of adulteration, as multiple unidentified spots were revealed under UV light and when developed with the Dragendorff-Ludy-Tenger reagent. Comparison with a reference heroin sample indicated the presence of heroin (**1c**, $RR_f = 0.43$) in all seven samples. Only one sample (SS-1) produced a TLC spot that matched the fentanyl reference sample (**2b**, $RR_f = 1.00$).

FT-IR analysis indicated the clear presence of heroin in samples SS-5 to SS-7, as spectra were very similar to that of the reference material. Samples SS-1 to SS-4 appear heavily adulterated. Figure 2.12 and Figure 2.13 show reference spectra for fentanyl and heroin, respectively, while Figure 2.14 and Figure 2.15 show representative spectra for adulterated heroin samples (SS-1 and SS-2). Though the presence of heroin is possible, based on the ester C=O bands at ~ 1756 and ~ 1727 cm^{-1} , formal identification of the drug is not possible due to the level of mixture. A band at ~ 1644 cm^{-1} , observed only in SS-1, may be indicative of fentanyl, but the level of mixture again makes identification impossible.

Table 2.12 shows the highest matches resulting from a library search for each seized sample. Sample SS-1 only shows heroin with a relatively low match score (69%). Samples SS-2 to 4 show multiple components, also with low match scores which may be due to adulteration. Heroin was not detected in SS-3 and SS-4 by FTIR. SS-5 to 7, on the other hand, all came back as heroin with a good score (89-90%), which may indicate the absence of infrared-active adulterants. Fentanyl or its analogues were not detected. Subtracting the highest match spectrum and searching the database again led to no significant match.

Table 2.12 Infrared match scores for seized heroin samples SS-1 to 7.

Seized sample	Highest matches (match scores)
SS-1	Heroin (69%)
SS-2	Acetaminophen (68%) Heroin (44%) Caffeine (43%)
SS-3	Acetaminophen (59%) Caffeine (56%)
SS-4	Caffeine (71%) Acetaminophen (61%)
SS-5	Heroin (89%)
SS-6	Heroin (89%)
SS-7	Heroin (90%)

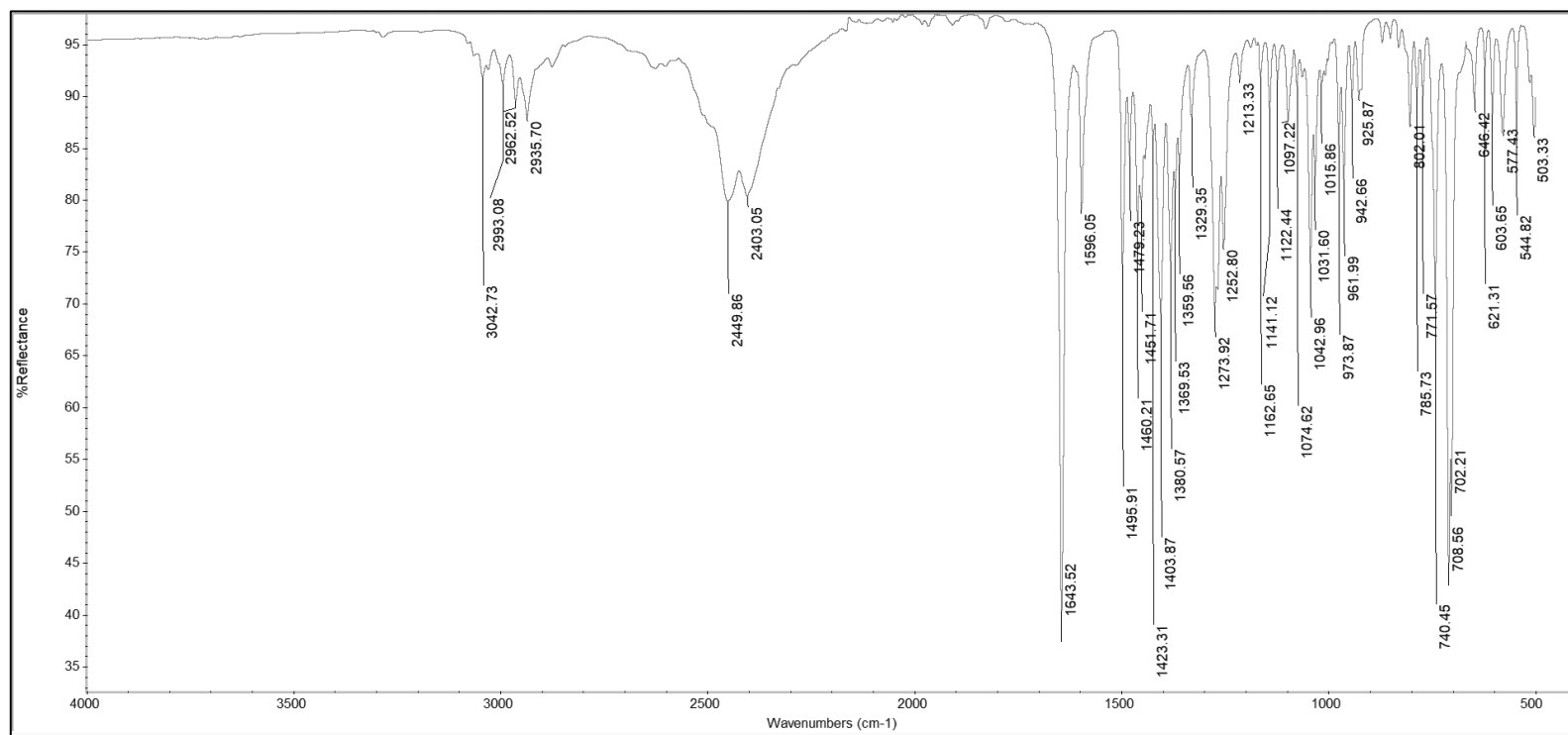


Figure 2.12. ATR-FTIR spectrum of fentanyl (**2b**).

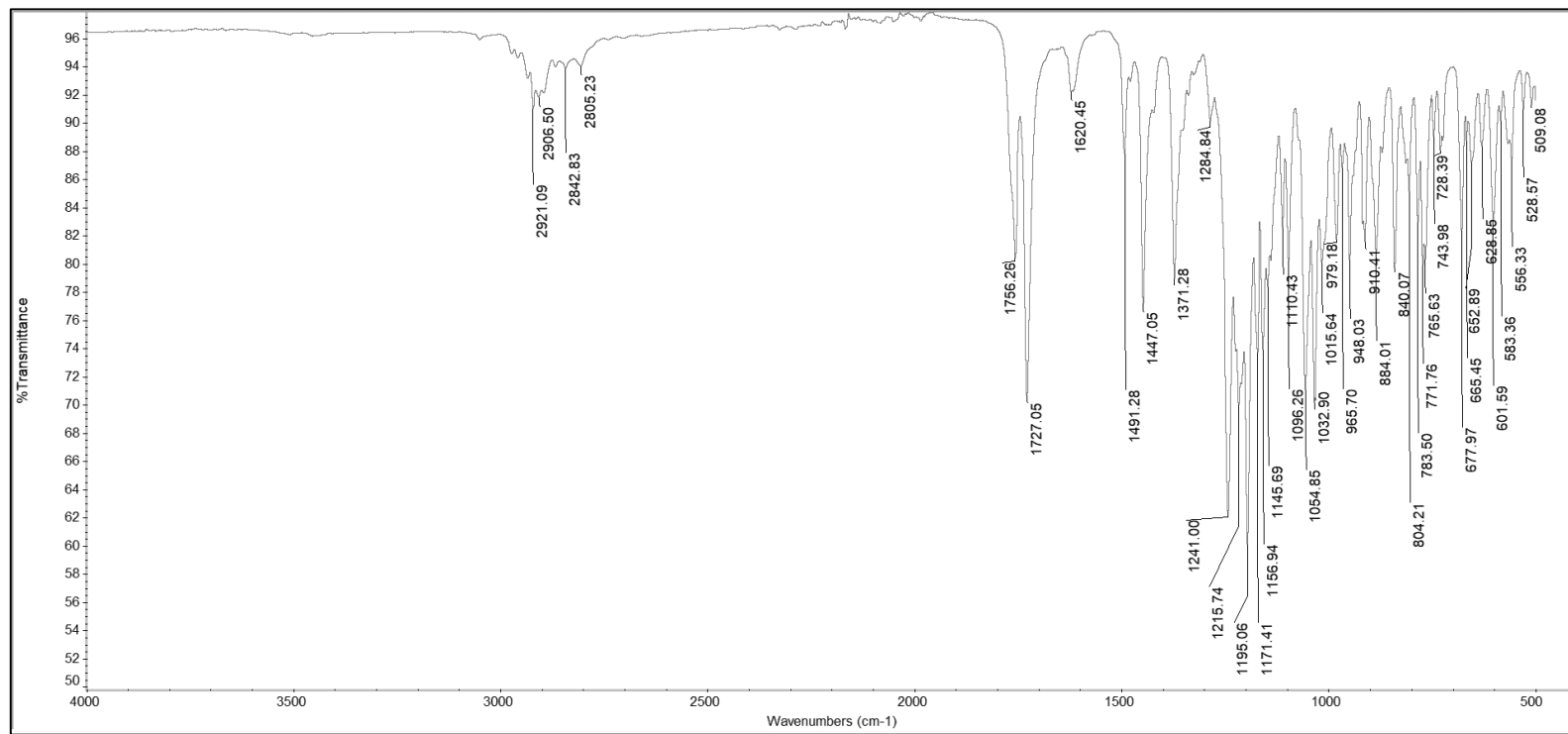


Figure 2.13. ATR-FTIR spectrum of heroin (**1c**).

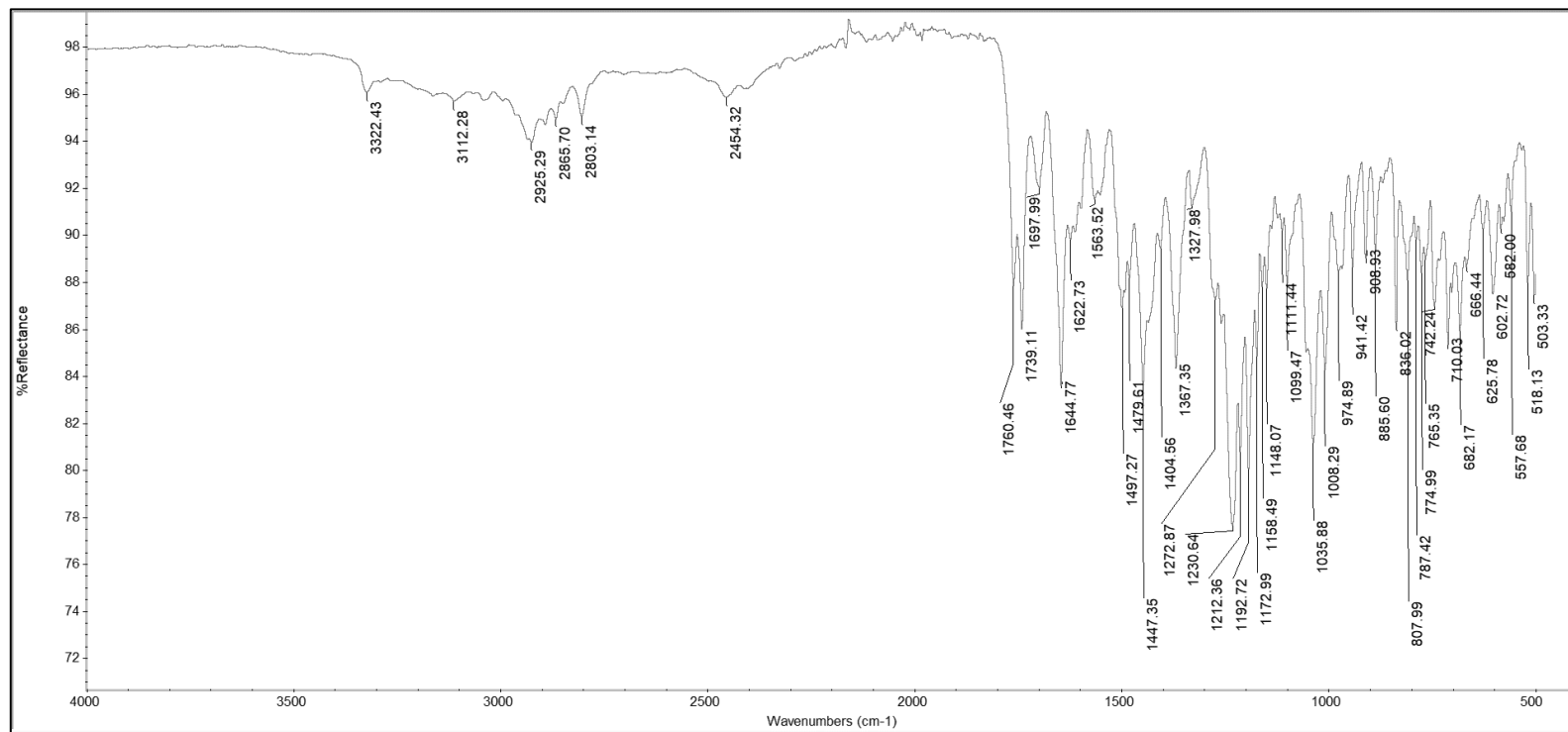


Figure 2.14. ATR-FTIR spectrum of seized heroin sample SS-1.

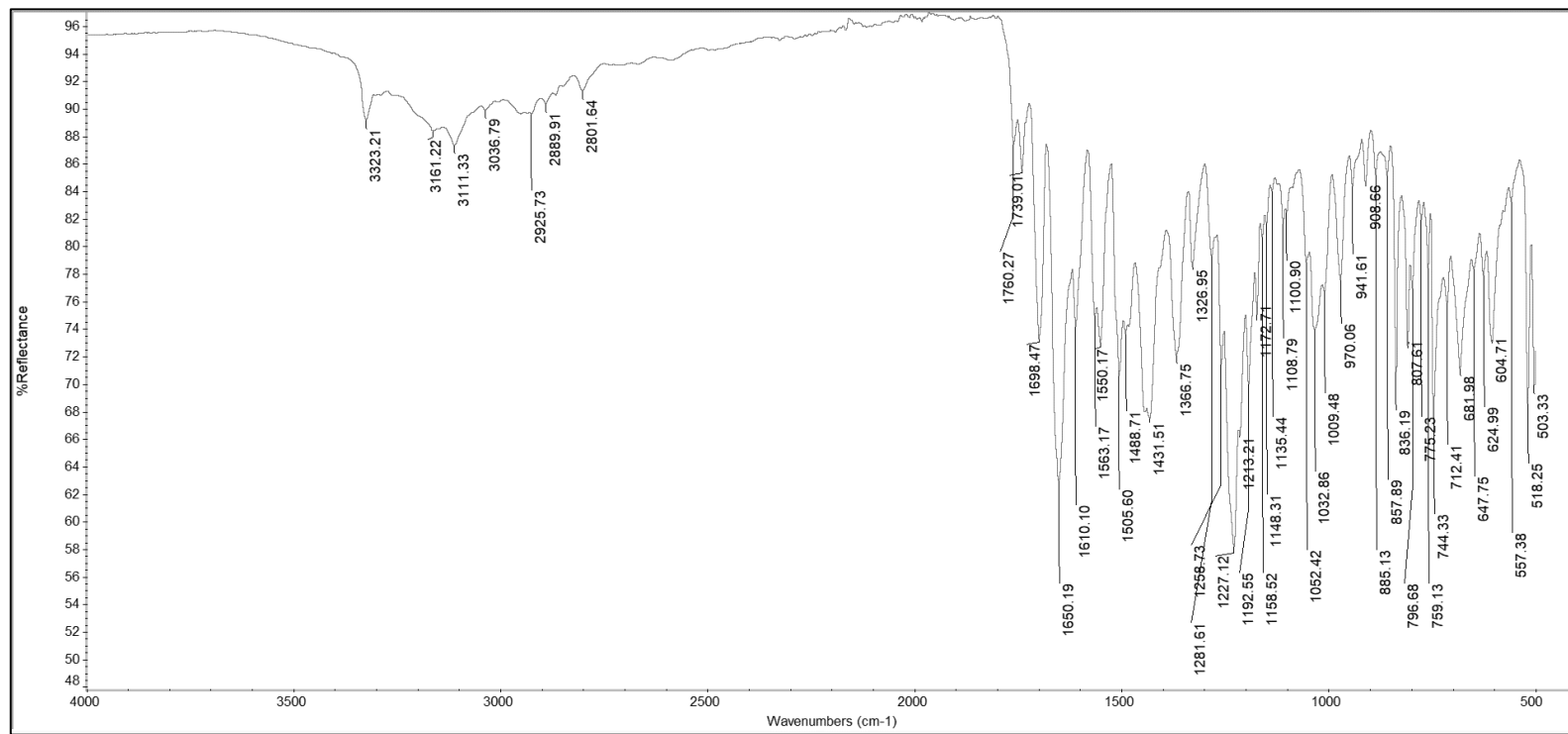


Figure 2.15. ATR-FTIR spectrum of seized heroin sample SS-2.

Preliminary GC-MS analysis of the samples was performed in scan mode. Representative chromatograms are shown in Figure 2.16. Qualitative analysis confirmed the presence of heroin (**1c**, $t_R = 11.1$ min) in all seven samples. Samples SS-1 – SS-4 also contained caffeine (**25**, $t_R = 3.0$ min) and paracetamol (**26**, $t_R = 2.4$ min) as the primary adulterants. Samples SS-2 – SS-4 contained a minor peak attributed to diacetamide (**40**, $t_R = 2.6$ min), confirmed by comparison to the NIST mass spectrum library. Compound **40** has been observed to form *via* transacetylation between paracetamol (**26**) and *o*-acetylsalicylic acid (aspirin) after storage for prolonged periods. [144] It may have arisen in these samples from a similar interaction between paracetamol (**26**) and heroin (**1c**). Samples SS-2 – SS-7 contained 6-mono-acetylmorphine (6-MAM, **41**, $t_R = 9.9$ min), as confirmed by comparison with a commercial 6-MAM reference solution. The presence of the hydrolysis product 6-MAM is postulated to arise if heroin samples are stored in damp conditions over a period of time. [145] The chemical structures of minor components **40** and **41** are shown in Figure 2.17. As shown in Figure 2.16, sample SS-1 was the only one to indicate the presence of fentanyl (**2b**, $t_R = 12.0$ min) in scan mode analysis, which agreed with the preliminary tests carried out on this sample.

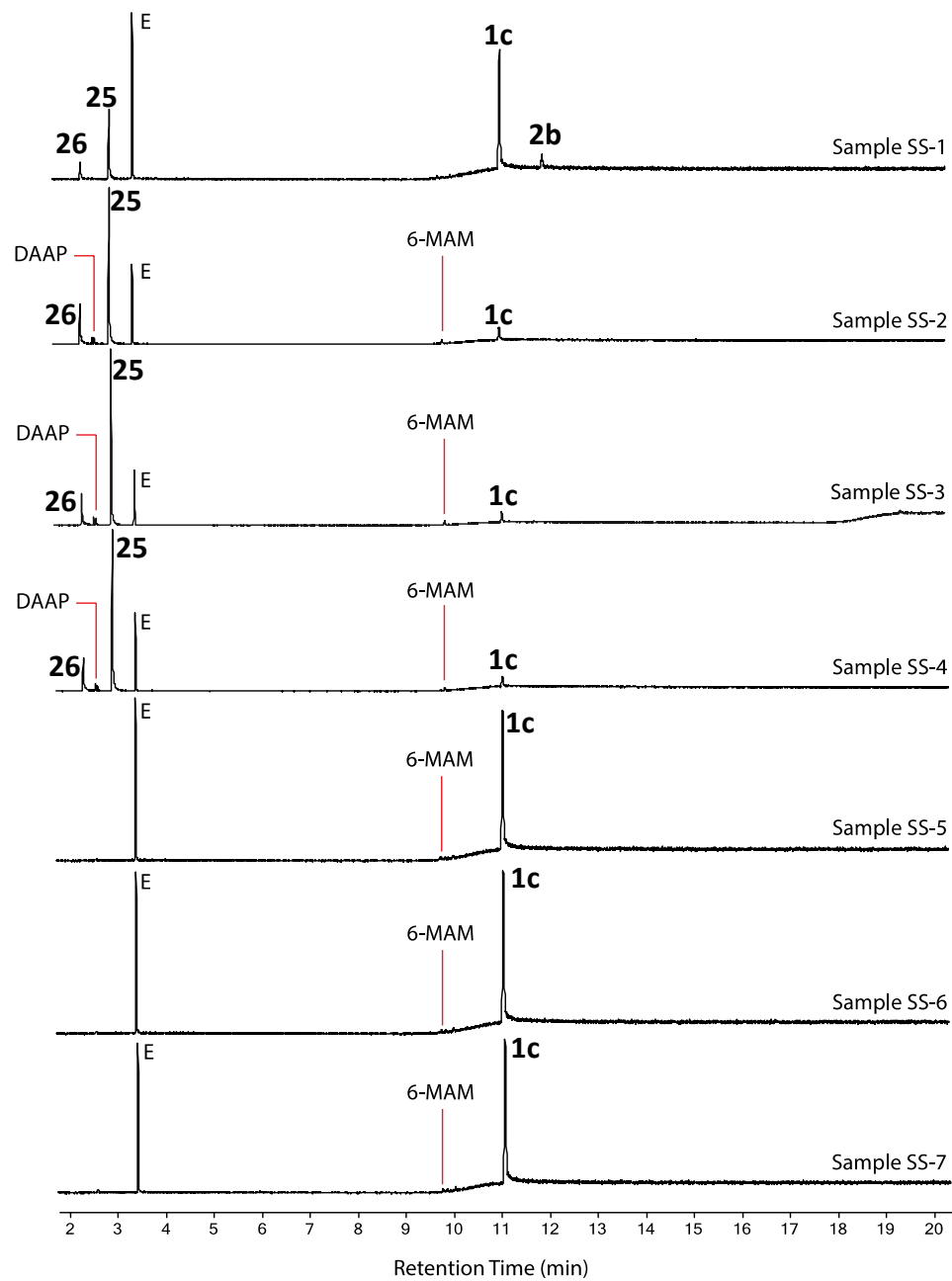


Figure 2.16. Qualitative scan mode GC–MS analysis of heroin samples SS-1 to SS-7 (0.1 mg/mL in methanol). Key: DAAP = N,O-diacetylaminophenol; 6-MAM = 6-monacetylmorphine; E = eicosane (internal standard).

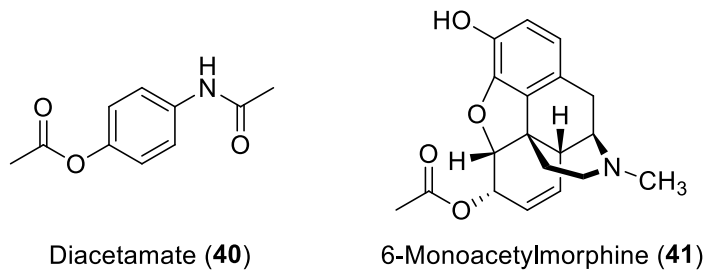


Figure 2.17. Chemical structure of compounds **40** and **41**, detected in seized heroin samples.

All samples were then submitted to the more sensitive SIM method, in case any low-concentration fentalogues had been missed in scan mode. Figure 2.18 shows a comparison of sample SS-1 analysed in scan (1.12a) and SIM (1.12b) mode. SIM analysis leads to a much lower baseline and improved sensitivity. Although it had been missed in scan mode (see Figure 2.18c), fentanyl was found in sample SS-2 when SIM analysis was performed, due to the enhanced sensitivity of this method (see Figure 2.18d). Figure 2.18e shows an example of the fentanyl SIM mass spectrum obtained from SS-1. Fentanyl, or one of its analogues, were not found in any other sample. As described previously (see section 2.7), ion ratios of the supposed fentanyl signals in SS-1 and SS-2 were compared to those obtained from fentanyl reference spectra (see Table 2.13). Relative ion intensities were within the tolerance windows prescribed by WADA guidelines when compared to the pure reference material, confirming the identification of fentanyl in SS-1 and SS-2. [142]

Table 2.13. Comparison of EI-MS ion ratios of the fentanyl reference and the supposed fentanyl signal in seized heroin samples SS-1 and SS-2.

2b	SIM ions	245.1	189.1	146.0
	Relative intensities (%)	100.0	44.0	58.5
	Precision (% RSD, n = 3)	-	0.9	1.0
SS-1 (2b)	SIM ions	259.1	189.1	146.0
	Relative intensities (%)	100.0	45.0	60.4
	Precision (% RSD, n = 3)	-	0.4	1.0
SS-2 (2b)	SIM ions	259.1	189.1	146.0
	Relative intensities (%)	100.0	52.8	65.5
	Precision (% RSD, n = 3)	-	2.0	0.7

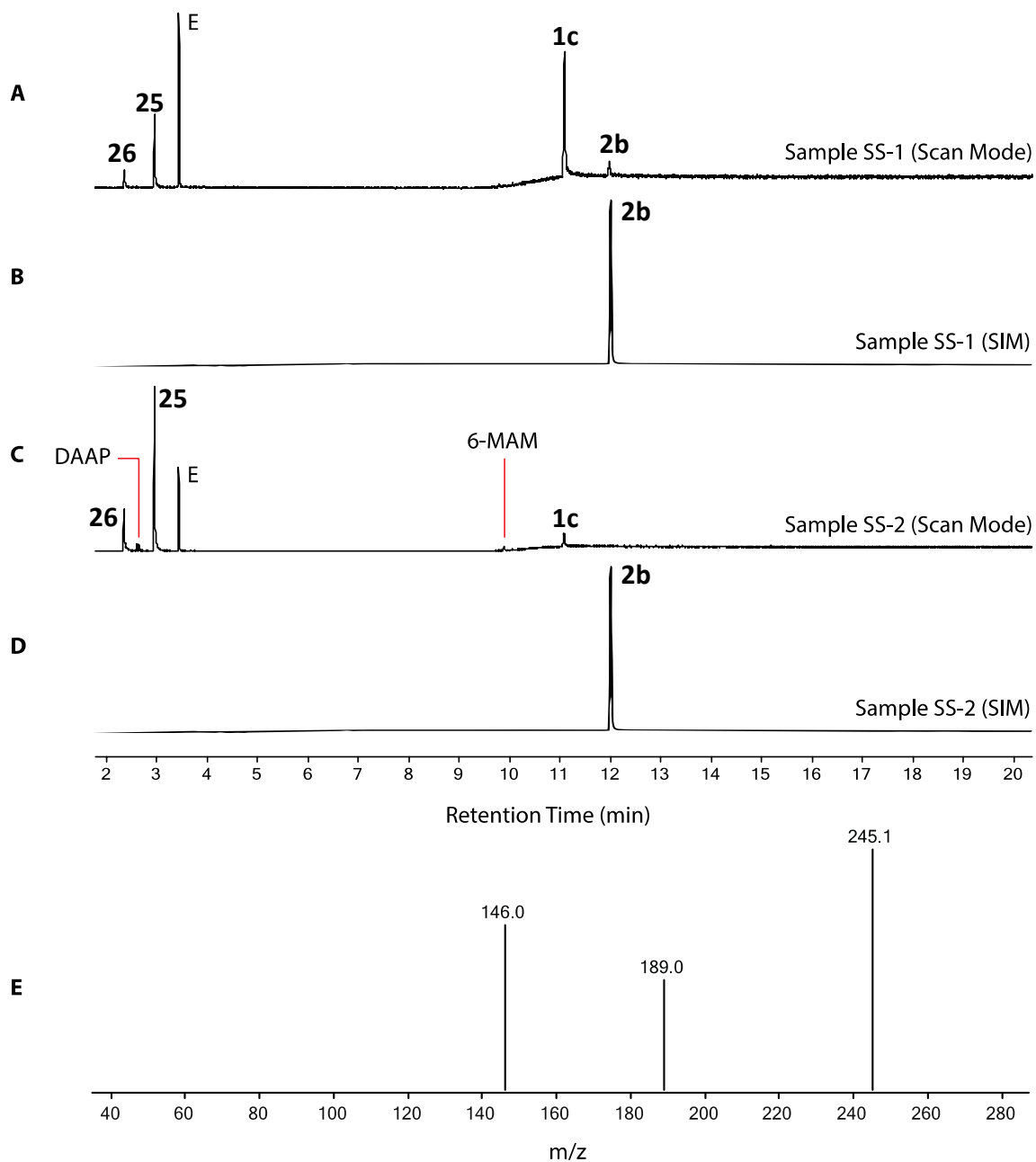


Figure 2.18. Qualitative GC-MS analysis heroin samples SS-1 and SS-2 (0.1 mg/mL in methanol). a) SS-1 in scan mode; b) Total ion chromatogram of SS-1 in SIM mode ($m/z = 245.1, 189.0, 146.0$); c) SS-2 in scan mode; d) Total ion chromatogram of SS-2 in SIM mode ($m/z = 245.1, 189.0, 146.0$); e) SIM spectrum of peak ($t_R = 12.0$ min) corresponding to fentanyl (**2b**).

In order to quantify the components present in seized samples, and especially fentanyl, SS-1 – SS-7 were reanalyzed (in triplicate) using the validated GC-MS method. Quantification results are reported in Table 2.14. All samples contained heroin at levels ranging between 17.8 – 82.9% w/w. The lower purity samples (SS-1 – SS4) contained significant levels of caffeine (3.7 – 20.5% w/w) and paracetamol (5.9 – 28.6% w/w). Samples SS-1 and SS-2 were found to contain fentanyl at $6.29 \pm 0.01\%$ w/w and $0.288 \pm 0.008\%$ w/w respectively. This corresponds to 4.403 ± 0.007 mg and 0.35 ± 0.01 mg within the bulk samples.

It should be noted that this analysis does not account for 100% of the mass of samples. This can be partly explained by the presence of varying amounts of insoluble materials in samples; dissolution of these samples in methanol for GC-MS analysis leaves brown insoluble material that was filtered off. Other compounds, such as sugars, may be soluble in methanol but not volatile enough for GC-MS analysis. Common heroin diluents include lactose, maltose, mannitol, sodium bicarbonate and starch. [146]

Table 2.14. Qualitative and quantitative analysis of seized samples (SS-1 – SS-7) obtained from Greater Manchester Police. Note: A dash indicates a compound was not detected.

Sample No.	Weight (g)	Heroin (% w/w)	Paracetamol (% w/w)	Caffeine (% w/w)	Fentanyl (% w/w)	Other components
SS-1	0.07	53.1±0.8	5.9±0.5	3.69±0.06	6.29±0.01	—
SS-2	0.12	20.5±0.8	26.8±1.5	14.8±0.8	0.288±0.008 ^a	Diacetyl- <i>p</i> -aminophenol (40), 6-Mono-acetylmorphine (41)
SS-3	0.11	25.5±0.7	27.1±0.6	16.9±0.7	—	Diacetyl- <i>p</i> -aminophenol (40), 6-Mono-acetylmorphine (41)
SS-4	0.73	17.8±0.4	28.6±2.0	20.5±1.3	—	Diacetyl- <i>p</i> -aminophenol (40), 6-Mono-acetylmorphine (41)
SS-5	1.04	82.9±2.7	—	—	—	6-Mono-acetylmorphine (41)
SS-6	0.95	74.7±1.6	—	—	—	6-Mono-acetylmorphine (41)
SS-7	0.15	82.2±3.1	—	—	—	6-Mono-acetylmorphine (41)

Key: ^aComponent only detected in SIM mode.

This is a clear demonstration that the method developed in this study is more suitable for fentanyl detection (and quantification) than previously available methods. Fentanyl was only detected in SS-1 because it was present at a very high concentration. Fentanyl present in SS-2, on the other hand, was missed by every available analytical method, including a generic GC-MS scan, which is normally used for routine analysis of seized samples. The newly developed method allows quantification of fentanyl at relevant concentrations and is, therefore, better suited for harm reduction and intelligence gathering.

It must be noted that due to the small number of samples (n = 7), these results are not representative of the prevalence of heroin samples contaminated with fentanyl in Manchester or the UK. A much wider sample range would need to

be analysed to establish general trends. The method presented would allow the production of such information, as it facilitates the routine screening of suspected heroin samples which may contain fentalogues, including at trace levels.

2.10 Conclusion

Analytical methods for the detection and quantification of 18 target fentalogues were tested and optimised using reference material synthesised in-house. Colorimetric tests, namely a combination of the Marquis and Eosin Y tests were shown to allow presumptive discrimination of fentalogues from common controlled drugs and adulterants. Thin-layer chromatography allowed partial separation of fentalogues from each other, and full separation from heroin. Formal separation and identification of fentanyl, however, requires more advanced techniques and was achieved using GC-EI-MS. Fragmentation patterns common to all fentalogues and fragments specific to certain compounds were described. A GC-MS separation method was optimised and fully validated for quantification at low concentrations (LOD: 0.008 – 0.125 µg/mL and LOQ: 0.025 – 0.415 µg/mL).

The analytical methods described were applied to seven seized heroin samples. The Eosin Y colour test and TLC analysis allowed the presumptive detection of fentanyl in one sample (SS-1). FTIR analysis only allowed the clear identification of heroin in samples containing no caffeine or paracetamol. It did not allow the detection of fentanyl in SS-1. An initial GC-MS screening confirmed the presence of fentanyl in only one sample (SS-1). The optimised SIM method showed a greatly improved sensitivity and allowed the detection of fentanyl in a second, lower-concentration sample (SS-2). Using the

optimised quantification method, fentanyl concentration was determined in both SS-1 and SS-2 at $6.29 \pm 0.01\%$ w/w and $0.288 \pm 0.008\%$ w/w, respectively.

This chapter focused on a selection of fentanyl analogues that were most relevant at the time this study was conducted. Though new derivatives are still emerging in seizures and early warning systems, this constituted an initial framework for fentanyl separation and detection by GC-MS in seized samples, to which new compounds can always be added. However, certain emerging compounds, such as fluorinated fentanyl regioisomers, may pose different analytical challenges and require the development of specific detection methods.

CHAPTER III

SYNTHESIS AND DETECTION OF FLUORINATED FENTANYL REGIOISOMERS

3.1 Overview

An increasingly common modification of the fentanyl structure is the introduction of a fluorine substituent. Most commonly, fluorine substitution occurs on the aniline ring of the fentanyl molecule. For instance, *ortho*-, *meta*- and *para*-fluorofentanyl have been reported across Europe and, in some cases, have been linked to overdoses (see Figure 3.1, **42a-c**). [57-60] Similar derivatives such as *para*-fluorobutyrfentanyl (**43**), *para*-fluoroisobutyrfentanyl (**44**) or ocfentanyl (**45**) have been reported in seizures as well as cases of acute poisonings. [61-64]

Fluorination in other positions has yet to be frequently observed. One difluorinated analogue, 2'-fluoro-*ortho*-fluorofentanyl (**47**), was identified within a seizure in China. [147] Although this was the first example of fluorination on the phenethyl moiety of fentanyl, it highlights the possibility that 2'-, 3'- and 4'-fluoro derivatives such as **46a-c** could appear. Spahn *et al.* reported that 3-fluorofentanyl (**48**, also known as NFEPP) only targeted inflamed tissue in mice and did not produce effects sought from opioid abuse (sedation, euphoria), making this compound unlikely to emerge on recreational drug markets. [1]

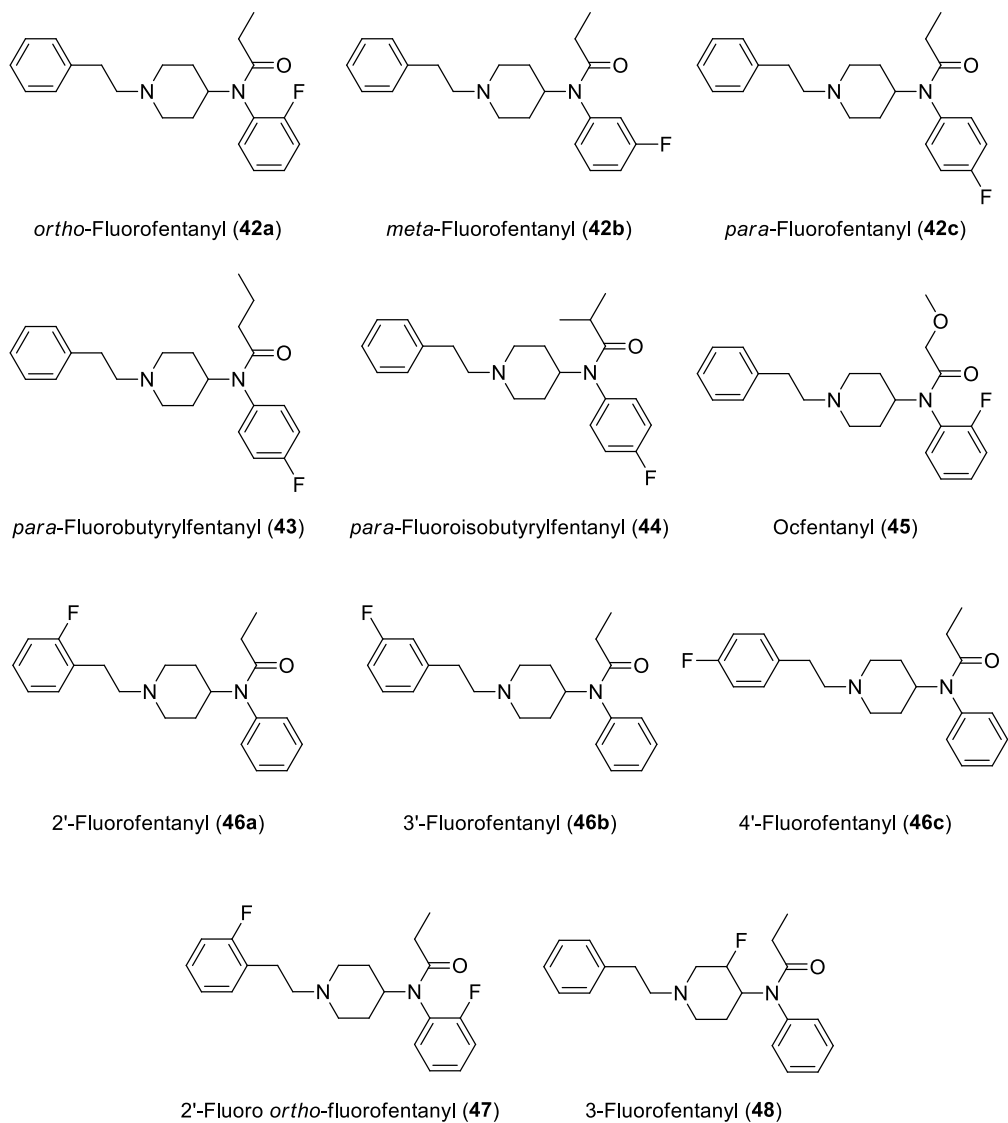


Figure 3.1. Chemical structure of known and potential fluorinated fentologues.

The emergence of regioisomeric derivatives of known synthetic drugs is a constant challenge in forensic casework. The availability of regioisomeric starting materials renders the synthesis of regioisomeric derivatives extremely simple. These compounds tend to exhibit similar chemical and

chromatographic properties, and their mass spectra are often equivalent. This complicates the identification of specific drug regioisomers, hence why specific analytical methods have been developed by other research groups to identify regioisomers of synthetic cannabinoids, fluoroamphetamines, chloroamphetamines and cathinones. [148-153]

The same challenge applies to the identification of regioisomers of fluorofentanyl. This chapter starts with the synthesis of reference material for eight fluorinated regioisomers of fentanyl (see Figure 3.2, **42a-c**, **46a-c**, **47**, **48**). Only propionyl derivatives were included, since this study focuses on the separation of regioisomers, while the differentiation of fentalogues bearing different amide chains was outlined in Chapter 2. Target compounds, as well as fentanyl, heroin, paracetamol and caffeine will be submitted to presumptive detection methods and GC-MS analysis. Because of the difficulty of discriminating fluorinated fentalogues using GC-MS, benchtop NMR will be evaluated as an orthogonal detection method for successful identification. NMR will also be validated for quantification of target compounds.

3.2 Synthesis

The hydrochloride salts of fluorofentanyls (**42a-c**, **46a-c**, **47**, **48**) were prepared using procedures adapted from the literature (see Figure 3.2). Starting from *N*-phenethylpiperidone **5**, anilines bearing a fluorine at different positions were introduced by reductive amination to obtain fluorinated 4-ANPP derivatives **49a-c**. Acylation with propionyl chloride and reaction with ethereal HCl produces target compounds **42a-c**. Synthesis of **46a-c** derivatives started with the acylation of 1-Boc-4-phenylaminopiperidine **50** to obtain compound **51**. Boc deprotection, alkylation with fluorophenethyl bromide regioisomers and reaction with HCl afforded compounds **46a-c**. Synthesis of **47** was performed

in a similar way, starting with an additional step consisting in the reductive amination between 1-Boc-4-piperidone **52** and 2-fluoroaniline. Finally, synthesis of 3-fluorofentanyl (**48**) followed the same steps, starting from 1-Boc-3-fluoro-4-piperidone (**55**).

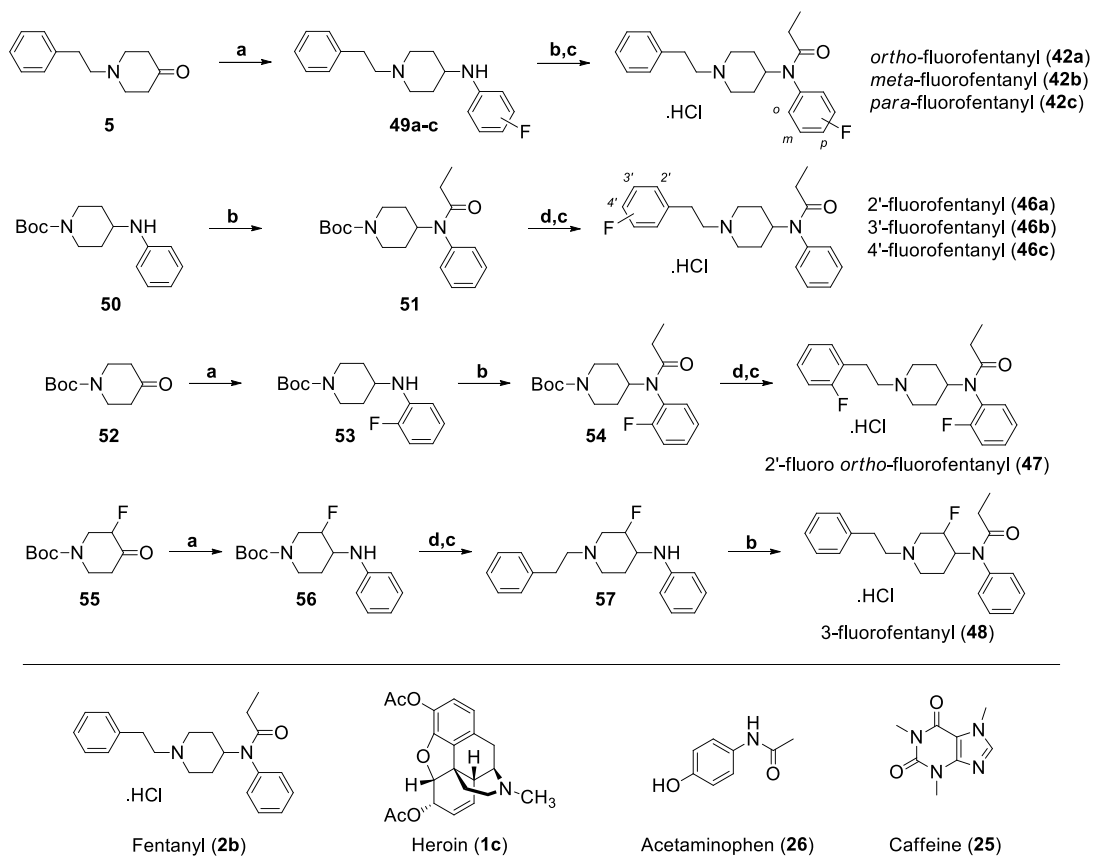


Figure 3.2. Synthesis of target fluorofentanyls (**42a-c**, **46a-c**, **47**, **48**) and structure of controlled drugs and adulterants included in this study. *Reagents and conditions*: (a) ArNH₂, AcOH, NaBH(OAc)₃, DCE, r.t., 48 h; (b) Propionyl chloride (2.0 eq.), iPr₂NEt (2.0 eq.), DCM (0.1 M), 0 °C to r.t., 2 h; (c) HCl (3 M in CPME, 1.0 eq.), Et₂O or acetone (0.1 M), r.t., 2 h; (d) 1. TFA/DCM (1:3) (0.3 M), 0 °C to r.t., 1 h, 2. Ar(CH₂)₂Br, Cs₂CO₃, ACN, reflux, 5 h.

The products were fully characterized: ATR-FTIR and NMR (^1H , ^{13}C , ^{19}F) and high-resolution mass spectrometry (HRMS) data are reported in Section 7.12. ATR-FTIR and NMR (^1H , ^{13}C , ^{19}F) spectra are reported in the Appendix. EI-MS spectra are reported in Section 3.6 (Figure 3.4).

It was shown in Chapter 2 that fentalogues produced ^1H NMR spectra that were indicative of their common backbone, and that specific derivatives could be differentiated based on signals associated with their amide chains. Most fluorinated regioisomers studied in this chapter share common features in their piperidine, ethyl chain and amide chain signals, as highlighted in Table 3.1. One glaring exception is 3-fluorofentanyl (**48**): its piperidine signals have different chemical shifts and couplings from the other derivatives, because of the presence of a fluorine atom. Another exception was observed in compounds **42a** and **47**, which bear a fluorine in the *ortho* position of the aniline ring. In most fentalogues, piperidine signals are split between axial and equatorial protons, because of differences in their chemical environments. For instance, protons 11-*axial* and 11-*equatorial* have different chemical shifts from each other. Incidentally, because fentanyl is symmetrical, 11-*axial* coincides with 13-*axial*, while 11-*equatorial* coincides with 13-*equatorial*. The corresponding signals were arbitrarily labelled 11a/11b and 13a/13b. In compounds **42a** and **47**, proton 11a has a different chemical shift from 13a, meaning that their chemical environments are not equivalent due to the presence of the *ortho* fluorine on the aniline ring. The presence of this fluorine must somehow slow down or prevent the rotation around the C₁₂-N bond, resulting in different chemical environments for protons 11 and 13.

Fluorinated regioisomers can be differentiated through differences in their aromatic region, as shown in Figure 3.3. Signal attribution required an analysis

of ^1H - ^1H and ^1H - ^{13}C correlation spectra and ^{13}C - ^{19}F coupling constants observed in ^{13}C NMR (reported in Section 7.10.2). While ^1H NMR spectra indicate a specific substitution pattern, the presence of a fluorine atom can only be determined by ^{19}F NMR and mass spectrometry.

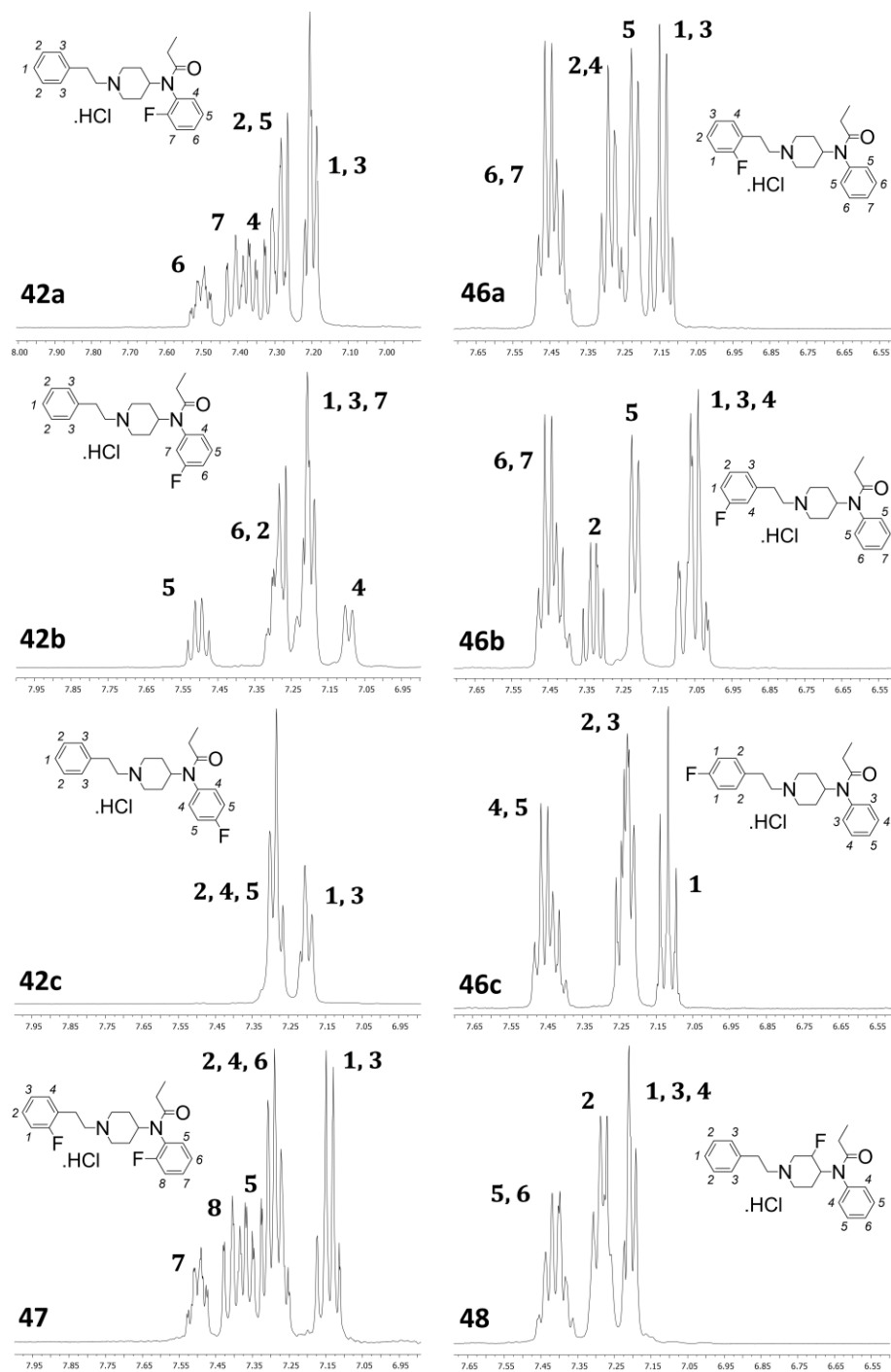
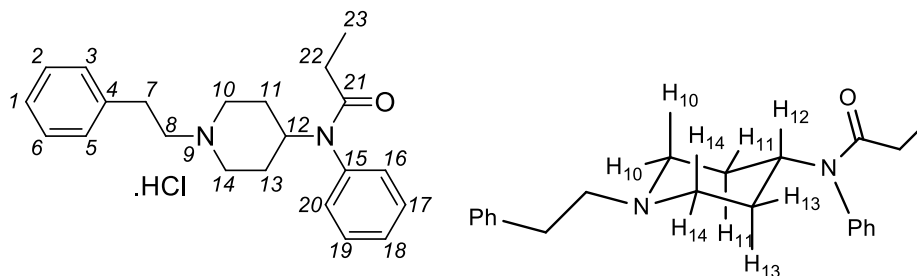


Figure 3.3. Aromatic region (7.025 – 7.750 ppm) of the high-field ^1H NMR spectra of fluorofentanyls **42a-c**, **46a-c**, **47**, **48** in $\text{DMSO-}D_6$.

Table 3.1. ¹H NMR attribution of fentalogues **42a-c**, **46a-c**, **47**, **48** and numbering reference for fentanyl (**2b**).

	Piperidine ring and ethyl chain protons ^a										Amide chain protons		
	12	10a	14a	10b	14b	8	7	13a	11a	11b	13b	22	23
42a	4.75 (tt)	3.52 (t)		3.21-3.04 (m)			3.01-2.92 (m)	1.98 (d)	1.93-1.49 (m)			1.93-1.49 (m)	0.89 (t)
42b	4.7 (t)	3.52 (d)		3.22-3.04 (m)			3.04-2.92 (m)	2.04-1.80 (m)		1.63 (qd)		2.04-1.80 (m)	0.89 (t)
42c	4.71 (t)	3.52 (d)		3.24-3.03 (m)			3.03-2.91 (m)	1.92 (m)		1.6 (qd)		1.83 (q)	0.88 (t)
46a	4.72 (tt)	3.53 (d)		3.19-3.06 (m)			3.05-2.97 (m)	1.93 (m)		1.6 (qd)		1.81 (q)	0.87 (t)
46b	4.69 (tt)	3.48 (d)		3.21-3.01 (m)			3.01-2.92 (m)	1.9 (m)		1.58 (qd)		1.79 (q)	0.84 (t)
46c	4.72 (tt)	3.51 (d)		3.21-3.03 (m)			2.99-2.90 (m)	1.93 (m)		1.58 (qd)		1.82 (q)	0.87 (t)
47	4.74 (tt)	3.54 (t)		3.23-3.08 (m)			3.08-2.95 (m)	2.00 (d)	1.95-1.49 (m)			1.95-1.49 (m)	0.89 (t)
48	4.81 (dd)	3.83 (t)	3.72-3.43 (m)		3.35-3.13 (m)		3.08-2.87 (m)	1.94-1.75 (m)	5.35 (d)	–	1.59 (qd)	1.94-1.75 (m)	0.9 (t)

Key: ^a a and b are axial and equatorial protons on the same carbon.



3.3 Presumptive colour tests

Fluorinated fentalogues, fentanyl and heroin were submitted to the Marquis, nitric acid and Eosin Y colorimetric tests; results are reported in Table 3.2. Heroin (**1c**) could easily be differentiated from fentanyl (**2b**) and its fluorinated analogues (**42a-c**, **46a-c**, **47**, **48**) using the nitric acid or Marquis' tests. Heroin produced a green colour with the former while fentalogues do not react, and a distinctive deep violet colour with the latter.

The results of Marquis' test, however, varied depending on the fluorofentanyl tested. Compounds **42a-c** and **48** reacted the same way as fentanyl, producing a dark brown colour. Interestingly, fluorination of the phenethyl ring (**46a-c**, **47**) appeared to hinder the reaction. This is most likely because it proceeds through formylation of the aromatic ring by formaldehyde, catalysed by sulfuric acid. [77] The presence of a fluorine atom deactivates the ring for electrophilic aromatic substitution.

This reveals an important fact about the potential mechanism of the reaction between fentalogues and Marquis' reagent: formylation mostly occurs at the phenethyl ring, not the aniline ring. Any modification of this moiety is therefore likely to prevent a conclusive colour change from appearing, leading to a false negative result. This illustrates how presumptive colour tests can prove unreliable when testing for emerging drug analogues.

The Eosin Y test allows effective discrimination between fentanyl analogues and common drugs and adulterants. This also applied to fluorinated fentalogues, except for **42c** and **48**, which produced a false negative result.

Table 3.2. Reactions of fluorofentalogues (**42a-c**, **46a-c**, **47**, **48**), fentanyl and heroin with the Marquis, nitric acid and Eosin Y tests. Note: A dash indicates the absence of a discernible colour change.

	Nitric Acid		Marquis		Eosin Y	
	Immediate colour	Colour after 5 min	Immediate colour	Colour after 5 min	Immediate colour	Colour after 5 min
1c	Yellow	Green	Violet	Violet	Light pink	Light pink
2b	—	—	Orange	Dark brown	Dark pink	Dark pink
42a	—	—	Orange	Dark brown	Dark pink	Dark pink
42b	—	—	Orange	Dark brown	Dark pink	Dark pink
42c	—	—	Orange	Dark brown	Light pink	Light pink
46a	—	—	Light orange	Orange-brown	Dark pink	Dark pink
46b	—	—	—	Light pink	Dark pink	Dark pink
46c	—	—	—	Pink	Dark pink	Dark pink
47	—	—	Light orange	Orange-brown	Dark pink	Dark pink
48	—	—	Orange	Dark brown	Light pink	Light pink

3.4 Thin-layer chromatography (TLC)

TLC analysis of the target compounds was carried out using an eluent of dichloromethane-methanol (9:1 v/v) containing 1% triethylamine. The plates were developed with modified Dragendorff-Ludy-Tenger reagent. The R_f values showed clear separation of the *ortho/meta/para* series (**42a-c**, $R_f = 0.52$, 0.49 and 0.46, respectively). Separation was less defined between **47** ($R_f = 0.50$) and **2b** ($R_f = 0.51$). **42c** ($R_f = 0.46$) co-eluted with **46a** ($R_f = 0.46$) and **46b** ($R_f = 0.47$). **46c** ($R_f = 0.44$) and **48** ($R_f = 0.64$) were clearly separated from all other derivatives. Despite their similar chromatographic properties, partial

discrimination of the target fluorofentanyl derivatives was possible under these TLC conditions.

Table 3.3 Thin-layer chromatography results for fentanyl derivatives **42a-c**, **46a-c**, **47**, **48** and fentanyl **2b**.

Compound	R _f ^a	RR _f ^b
42a	0.52	1.01
42b	0.49	0.96
42c	0.46	0.91
46a	0.46	0.91
46b	0.47	0.93
46c	0.44	0.87
47	0.50	0.99
48	0.64	1.26
2b	0.51	1.0

Key: ^aRetention factor (DCM-MeOH (9:1 v/v) with 1% Et₃N); ^bRelative Retention Factor (with respect to fentanyl, **2b**).

3.5 Infrared spectroscopy

ATR-FTIR spectra of fentanyl derivatives **42a-c**, **46a-c**, **47** and **48** are reported in Section 7.13. Similarly to the compounds studied in Chapter II, they are characterised by weak to medium aromatic and aliphatic C-H bands (~3050-2850 cm⁻¹), weak to medium ammonium salt N-H bands (~2600-2400 cm⁻¹) and a strong amide C=O stretching band (~1660-1640 cm⁻¹). A C-F stretch should be observed in the fingerprint region, around 1200 cm⁻¹, [154] but is difficult to identify.

Again, a leave-one-out validation was performed (Table 3.4). All match scores are less than or equal to 73%, which indicates a good ability to discriminate compounds.

Table 3.4. Leave-one-out validation of the ATR-FTIR method with analogues **42a-c**, **46a-c**, **47**, **48**.

Compound	Second highest match	Match score
42a	47	72%
42b	2e	39%
42c	2g	32%
46a	47	65%
46b	2b	73%
46c	46a	57%
47	42a	72%
48	2k	58%

3.6 Electron ionisation mass spectrometry

Electron ionisation mass spectra of fentalogues **42a-c**, **46a-c**, **47**, **48** are reported in Figure 3.4.

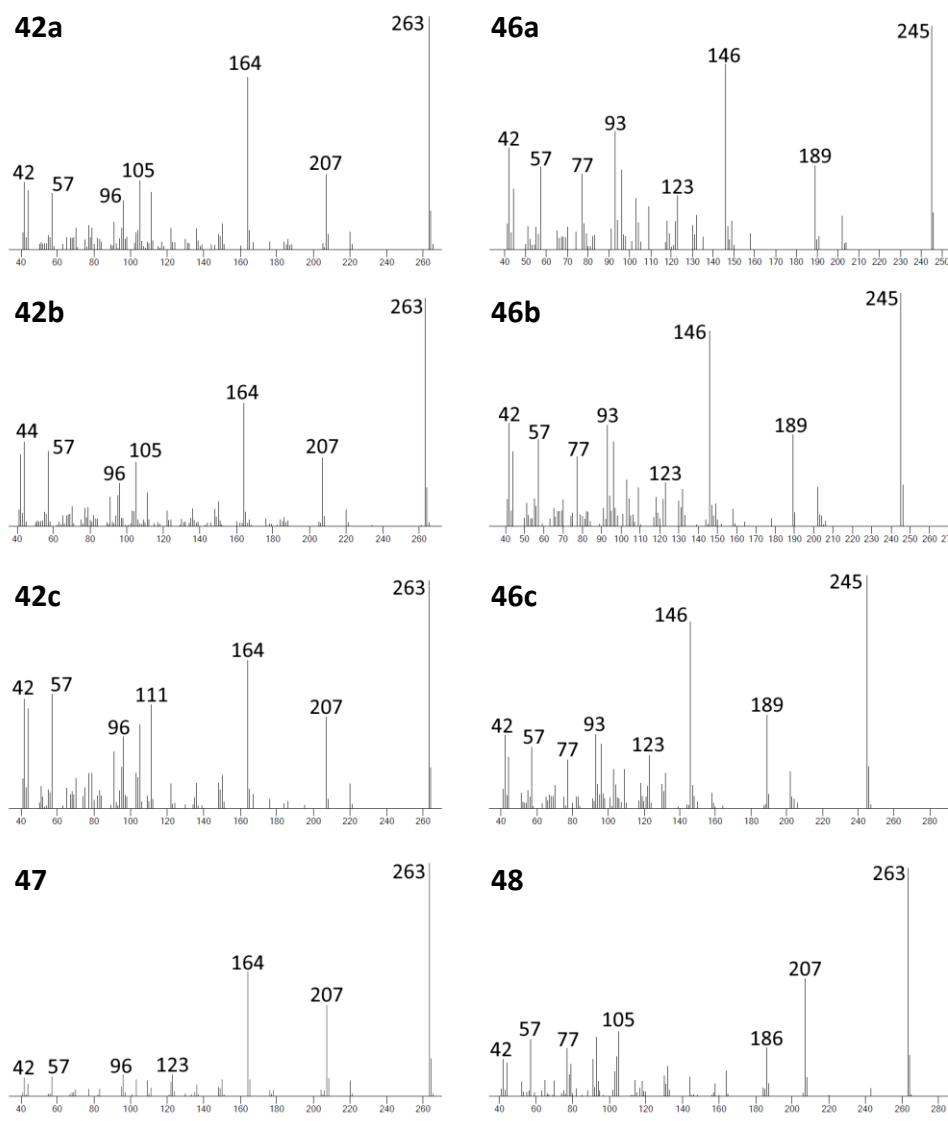


Figure 3.4. Electron ionisation mass spectra of fentalogues **42a-c**, **46a-c**, **47**, **48**.

The general EI-MS fragmentation pattern of fentanyl has been discussed and is represented in Figure 2.6. The main initial loss of a benzyl radical produced a fragment at $m/z = 245$, followed by three major fragments of $m/z = 202$, 189

106

and 146. In the same way, fluorofentanyl isomers **46a-c**, readily lose a benzyl cation upon fragmentation to form a cation of $m/z = 245$ (Figure 3.5). Their main fragments did not contain a fluorine atom and were therefore equivalent to those of fentanyl. The only difference with fentanyl was a fragment of $m/z = 109$, which could be attributed to a fluorinated tropylium ion. In fentanyl, the corresponding tropylium ion has an m/z of 91.

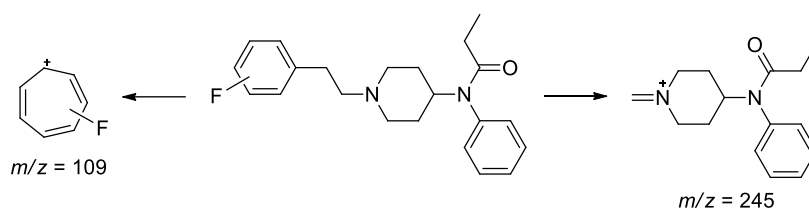


Figure 3.5. Initial EI-MS fragmentations of 2'-, 3'- and 4'-fluorofentanyl (**46a-c**).

Isomers **42a-c** all retained a fluorine atom in their main fragments (see Figure 3.6). They were thus easily differentiated from fentanyl, but not from each other, by their mass spectra.

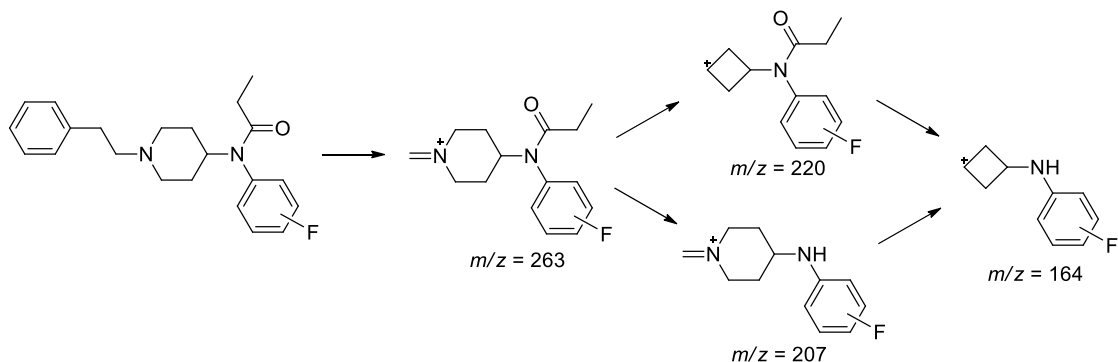


Figure 3.6. EI-MS fragmentation of *ortho*-, *meta*-, *para*-fluoro fentanyl (**42a-c**).

Compound **47**, by losing a fluorobenzyl radical, produced essentially the same fragment ions as compounds **42a-c**, outlined in Figure 3.6. However, its three heaviest fragments ($m/z = 263$, 207 and 164) were of disproportionately strong intensity compared to **42a-c**. **48** produced fragment ions with the same mass as those reported in Figure 3.6, with one additional ion at $m/z = 186$, which was not readily explained.

3.7 Qualitative GC-MS analysis

A GC-MS method was optimized to separate the target compounds (see Figure 3.7), using the following temperature gradient: 100 to 200 °C at 30 °C/min, 200 to 230 at 10 °C/min, 230 to 260 at 30 °C/min, 260 to 265 at 1 °C/min, hold for 1 min for a 13.3 min total runtime. Only partial chromatographic resolution was achieved, due to their similar chromatographic properties. Target fentalogues were fully separated from heroin (**1c**) and adulterants acetaminophen (**26**) and caffeine (**25**). The method also separated compounds **42a-c**. Despite an optimization of the temperature program, however, compounds **46a-c** co-eluted and could not be resolved by SIM analysis as they produced the same

fragment ions. SIM ions and their relative intensities are reported in Table 3.5. In a similar way, **42b** partially co-eluted with **47**, and the two produced the same MS ions. Although **48** co-eluted with **2b**, they were differentiated in SIM mode.

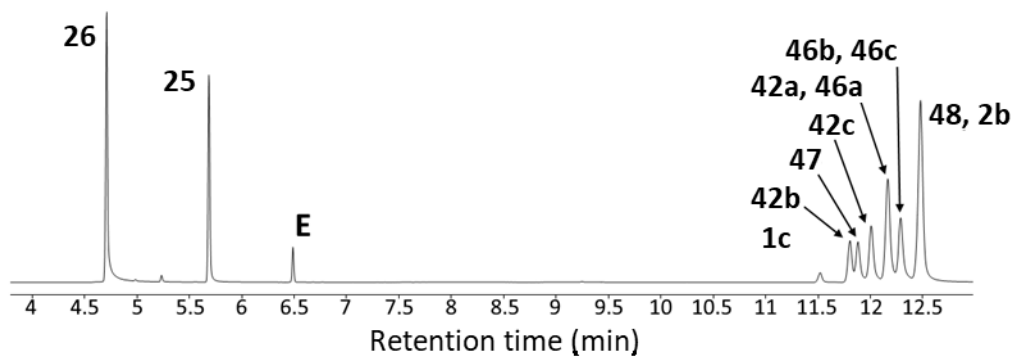


Figure 3.7. Exemplar GC-MS chromatogram of target fluorofentanyl (s) (**42a-c**, **46a-c**, **47**, **48**), fentanyl (**2b**), heroin (**1c**), acetaminophen (**26**), caffeine (**25**) and eicosane (internal standard, **E**).

Table 3.5. EI-MS ions used for identification of analytes via Selective Ion Monitoring (SIM), relative intensity of each ion (relative to base peak) and precision (%RSD) of the relative intensities.

26	SIM ions	109.0	151.0	80.0	42a	SIM ions	263.1	207.0	164.0
	Relative intensities (%)	100.0	36.0	20.1		Relative intensities (%)	100.0	39.1	51.7
	Precision (% RSD, n = 3)	N/A	0.5	0.3		Precision (% RSD, n = 3)	N/A	0.5	1.1
25	SIM ions	194.1	109.0	82.0	46a	SIM ions	245.1	189.1	146.0
	Relative intensities (%)	100.0	46.9	19.8		Relative intensities (%)	100.0	35.5	49.7
	Precision (% RSD, n = 3)	N/A	0.7	0.6		Precision (% RSD, n = 3)	N/A	0.8	0.3
1c	SIM ions	369.2	327.2	268.1	46b	SIM ions	245.1	189.1	146.0
	Relative intensities (%)	66.5	100.0	62.3		Relative intensities (%)	100.0	36.0	49.3
	Precision (% RSD, n = 3)	1.2	N/A	1.9		Precision (% RSD, n = 3)	N/A	1.3	1.3
42b	SIM ions	263.1	207.0	164.0	46c	SIM ions	245.1	189.1	146.0
	Relative intensities (%)	100.0	32.4	38.2		Relative intensities (%)	100.0	36.6	52.8
	Precision (% RSD, n = 3)	N/A	1.0	0.3		Precision (% RSD, n = 3)	N/A	0.4	0.8
47	SIM ions	263.1	207.0	164.0	2b	SIM ions	245.1	189.1	146.0
	Relative intensities (%)	100.0	38.9	52.1		Relative intensities (%)	100.0	35.2	47.5
	Precision (% RSD, n = 3)	N/A	1.8	0.5		Precision (% RSD, n = 3)	N/A	1.1	1.9
42c	SIM ions	263.1	207.0	164.0	48	SIM ions	263.1	207.0	164.0
	Relative intensities (%)	100.0	30.9	42.3		Relative intensities (%)	100.0	52.8	8.3
	Precision (% RSD, n = 3)	N/A	1.2	0.9		Precision (% RSD, n = 3)	N/A	2.6	3.8

3.8 Quantitative GC-MS analysis

The quantitative GC-MS method (SIM mode), was developed and validated in accordance with the ICH guidelines. [143] To avoid peak overlap between analytes which produced indistinguishable SIM ions, target compounds were organized into three groups, each validated separately from the others

(Group I: heroin **1c**, fentanyl **2b**, caffeine **25**, acetaminophen **26** and **46b**; Group II: **42a-c** and **46c**; Group III: **46a**, **47** and **48**).

A summary of GC-MS validation data is reported in Table 3.6. As discussed previously, fentalogues are well resolved from heroin and its adulterants, but poorly resolved from each other. Fluorinated fentalogues peaks proved very symmetrical (A_s value close to 1). Limits of detection and quantification were determined based on signal-to-noise (S/N) ratio. For fentalogues, these were 0.009 – 0.020 $\mu\text{g/mL}$ (LOD) and 0.031 – 0.067 $\mu\text{g/mL}$ (LOQ). For other controlled substances and adulterants they were 0.034 – 0.068 $\mu\text{g/mL}$ (LOD) and 0.113 – 0.227 $\mu\text{g/mL}$ (LOQ). This is comparable to the method reported in Chapter II (see Section 2.8). Limits of detection and quantification in SIM mode were compared to those calculated for scan mode (Table 3.7). For fentalogues, the SIM method proved between 455 – 1261 times more sensitive than scan mode.

Calibration standards were prepared over a 5.0–25.0 $\mu\text{g/mL}$ concentration range, using eicosane as an internal standard, to produce a calibration curve for each analyte (see calibration curve equations below Table 3.6). All substituted fentalogues demonstrated a linear response ($r^2 = 0.998\text{--}0.999$) with satisfactory repeatability (RSD = 0.3 – 3.9%, $n = 6$). The method was also suitable for quantification of the other controlled substances and adulterants, demonstrating linear response ($r^2 = 0.993\text{--}0.998$) with reasonable repeatability (RSD = 1.1 – 7.4 %, $n = 6$).

The accuracy of the method was determined using a percentage recovery study (see Table 3.8). Spiked samples were prepared in triplicates at three concentration levels over a range of 80–120% of a target concentration

(15 µg/mL). The result of these injections is fed back into the calibration curve and the experimental concentration is compared with the theoretical concentration (assay recovery). The relative error shows how the mean assay recovery diverges from an expected 100%. Acceptable recoveries ($100 \pm 3\%$) were obtained for all analytes.

The precision (inter- and intraday precision) was calculated from six replicate injections of a spiked sample (10 µg/mL) and analysed on two consecutive days (see Table 3.9). Most analytes showed acceptable precision, with intraday RSDs between 1.7 and 4.6%, apart from paracetamol (interday: 6.5%), similar to the method developed in Chapter II.

Although the GC-MS analysis of fluorinated fentalogues was fully validated, co-elution of compounds with the same *m/z* ions (**46a-c**) prevented the identification of specific regioisomers. Identification of regioisomers would have to be confirmed using a different technique, such as NMR. ¹H and ¹⁹F NMR spectroscopy are proposed as alternative detection and quantification techniques to resolve this issue.

Table 3.6. Summary of GC-MS validation data (SIM mode) for the quantification of fentalogues (**2b**, **42a-c**, **46a-c**, **47**, **48**), heroin (**1c**) and common adulterants (**25**, **26**). NB. t_R (eicosane, IS) = 3.47 min (see Figure 3.7 for chromatogram).

Analyte	t_R (min)	RRT ^a	R_s	A_s	N (plates)	r^2	LOQ ⁿ ($\mu\text{g/mL}$)	LOD ^o ($\mu\text{g/mL}$)	Precision (%RSD, n = 6)				
									5 $\mu\text{g/mL}$	10 $\mu\text{g/mL}$	15 $\mu\text{g/mL}$	20 $\mu\text{g/mL}$	25 $\mu\text{g/mL}$
26	4.88	0.39	-	6.1	418362	0.993 ^b	2.074	0.622	7.4	4.7	4.3	5.9	3.3
25	5.69	0.46	33.0	1.8	501999	0.997 ^c	0.113	0.034	4.0	2.1	1.9	2.5	2.4
IS	6.49	0.52	27.8	1.1	871966	N/A	N/A	N/A	N/A	N/A	N/A	N/A	N/A
1c	11.51	0.93	109.0	1.0	553506	0.998 ^d	0.227	0.068	5.3	4.8	1.4	2.1	1.1
42b	11.79	0.95	4.3	1.0	564224	0.999 ^e	0.040	0.012	2.8	0.3	2.4	1.3	1.1
47	11.87	0.95	1.1	1.0	514321	0.999 ^f	0.044	0.013	1.1	1.6	1.5	1.6	1.1
42c	11.99	0.96	1.7	1.0	506423	0.998 ^g	0.045	0.013	2.1	1.0	2.4	1.2	1.2
42a	12.14	0.98	2.1	1.1	459280	0.999 ⁱ	0.057	0.017	3.1	1.2	1.4	1.2	1.2
46a	12.16	0.98	0	1.0	533666	0.999 ^h	0.031	0.009	1.2	0.6	1.3	1.5	0.9
46b	12.24	0.98	1.6	1.1	450960	0.999 ^j	0.057	0.017	3.7	1.9	1.6	2.2	1.7
46c	12.27	0.99	0	1.2	433778	0.998 ^k	0.045	0.013	2.2	1.3	2.1	1.0	1.4
2b	12.44	1.00	2.4	1.1	468388	0.999 ^l	0.055	0.017	3.9	2.4	1.0	2.5	1.3
48	12.47	1.00	0	1.1	464368	0.999 ^m	0.067	0.020	1.9	1.6	1.2	1.3	1.5

Key: ^a Relative retention time (in relation to fentanyl); ^b $y=0.1438x-0.6305$; ^c $y=0.1920x-0.0628$; ^d $y=0.0597x - 0.0761$; ^e $y=0.2547x-0.0635$; ^f $y=0.1804x-0.0761$; ^g $y=0.2546x-0.1061$; ^h $y=0.2463x-0.1634$; ⁱ $y=0.2070x-0.0634$; ^j $y=0.2295x-0.2382$; ^k $y=0.2442x-0.0907$; ^l $y=0.2173x-0.4763$; ^m $y=0.2420x-0.2908$; ⁿ Limit of detection (calculated using a signal-to-noise ratio of 3:1); ^o Limit of quantification (calculated using a signal-to-noise ratio of 10:1).

Table 3.7. Comparison of GC-MS limits of detection/quantification determined in scan mode and selective ion monitoring (SIM) mode for fentalogues (**2b**, **42a-c**, **46a-c**, **47**, **48**), heroin (**1c**) and common adulterants (**25**, **26**).

Analyte	t _R (min)	Scan mode		Selective ion monitoring (SIM) mode	
		LOD ^a (µg/mL)	LOQ ^b (µg/mL)	LOD ^a (µg/mL)	LOQ ^b (µg/mL)
26	4.88	76.5	23.0	2.074	0.622
25	5.69	1.6	0.5	0.113	0.034
1c	11.51	62.0	18.6	0.227	0.068
42b	11.79	33.0	9.9	0.040	0.012
47	11.87	29.8	8.9	0.044	0.013
42c	11.99	30.8	9.2	0.045	0.013
42a	12.14	35.9	10.8	0.057	0.017
46a	12.16	39.1	11.7	0.031	0.009
46b	12.24	27.3	8.2	0.057	0.017
46c	12.27	27.3	8.2	0.045	0.013
2b	12.44	25.0	7.5	0.055	0.017
48	12.47	36.3	10.9	0.067	0.020

Key: ^aLimit of detection (calculated using a signal-to-noise ratio of 3:1); ^bLimit of quantification (calculated using a signal-to-noise ratio of 10:1).

Table 3.8. GC-MS recovery results for fentalogues (**2b**, **42a-c**, **46a-c**, **47**, **48**), heroin (**1c**) and common adulterants (**25**, **26**).

Analyte	Assay recovery ^a			Mean recovery (%)	%RSD (n = 3)	Relative Error ^b (%)
	12 µg/mL (% , n = 3)	15 µg/mL (% , n = 3)	18 µg/mL (% , n = 3)			
42b	98.4	97.3	97.0	97.6	0.8	-2.4
47	98.7	98.2	99.0	98.6	0.4	-1.4
42c	97.5	97.0	97.0	97.2	0.3	-2.8
42a	98.1	97.5	98.8	98.1	0.7	-1.9
46a	99.7	98.2	99.2	99.0	0.7	-1.0
46b	103.0	103.1	99.6	101.9	2.0	1.9
46c	98.1	97.9	96.7	97.6	0.7	-2.4
2b	102.7	102.8	100.1	101.9	1.5	1.9
48	98.0	98.6	98.9	98.5	0.4	-1.5
1c	102.8	102.8	100.3	102.0	1.4	2.0
26	102.0	102.6	102.3	102.3	0.3	2.3
25	103.1	100.3	100.6	101.3	1.5	1.3

Key: ^a Determined as a percentage ratio between the experimental concentration (calculated from the calibration curve) and the known concentration (12, 15 or 18 µg/mL); ^b Deviation between the average experimental recovery and a 100% recovery.

Table 3.9. Summary of GC-MS repeatability (intraday precision) and intermediate precision (interday precision) for fentalogues (**2b**, **42a-c**, **46a-c**, **47**, **48**), heroin (**1c**) and common adulterants (**25**, **26**).

Analyte	Intraday precision ^a (%RSD, n = 12)	Interday precision ^b (%RSD, n = 12)
26	4.6	6.5
25	2.9	2.6
1c	2.8	1.9
42b	1.8	3.6
47	3.8	3.9
42c	3.8	3.1
42a	3.3	3.1
46a	3.7	3.7
46b	3.7	3.5
46c	1.7	4.1
2b	3.4	4.2
48	4.3	3.6

Key: ^aRelative standard deviation of twelve injections (10 µg/mL) performed over a short time interval; ^bRelative standard deviation of twelve injections (10 µg/mL) performed over two consecutive days.

3.9 Qualitative NMR analysis

It was highlighted in Section 3.2 that ^1H NMR could be used to differentiate fluorinated fentanyl analogues based on their aromatic signals. A recent study also reported using ^1H benchtop NMR for the qualitative identification of certain fluorofentanyls (**42a-c** and **48**). [95]

Although ^1H NMR allowed the identification of fluorofentanyl regioisomers, and potentially their quantification, its effectiveness may be limited in adulterated mixtures where signal overlaps are likely. The use of ^{19}F NMR circumvents this issue – fluorine atoms do not typically occur in the drugs and adulterants commonly mixed with fentanyl, such as heroin, acetaminophen and caffeine. ^{19}F NMR would therefore allow the quantification of fluorofentanyls in mixtures.

Overlaid ^{19}F NMR spectra of the target fluorofentanyls are shown in Figure 3.8 and chemical shifts of each fluorine signal are reported in Table 3.10. The same pattern was observed for each aromatic ring: the ^{19}F NMR signals of the *ortho* and *para* isomers were shielded by the electron-donating effect of the substituent (amide or alkyl chain), and this effect was more observable in the *ortho* compounds. In 3-fluorofentanyl (**48**), the fluorine is located on an aliphatic ring and thus is extremely shielded (-119.4 ppm). All target compounds produced fully resolved signals using high-field ^{19}F NMR and could easily be identified and separated in a potential mixture (Figure 3.8b). This shows that, confronted with a suspected fluorofentanyl sample, ^{19}F NMR can be used to inform which ring is substituted and at which position. Difluorinated compound **47** produced two signals, equivalent to those of 2'-fluorofentanyl **46a** and *ortho*-fluorofentanyl **42a** (Figure 3.8b). This simplifies the identification of potential new difluorinated compounds, as a simple ^{19}F NMR analysis and comparison

to reference chemical shifts can help determine the fluorine substitution pattern, without the need for more complex and time-consuming 2D analysis.

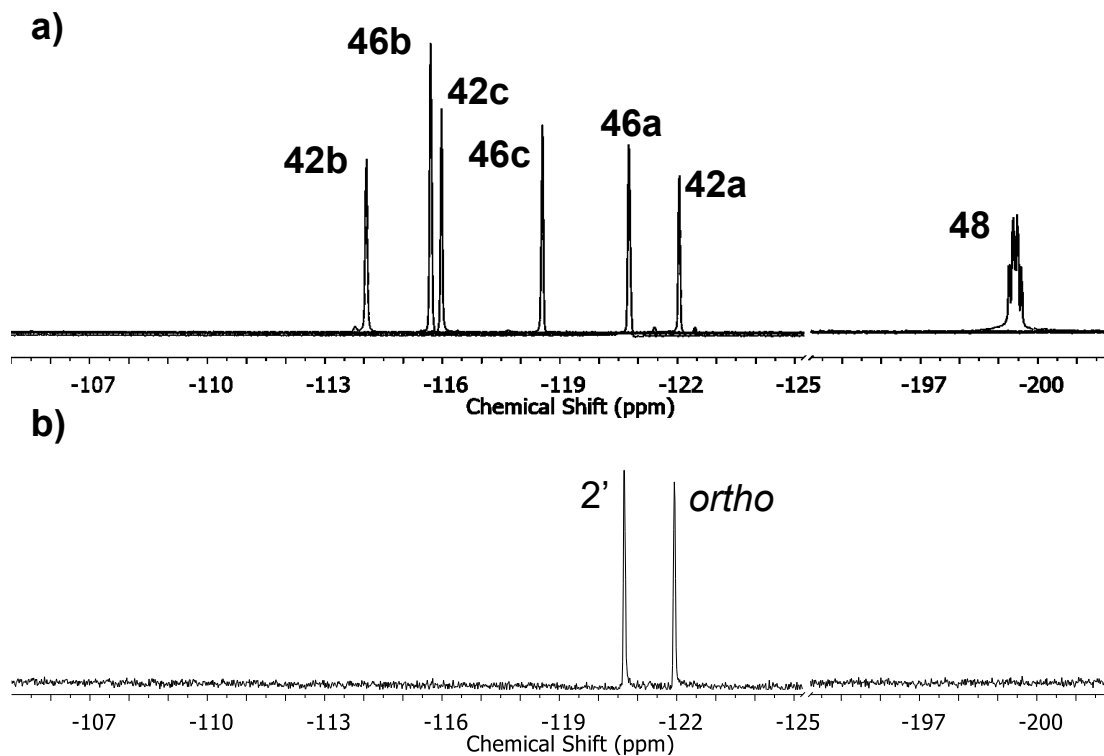


Figure 3.8. (a) Overlay of high-field ^{19}F NMR spectra of target fluorofentanyls (42a-c, 46a-c, 48); (b) High-field ^{19}F NMR of compound 47.

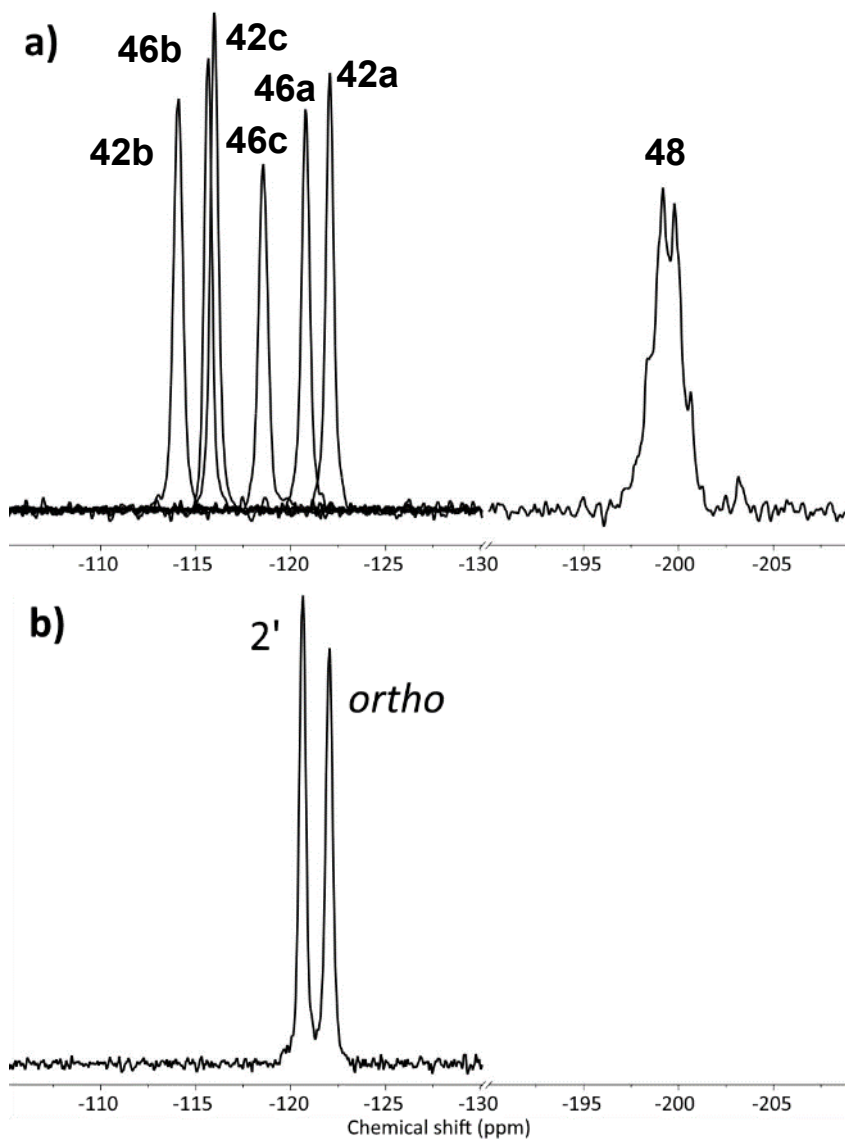


Figure 3.9. (a) Overlay of low-field ^{19}F NMR spectra of target fluorofentanyls (**42a-c**, **46a-c**, **48**); (b) Low-field ^{19}F NMR of compound **47**.

Low-field ^{19}F NMR detection of fluorofentanyls was also investigated. Low-field benchtop NMR instruments have the advantage of being much more affordable than their high-field counterparts, easier to use and potentially field-deployable. Previous studies have reported the reliable identification of illicit drugs [93] and

fentanyl derivatives [95] by low-field ^1H NMR. Figure 3.9 shows an overlay of the low-field ^{19}F NMR spectra of target fluorofentanyls. The use of benchtop NMR resulted in a loss of resolution: two signals coincide (**46b** and **42c**) but are still partially resolved. Benchtop ^{19}F NMR proved suitable for the discrimination of fluorinated regioisomers of fentanyl (except **46b** and **42c**). These also co-elute by TLC, so proper identification of these derivatives would require ^1H NMR or GC-MS analysis.

Another scenario which must be accounted for is the unlikely, but possible, analysis of a mixture of two fluorofentanyls, for instance **42a** and **46a**. Combinations of different fentalogues have previously been found in casework. [155-157] This mixture would appear similar to difluorinated compound **47**, which produces the same ^{19}F NMR signals. A sample of 2'-fluoro *ortho*-fluorofentanyl would easily be differentiated from a mixture of 2'-fluorofentanyl (**46a**) and *ortho*-fluorofentanyl (**42a**) by TLC or GC-MS, or alternatively by measuring the ratio between both fluorine signals in the ^{19}F NMR spectrum.

Five standard solutions containing varying ratios of **46a/42a** were prepared. Benchtop ^{19}F NMR spectra of each sample were acquired; the integration of **46a** (2' fluorine signal) was divided by the sum of both signals. The resulting graph is shown in Figure 3.10. A linear relationship is obtained which enables the quantification of the proportion of **46a** and **42a** present in a mixture by analysing the ratio of their signals. A solution containing only difluorinated **47** was run, and a signal ratio of 0.524 was obtained (see Figure 3.10, orange line).

While this ratio will always be constant for compound **47**, only a mixture of 51:49 **46a/42a** would produce the exact same ratio as **47** – any other

concentration would produce a different ratio and be easily differentiable. In the rare case where a signal ratio of 51:49 was obtained, other methods previously discussed are required to correctly identify the sample.

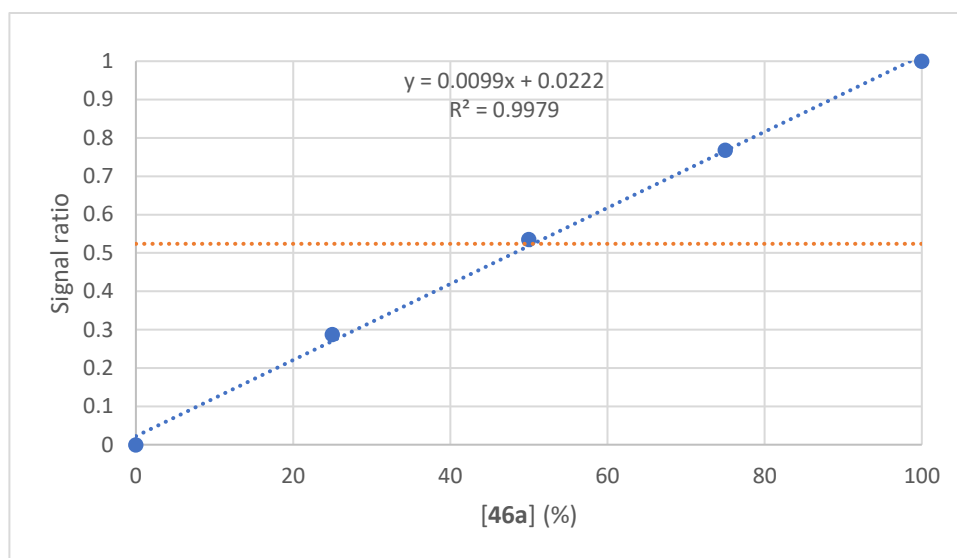


Figure 3.10. ^{19}F NMR signal ratio of a **46a** and **42a** mixture (integration of **46a**/**(46a+42a)**) against the concentration of **46a**. The orange line marks the signal ratio observed in a pure solution of **47**.

3.10 Quantitative low-field ^{19}F NMR analysis

A quantitative low-field ^{19}F NMR method was developed and validated in accordance with the ICH guidelines. [143] A summary of NMR validation data is reported in Table 3.10. The LOD and LOQ (based on signal-to-noise ratio) were of $73.8 - 403.3 \mu\text{g mL}^{-1}$ and $286.9 - 1344.3 \mu\text{g mL}^{-1}$ respectively. Though this technique is not nearly as sensitive as GC-MS (LOD = $0.009 - 0.020 \mu\text{g/mL}$), this data shows that fentalogue detection would be possible at the low concentrations expected in seized samples.

Calibration standards were prepared over a 5.0–15.0 mg/mL concentration range to produce a calibration curve for each analyte. TFA was added as a chemical shift reference, but no internal standard was necessary to normalise analyte signals. All substituted fentalogues demonstrated a linear response ($r^2 = 0.994–0.999$) with satisfactory repeatability (RSD = 0.9 – 9.7 %, $n = 6$).

The accuracy of the method was determined using a percentage recovery study (see Table 3.11). Spiked samples were prepared in triplicates at three concentration levels over a range of 80–120% of a target concentration (10 mg/mL). Acceptable recoveries ($100 \pm 3\%$) were obtained for all analytes.

Table 3.10. Low-field ^{19}F NMR validation data for the quantification of fluorofentanyls (**42a-c**, **46a-c**, **47**, **48**). See Figure 3.9 for representative spectra.

Analyte	Chemical shift (ppm) ^a	r^2	LOD ^b ($\mu\text{g/mL}$)	LOQ ^c ($\mu\text{g/mL}$)	Precision (%RSD, $n = 6$)				
					5 mg/mL	8 mg/mL	10 mg/mL	12 mg/mL	15 mg/mL
42b	-114.064	0.999	105.2	350.7	3.3	2.2	2.4	1.6	1.4
46b	-115.698	0.999	104.1	347.0	4.1	2.8	2.8	2.0	1.6
42c	-115.977	0.996	75.6	251.8	4.8	4.7	2.5	2.3	3.0
46c	-118.556	0.995	130.6	435.3	5.3	2.5	4.2	1.8	2.3
46a	-120.762	0.999	86.1	286.9	4.3	3.3	0.9	2.4	1.1
42a	-122.048	0.995	73.8	246.1	5.8	4.8	2.6	4.1	2.4
48	-199.434	0.996	403.3	1344.3	9.7	4.5	2.7	5.2	4.7
47 (2')	-120.657	0.994	108.6	361.9	3.1	4.0	3.5	4.0	2.9
47 (o)	-122.047	0.994	117.9	393.0	6.1	4.5	4.7	4.3	2.2

Key: ^a Referenced to trifluoroacetic acid (TFA); ^b Limit of detection (determined using a signal-to-noise ratio of 3:1); ^c Limit of quantification (determined using a signal-to-noise ratio of 10:1).

Table 3.11. Low-field ^{19}F NMR recovery results for fentalogues (**42a-c**, **46a-c**, **47**, **48**).

Analyte	Assay recovery ^a			Mean recovery (%)	%RSD (n = 3)	Relative Error ^b (%)
	8 mg/mL (% , n=3)	10 $\mu\text{g/mL}$ (% , n=3)	12 $\mu\text{g/mL}$ (% , n=3)			
42b	98.5	100.3	99.4	99.4	0.9	-0.6
46b	97.7	103.6	102.2	101.2	3.0	1.2
42c	96.9	100.4	96.6	98.0	2.1	-2.0
46c	101.6	103.3	102.7	102.5	0.8	2.5
46a	99.4	101.9	102.3	101.2	1.5	1.2
42a	101.8	103.1	96.7	100.6	3.4	0.6
48	100.9	102.4	100.2	101.2	1.1	1.2
47 (2')	103.9	99.8	102.7	102.1	2.1	2.1
47 (o)	97.6	98.4	100.7	98.9	1.6	-1.1

Key: ^a Determined as a percentage ratio between the experimental concentration (calculated from the calibration curve) and the known concentration (12, 15 or 18 $\mu\text{g/mL}$); ^b Deviation between the average experimental recovery and a 100% recovery.

Finally, the possibility to detect a fluorinated fentanyl in a mixture with heroin using this method was tested. A solution containing 42 mg/mL heroin (**1c**) and 1 mg/mL *ortho*-fluorofentanyl (**42a**) was prepared. This corresponds to a **42a/1c** ratio of 2.4% w/w. The solution was first analysed by benchtop ^1H NMR using the Pulsar benchtop NMR spectrometer. The resulting spectrum appeared to be that of pure heroin (see Figure 3.11a). When compared against a previously developed low-field ^1H NMR drug database, [93] which includes *ortho*-fluorofentanyl **42a**, heroin was the only component identified in the sample with a 97.4% match score, while **42a** was not detected. Increasing the number of scans in increments from 16 – 4096 yielded the same result, with negligible change in the match score.

Low-field ^{19}F NMR analysis using the developed method revealed the presence of **42a**, within the LOQ, demonstrating the applicability of this method to adulterated heroin samples (see Figure 3.11b).

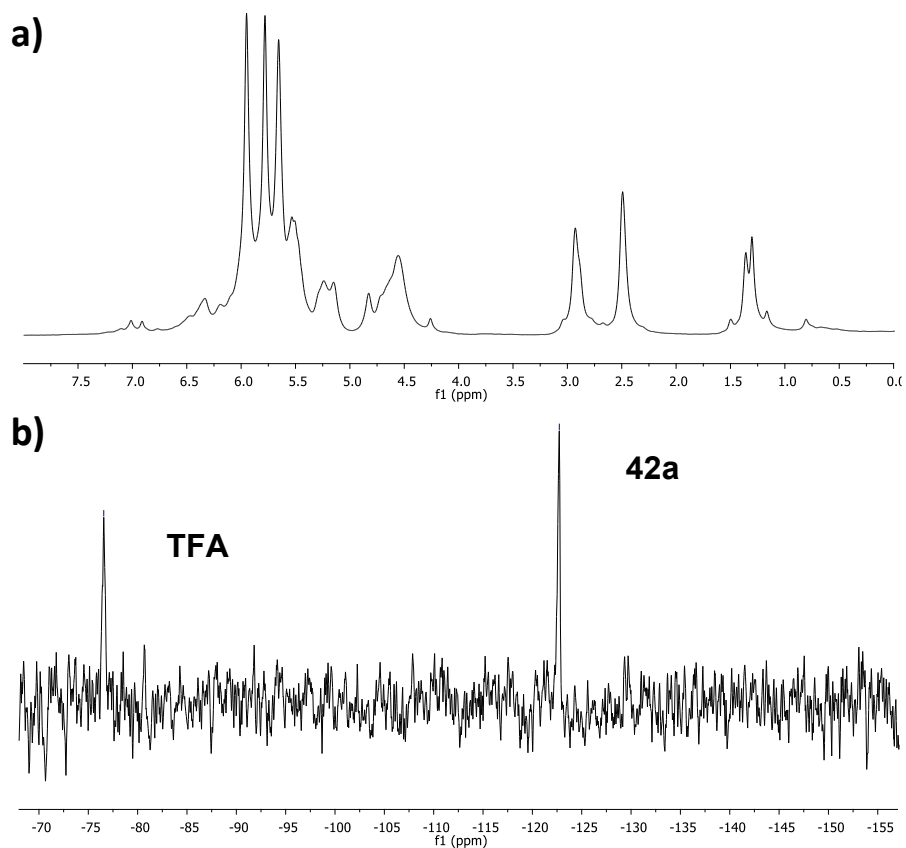


Figure 3.11. (a) Low-field ^1H NMR spectrum of an *ortho*-fluorofentanyl (**42a**)/heroin (**1c**) mixture (2.4 %w/w); (b) Low-field ^{19}F NMR spectrum of an *ortho*-fluorofentanyl (**42a**)/heroin (**1c**) mixture (with TFA as reference).

The specificity of this technique must be discussed. When confronted with a seized heroin sample, the detection of a fluorine peak cannot lead to the formal identification of a fluorinated fentanyl. However, it should be considered that none of the adulterants commonly mixed with heroin bear fluorine atoms. Considering this context, the detection of a fluorine peak, at a chemical shift consistent with a fluorofentanyl, should be a cause of suspicion which leads to

the use of other confirmatory methods. In that sense, ^{19}F NMR can be used orthogonally to other techniques, as well as for quantification.

3.11 Conclusion

In conclusion, it was shown that fluorinated regioisomers of fentanyl, which are increasingly common on drug markets, cannot be fully discriminated using methods outlined in Chapter II (*i.e.* colour tests, TLC, infrared spectroscopy or GC-MS). GC-MS afforded partial discrimination, but the co-elution of compounds with the same major m/z fragments prevented a conclusive identification. A GC-MS quantification method was developed, as it could still be useful for single-component samples or samples containing non co-eluting compounds. ^{19}F benchtop NMR was proposed as an orthogonal method for the identification and quantification of fluorinated regioisomers of fentanyl. Most fentalogues investigated, except **42c** and **46b**, produced distinct signals in low-field ^{19}F NMR and a quantification method was developed using this technique. Benchtop NMR is a simpler, faster and cheaper method than GC-MS. Despite its lower sensitivity than GC-MS, benchtop ^{19}F NMR showed sufficiently low LODs and LOQs, and it was shown that it could detect *ortho*-fluorofentanyl **42a** in a 2.4 %w/w heroin mixture, a common challenge for the detection of fentanyl analogues.

CHAPTER IV

INVESTIGATION OF THE EOSIN Y COLORIMETRIC TEST

4.1 Overview

Eosin Y (**22**, see Figure 4.1 for structure) has been used in chemical dye sensors because of its ability to change colour in contact with various analytes. As is the case for many presumptive colour tests, the chemical mechanism leading to this colour change has yet to be explained. A recent study reported that the dye reacts with fentanyl, and not cocaine, to produce a characteristic deep pink colour. [158] Results reported in Chapter II and III show that the dye reacts in the same way with a variety of fentanyl analogues, while none of the other drugs and adulterants investigated did. This specificity could be harnessed for the reliable detection of fentanyl analogues using a simple eosin Y test, usable onsite by police enforcement, by drug users for personal harm reduction, etc. Commercial versions of the Marquis test are already available for opioid detection, but they are known to be unreliable, especially in mixtures or with low concentrations of analyte. This chapter will therefore focus on the validation of the eosin Y test for the detection of fentanyl. The mechanism of the reaction between eosin Y and fentanyl will be investigated, objective methods (spectrophotometry, RGB detection) will be assessed for colour change detection and if the eosin Y colour test can be used quantitatively will be determined.

4.2 Detection of fentalogues

In previous chapters, the eosin Y test proved particularly useful for discriminating fentalogues from other controlled drugs, their adulterants and even the precursor 4-ANPP (see Table 4.1). Table 4.2 presents the identification of compounds based on the test, to highlight the percentage of false positives/negatives. 36 compounds were tested, including 25 fentalogues. All non-fentalogues were correctly identified, while only 3 fentalogues did not react (8.3% false negatives).

Table 4.1. Results of the eosin Y test with compounds investigated in Chapter II and III.

Compound	Colour after 5 min	Compound	Colour after 5 min	Compound	Colour after 5 min
4	Light pink	2m	Light pink	1b	Light pink
2a	Dark pink	2n	Dark pink	1c	Light pink
2b	Dark pink	2o	Dark pink	42a	Dark pink
2c	Dark pink	2p	Dark pink	42b	Dark pink
2d	Dark pink	2q	Dark pink	42c	Light pink
2e	Dark pink	2r	Dark pink	46a	Dark pink
2f	Dark pink	23	Light pink	46b	Dark pink
2g	Dark pink	24a	Peach	46c	Dark pink
2h	Dark pink	24b	Light pink	48	Light pink
2i	Dark pink	25	Light pink	47	Dark pink
2j	Dark pink	26	Light pink		
2k	Dark pink	27	Light pink		
2l	Dark pink	1a	Light pink		

Table 4.2. Identification of fentalogues and other drugs and adulterants made using the eosin Y test.

Eosin Y identification	Fentalogue	Other
Fentalogue	22/25 (91.7% true positive)	0/11 (0% false positive)
Other	3/25 (8.3% false negative)	11/11 (100% true negative)

However, simply knowing the empirical effectiveness of a test is not enough to determine its applicability in real-life situations. Applying any analytical technique without knowing how it works is dangerous and increases the risk of unforeseen false positives/negatives. Knowledge of the mechanism of the chemical reaction leading to a colour change is essential and must be investigated before a presumptive test is used in forensic casework.

4.3 Investigation of the reaction mechanism

The eosin Y reaction mechanism was investigated using three analytes: caffeine, heroin and fentanyl. While the first two produce the same colour change, caffeine was included as a control, since its reaction with eosin Y has been partially investigated in a previous study. [159] NMR was used as the main diagnostic tool to monitor changes in eosin Y and the target molecules. Experiments were conducted in DMSO-D₆ and D₂O buffered to pH = 7.

¹H and ¹³C NMR spectra of commercial eosin Y, commercial caffeine free-base and synthesised fentanyl hydrochloride in DMSO-D₆ and buffered D₂O are reported in Section 7.12 for reference. Analysis of the DMSO-D₆ ¹H NMR spectrum of commercial eosin Y revealed that it was in its fully protonated form (as shown in Figure 1.10), as evidenced by a carboxylic acid and a phenol OH signal. Small peaks are visible in the aromatic region which may belong to the deprotonated products or other impurities (95% purity, according to the retailer).

As heroin is an expensive reference material, especially in the quantities required to perform this study, it was isolated from seized heroin samples in its free-base form (see Section 7.12.4 for procedure). ¹H and ¹³C NMR spectra

are reported in Section 7.12.4; attribution of signals was done using ^1H - ^1H and ^1H - ^{13}C NMR correlation spectra, which are also reported.

4.3.1 NMR experiments (DMSO)

Original tests were carried out in DMSO- D_6 , as it dissolves the target analytes and is aprotic, thus limiting the impact of the solvent in eventual acid-base reactions.

Caffeine did not react with eosin Y in DMSO: no colour change was observed, and their NMR signals remained unchanged in the spectrum of the mixture (see Figure 4.1). Caffeine has been reported to react with eosin Y in an aqueous buffer, [159] indicating that this reaction is dependent on the choice of solvent. This may be due to the fact that, as proposed by Okuom *et al.*, the colour change is due to the deprotonation of caffeine by eosin Y. [159] However, acid dissociation constants are solvent-dependent: water would dissolve the resulting caffeine anion better than DMSO, making caffeine less acidic in the latter solvent. [160] Eosin Y may also need to be in its deprotonated form to react, which it is at pH = 7 in water, but not in DMSO.

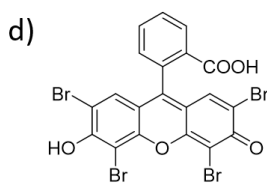
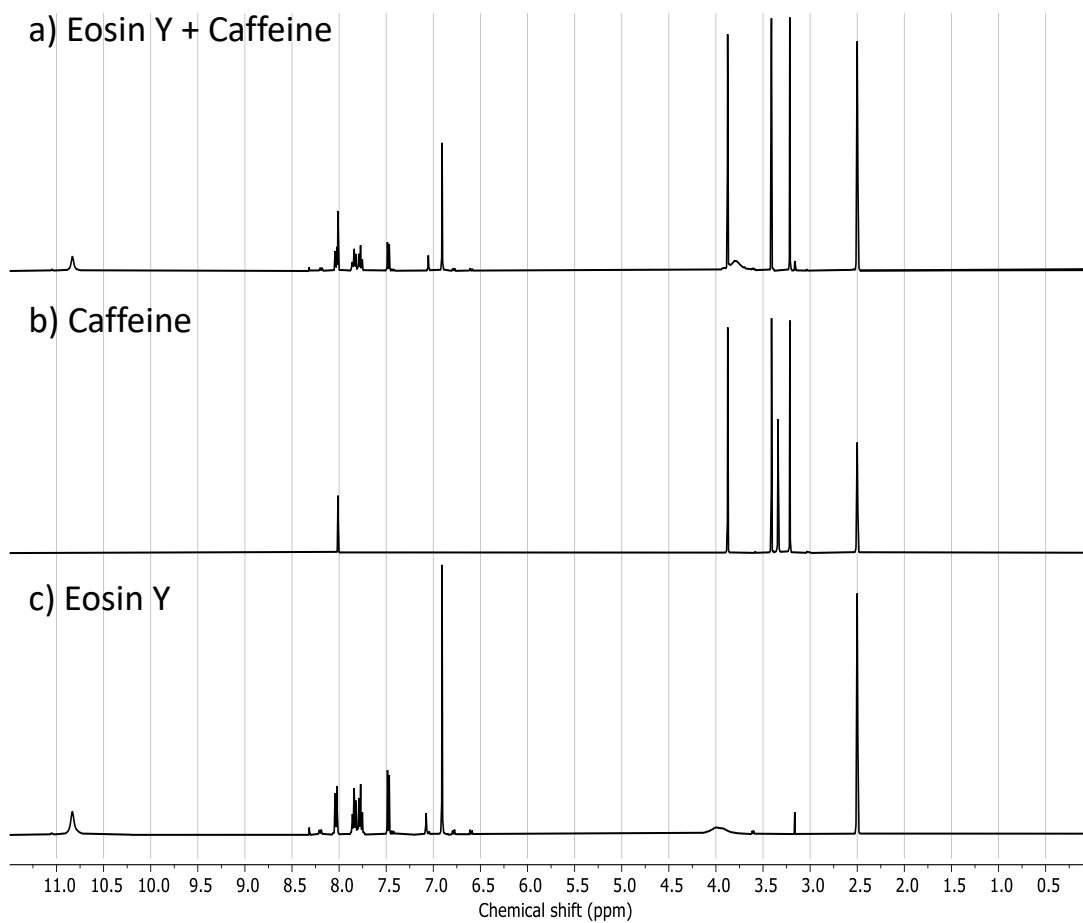


Figure 4.1. ^1H NMR spectra (400 MHz, DMSO-D_6) of a) Eosin Y and caffeine; b) Caffeine; c) Eosin Y; d) Chemical structure of eosin Y.

Heroin, which is more strongly basic than caffeine, did react with eosin Y in DMSO, producing a colour change from orange to pink in the NMR tube. In the ^1H NMR spectrum, the disappearance of eosin's carboxylic acid peak and a

shift of the heroin signals was observed (see Table 4.3 and Figure 4.2). Protons 9, 15, 16 and 19 (see Figure 4.2d for reference), which are in proximity to the *tertiary* amine, are especially deshielded. This could indicate the protonation of heroin by the eosin Y carboxylic acid. This is confirmed by reacting heroin free-base with anhydrous HCl (1.0 eq.) and isolating the resulting salt to acquire an NMR (see Figure 4.2c); a comparison of NMR signals in heroin HCl and the eosin Y – heroin mixture supports the hypothesis that there has been protonation. The colour change would thus result from the deprotonation of eosin Y and the delocalisation of the resulting electron pair across the aromatic rings. This hypothesis was reinforced with a simple experiment, using a simpler *tertiary* amine: eosin Y and triethylamine were mixed in DCM, which resulted in a drastic colour change.

Table 4.3. ^1H NMR chemical shifts of heroin and the eosin Y – heroin mixture (DMSO- D_6)

Proton	2	1	7/8	6	5	9	10'	14	16'	19	10	17	16	18	15'	15
Heroin (ppm)	6.73	6.59	5.50	5.15-5.10	5.03	3.32	2.97	2.73	2.47	2.32	2.27	2.22	2.17	2.07	2.02	1.60
Heroin + Eosin (ppm)	6.87	6.71	5.20	5.67	5.5	4.17	3.32	3.00	2.80	2.92	2.80	2.24	2.26	2.06	2.05	1.91

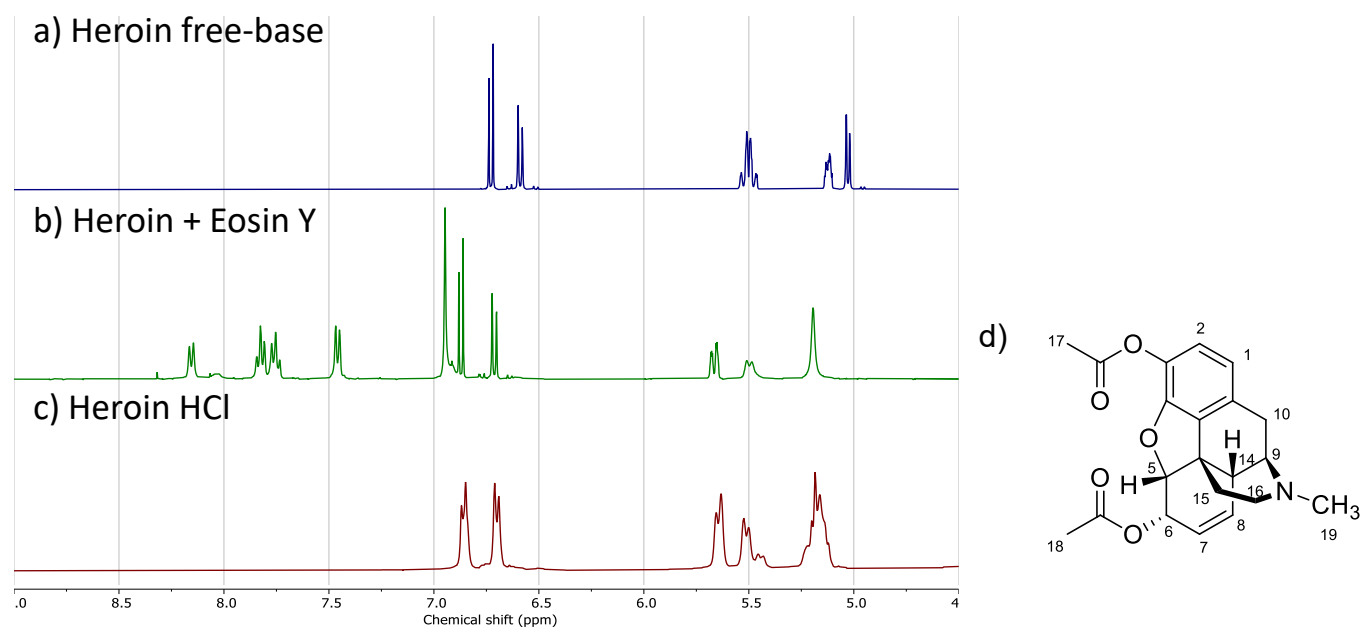


Figure 4.2. ^1H NMR spectra (400 MHz, DMSO- D_6) of a) Heroin free-base; b) Heroin free-base and eosin Y; c) Heroin protonated with HCl (1.0 eq.); d) Chemical structure of heroin.

All the eosin Y signals in the mixture were slightly shifted from the pure eosin Y solution (see Figure 4.3c-d). To establish what species was being observed, eosin Y was reacted with 1 equivalent NaOH to selectively form its monoanion, and 2 equivalents for the dianion. ^1H NMR spectra of these two mixtures were acquired (Figure 4.3a-b). Proton signals in the mixture match up perfectly with the monoanionic species, pointing to a 1:1 acid-base reaction between eosin Y and heroin.

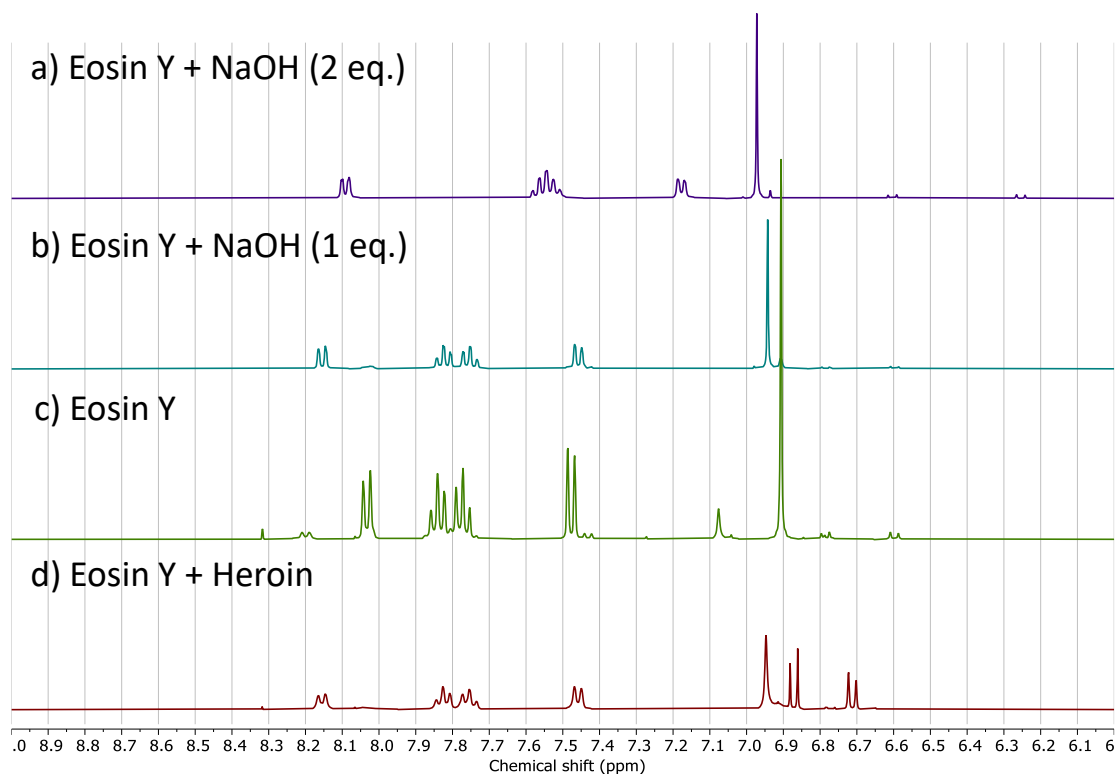


Figure 4.3. ^1H NMR spectra (400 MHz, DMSO-D_6) of a) Eosin Y deprotonated with NaOH (2 eq.); b) Eosin Y deprotonated with NaOH (1 eq.); c) Eosin Y; d) Eosin Y and heroin free-base.

Fentanyl HCl was investigated next. Though it bears a *tertiary* amine, like heroin, fentanyl is already protonated. It did not react with eosin Y in DMSO (see Figure 4.4). Therefore, like with caffeine, the reaction between fentanyl and eosin Y is dependent on the solvent.

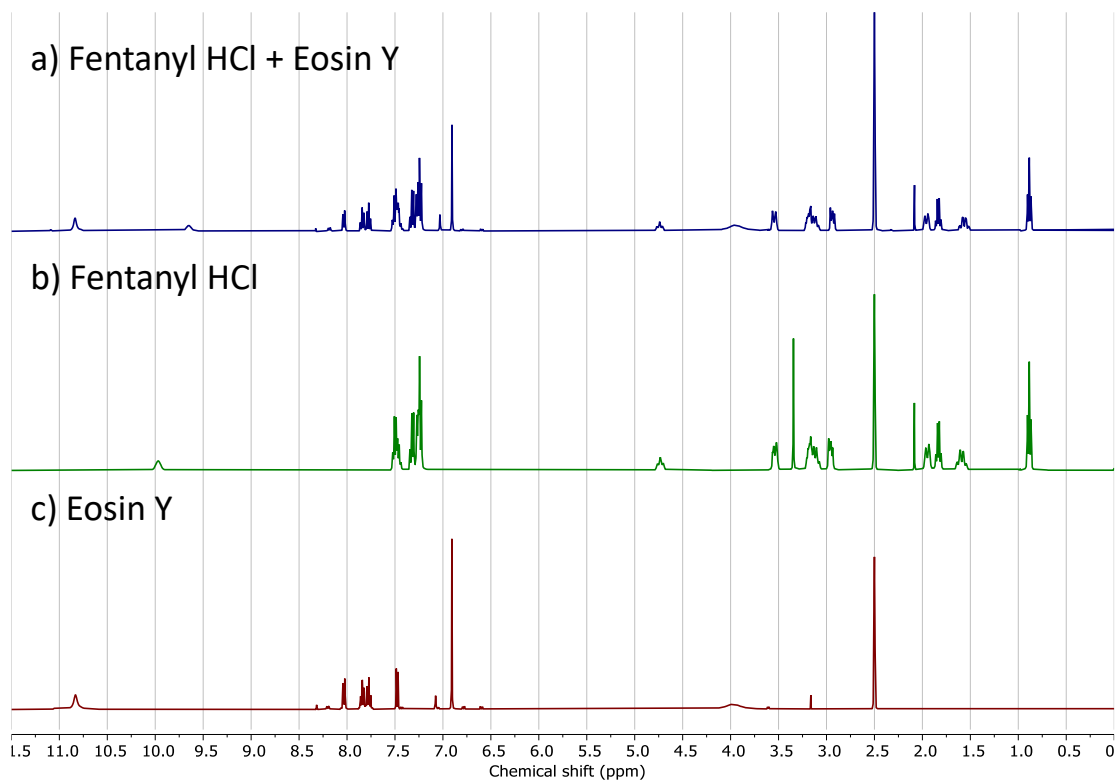


Figure 4.4. ¹H NMR spectra (400 MHz, DMSO-D₆) of a) Fentanyl HCl and eosin Y; b) Fentanyl HCl; c) Eosin Y.

Reacting fentanyl free-base with eosin Y does lead to a reaction, however. As it did with heroin, eosin Y appears to be deprotonated to the monoanionic species (Figure 4.5) while the fentanyl free-base appears to be protonated (Figure 4.6), pointing to a 1:1 acid-base reaction.

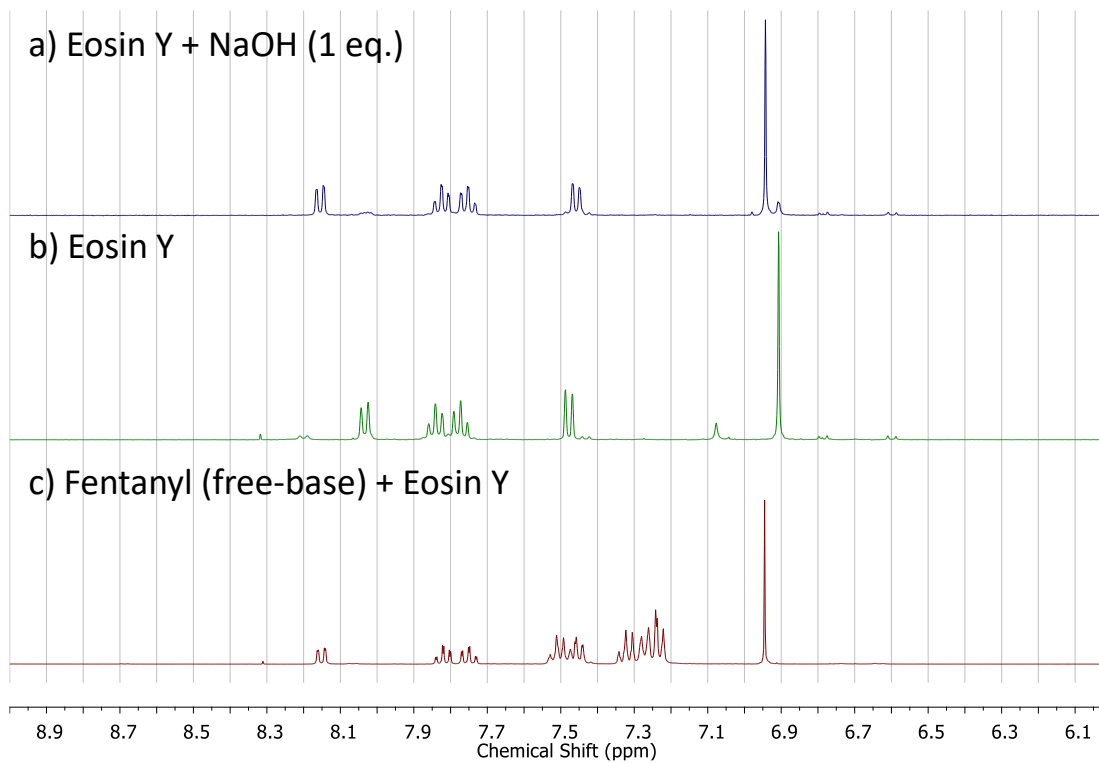


Figure 4.5. ¹H NMR spectra (400 MHz, DMSO-D₆) of a) Eosin Y deprotonated with NaOH (1 eq.); b) Eosin Y; c) Fentanyl free-base and eosin Y.

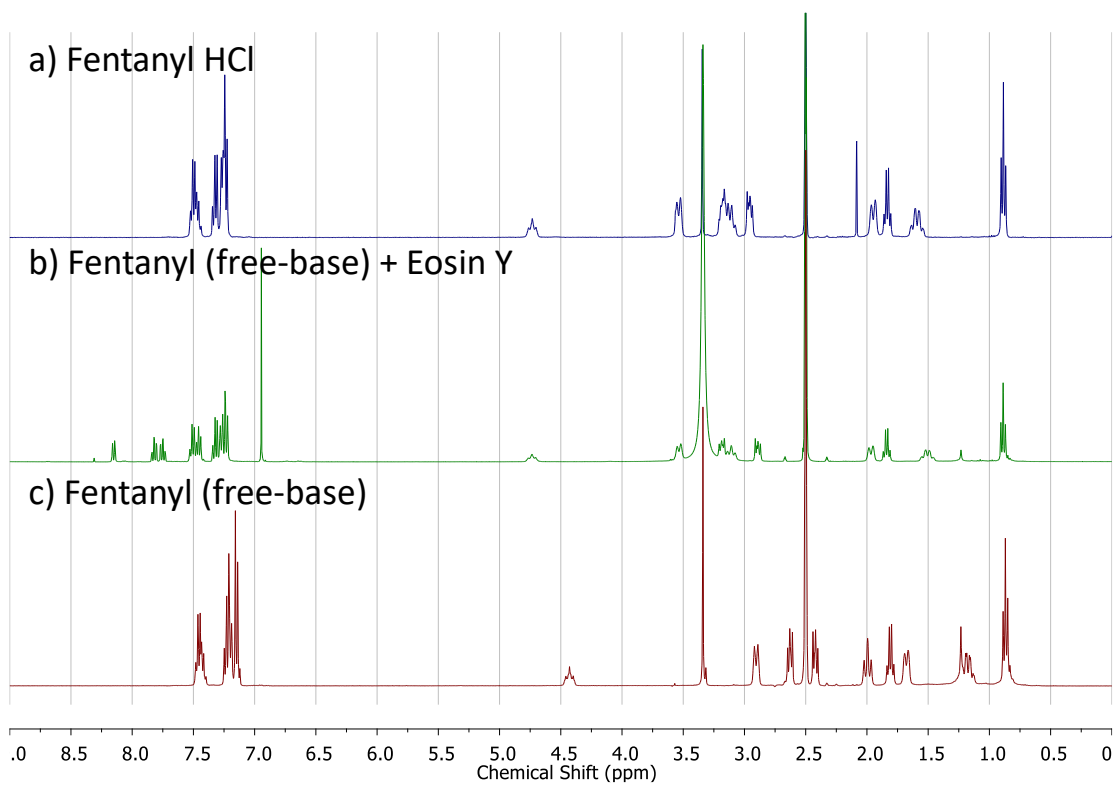


Figure 4.6. ¹H NMR spectra (400 MHz, DMSO-D₆) of a) Fentanyl HCl; b) Fentanyl free-base and eosin Y; c) Fentanyl free-base.

4.3.2 NMR Experiments (D₂O)

Further tests were conducted in D₂O, buffered with anhydrous K₂HPO₄ and adjusted to pH = 7 with concentrated DCl, to mimic typical test conditions. The residual water peak was removed from ¹H NMR spectra using solvent suppression; chemical shifts were referenced to 3-(trimethylsilyl)propionic-2,2,3,3-*d*₄ acid.

Figure 4.7 compares the individual spectra of caffeine and eosin Y in buffered D₂O against the mixture. At pH = 7, caffeine exists in its neutral form (pK_a of the C-8 proton = 14.0, pK_a of the ammonium salt = 0.6). [161] A shift could be observed in the eosin Y signals (Figure 4.7d-e), but the caffeine protons remained relatively unchanged (Figure 4.7a-b). This is very different to what was reported by Okuom *et al.* [159] Though they observed a very similar shift in eosin Y signals, they also saw substantial shielding of the caffeine signals. Comparison of chemical shifts shows that the caffeine reference spectrum in Figure 4.7 is consistent with theirs, and the difference lies in the mixture spectrum.

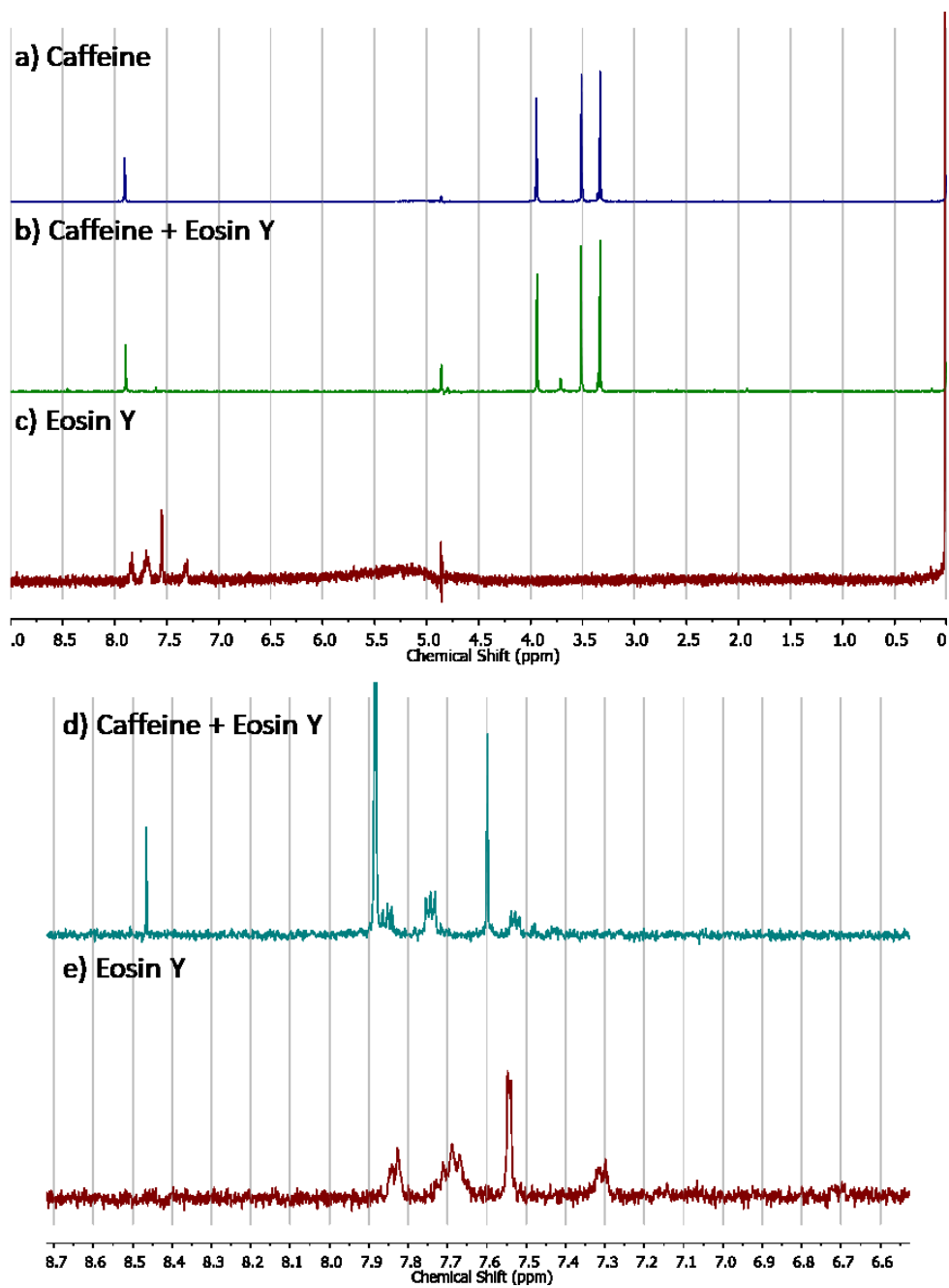


Figure 4.7. ^1H NMR spectra (400 MHz, D_2O) of a) Caffeine; b) Caffeine and eosin Y; c) Eosin Y; d) Caffeine and eosin Y (6.5–8.7 ppm region); e) Eosin Y (6.5–8.7 ppm region)

To try to explain the eosin Y shift, the eosin Y monoanion and dianion previously obtained were analysed in D₂O and compared to the neutral compound. Unsurprisingly, no difference could be observed between the three spectra. Eosin Y, which bears two acidic protons (pK_a = 2.0, 3.8), [162] should exist in its dianionic form at pH = 7. Neutral eosin Y and the monoanion were therefore deprotonated by the buffer, and the observed spectrum corresponds to the dianionic species. This may seem like a trivial experiment, but it indicates that whatever transformation occurs in the caffeine mixture is unlikely to be only a protonation of eosin Y; the buffer would simply deprotonate the conjugate acid of lower pK_a. There must, therefore, be some form of equilibrium or interaction with caffeine, which prevents this transformation from reverting.

What Okuom *et al.* propose is that eosin Y carboxylate (pK_a of the conjugate acid = 3.8) [162] deprotonates caffeine at the C-8 position (pK_a = 14.0), positing that “this proton is very labile and can be abstracted easily at pH = 7.” [159] This is simply untrue: the equilibrium depicted in Figure 4.8 should favour the formation of the weakest acid/base pair, or the “acid” with the highest pK_a. The dianionic eosin Y is not a strong enough base, as evidenced by the pK_a of its conjugate acid, to deprotonate caffeine. While the study reported a decrease in the relative intensity of the “labile” C-8 proton peak, this was not observed here. Also, though the authors imply that there is a mixture of protonated and deprotonated caffeine is present in solution, they only report one set of peaks.

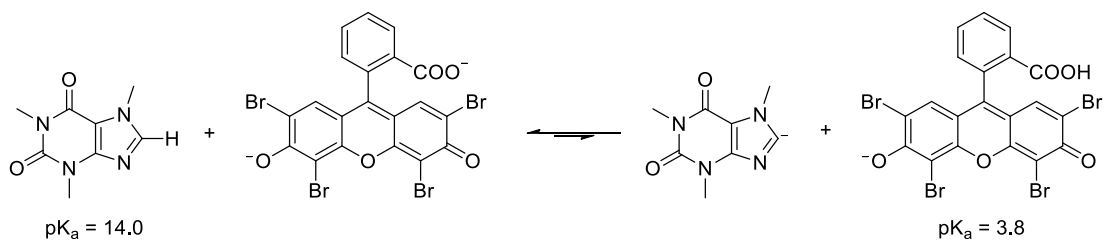


Figure 4.8. Acid-base equilibrium between caffeine and eosin Y.

Heroin was investigated next. With a pK_a of 7.95 in water, [163] 90% of the drug should be ionised in the $pH = 7$ buffer, making it mostly soluble. Therefore, the NMR spectrum of heroin (Figure 4.9a) is that of a soluble protonated species, but the ammonium proton signal is not visible as it is being exchanged with the solvent. When heroin was mixed with eosin Y, no change was observed in the heroin signals (Figure 4.9). The eosin Y signals in the mixture were shifted downfield or upfield by up to 0.1 ppm, depending on the signal. (Figure 4.10) This is similar to the results obtained with caffeine.

Again, if eosin Y were protonated by heroin in these conditions, it would instantly be deprotonated by the buffer. There must be an interaction between eosin Y and heroin, causing the shift in eosin Y signals.

Eosin Y was not completely soluble in the buffer, and particles had to be removed by decantation, which may explain why eosin Y signals in Figure 4.9c are much weaker than the heroin signals. Even a minute quantity of eosin Y reacting with heroin may cause a noticeable colour change; the overwhelming excess of heroin would remain unreacted, and no significant change in chemical shift or integration of the heroin signals may be detected. This may

also be the reason why no shift was observed in the caffeine signals in Figure 4.7.

Looking at eosin Y and heroin, the simplest explanation may be an ionic interaction between the two. Eosin Y would go from a free dianionic species to one where its carboxylate interacts with heroin. This involvement of the carboxylate electrons in an ionic interaction may be enough to shift the aromatic proton signals, but also produce a colour change.

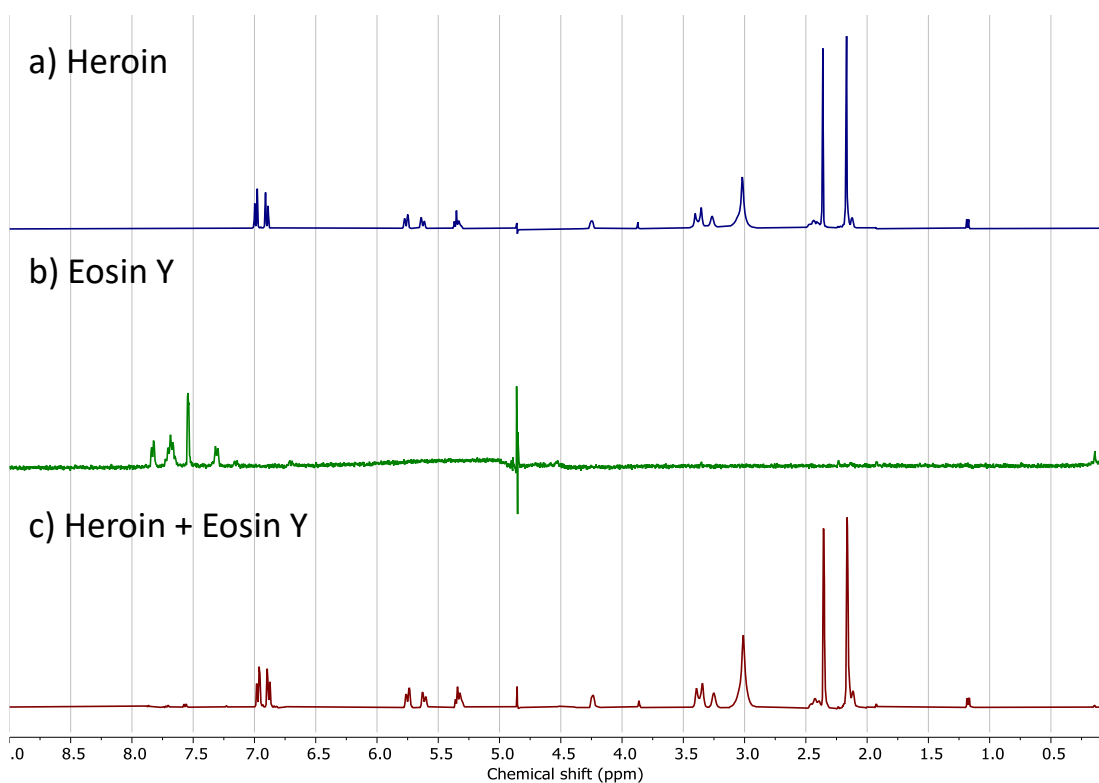


Figure 4.9. ^1H NMR spectra (400 MHz, D_2O) of a) Heroin free-base; b) Eosin Y; c) Heroin free-base and eosin Y.

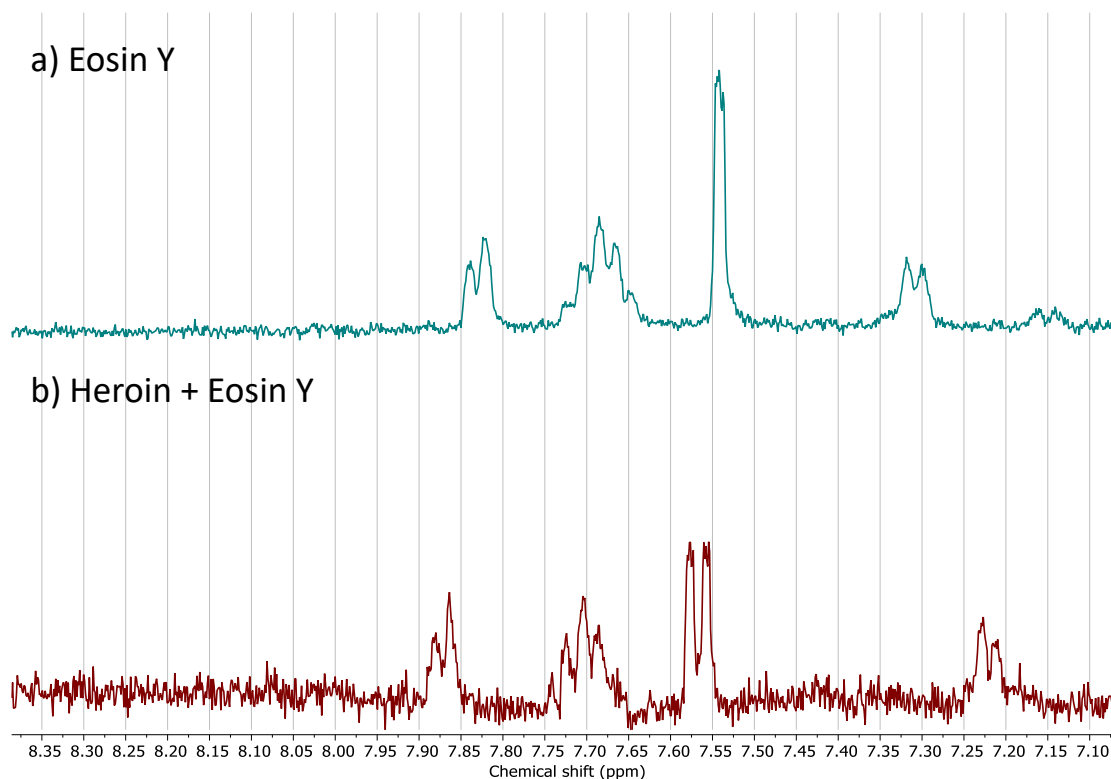


Figure 4.10. Aromatic region of the ^1H NMR spectra (400 MHz, D_2O) of a) Eosin Y; b) Heroin free-base and eosin Y.

Fentanyl was investigated next. In buffered D_2O , fentanyl HCl should exist in its protonated form ($\text{pK}_a = 8.4$). This is confirmed by a comparison with spectra of fentanyl HCl and free-base in DMSO; the $\text{pH} = 7$ spectrum corresponds almost exactly to the HCl salt spectrum in DMSO.

The reaction between fentanyl and eosin Y produces a deep pink precipitate. Filtration removes this precipitate, leaving a colourless solution. Analysis of the supernatant reveals only unmodified fentanyl HCl (Figure 4.11).

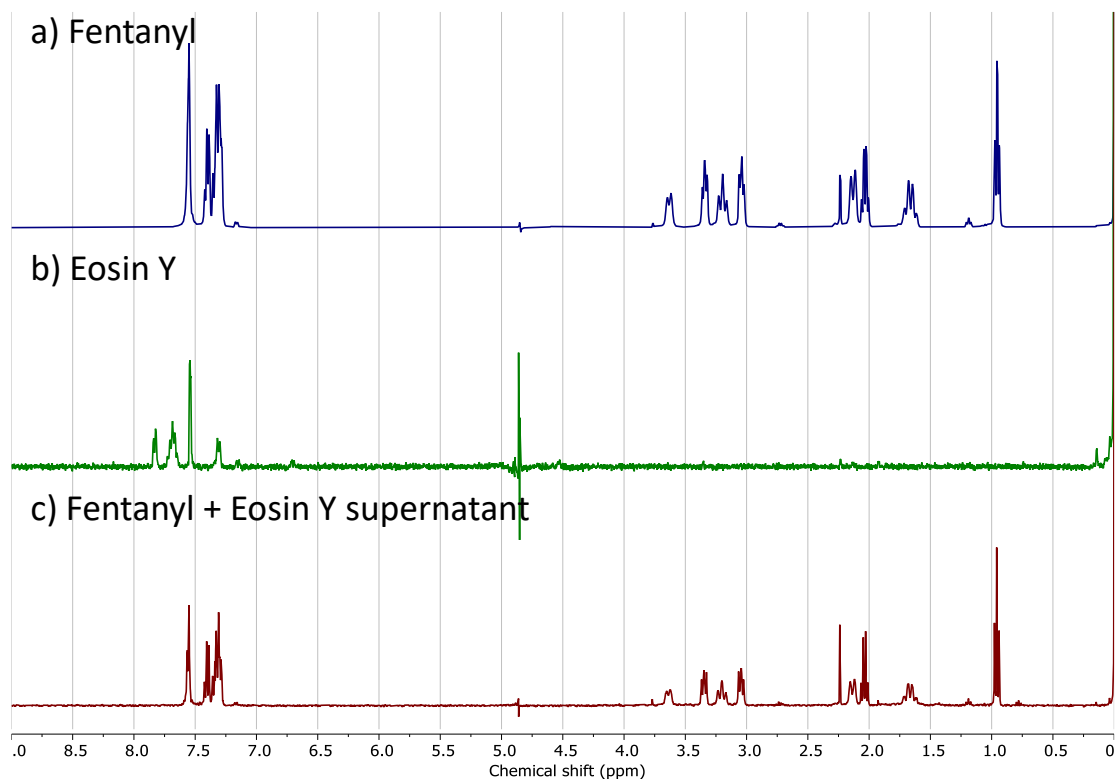


Figure 4.11. ¹H NMR spectra (400 MHz, D₂O) of a) Fentanyl HCl; b) Eosin Y; c) The supernatant obtained from mixing fentanyl HCl and eosin Y.

The precipitate was analysed in DMSO-D₆, as it was insoluble in water (see Figure 4.12c). No eosin Y peak was observed. The aromatic region remains mostly unchanged from fentanyl (Figure 4.12b), apart from a slight deshielding in some of the signals. The propionyl signals are consistent with fentanyl, but the piperidine ring and phenethyl-chain signals are shifted and very broad, and no NH⁺ signal is visible. This points to a deprotonation of the ammonium salt, confirmed by a comparison with fentanyl free-base (Figure 4.12a). Figure 4.13 clearly shows the similarity between the precipitate and fentanyl free-base, except for small differences in chemical shifts and the broadening of piperidine

and phenethyl signals. The same phenomenon occurred in ^{13}C NMR spectra: no difference in shift is observed in the aliphatic region, only a broadening of certain signals (see Figure 4.14).

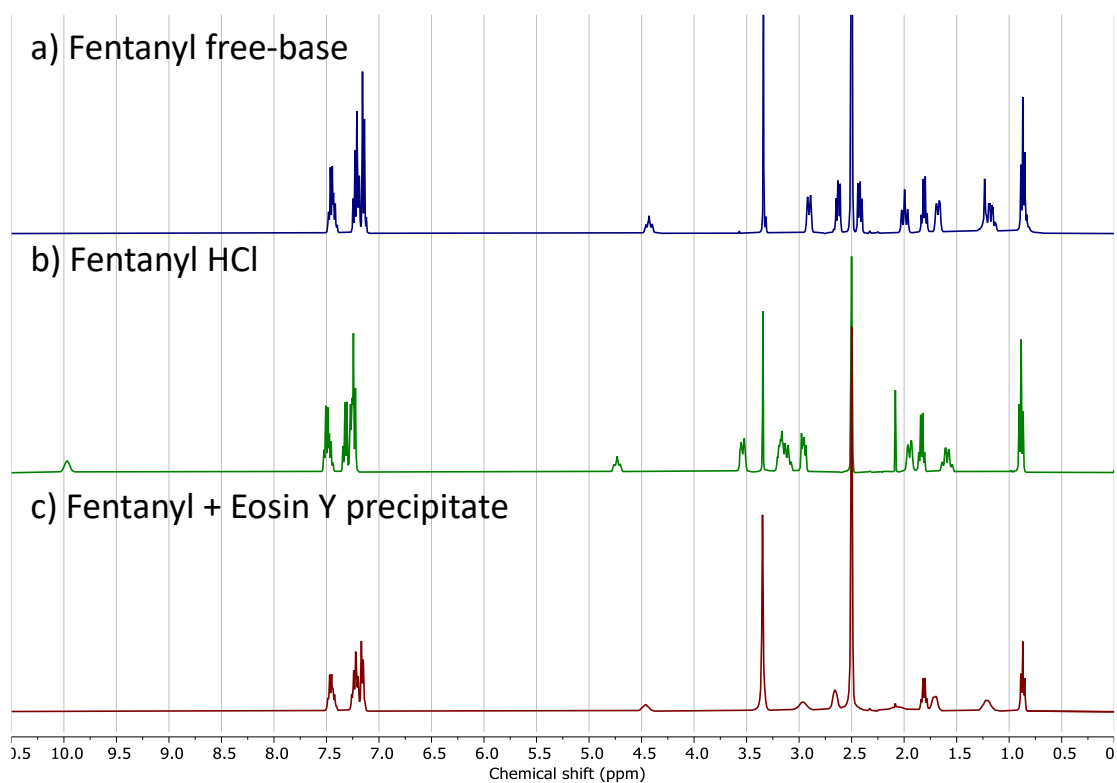


Figure 4.12. ^1H NMR spectra (400 MHz, DMSO-D_6) of a) Fentanyl free-base; b) Fentanyl HCl; c) The precipitate obtained from mixing fentanyl HCl and eosin Y.

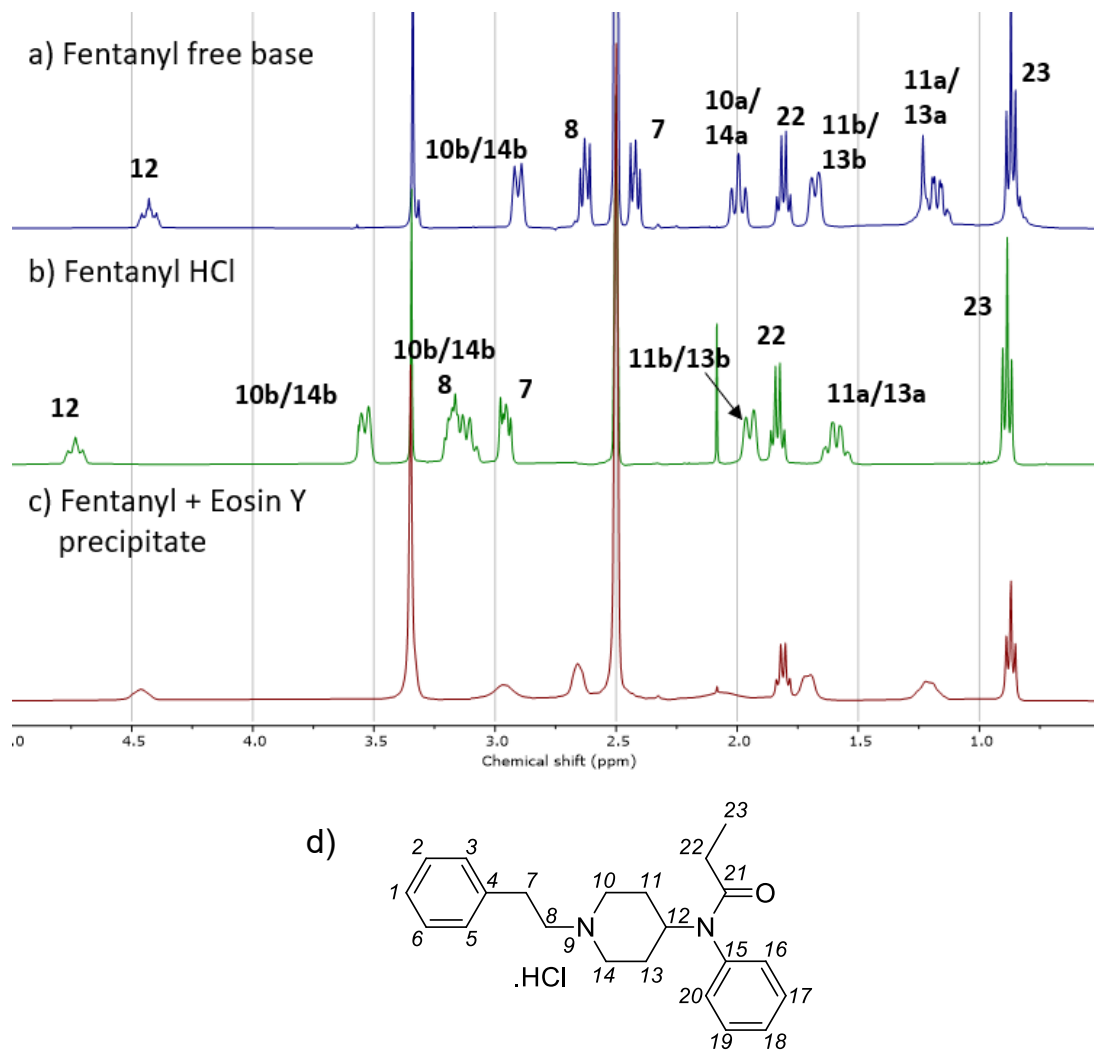


Figure 4.13. Chemical structure of fentanyl and ^1H NMR spectra (400 MHz, DMSO-D_6) of a) Fentanyl free-base; b) Fentanyl HCl; c) The precipitate obtained from mixing fentanyl HCl and eosin Y; d) Chemical structure of fentanyl.

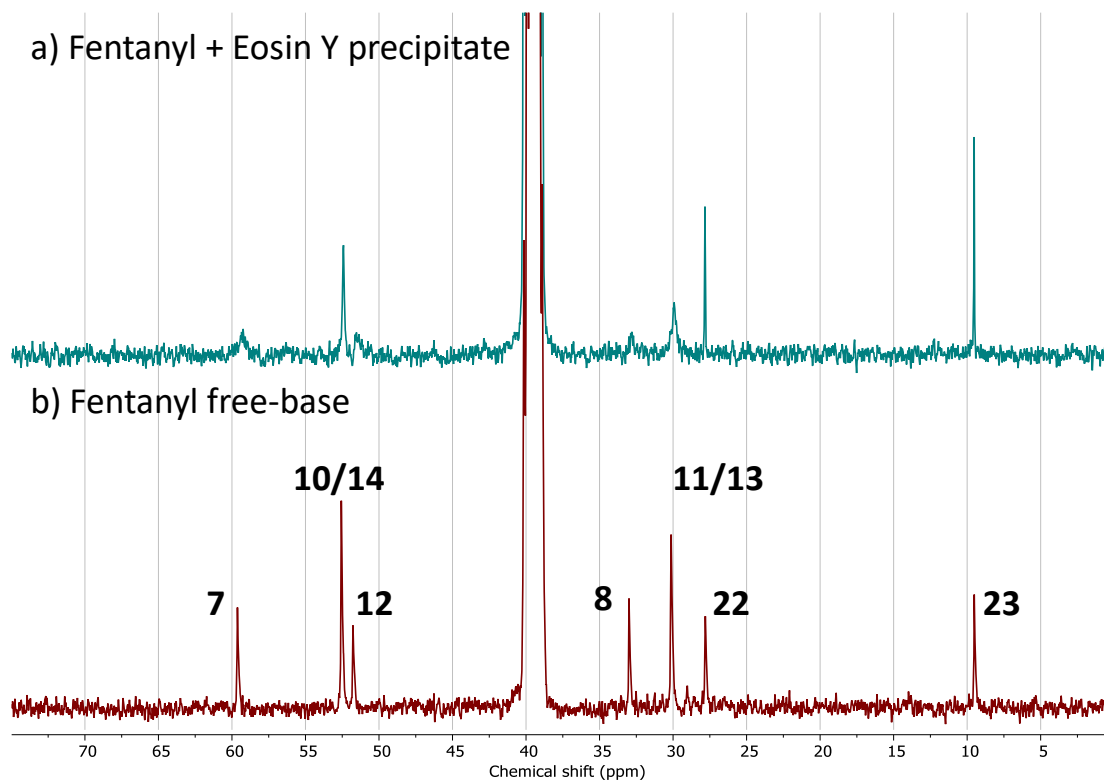


Figure 4.14. ¹³C NMR spectra (400 MHz, DMSO-D₆) of a) The precipitate obtained from mixing fentanyl HCl and eosin Y; b) Fentanyl free-base.

A comparison of IR spectra is consistent with the NMR analysis. The spectrum of the precipitate (Figure 4.15), when compared with fentanyl HCl (Figure 4.16), shows the absence of ammonium salt peaks at 2449 and 2403 cm⁻¹. The precipitate looks very similar to fentanyl free-base (Figure 4.17), but small differences in wavenumbers set both compounds apart.

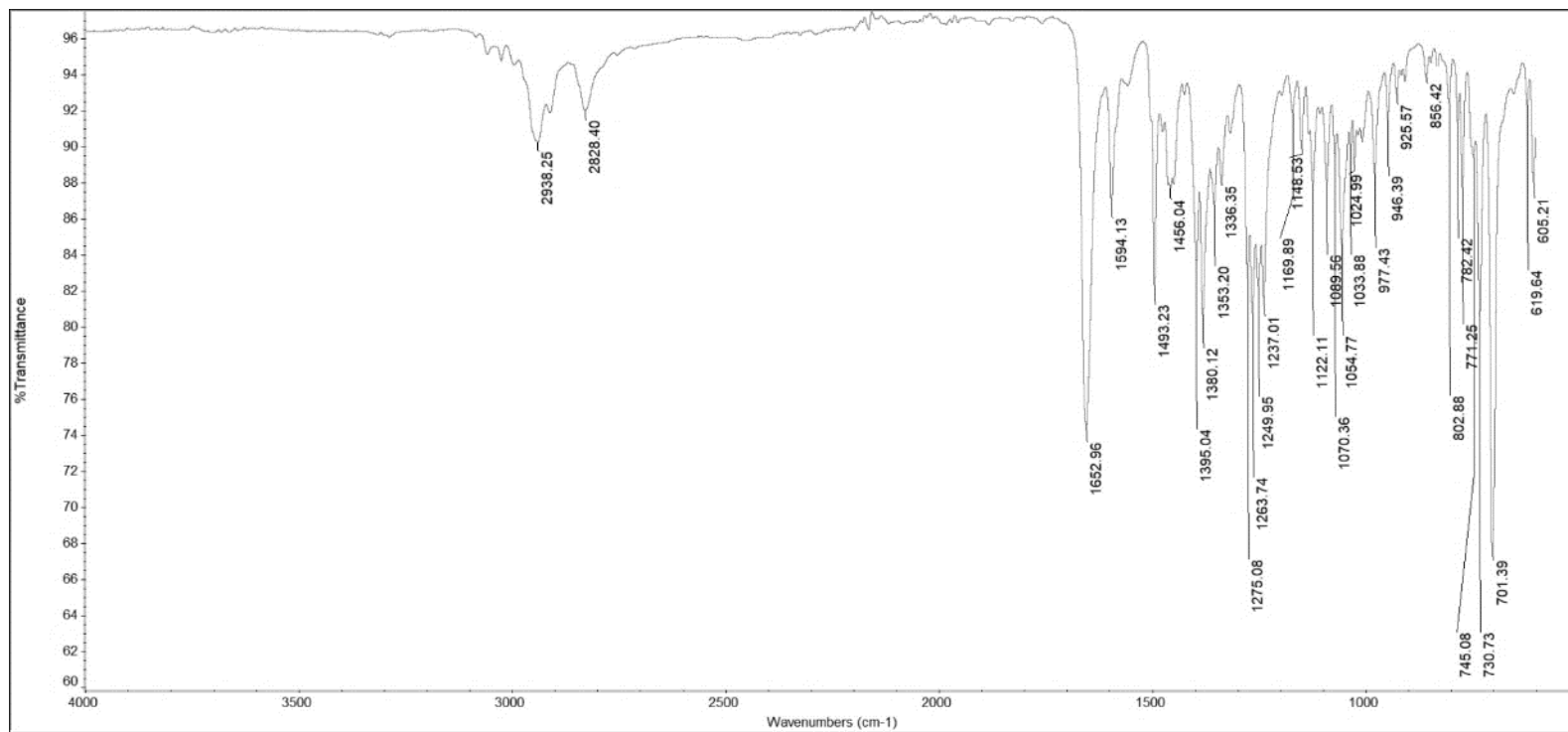


Figure 4.15. ATR-FTIR spectrum of the precipitate obtained from fentanyl and eosin Y.

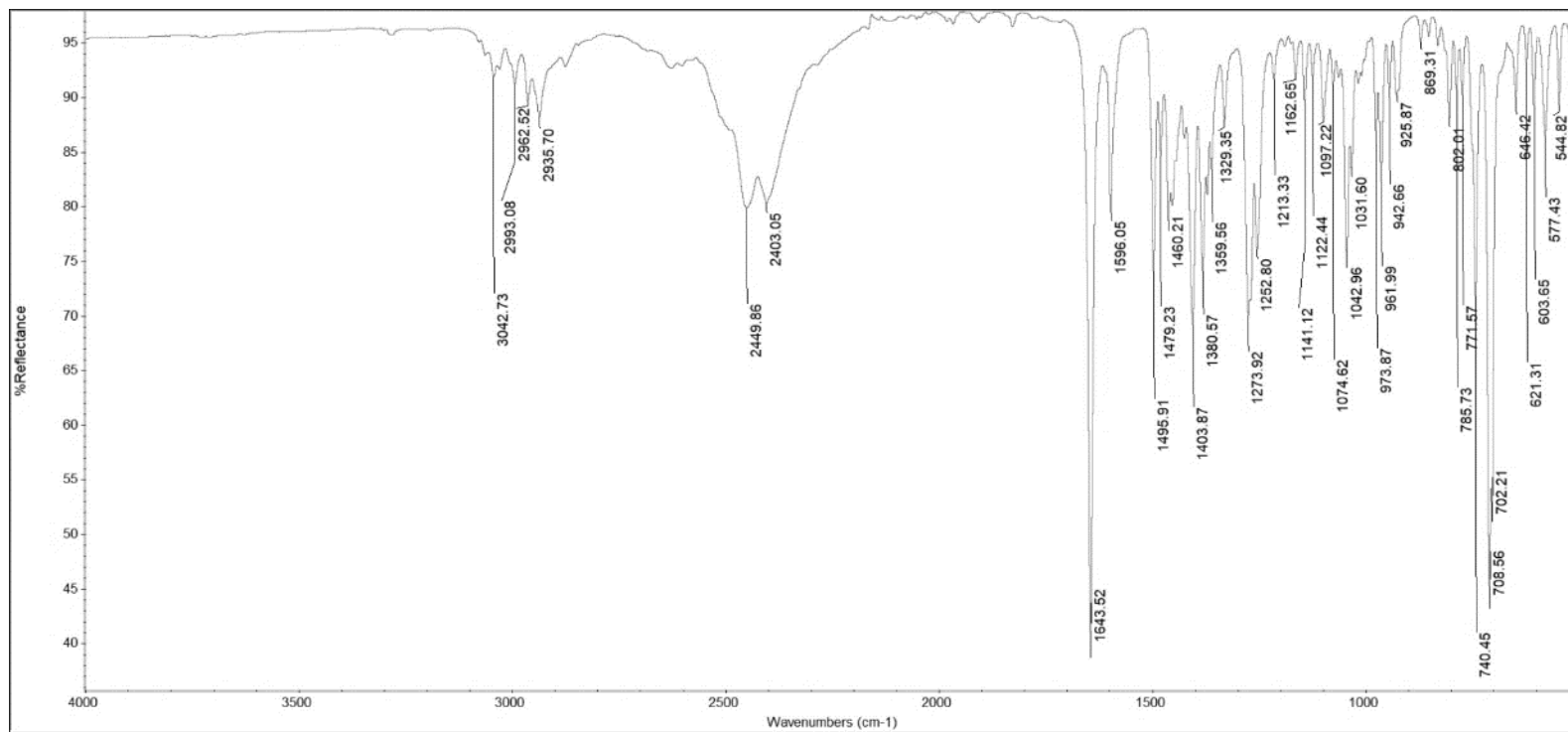


Figure 4.16. ATR-FTIR spectrum of fentanyl hydrochloride.

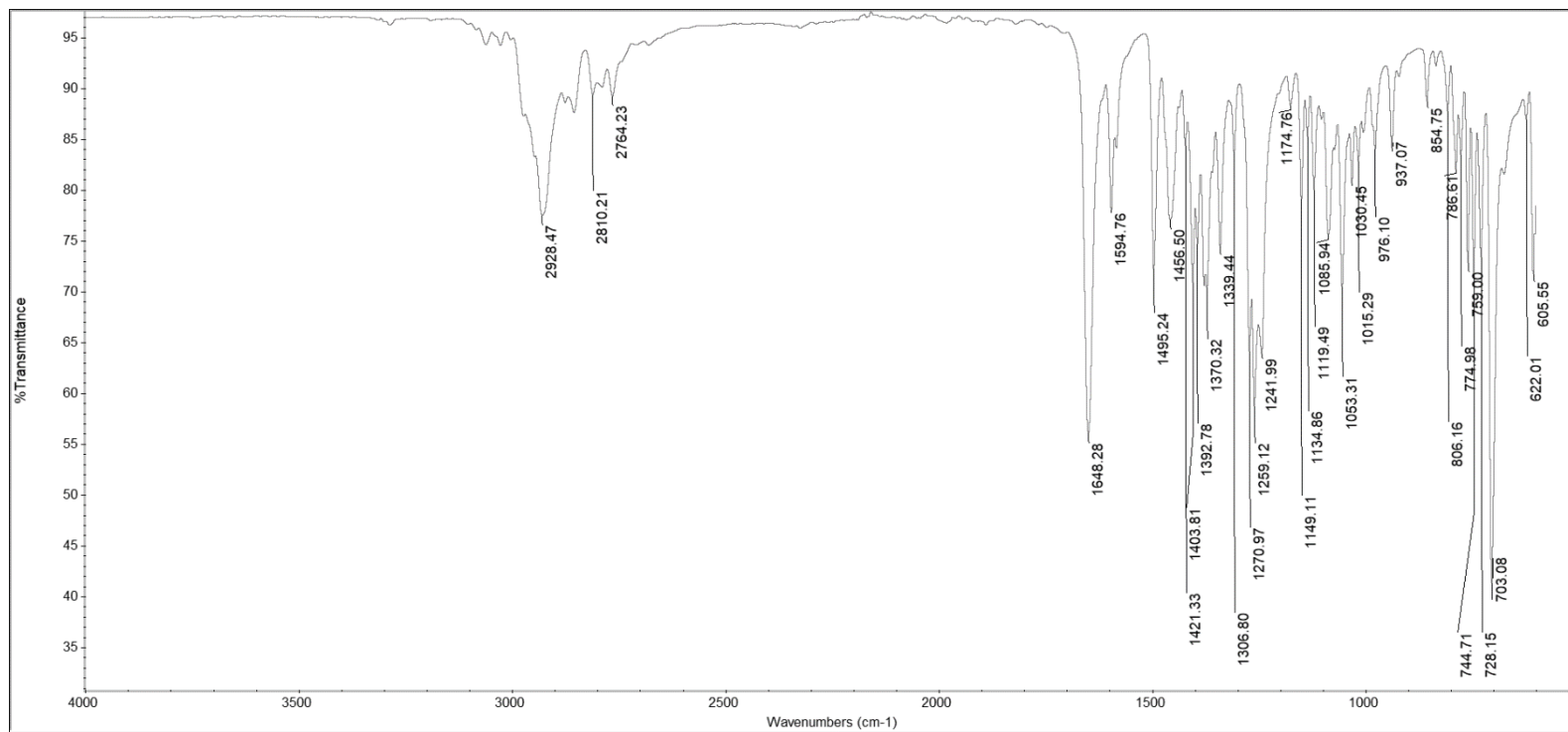


Figure 4.17. ATR-FTIR spectrum of fentanyl free-base.

Because the precipitate is pink, it follows that some eosin Y has precipitated with fentanyl. Eosin Y peaks are invisible in the precipitate, but even in amounts undetectable by NMR, eosin Y, which is a very potent dye, can produce an intense coloration. Moreover, eosin Y peaks were already quite weak in the original stock solution (see Figure 4.11b), because of its low solubility in buffered D₂O. It is also possible that some eosin Y remains in solution and gets trapped in the filter when the filter is isolated: it has been observed that filtration of an aqueous solution of eosin Y through a 0.45 μm filter completely removes the dye, resulting in a colourless solution. The filter can then be washed with methanol to release an orange eosin Y solution. It is thus conceivable that the quantity of eosin Y remaining in the precipitate is undetectable by NMR. GC-MS analysis of the precipitate only reveals the presence of fentanyl, but eosin Y is not volatile enough to be detected.

In ¹H-¹H COSY (see Figure 4.18), couplings are only observable in the propionyl chain and in the aromatic region. All couplings between the broadened piperidine and phenethyl signals have disappeared, which is very unlike fentanyl free-base.

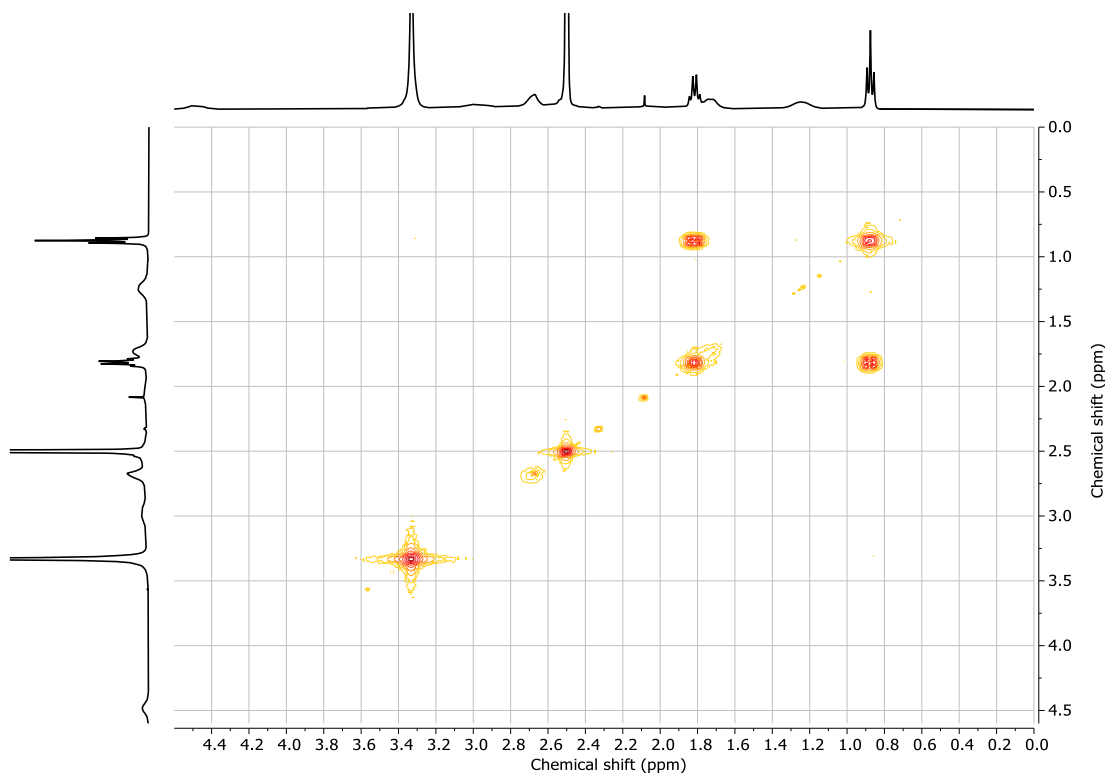


Figure 4.18. ^1H - ^1H COSY spectrum of the precipitate obtained from fentanyl and eosin Y (400 MHz, DMSO-D_6).

The fact that only part of the molecule is so affected points to a certain exchange or “fluxionality” happening in this portion of the molecule on the NMR timescale. [164, 165] As an example, if the $\text{CH}_2\text{-CH}_3$ bond of the fentanyl molecule were fixed in space, all protons of the methyl group would have different chemical environments. In reality, rotation around this bond happens so quickly in comparison to the NMR timescale that all CH_3 protons have effectively the same chemical environment, resulting in an averaged signal of a neatly defined triplet. However, if such a process happened at a slower rate, it could be observed in NMR as a widening of peaks as signals would be only

partially averaged. The rate of some such processes can be changed simply by modifying observation conditions such as temperature or pH. [164]

In this case, a possible candidate for such a process is the axial-equatorial equilibrium of the piperidine ring. Jones *et al.* reported the conformational ΔG° values of a similar molecule, 4-*p*-chlorophenyl-1-ethylpiperidine (see Figure 4.19). [166] They noted that the aromatic substituent favoured an equatorial conformation by a ΔG° of 3.0 kcal/mol, but that inversion of the *N*-ethyl chain occurred much more readily, with a ΔG° of only 0.87 kcal/mol (in benzene). According to their calculations, this meant that 81% of the population existed as the equatorial-equatorial conformer and 19% as the equatorial-axial. In normal conditions, inversion between both conformers would occur very quickly and would not be detectable by NMR spectroscopy.

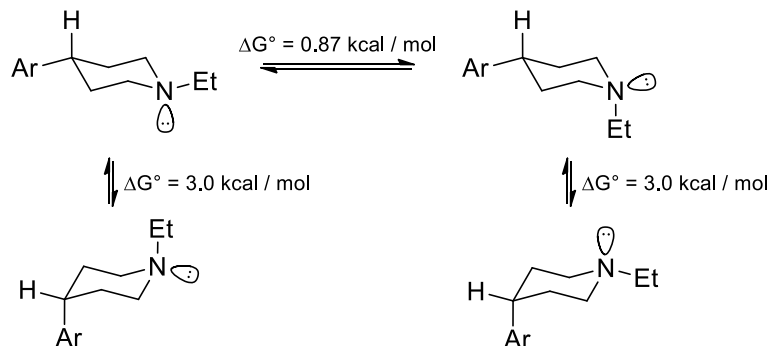


Figure 4.19. Conformational equilibria of 4-*p*-chlorophenyl-1-ethylpiperidine and corresponding ΔG° values calculated by Jones *et al.* [166]

As reported by Jackman and Sternhell in their explanation of time-dependent effects in NMR spectroscopy, the rate of certain intramolecular motions can be changed by a modification of pH. [164] The conformational equilibrium between

equatorial and axial piperidine conformers can conceivably be slowed down by an acid-base equilibrium induced by the presence of small quantities of a weak acid, since protonation of the piperidine would make the inversion more difficult. Protonated eosin Y is a weak acid, and the presence of eosin Y in the pink precipitate is, after all, what differentiates it from regular fentanyl free-base.

To test the hypothesis of fluxionality, ^1H NMR spectra were taken at increasing temperatures (see Figure 4.20). A noticeable change occurred in the signal at 1.91 ppm, tentatively attributed to protons 11/13 of the piperidine ring, which started to split at higher temperatures. This is consistent with a quicker conformational inversion of the piperidine ring. In contrast, the CH_2 quartet (1.83 ppm) started to coalesce at higher temperatures. A shift was observed in most of the other signals, but no significant change in multiplicity.

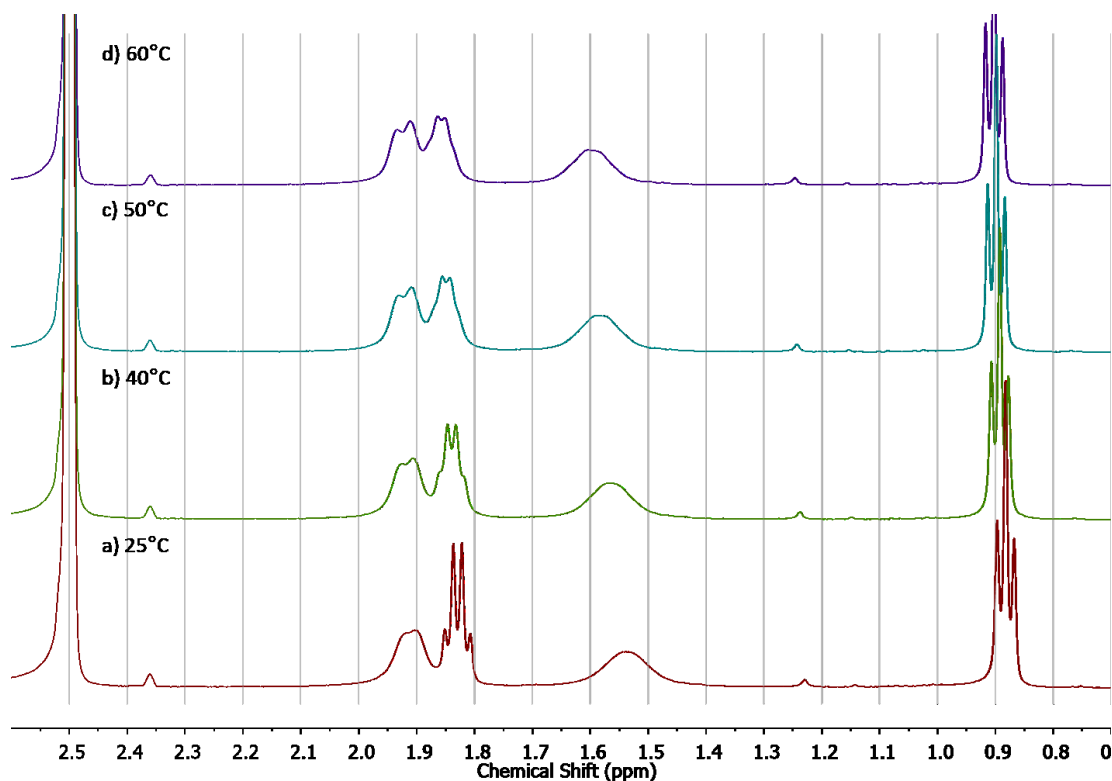


Figure 4.20. ^1H NMR spectra (400 MHz, DMSO-D_6) of the precipitate obtained from fentanyl and eosin Y, taken at 25, 40, 50 and 60°C .

The observed colour change may thus partly be explained by the deprotonation of fentanyl by eosin Y. After all, fentanyl does not readily form an insoluble free-base when dissolved in the buffer, so it follows that it is being deprotonated by eosin Y. Then, eosin Y co-precipitates with fentanyl free-base. The colour of eosin Y depends on what solvent it is dissolved in, and it has a different colour in its solid state. The characteristic colour of the precipitate is therefore due to it containing eosin Y as a solid (deep pink) rather than being dissolved on its own in water (peach) or in a mixture with caffeine/heroin (light pink).

Some trends can be observed in this study. First of all, eosin Y reacts with amines. This includes *tertiary* and aromatic amines (fentanyl, heroin, caffeine) but results from Table 4.1 show that it also reacts with MDMA, a secondary amine. It did not react with benzocaine (aromatic amine) but it did with procaine, which only differs from the former in that it contains an aliphatic *tertiary* amine on its ester chain.

Secondly, with reactive analytes, the colour change produced depends on whether the analyte precipitates when it comes in contact with eosin Y. This is the case for most fentanyl analogues, but not all. For instance, 3-fluorofentanyl does not precipitate and produces the same colour change as heroin. The colour change may thus solely depend on the pK_a of the amine. While fentanyl HCl has a pK_a of 8.44 in water, 3-fluorofentanyl HCl has a lower pK_a of 6.8, closer to that of heroin. [1, 167]

It may seem that, because eosin Y can react with all *tertiary* amines in a certain pK_a range, this test lacks in selectivity for forensic purposes. However, compounds that are likely to be found in mixtures with fentanyl do not bear such an amine. That is, to be truly effective, a presumptive test does not need to exclude all existing chemical compounds, but simply the suspected population of substances that may be encountered with or confused for fentanyl in forensic cases. The fact that it produces a specific colour change with fentanyl derivatives and not with heroin, cocaine, MDMA and their adulterants is proof enough of the selectivity of this test.

However, another issue must be addressed to make this eosin Y test reliable, and that is the inherent subjectivity of presumptive colour tests.

4.4 Standardisation of colorimetric tests

The results shown in Table 4.1 are based on an appreciation of the colour change with the naked eye. Colour perception is deeply subjective, making presumptive colour tests less reproducible across different experimenters. This can be avoided by defining colour in quantitative terms: when a substance absorbs certain wavelengths in the visible light spectrum, its colour is a result of the remaining (reflected) wavelengths.

4.4.1 Visible light spectrophotometry

The colour of a substance is directly linked to its visible light absorption spectrum, and the fentanyl-eosin Y colour change can be measured using spectrophotometry. Figure 4.21 shows the visible light absorption spectra of eosin Y on its own and as a mixture with heroin and fentanyl. While the eosin Y solution has an absorbance maximum at $\lambda = 517$ nm, a shoulder is clearly visible in the fentanyl-eosin spectrum at $\lambda = 550$ nm. Fentanyl does not absorb in the visible light spectrum, so it can reasonably be assumed that the peak at 550 nm results from the fentanyl-eosin interaction and leads to the colour change.

The eosin Y – heroin mixture should produce a pink colour, which appears distinct from that of eosin Y on its own. This is not observed in Figure 4.21a, because the colour change is susceptible to the concentration of the eosin Y solution used. Spectra in Figure 4.21 were acquired at only 20 μ M eosin Y, rather than the 150 μ M used for presumptive tests. This is because a 150 μ M eosin Y solution saturates the detector of the spectrophotometer, and absorbance maxima cannot be detected. While fentanyl still reacts at this lower concentration, it takes a much higher dye content to produce a colour change

with heroin, hence why the heroin-eosin Y spectrum shows no difference from the eosin Y solution. This higher sensitivity for fentanyl may allow the detection of fentanyl in heroin samples, as was previously observed in Chapter 2 with sample SS-1.

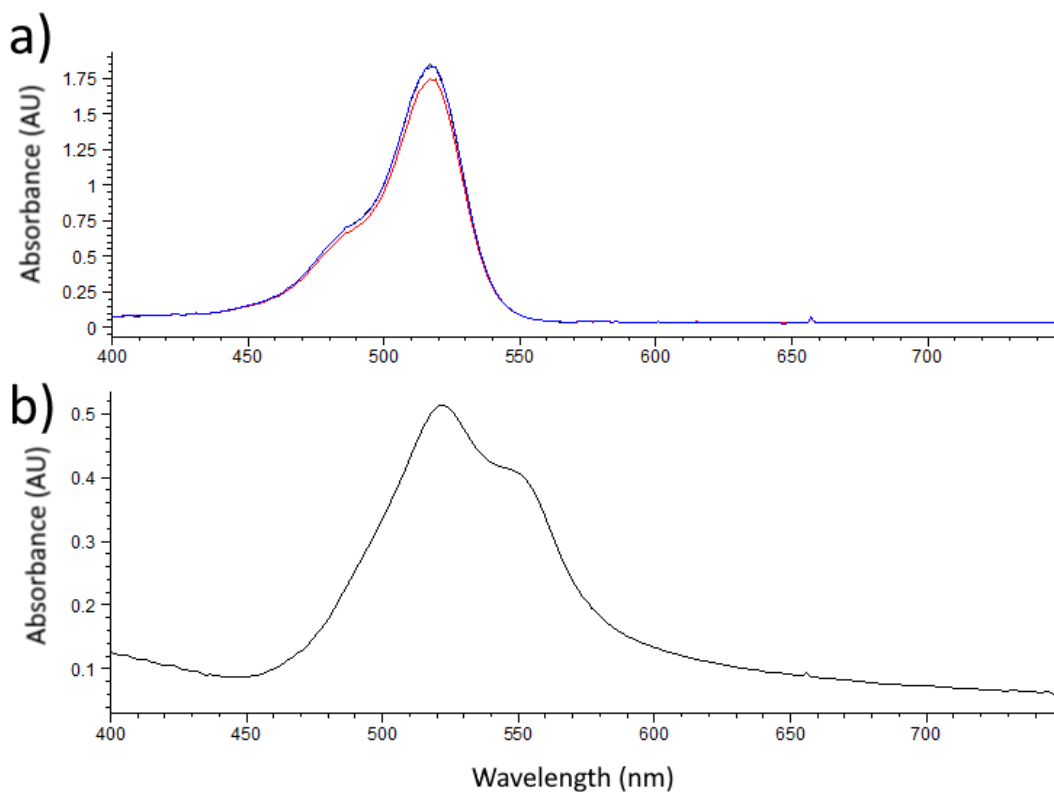


Figure 4.21. a) Visible light absorption spectra of eosin Y (red) and a heroin/eosin Y mixture (blue); b) Visible light absorption spectrum of a fentanyl/eosin Y mixture.

Using this technique, the absorbance at a wavelength specific to the eosin Y – fentanyl mixture can be measured. Because absorbance is proportional to the

concentration of the attenuating species, according to the Beer-Lambert law, this technique could be used to quantify fentanyl.

To achieve this, the optimal concentration of eosin Y had to be determined. A stock solution of fentanyl was prepared at 1 mg/mL in methanol. Volumes ranging between 0.1 – 1 mL (0.1 – 1 mg fentanyl) were transferred to vials and evaporated *in vacuo*. The dried solids were reconstituted in aqueous eosin Y at varying concentrations (150, 500, 750 or 1500 μM). Before acquisition, the eosin Y solution was used as a blank on the spectrophotometer. This subtracts the high-intensity absorbance due to the excess eosin Y. Figure 4.22 shows the resulting spectrum, with the subtracted region between 450 – 550 nm, and a defined fentanyl – eosin Y maximum centred on $\lambda = 568 \text{ nm}$.

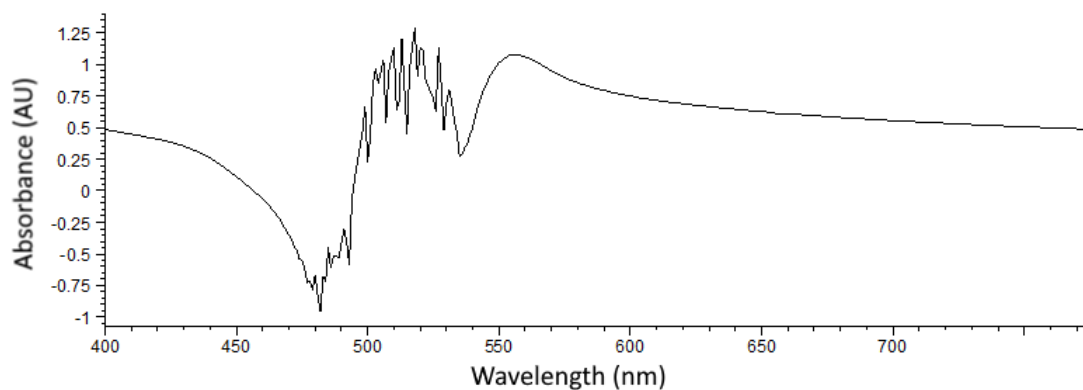


Figure 4.22. Visible light absorption spectrum of 500 mg fentanyl reconstituted in 150 μM eosin Y (2 mL) after eosin Y subtraction.

Reconstitution in 2 mL eosin Y at concentrations 150, 500 or 750 μM proved insufficient to fully react with higher amounts of fentanyl. Figure 4.23 shows an example calibration graph using 2 mL of the 750 μM solution, which plateaus at 800 mg fentanyl. The 1500 μM eosin Y solution proved unusable: its absorbance was so intense that the blank subtracted the fentanyl – eosin Y peak. Instead, samples were reconstituted in 5 mL of the 750 μM eosin Y solution. Though this dilutes samples more and thus decreases sensitivity, it provides a high enough quantity of eosin Y to completely react with 1 mg fentanyl.

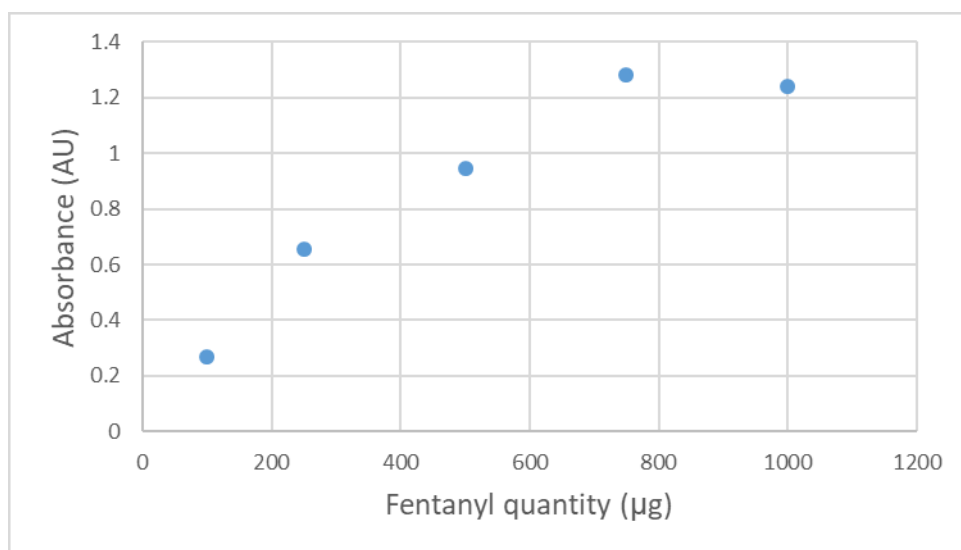


Figure 4.23. Absorbance at $\lambda = 568 \text{ nm}$ of fentanyl reconstituted in eosin Y 750 μM (2 mL).

The detection wavelength was optimised next. Using the same five solutions of fentanyl reconstituted in 5 mL eosin Y at 750 μM , absorbance was measured at wavelengths ranging from 568 to 600 nm. The resulting calibrations graphs

were plotted and the R^2 calculated to determine which wavelength resulted in the most linear graph. Results are reported in Table 4.4. Increasing the detection wavelength to $\lambda = 590$ nm resulted in the most linear graph, likely because the subtracted region of the absorbance spectrum is noisier and less reproducible. This comes with a loss of sensitivity, however, and wavelengths higher than 590 nm could not be used, as they returned an absorbance of 0 for the 0.1 mg fentanyl sample. The resulting calibration graph at 590 nm is shown in Figure 4.24.

To determine whether this method was also suitable to detect fentanyl in heroin samples, 1 mg heroin was reconstituted in 5 mL eosin Y (750 μ M). At $\lambda = 590$ nm, a negligible absorbance of 0.0035 AU was obtained. In comparison, 0.1 mg fentanyl results in an absorbance of 0.0700 AU, showing that there is minimal interference from heroin at this wavelength.

Table 4.4. Determination coefficient (R^2) of the fentanyl calibration graph (0.1 – 1.0 mg reconstituted in 5 mL eosin Y 750 μ M) at different detection wavelengths.

Wavelength (nm)	R^2
568	0.9788
570	0.9811
575	0.9854
580	0.9880
585	0.9898
590	0.9908

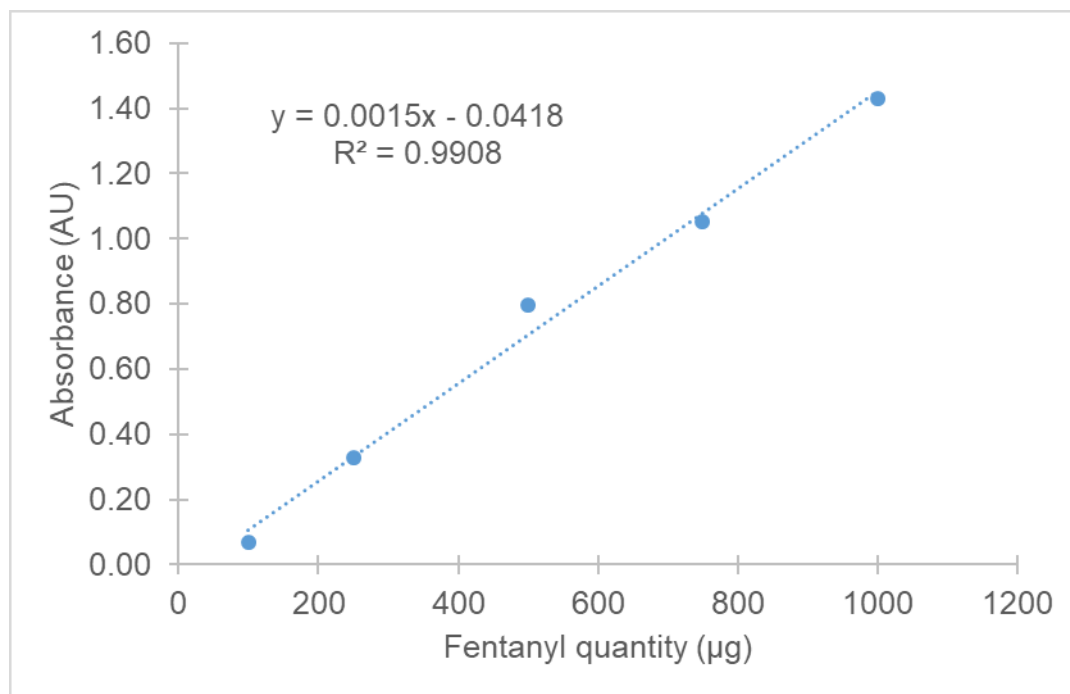


Figure 4.24. Absorbance at $\lambda = 590$ nm of fentanyl reconstituted in eosin Y 750 μM (5 mL).

With encouraging first results, a full calibration was prepared, with six replicates for each concentration. Results are shown in Table 4.5. This experiment highlighted a lack of reproducibility across multiple replicates of the same concentration, as evidenced by the very high relative standard deviation values. This time, absorbance at 1.00 mg fentanyl was lower than at 0.50 or 0.75 mg. This is most likely due to suspensions in solution: as discussed previously, the reaction between fentanyl and eosin Y causes fentanyl free-base to precipitate. The presence of solid matter in the light path causes the absorbance to be unreproducible. Filtration before analysis is not an option, as this removes all colour from the solution. The addition of a co-solvent was also

tested: methanol does not completely dissolve the particles, while DMSO results in the loss of the pink colour.

Table 4.5. Calibration of fentanyl reconstituted in 5 mL eosin Y 750 μ M.

Fentanyl quantity (mg)	Average absorbance (n = 6)	%RSD (n = 6)
0.10	0.0479	41.4
0.25	0.1621	29.5
0.50	0.6747	28.6
0.75	0.6806	9.4
1.00	0.5852	12.3

Visible light spectrophotometry remains very useful as a way of standardising presumptive colour tests. In the case of eosin Y, it provides quick and simple detection of fentanyl in seized heroin samples. However, it is only suitable for qualitative, and not quantitative, analysis. Solgels were explored as an alternative solution to this problem.

4.4.2 Qualitative solgel analysis

Solgels are polymer gels made from colloidal solutions of monomers. In this case, they were synthesised from a solution of tetraethoxysilane and eosin Y, so the test reagent would be incorporated in the resulting gel after polymerisation. Solgels have been used previously as a support for the Simon presumptive reagent, and were used for MDMA quantification. [168] Results were photographed using a smartphone and quantification was based on RGB values. The advantage is that solgels create a homogeneous medium, even if particulates are present, and the measurement of RGB values is based entirely on colour, or reflected light, rather than absorbance.

An initial optimisation of the solgel preparation was performed. A 2:1:2 mixture of tetraethoxysilane, aqueous HCl (0.04 M) and ethanol was prepared (solution A) and mixed with eosin Y in an aqueous pH = 7 buffer (solution B). Solutions A and B were mixed in a 1:2 ratio and 75 μL of the resulting solgel was quickly transferred to a 200 μL Eppendorf tube before the polymerisation started. 150 μL of a 0.1 mg/mL fentanyl solution in methanol was added to the polymerised solgel. Tests performed using 150 or 500 μM eosin Y as solution B showed no visible colour change, while 1000 μM proved optimal. Colour changes at this concentration were observed from 0.1 to 1.0 mg/mL fentanyl (see Table 4.6). Photographs were taken with a Huawei Mate 10 Pro smartphone and RGB values were measured with the paint.net free software (version 4.2.12), using the average from a 51 x 51 pixels grid in the center of the vial. While the R value remained mostly stable, the G value decreased and the B value increased with the fentanyl concentration. The G value showed the highest relative change. Though tubes were photographed in similar conditions, differences in lighting can explain the imperfect relationship between G value and concentration observed in Table 4.6.

Table 4.6. RGB values for solgels prepared with 1000 μM eosin Y mixed with increasing concentrations of fentanyl.

Fentanyl concentration (mg/mL)	R value ^a	G value ^a	B value ^a
0	162	72	50
0.10	158	69	47
0.25	158	72	52
0.50	158	63	49
0.75	159	48	54
1.00	161	35	64

Key: ^a RGB values determined from a photograph of the solgel vial, by sampling a 51 x 51 pixels grid using the paint.net software.

The MDMA study was conducted using a custom-built photography box, with a white interior and uniform LED lighting, in which the samples were introduced before being photographed. [168] Though the use of a smartphone is a clear advantage of this acquisition method, by making detection accessible to virtually anyone, the requirement of a special photography box negates this advantage. Ideally, one should be able to take the photograph in any kind of environment and still get a reliable result, but RGB values are extremely susceptible to lighting conditions.

Figure 4.25 shows an example of this. Each picture shows the same two solgel vials photographed in three different settings. Blank methanol (150 μ L) was added to the vial on the left and a 1 mg/mL solution of fentanyl (150 μ L) to the one on the right. Photographs were taken at varying angles, with different lighting conditions. In Figure 4.25a, which was taken in natural light, heterogeneous shadows and lightings can be seen on the surface. The photograph in Figure 4.25b was taken in a lower lighting environment, which the phone camera automatically compensates for, resulting in higher R and G values. The third photograph (Figure 4.25c) was taken with back-lighting coming from the windows, causing the solgels to appear darker.

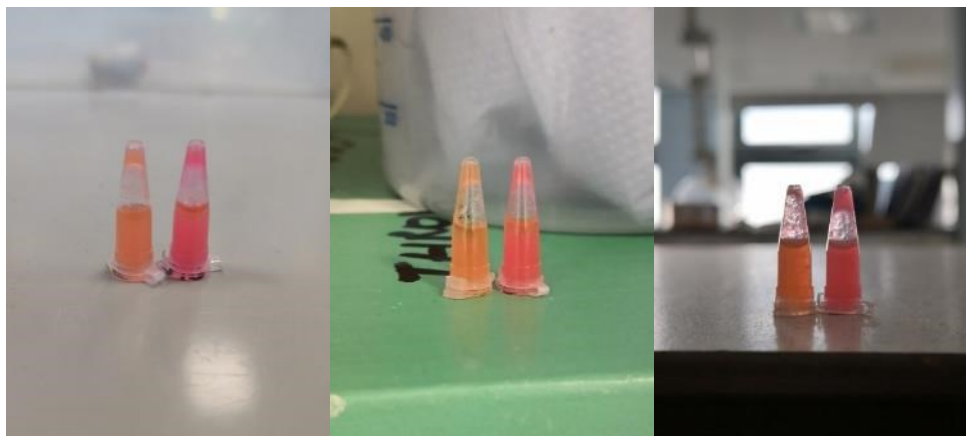


Figure 4.25. Photographs of solgels taken in three different lighting conditions, reacted with blank methanol (left) and 1 mg/mL fentanyl (right). RGB values of the fentanyl-solgel mixture: a) R: 191, G: 62, B: 74; b) R: 215, G: 81, B: 71; c) R: 153, G: 49, B: 47

RGB values can vary greatly depending on the position and intensity of light sources, the position of windows, the time of day, how close the experimenter is from the samples, and so forth. This poses a problem when trying to standardise colorimetric tests based on RGB values: all photographs must be taken in a standard environment with constant, even lighting. To try and circumvent this issue, results obtained in thirteen different lighting conditions were analysed (Table 4.7). Each time, the same vials containing blank methanol and fentanyl (1 mg/mL) were photographed side-by-side.

Table 4.7. RGB values of solgel vials photographed side-by-side in different lighting conditions (see Section 7.9 for photographs).

Lighting Conditions	Blank			Fentanyl 1 mg/mL		
	R	G	B	R	G	B
1	187	93	62	194	62	70
2	193	96	70	195	68	74
3	190	94	68	191	62	74
4	212	116	93	209	81	105
5	177	82	45	172	58	56
6	155	69	39	153	49	47
7	171	81	55	164	53	62
8	164	79	52	156	50	57
9	177	86	59	175	59	66
10	205	110	57	215	81	71
11	156	76	45	166	54	51
12	202	107	74	208	78	83
13	142	71	46	146	51	52

Table 4.8 reports the average G value for the conditions tested (G_{std}). As discussed previously, the green value tends to decrease proportionally to the concentration of fentanyl, and it could be used for detection. However, with varying lighting conditions, a high variability (19% RSD) in the G value of the standard solution was observed (see Table 4.8, G_{std}). In an effort to reduce this variability, the red value, which remains constant between samples, was used as a sort of internal standard to account for differences between samples. By using the G/R ratio of the vial containing the fentanyl standard, the RSD decreased to 7.0%. To decrease this further, the blank vial was used as an external standard to account for differences in lighting conditions. After all, the blank should always have the same colour, independent of the fentanyl concentration. The sample G/R ratio was divided by the blank G/R ratio, and a standard deviation of 3.7% was obtained.

Table 4.8. Comparison of RGB standardisation methods with eosin Y solgels.

	RGB Standardisation		
	G_{std}	$(G / R)_{std}$	$\frac{(G / R)_{std}}{(G / R)_{blank}}$
Average (n = 13)	62	0.34	0.69
Standard deviation (n = 13)	12	0.02	0.03
Relative standard deviation (%) (n = 13)	19	7.0	3.7

This simple modification made the test much more reliable across all conditions tested and eliminated the need for a specialised photography set or box. This technique could easily be applied to standardise other colour tests.

4.4.3 Quantitative solgel analysis

The possibility to quantify fentanyl using the eosin Y solgel test was then tested. To obtain a calibration curve, six replicate samples were tested at ten concentrations of fentanyl from 0.1 to 1.0 mg/mL. Results were standardised using the G/R ratio of the standard divided by the blank. The resulting calibration graph is shown in Figure 4.26.

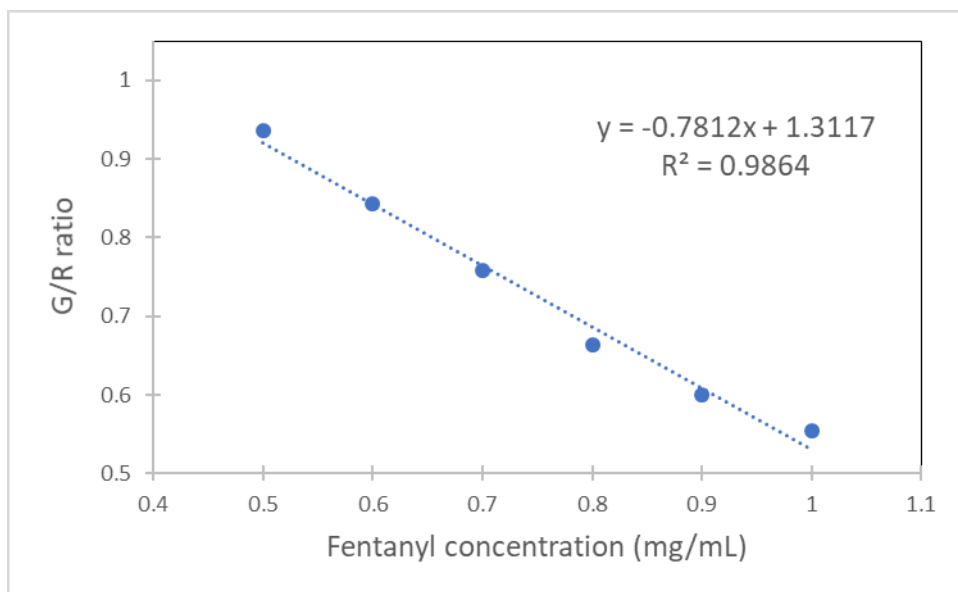
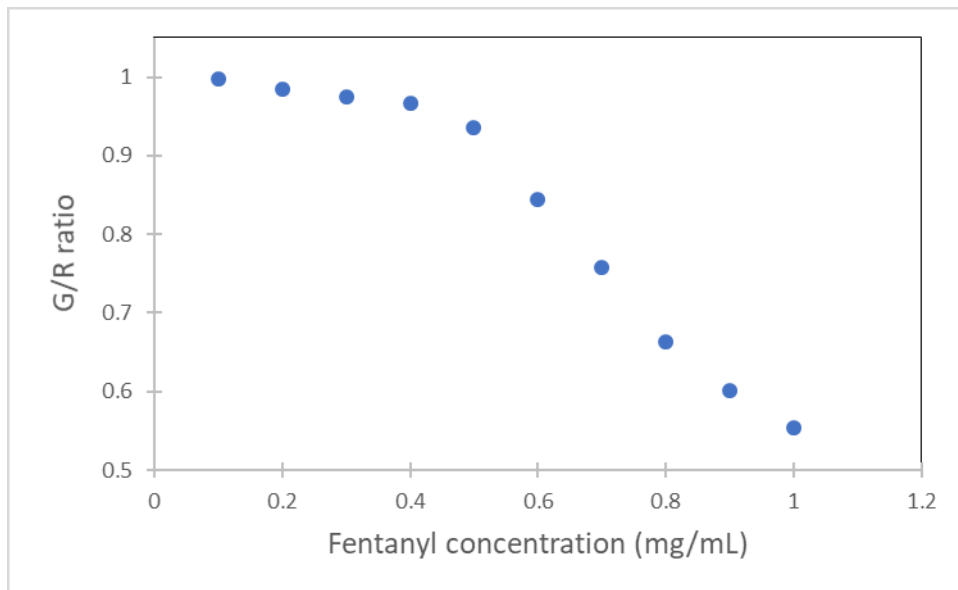


Figure 4.26. Calibration of fentanyl with eosin Y solgel RGB detection, a) 0.1 – 1.0 mg/mL concentration range; b) 0.5 – 1.0 mg/mL concentration range.

At low concentrations, between 0.1 and 0.4 mg/mL, the measured colour change is relatively weak, resulting in a non-linear calibration curve. However, a linear response range can be observed between 0.5 and 1.0 mg/mL, with a relatively good R^2 of 0.986, as shown in Figure 4.26b. Samples can easily be diluted to fall within this range. The lowest concentration (0.5 mg/mL) corresponds to only 75 μg of fentanyl in a volume of 150 μL , showing the surprisingly high sensitivity of this method.

However, the technique did not prove selective enough for fentanyl detection. A variety of common drugs and adulterants were reacted with the eosin Y solgel (see Table 4.9). A G/R ratio close to 1.00 indicates an absence of reaction. All compounds tested reacted with the solgel at this concentration. Two heroin samples which did not contain fentanyl, SS-4 and SS-5, were also tested and reacted with the solgel.

Table 4.9. Test results of common drugs and adulterants and seized heroin samples SS-4 – 5.

Test compound (5 mg/mL)	G/R ratio
MDMA	0.76
Codeine	0.82
Procaine	0.56
Caffeine	0.82
Paracetamol	0.78
Benzocaine	0.96
Morphine	0.90
Heroin	0.97
SS-4	0.62
SS-5	0.88

Therefore, the solgel method could not be applied to quantify fentanyl in mixtures with the substances tested, greatly reducing its usefulness. This is due to the lack of specificity of the RGB method of detection: even though fentanyl and MDMA, for instance, produce visibly different colours when reacting with eosin Y, the RGB measurement cannot differentiate them. This was an advantage of visible light spectrophotometry over RGB detection, because it allowed the monitoring of very specific wavelengths. Thus, the solgel detection method was not investigated further.

4.5 Conclusion

In conclusion, the reaction between the eosin Y dye and illicit drugs, including heroin and fentanyl, was investigated. It was determined that eosin Y reacts with heroin through an acid-base reaction, resulting in a colour change from peach to pink, a result which is observed with most amines. It reacts similarly with fentanyl, with the exception that the reaction leads to the precipitation of fentanyl free-base. It is suggested that the characteristic deep pink colour observed with fentanyl is due to the co-precipitation of eosin Y, which has a different colour in solid form than in solution.

Although the test cannot be used for the quantification of fentanyl in mixtures, it can still be used for qualitative analysis. This is especially reliable when using UV-Vis spectrophotometry, because the fentanyl – eosin Y mixture absorbs at a specific wavelength. Solgel detection coupled with RGB measurement, on the other hand, can be indicative of the presence of fentanyl but it lacks in selectivity, and is susceptible to interference from other components found in mixtures (e.g. heroin, caffeine, paracetamol).

Nevertheless, the developed methodology can, and should, be applied to the standardisation of colorimetric tests. For instance, the RGB standardisation method described in this chapter could serve to make MDMA detection with the solgel Simon test much more accessible, by eliminating the need for specialist photography equipment. [168] In a broader perspective, the reaction mechanisms leading to colour changes should be investigated, using NMR and other techniques, to better understand colour tests. Interference tests should always be carried out with compounds likely to be found in mixtures with the drug of interest, to assess the risks of false positives. Where possible, tests should not rely on visual examination but on objective colour detection methods, such as UV-Vis spectrophotometry or RGB detection.

CHAPTER V

PRINCIPAL COMPONENT ANALYSIS MODEL FOR FENTANYL ANALOGUE CLASSIFICATION

5.1 Overview

This quick emergence of synthetic analogues of controlled drugs constitutes a challenge for their identification, because of the time it takes before extensive chemical characterisation of these analogues is disseminated in academic journals or specialised databases. [19, 28] Because fentanyl (**2b**) is synthesised using simple reagents, modifications of its structure are easily introduced by using different starting materials, resulting in completely new drugs. These novel analogues can be harder to identify, because they have yet to be added to mass spectral databases. The development of detection methods, as discussed in Chapters II and III, aims to make the detection of known analogues more accessible, to help harm reduction and decrease under-reporting. However, it is inherently a reactive approach to the issue, and as long as new analogues keep appearing, new detection methods will have to be developed. Proactive solutions should, therefore, be considered to quickly identify future analogues. Efforts should focus on the development of predictive models which, when confronted with an unknown drug analogue, not present in their database, can still identify common features and discern how the analogue differs from the parent drug.

Mass spectrometry data appears to be the ideal technique for this purpose, partly because of its widespread use: multiple gas chromatography-mass spectrometry (GC-MS) methods have been reported for the detection of fentanyl and its derivatives. [108, 109, 111, 169] Moreover, m/z ions are indicative of specific modifications and their position on the molecule. How easily characteristic fragments can be identified by an experimenter depends on the complexity of mass spectra: fentanyl analogue spectra can comprise hundreds of m/z peaks. Techniques based on dimensionality reduction, such as principal component analysis (PCA), are therefore perfectly suited for this type of analysis and can highlight unsuspected trends in spectral data. New observations can also be projected onto the PCA model to see how they relate to known analogues. [170]

Multivariate analysis has previously been used to determine the synthetic route used to manufacture fentanyl samples based on an inventory of compounds detected by GC-MS, LC-MS/MS and ICP-MS. [112] It also helped identify fentanyl analogues based on their Raman spectra. [88] Principal component analysis has been used to differentiate regioisomeric synthetic drugs, including regioisomers of fluorofentanyl (**42a-c**), by highlighting differences in specific m/z ion ratios. [113-115]

Recently, spectral similarity mapping was applied to group fentanyl analogues based on their mass spectra. [116] Clustering separated compounds in three groups, based on the number of major peaks that shifted (0, 1 or 3) between an analogue and fentanyl. For instance, group 1 (0 shifts) was composed of fentanyl and the analogues modified at the phenethyl chain, because this modification does not cause a shift in the base peaks, which result from a loss of this chain. Modifications of the amide chain caused one major shift and

substitution of the aniline ring caused three, resulting in only three classes. This was a limitation of the model, in that it worked with the position rather than the nature of substituents: for instance, compounds bearing a fluorine, chlorine, methoxy or methyl substituent on their aniline ring would still cluster together, which makes little sense.

This chapter deals with the elaboration of a model which separates data into more meaningful classes, based on the nature and position of their substituents. The model was built using principal component analysis (PCA) to organise analogues based on the intensity of their common *m/z* ions. Coupled with hierarchical clustering, this allowed the reliable classification of fentanyl analogues into structural classes. The model used the mass spectra of 54 analogues; an evaluation of the model, using 67 analogues not previously included, showed that it can accurately identify structural modifications in “unknown” compounds.

5.2 Data handling

The 121 analogues used in this study are reported in Table 5.1 (see section 7.12.3 for a full description of their chemical structures). Compounds highlighted in green have been synthesised in-house; this includes a combination of compounds reported in Chapters II (**2a-r**) and III (**42a-c**, **46a-c**, **47**, **48**), as well as additional analogues synthesised specifically to increase the numbers of compounds available in certain classes. The latter analogues may not have been encountered in forensic casework, but they are plausible structures based on a combination of commonly observed modifications of fentanyl (**2b**). The synthesis of these analogues is described in Section 7.11. Mass spectra were acquired by GC-MS, as described in Section 7.4.

The mass spectra of the remaining compounds were available on the online SWGDRUG spectral library (version 3.7, released June 4th, 2020). [171]

Table 5.1. List of fentanyl analogues included in this study.

MODEL BUILDING			
Fentanyl analogue	N°	Fentanyl analogue	N°
Isobutyryl <i>N</i> -benzyl-	58	Acryl-	2q
<i>N</i> -Benzyl-	59	Butyryl-	2c
Cyclopropyl- <i>N</i> -benzyl-	60	Propionyl- [aka. Fentanyl]	2b
<i>p</i> -Fluoro-isobutyryl- <i>N</i> -benzyl-	61	Cyclopropyl-	2f
<i>p</i> -Fluoro- <i>N</i> -benzyl-	62	Isobutyryl-	2j
Phenyl- <i>N</i> -benzyl-	63	3'-Fluoro-	46b
<i>p</i> -Fluoro-acetyl- <i>N</i> -benzyl-	64	4'-Fluoro-	46c
<i>m</i> -Methyl-	65	2'-Fluoro-	46a
<i>o</i> -Methyl-acetyl-	66	<i>m</i> -Fluoro-acryl-	82
<i>m</i> -Methyl-acetyl-	67	<i>m</i> -Fluoro-methoxyacetyl-	83
4'-Methyl-acetyl-	68	<i>p</i> -Fluoro-acryl-	84
β -Methyl-acetyl-	69	<i>p</i> -Fluoro-acetyl-	85
2'-Methyl-	70	<i>p</i> -Fluoro-cyclopropyl-	86
<i>p</i> -Methyl-tetrahydrofuranyl-	71	3-Fluoro-butyryl-	87
Tetrahydrofuranyl- (3-isomer)	72	3-Fluoro-tetrahydrofuranyl-	88
β -Methyl-	73	3-Fluoro-	48
Heptanoyl-	74	<i>p</i> -Chloro-butyryl-	89
<i>m</i> -Methyl-furanyl-	75	<i>p</i> -Chloro-	90
(<i>E</i>)-2-Methyl-2-butenoyl-	76	<i>p</i> -Chloro-cyclopentyl-	91
4'-Fluoro-cyclopropyl-	77	<i>p</i> -Methoxy-acryl-	92
Benzoyl- (phenyl)	2r	<i>p</i> -Methoxy-methoxyacetyl-	93
2,2,3,3-Tetramethylcyclopropyl-	78	<i>p</i> -Methoxy-	94
2,2-Dimethylpropanoyl-	79	<i>p</i> -Methoxy-valeryl-	95
4'-Fluoro-butyryl-	80	<i>o</i> -Methoxy-butyryl-	96
Furanyl-	2o	<i>m</i> -Fluoro-	42b
4'-Fluoro-methoxyacetyl-	81	<i>o</i> -Fluoro-	42a
Methoxyacetyl-	2n	<i>p</i> -Fluoro-	42c

Table 5.1. List of fentanyl analogues included in this study. (cont.)

EVALUATION			
Fentanyl analogue	N°	Fentanyl analogue	N°
<i>m</i> -Fluoro- <i>N</i> -benzyl-	97	Thiophenyl- (3-isomer)	129
<i>p</i> -Fluoro- <i>N</i> -benzyl-furanyl-	98	3'-Methyl-	130
Acetyl- <i>N</i> -benzyl-	99	<i>o</i> -Fluoro-furanyl-	131
Furanyl- <i>N</i> -benzyl-	100	Acetyl-	2a
Methoxyacetyl- <i>N</i> -benzyl-	101	<i>iso</i> -Valeryl-	2k
Butyryl- <i>N</i> -benzyl-	102	Valeryl-	2d
Acryl- <i>N</i> -benzyl-	103	Hexanoyl-	2e
<i>p</i> -Fluoro- <i>N</i> -benzyl- cyclopropyl-	104	Cyclobutyryl-	2g
Tetrahydrofuranyl- <i>N</i> -benzyl-	105	2'-fluoro- <i>o</i> -fluoro-	47
4-ANPP	4	<i>p</i> -Fluoro-butyryl-	132
((<i>E</i>)-But-2-enoyl)-	106	<i>p</i> -Fluoro-isobutyryl-	133
(2-Methyl)butyryl-	107	<i>p</i> -Fluoro-cyclopentyl-	134
Ethoxyacetyl-	108	<i>p</i> -Fluoro-tetrahydrofuranyl-	135
Cyclopropylacetyl-	109	<i>p</i> -Fluoro-crotonyl-	136
<i>o</i> -Methyl-acryl-	110	<i>m</i> -Fluoro-isobutyryl-	137
<i>p</i> -Methyl-acetyl-	111	<i>o</i> -Fluoro-butyryl-	138
<i>o</i> -Methyl-	10	<i>o</i> -Fluoro-isobutyryl-	139
<i>m</i> -Methyl-cyclopropyl-	112	<i>p</i> -Fluoro-valeryl-	140
<i>o</i> -Methyl-furanyl-	113	<i>p</i> -Fluoro-furanyl- (3-isomer)	141
<i>p</i> -Methyl-furanyl-	114	2,3-Benzodioxoyl-	142
<i>m</i> -Methyl-methoxyacetyl-	115	<i>p</i> -Chloro-furanyl-	143
<i>o</i> -Methyl-cyclopropyl-	116	<i>m</i> -Fluoro-butyryl-	144
4'-Fluoro-furanyl-	117	<i>p</i> -Fluoro-furanyl-	145
<i>m</i> -Methoxy-furanyl-	118	<i>m</i> -Fluoro-furanyl-	146
<i>o</i> -Methoxy-furanyl-	119	<i>m</i> -Fluoro-isobutyryl	147
<i>p</i> -Methoxy-furanyl-	120	3-Fluoro-isobutyryl	148
<i>p</i> -Chloro-furanyl- (3-isomer)	121	<i>p</i> -Chloro-cyclobutyryl-	149
3'-Methyl-acetyl-	122	<i>p</i> -Chloro-isobutyryl-	150
4'-Methyl-	123	<i>p</i> -Chloro-methoxyacetyl-	151
α -Methyl-acetyl-	124	<i>p</i> -Chloro-valeryl-	152
α -Methyl-butyryl-	125	<i>p</i> -Chloro-acryl-	153
α -Methyl-	126	<i>p</i> -Methoxy-butyryl-	154
4'-Fluoro-acetyl-	127	<i>p</i> -Methoxy-methoxyacetyl-	155
2'-Methyl-acetyl-	128		

Compounds were separated into generic structural classes. Approximately half the compounds in each class (at least three) were selected to build the model, for a total of 54 compounds. These classes did not inform the clustering performed in Section 5.4, but served to have an even representation of possible

structural modifications in the model. The remaining 67 compounds were retained for a subsequent evaluation of the model's accuracy.

EI-MS spectra for compounds were extracted in .csv format. Relative intensities were calculated from $m/z = 41$ to $m/z = 352$, with the base peak normalised to 1 (see Table 5.2 for an excerpt of the dataset). The full dataset contained 54 observations (compounds) of 312 variables (m/z ions). This represents too many variables to extract meaningful information at a glance, making it difficult to evaluate whether compounds which share structural features also share common m/z ions for instance. Principal component analysis (PCA), by reducing the number of variables, will make these trends more easily visible. A full description of this procedure is reported in Section 7.10.

Table 5.2. Relative intensities for five fentanyl analogues.

Compound	Relative intensity (%)							
	$m/z = 41$	$m/z = 42$	$m/z = 43$	$m/z = 44$	$m/z = 45$	$m/z = 46$...	$m/z = 352$
Fentanyl (2b)	0.113	0.417	0.067	0.000	0.000	0.000	...	0.000
Butyryl fentanyl (2c)	0.144	0.279	0.361	0.184	0.000	0.000	...	0.000
Methoxyacetyl fentanyl (2n)	0.088	0.338	0.058	0.000	0.623	0.020	...	0.000
Cyclopropyl fentanyl (2f)	0.514	0.391	0.063	0.141	0.000	0.000	...	0.000
Isobutyryl fentanyl (2j)	0.246	0.393	0.867	0.198	0.000	0.000	...	0.000

The dataset was imported into the *R* statistical computing software (version 3.6.3). Further data clean-up was performed to remove noise. Variables (m/z ions) with a variance below 0.0001 were excluded as an initial clean-up, which reduced the dataset to 176 variables. This removed ions absent from all analogues, or ions that occurred very strongly in only one (or very few)

compounds. Higher variance thresholds were tested and led to a loss of valuable information when building the model.

Principal component analysis was performed with mean centering and data scaling using the PCA function from the *FactoMineR* package (version 2.2). [172] Data visualisation was performed using the *factoextra* (version 1.0.7) and), *ggcorrplot* (version 0.1.3) and *clustertend* (version 1.4) packages. [173-175]

PCA was used to reduce the number of dimensions to a small number of principal components (PCs). Before selecting how many PCs should be retained, the information represented by each of the first principal components was examined.

Figure 5.1a shows a projection of the model compounds on PCs 1 and 2. This is only a representation of the first two principal components, but the PCA generated 53 components in total. The first principal component, PC1, is the one that explains the most variance in the data, PC2 explains the second most variance, and so forth, until 100% of the total variance is explained. Later components explain only a trivial portion of the variance and need not be retained in the model. There is no strict criterion to decide how many PCs should be retained when building a PCA model. According to Kaiser, this can be determined using eigenvalues, a measure of the variance explained by each principal component. [176] Each PC has an inherent eigenvalue; when normalised so that the sum of eigenvalues across all PCs is 10, a PC with an eigenvalue greater than 1 should be retained. Eigenvalues for each PC are reported in a Scree plot (Figure 5.2). Only PC1 fits Kaise's criterion, while PC2 is slightly under. However, in this case, the first PCs explain only a small portion

of the data. This may be due to the nature of the data, and the overall variability of m/z ions: much of the variance can remain in further PCs. This, however, does not mean that the first few PCs are not sufficient to highlight relevant trends in the data. A recent study using mass spectral data from synthetic phenethylamines and tryptamines obtained similarly low values of variance explained by the first PCs. [177] In this case, PCs were selected based on their importance in separating structural classes, rather than on the eigenvalue criterion.

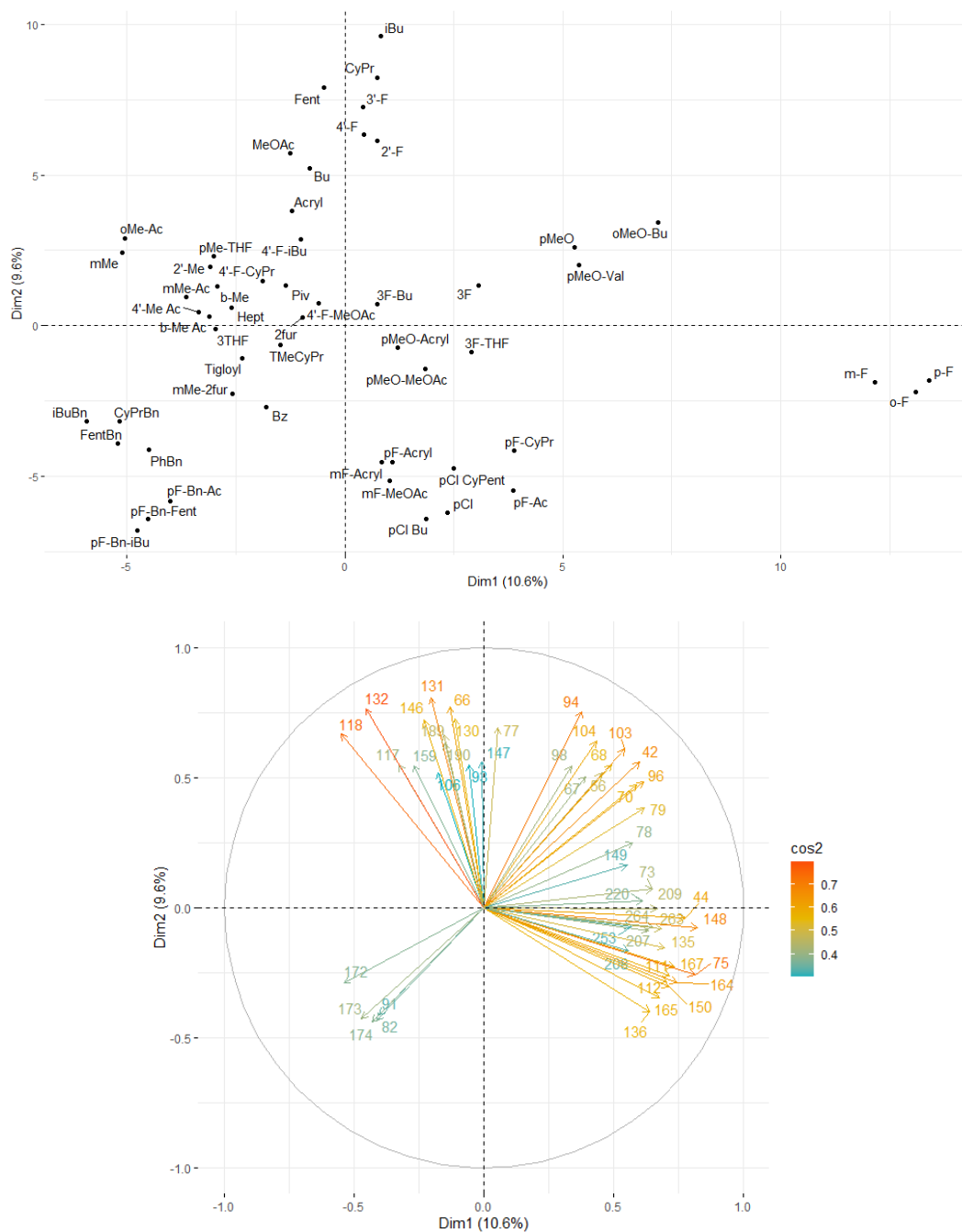


Figure 5.1. a) Projection of model fentanyl analogues on principal components PC1 and PC2; b) Correlation circle of m/z values projected on principal components PC1 and PC2, coloured according to \cos^2 values ($\cos^2 > 0.3$).

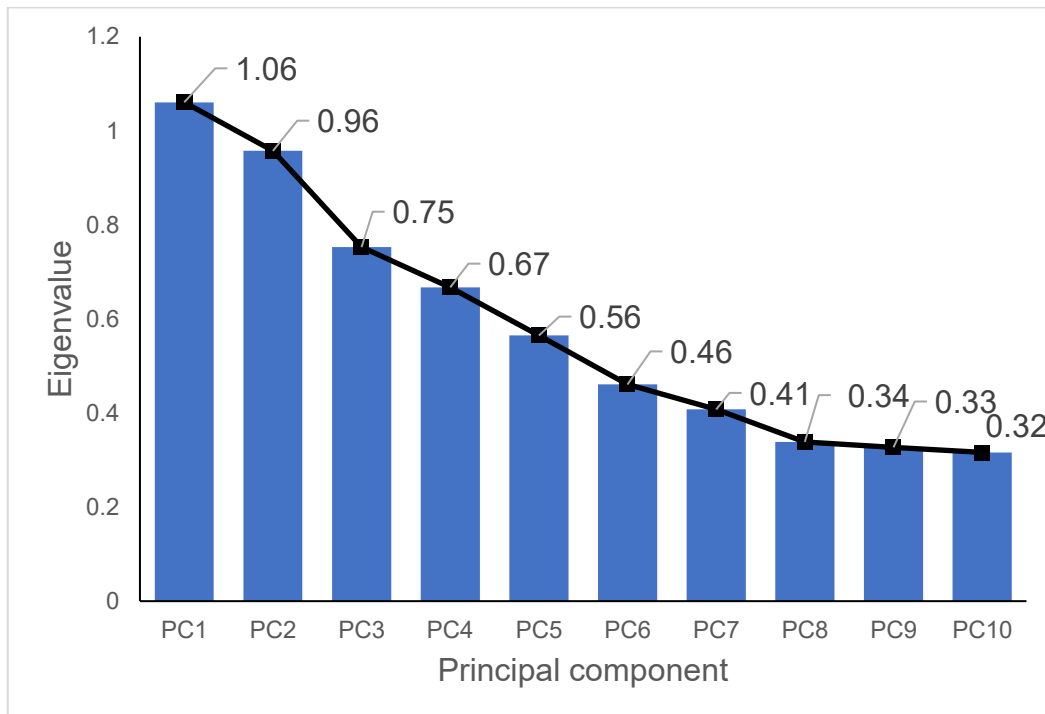


Figure 5.2. Scree plot of the eigenvalues for the first ten principal components.

Therefore, before eliminating any PCs, the ions best represented by each component were examined. This gives a better understanding of the underlying dynamics behind each PC, and helps determine if valuable information is lost by eliminating specific PCs. Figure 5.1b shows a correlation circle of all variables (ions) projected onto PC1 and PC2. Variables are coloured based on their \cos^2 , a measure of their distance from the center of the plot. Variables with a high \cos^2 (orange) are best represented by the principal components. Incidentally, variables in the same quadrant of the circle are positively correlated to each other, while variables in opposite quadrants are negatively correlated. This explains why, for instance, some variables have a positive value when projected onto PC1 (e.g. $m/z = 148$) and others a negative (e.g.

$m/z = 172$ and 173), although the positive/negative sign is arbitrary. Ultimately, ions with the highest \cos^2 are most characteristic of compounds projected in a given direction. Only the major fragment ions of fentanyl have been characterised, so the structure of ions of low mass or weak intensity may not be known. Still, PCA shows that these unknown ions can be characteristic of certain classes of compounds, revealing previously unsuspected trends which allow clustering. This is a clear advantage of using PCA: its potential for abstraction. Without knowing how every single ion arise, they can still be used by the model to establish fentanyl classes. Certain ions will be discussed here to describe the first PCs; a more in-depth discussion of the structures of characteristic ions will be done in Section 5.4.

PC1 on its positive axis, appears strongly characteristic of fluorinated derivatives ($m/z = 164, 207$), especially those bearing a propionyl amide chain ($m/z = 263$, **42a-c**). It also separates 3-fluoro- (**48, 87-88**) and methoxyaniline (**92-96**) derivatives from the bulk, to a lesser extent. Positive values of PC2 characterises most amide derivatives and fluorophenethyl- (**46a-c, 77, 80-81**) compounds, while negative values are representative of chloro- (**89-91**) and fluoro-aniline (**42a-c, 82-86**) compounds. *N*-Benzyl analogues (**58-64**) gather in the lower left quadrant (Figure 5.1a) and are most strongly characterised by $m/z = 82, 91, 172, 173$ and 174 (Figure 5.1b). These are piperidine or tropylium ($m/z = 91$) fragments which arise more strongly in *N*-benzyl than *N*-phenethyl derivatives. [178]

Projections on PCs 3-4 are shown in Figure 5.3 and PCs 5-6 in Figure 5.4. PC3 characterises chloro-aniline compounds (**89-91**), and PC4 is representative of methoxy-aniline compounds (**92-96**). PC5 serves mainly to discriminate 3-fluoro compounds (**48, 87-88**) from the bulk. PC6 does not appear to contribute

significantly to clustering, showing a rather even distribution of compounds along its axis. Few m/z ions are strongly represented by PC6. PCs beyond PC6 explain decreasing proportions of the total variance and are unlikely to contribute to the model. Therefore, the first five PCs were retained, which explain 40.0% of the total variance in the data.

The ion at $m/z = 263$ is specific to *ortho*-, *meta*- and *para*-fluorofentanyl (**42a-c**), and includes the propionyl amide chain. It is strongly characterised by PC1, leading the three derivatives to project far on this axis. Ions bearing an amide moiety tend to be compound-specific and poorly explain variance in the data. The difference with $m/z = 263$ is that it is found in multiple compounds which all produce very similar mass spectra. This means a disproportionate number of derivatives produce the $m/z = 263$ ion, which may be skewing the PCA. The same phenomenon occurs for 2'-, 3'- and 4'-fluorofentanyl (**46a-c**), which project far away from other 4'-fluorinated derivatives on the PC4 axis. The inclusion of more derivatives of each class would probably lessen this phenomenon. This is not problematic *per se*, but it must be kept in mind when defining what constitutes a "class" of fentalogues within this model.

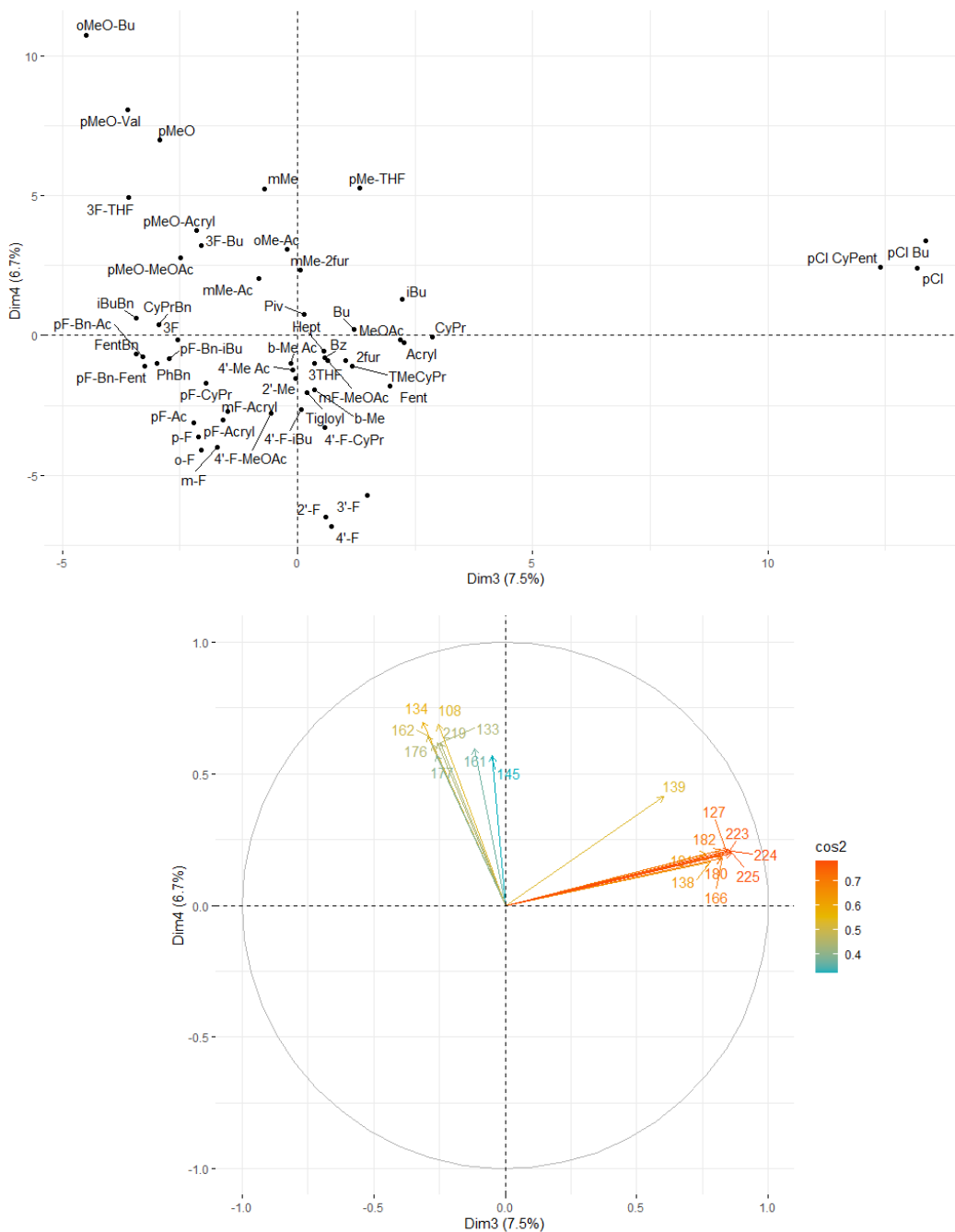


Figure 5.3. a) Projection of model fentanyl analogues on principal components PC3 and PC4; b) Correlation circle of *m/z* values projected on principal components PC3 and PC4, coloured according to *cos*² values (*cos*² > 0.3).

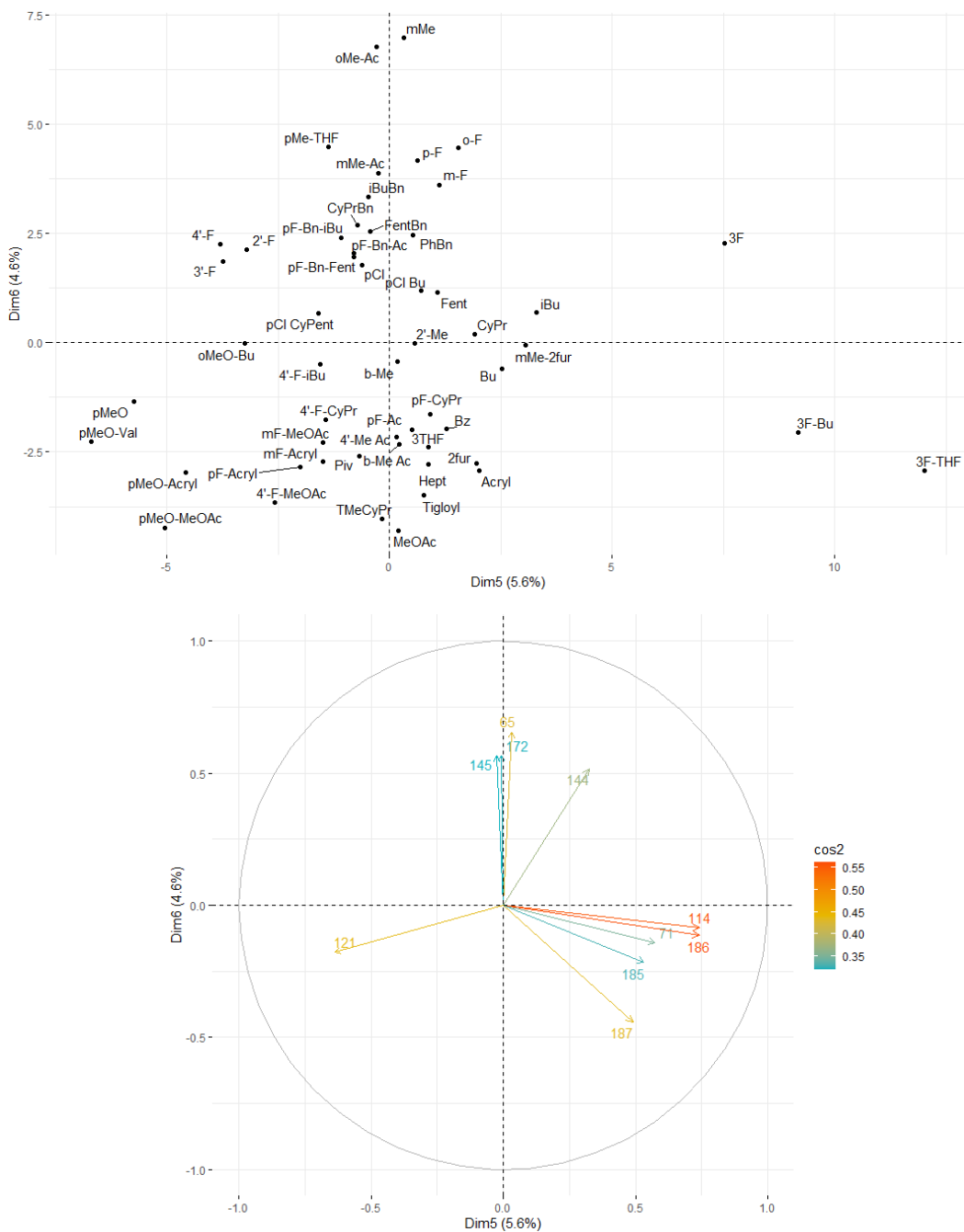


Figure 5.4. a) Projection of model fentanyl analogues on principal components PC5 and PC6; b) Correlation circle of m/z values projected on principal components PC5 and PC6, coloured according to \cos^2 values ($\cos^2 > 0.3$).

5.3 Hierarchical clustering

The next step in this process was to assign samples into clusters based on their proximity in the PCA space. First, the clustering tendency of the data was assessed. This is important because clustering algorithms will force random data into clusters, even if they are not statistically significant. The Euclidean distance was used as a measure of the similarity of two elements in a distribution and is defined in Equation 1:

$$d(p, q) = \sqrt{\sum_{i=1}^n (p_i - q_i)^2} \quad \text{Eqn. 1}$$

where p and q are two vectors of length n . Thus, it measures the distance between two points or individuals in n dimensions.

The clustering tendency was assessed using the Hopkins method, which randomly samples n points (p_1, \dots, p_n) from the dataset. For each point p_i , it finds its nearest neighbour p_j and calculates the Euclidean distance between them, noted as $x_i = d(p_i, p_j)$. A random dataset is then generated containing n points (q_1, \dots, q_n) with the same variation as the original dataset. The same process is applied to calculate $y_i = d(q_i, q_j)$, the Euclidean distance between points in the “simulated” dataset. The Hopkins statistic is defined in Equation 2:

$$H = \frac{\sum_{i=1}^n y_i}{\sum_{i=1}^n x_i + \sum_{i=1}^n y_i} \quad \text{Eqn. 2}$$

The Hopkins statistic compares sum of the distance between points in the dataset of interest (x_i) and a random dataset (y_i), the assumption being that

the data in the random dataset should be evenly distributed. If H is close to 0.5, the data is uniformly distributed. Values closer to 0 indicate a non-uniform distribution, or a high clustering tendency. Using the *hopkins* function from the *clustertend* R package, $H = 0.203$ was obtained, meaning the data has a tendency to cluster. This value does not, however, the number of clusters or which individuals they include.

A visual exploration of clusters can be done using a dissimilarity matrix (see Figure 5.5). The colour is proportional to the distance between individuals; red means the distance between individuals is close to 0, while blue means the distance is maximal within this dataset. The appearance of red boxes across the diagonal axis indicates the presence of clusters. This is clearly visible here, as a number of clusters appear in the data, which generally correlate with analogue structural classes. From bottom left to top right, groups of compounds include: 1) methoxyaniline derivatives (**92-96**); 2) fluoroaniline propionyl derivatives (**42a-c**); 3) 3-fluoro derivatives (**48, 87-88**); 4) chloroaniline derivatives (**89-91**); 5) fluorophenethyl propionyl derivatives (**46a-c**); 6) a large group of poorly separated derivatives containing potential sub-clusters; 7) *N*-benzyl derivatives (**58-64**); 8) fluoroaniline derivatives (**82-86**).

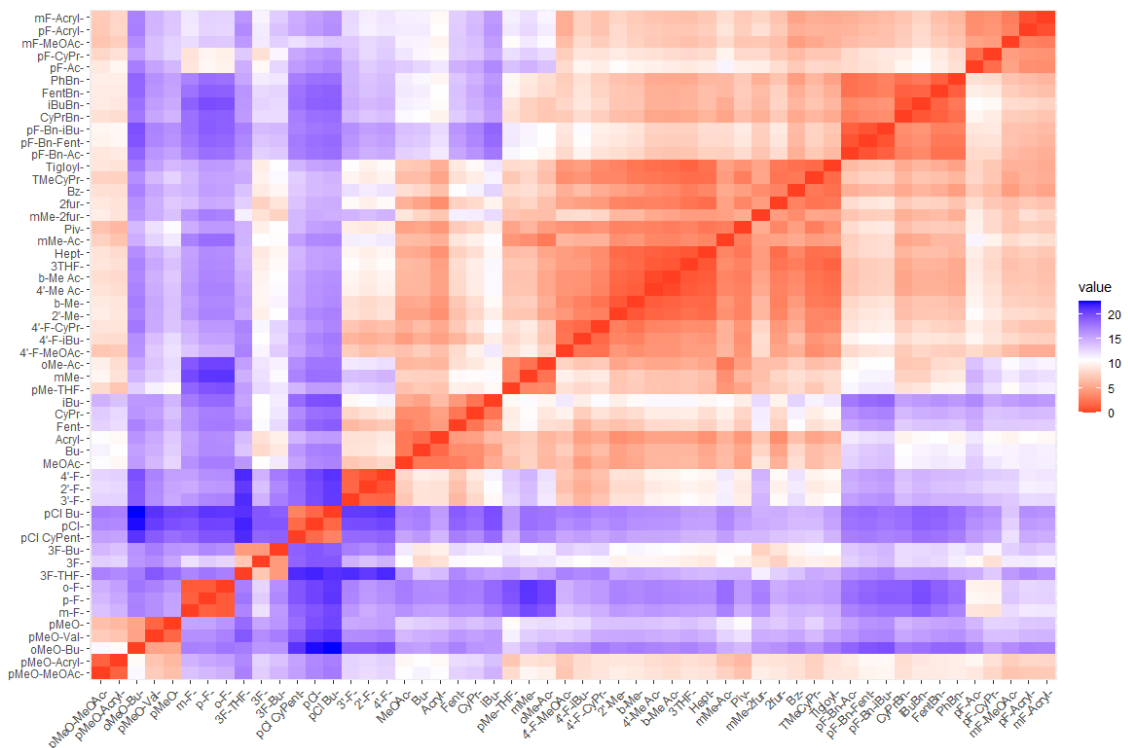


Figure 5.5. Dissimilarity matrix of the 54 fentanyl derivatives PCA.

Hierarchical ascendant classification was then applied to the model using the *HCPC (Hierarchical Clustering on Principal Components)* algorithm from *FactoMineR*. This is based on an *agnes (agglomerative nesting)* clustering algorithm. This type of algorithm classes individuals hierarchically based on their proximity in the PCA space; it starts with as many classes as there are individuals, then groups classes in a way that maximises intervariability, or the difference between classes. [172, 179]

Inter-variability is represented by the inter-class inertia which is defined in Equation 3:

$$\sum_{q=1}^Q \sum_{i=1}^I (x_{iq} - \bar{x})^2 = \sum_{q=1}^Q \sum_{i=1}^I (x_{iq} - \bar{x}_q)^2 + \sum_{q=1}^Q \sum_{i=1}^I (\bar{x}_q - \bar{x})^2 \quad \text{Eqn. 3}$$

Total inertia
Intra-class inertia
Inter-class inertia

where x_{iq} represents the PCA coordinates of the i^{th} individual from cluster q , \bar{x}_q is the average (or center of gravity) of cluster q , \bar{x} is the average of the full dataset, Q is the total number of clusters and I the total number of individuals. Inter-class inertia is the sum of the squared distances between the mean of each cluster and the mean of the full dataset, and thus represents how different clusters are from each other. By contrast, intra-variability, or intra-class inertia, is the sum of the squared distances between each member of a class and the average of that class, and thus represents the homogeneity of a given cluster. Ideally, the best partition should maximise inter-class inertia and minimise intra-class inertia.

The ascendant hierarchical classification starts with as many classes as there are individuals; at this point, classes are completely homogeneous. As such, the intra-class inertia is 0, while inter-class inertia is maximised. Although this is technically a perfect partition, it does not group individuals into useful, understandable classes. To achieve this, the model must suffer a certain loss of inter-class inertia, for the benefit of having a more general classification; the trick is in mitigating this loss of inertia. Grouping classes together can only lead to a decrease in the inter-class inertia, because the intra-class inertia increases

(i.e. classes become less homogeneous). Equation 4 describes how the inertia of two classes a and b decreases when they are grouped together:

$$Inertia(a) + Inertia(b) = Inertia(a \cup b) - \frac{m_a m_b}{m_a + m_b} d^2(a, b) \quad \text{Eqn. 4}$$

where m_a and m_b are the numbers of individuals in classes a and b and $d^2(a,b)$ is the squared distance between the centers of gravity of a and b . Thus, when a and b are grouped together, inertia is decreased by a value proportional to the distance between both classes, weighted by the number of individuals in each class. *HCPC* uses Ward's method, which aims to make the negative term of this equation as small as possible; it starts with as many classes as there are individuals, then groups the two classes that lead to the smallest loss of inertia, then the next smallest loss, and so forth until this iterative process builds a full dendrogram. [172, 179] The height of a branch represents the loss of inertia when two sub-groups are grouped together. The resulting dendrogram for the present model is shown in Figure 5.6.

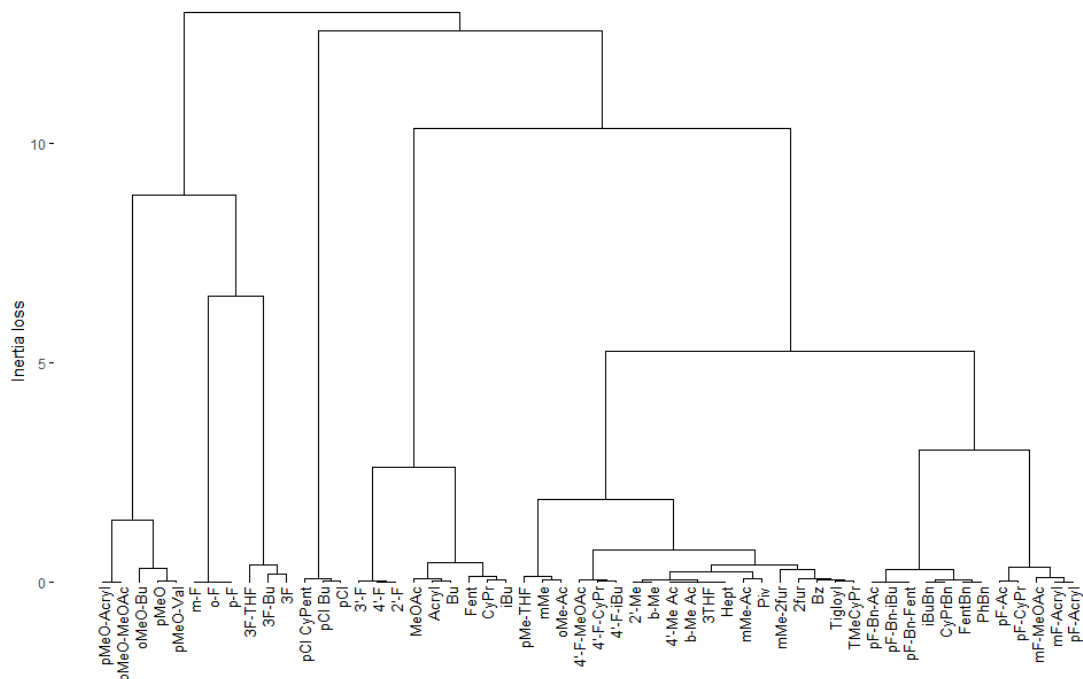


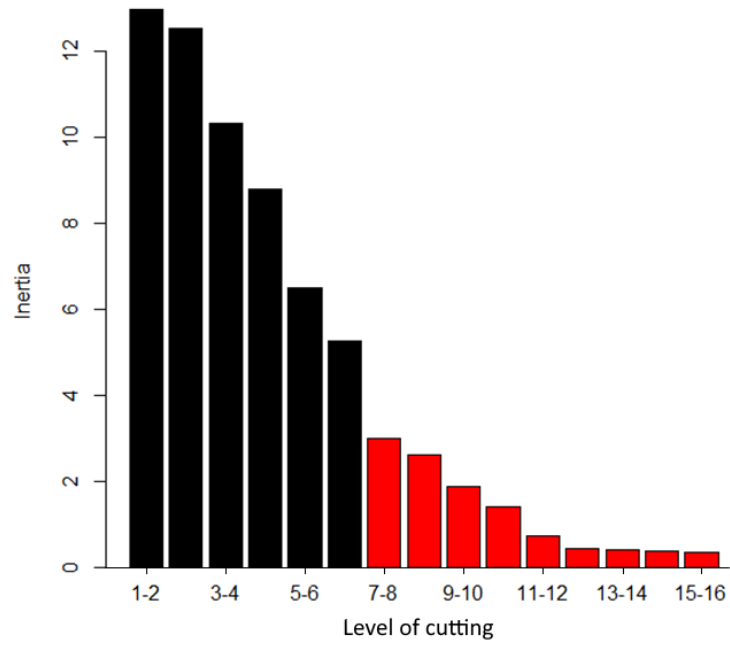
Figure 5.6. Initial hierarchical dendrogram of fentanyl analogues data.

Clusters generated through HCPC are defined by “cutting” the dendrogram at an appropriate level. Therefore, the number of classes can be defined by the user, but the composition of these classes arises solely from the clustering algorithm described. Again, no absolute criterion exists to determine the optimal number of clusters.

One possible criterion is the relative inertia gain. Table 5.2 shows how much inter-class inertia is gained by separating a class in two. For instance, starting from the top of the dendrogram, separating the whole dataset into two classes results in an inertia gain of 13.0, or 18.4% of the total inertia. HCPC considers the grouping with the highest relative gain as the optimal partition, forming ten

classes in this case. The resulting partition is shown in Figure 5.7a. This grouping accounts for 80.1% of the total inertia and, beyond that, the gain in inertia is relatively small (Table 5.3). The problem can also be considered in reverse: by grouping individuals in 7 classes, 19.9% of the inter-class inertia was lost, but the creation of relevant classes potentially made the model more general. Grouping more classes together, however, might result in too high a loss of inertia.

Table 5.3. Inter-cluster inertia gains.



Grouping	1-2	2-3	3-4	4-5	5-6	6-7	7-8	8-9	9-10	10-11	11-12	12-13	13-14	14-15	15-16
Inertia gain	13.0	12.5	10.3	8.8	6.5	5.3	3.0	2.6	1.9	1.4	0.8	0.4	0.4	0.4	0.3
% inertia gain	18.4	17.8	14.7	12.5	9.3	7.5	4.3	3.7	2.7	2.0	1.1	0.6	0.6	0.6	0.5
Cumul. %	18.4	36.2	50.9	63.4	72.6	80.1	84.4	88.1	90.8	92.8	93.9	94.5	95.1	95.6	96.1

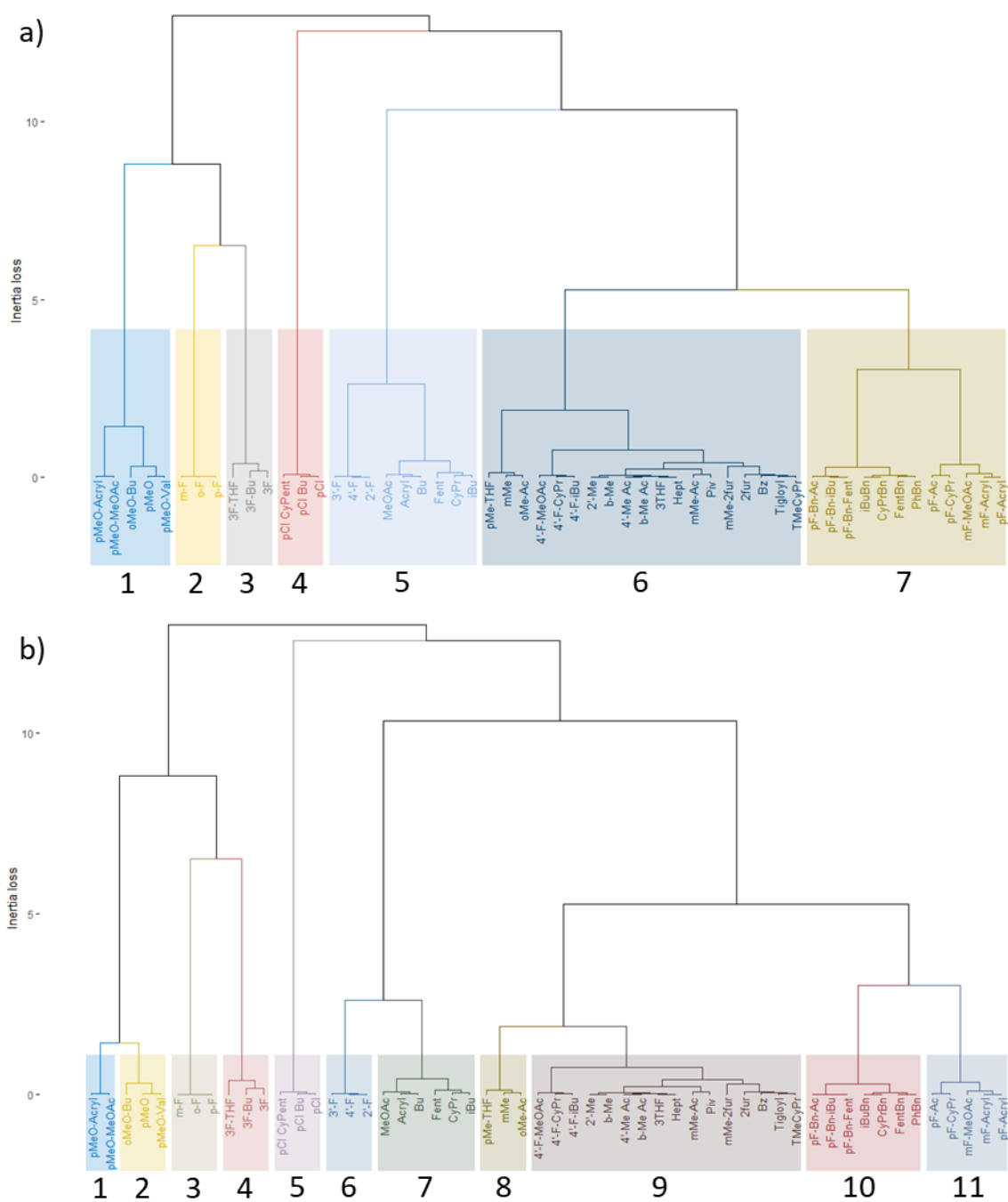


Figure 5.7. Dendrograms created from the hierarchical clustering of fentanyl analogues. a) $k = 7$ clusters; b) $k = 11$ clusters.

A more formal approach developed by Tibshirani *et al.* uses the “gap statistic” to determine an optimal number of clusters. [180] The gap statistic is defined in Equation 5:

$$Gap(k) = \frac{1}{B} \sum_{b=1}^B \log(W_{kb}) - \log(W_k) \quad \text{Eqn. 5}$$

This method calculates the total intra-cluster variation W_k in the dataset for an increasing number of clusters $k = 1, \dots, k_{max}$. B datasets with a random uniform distribution are then generated and separated into $k = 1, \dots, k_{max}$ clusters to determine their total intra-cluster variation W_{kb} . The gap statistic measures how much the present clustering deviates from the random distribution. For a larger gap statistic, it can be inferred that clustering is supported by the data and is unlikely to arise from a random distribution. The algorithm then looks for the smallest value of k for which $Gap(k)$ is within one standard deviation of $Gap(k + 1)$. In the present case, calculated with $k_{max} = 12$ and $B = 1000$, the optimal number of clusters according to the gap statistic is 11 (Figure 5.8). The resulting classification is shown in Figure 5.7b.

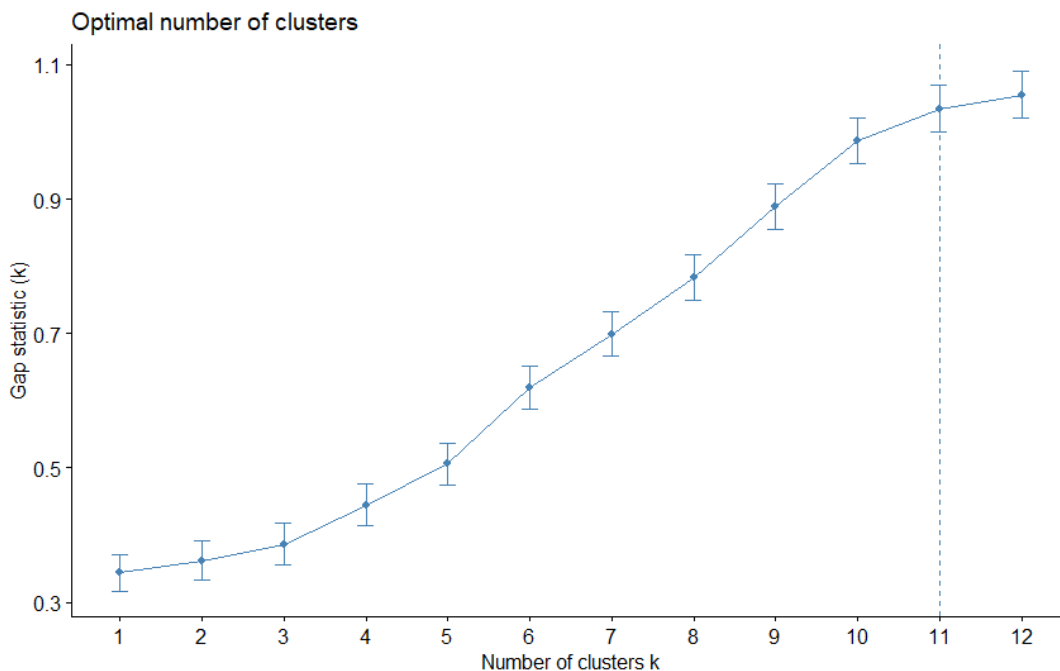


Figure 5.8. Gap statistic for each number of clusters ($k_{max} = 12$, $B = 1000$). Note: Error bars represent one standard deviation of $Gap(k)$ ($n = 1000$).

Arguably, the most important criterion is the ability to interpret why classes arise. It is counterproductive to divide a class without understanding the distinction between the two newly formed classes. Dividing the model into too many classes can also lead to “over-fitting”, which means it will perform poorly in the evaluation, when classifying test samples. It may therefore be relevant to use an empirical criterion, or prior knowledge about the derivatives included in the model, to evaluate the proposed classification. For instance, looking at Figure 5.7a ($k = 7$), clusters 5 and 7, which are the most heterogeneous according to their branch height, make little sense. Cluster 5 groups fluorophenethyl derivatives with non-fluorinated analogues, while cluster 7 groups *N*-benzyl derivatives with fluoroaniline analogues, and each could

arguably be cut in half. In contrast, the partition obtained from the gap statistic, shown in Figure 5.7b ($k = 11$), contains too many groups. Clusters 1 and 2 separate two methoxyaniline derivatives (*para*-methoxyacrylfentanyl (**92**) and *para*-methoxymethoxyacetylfentanyl (**93**)) from the others, which does not seem to be a useful distinction. Cluster 7 is composed only of methylaniline derivatives, but closely related compounds *meta*-methylacetylfentanyl (**67**) and *meta*-methyl-2-furanylfentanyl (**75**) fall in cluster 8.

In fact, cluster 8 itself makes little sense. Considering the variety of analogues included, it is unlikely that the model would detect the minute mass spectral differences between all structural classes. Cluster 8 regroups analogues which remain close to the center of the PCA space, compounds which could potentially be resolved from the rest of the group by subtle differences in their mass spectra, which explain a low percentage of the variance in this dataset. This is a limitation of this model which will be remedied later. In the meantime, clusters 7 and 8 will be grouped together into one cluster of “inconclusive” compounds, resulting in a partition of 9 clusters. This partition is called “Classifier 1” and is shown in Figure 5.9. Figure 5.10 shows the same partition in the PCA space, on the PC1-PC2 plane, although PCs 3-5 are omitted and also contribute to the clustering. A detailed list of the compounds in each cluster is reported in Table 5.4.

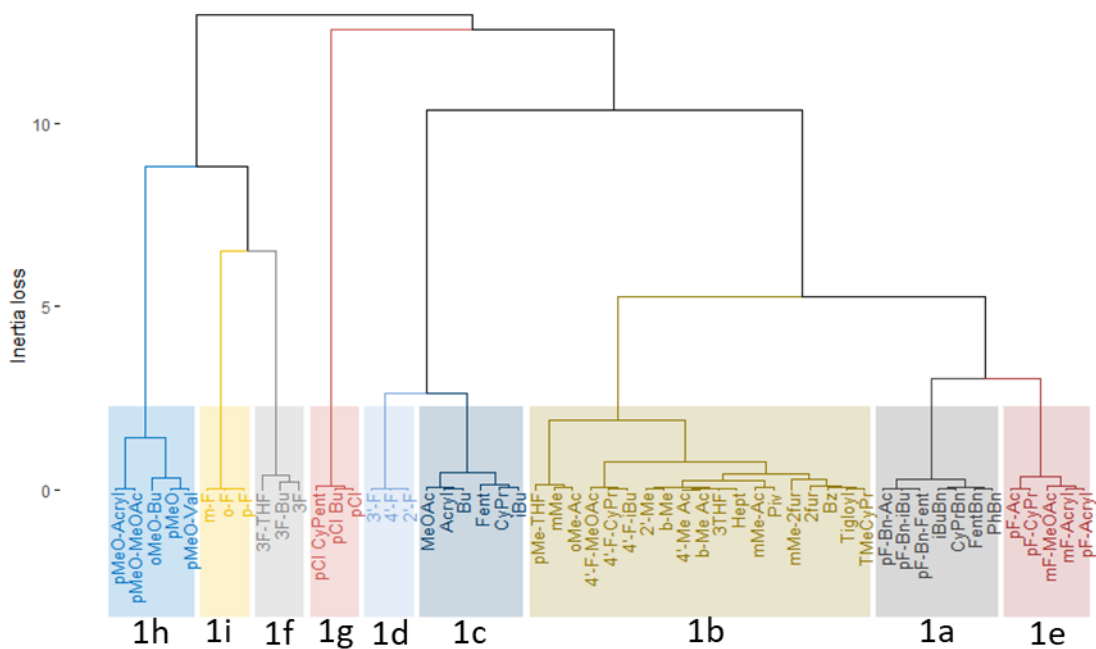


Figure 5.9. Classifier 1 dendrogram created from the hierarchical clustering of fentanyl analogues. *Note:* The vertical axis represents the loss of inertia caused by each grouping.

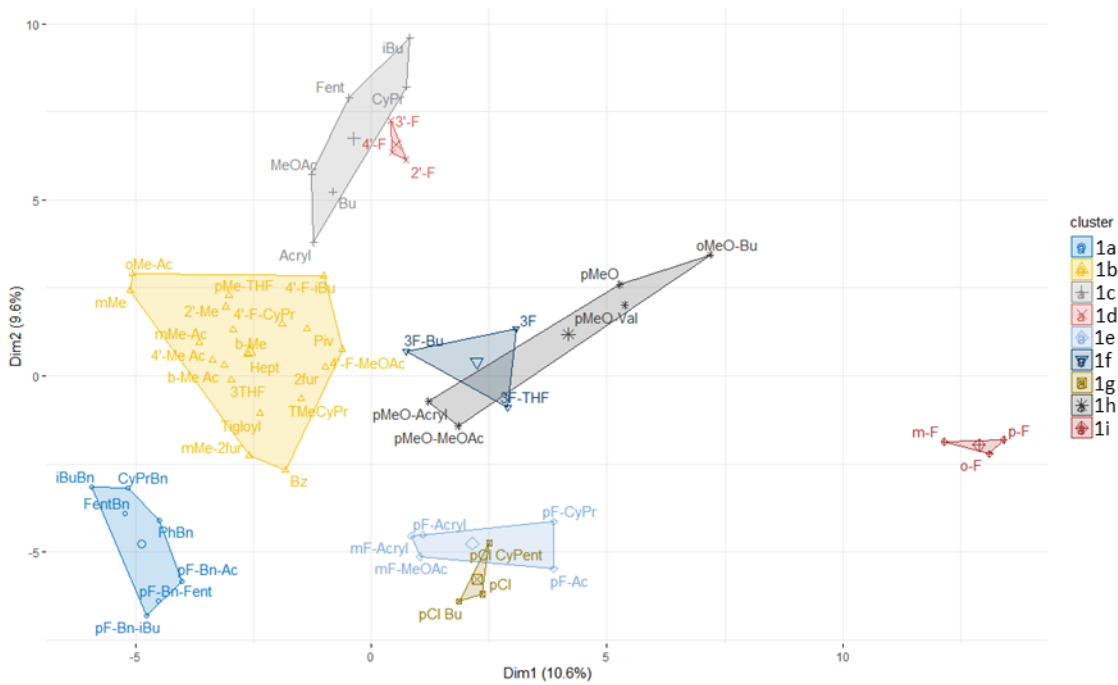


Figure 5.10. Classifier 1 hierarchical clustering shown on the PC1-PC2 plane. *Note:* PCs 3-5 are not shown but also contribute to the clustering.

Table 5.4. Individuals in each cluster of Classifier 1.

Cluster		Fentanyl analogue	Abbreviation	N°	Cluster		Fentanyl analogue	Abbreviation	N°
1a	N-Benzyl-	Isobutyryl <i>N</i> -benzyl-	iBuBn	58	1c	Amides	Acryl-	Acryl	2q
		<i>N</i> -Benzyl-	FentBn	59			Butyryl-	Bu	2c
		Cyclopropyl- <i>N</i> -benzyl-	CyPrBn	60			Propionyl-	Fentanyl	2b
		<i>para</i> -Fluoro-isobutyryl- <i>N</i> -benzyl-	pF-Bn-iBu	61			Cyclopropyl-	CyPr	2f
		<i>para</i> -Fluoro- <i>N</i> -benzyl-	pF-Bn-Fent	62			Isobutyryl-	iBu	2j
		Phenyl- <i>N</i> -benzyl-	PhBn	63	3'-Fluoro-	3'-F	46b		
		<i>para</i> -Fluoro-acetyl- <i>N</i> -benzyl-	pF-Bn-Ac	64	4'-Fluoro-	4'-F	46c		
1b	Inconclusive	<i>meta</i> -Methyl-	mMe	65	1d	Fluorophenethyl (Propionyl)	2'-Fluoro-	2'-F	46a
		<i>ortho</i> -Methyl-acetyl-	oMe-Ac	66			<i>meta</i> -Fluoro-acryl-	mF-Acryl	82
		<i>meta</i> -Methyl-acetyl-	mMe-Ac	67			<i>meta</i> -Fluoro-methoxyacetyl-	mF-MeOAc	83
		4'-Methyl-acetyl-	4'-Me Ac	68	1e	Fluoroanilines	<i>para</i> -Fluoro-acryl-	pF-Acryl	84
		β -Methyl-acetyl-	b-Me Ac	69			<i>para</i> -Fluoro-acetyl-	pF-Ac	85
		2'-Methyl-	2'-Me	70			<i>para</i> -Fluoro-cyclopropyl-	pF-CyPr	86
		<i>para</i> -Methyl-tetrahydrofuranyl-	pMe-THF	71			3-Fluoro-butyryl-	3F-Bu	87
		Tetrahydrofuranyl- (3-isomer)	3THF	72	1f	3-Fluoro-	3-Fluoro-tetrahydrofuranyl-	3F-THF	88
		β -Methyl-	b-Me	73			3-Fluoro-	3F	48
		Heptanoyl-	Hept	74			<i>para</i> -Chloro-butyryl-	pCl Bu	89
		<i>meta</i> -Methyl-furanyl-	mMe-2fur	75	1g	Chloroanilines	<i>para</i> -Chloro-	pCl	90
		((<i>E</i>)-2-Methyl-2-butenoyl)-	Tigloyl	76			<i>para</i> -Chloro-cyclopentyl-	pCl CyPent	91
		4'-Fluoro-cyclopropyl-	4'-F-CyPr	77	1h	Methoxyanilines	<i>para</i> -Methoxy-acryl-	pMeO-Acryl	92
		Benzoyl- (phenyl)	Bz	2r			<i>para</i> -Methoxy-methoxyacetyl-	pMeO-MeOAc	93
		2,2,3,3-Tetramethylcyclopropyl-	TMeCyPr	78			<i>para</i> -Methoxy-	pMeO	94
		2,2-dimethylpropanoyl-	Piv	79			<i>para</i> -Methoxy-valeryl-	pMeO-Val	95
		4'-Fluoro-butyryl-	4'-F-Bu	80			<i>ortho</i> -Methoxy-butyryl-	oMeO-Bu	96
		Furanyl-	2-fur	2o			<i>meta</i> -Fluoro-	m-F	42b
		4'-Fluoro-methoxyacetyl-	4'-F-MeOAc	81	1i	Fluoroanilines (Propionyl)	<i>ortho</i> -Fluoro-	o-F	42a
		Methoxyacetyl-	MeOAc	2n			<i>para</i> -Fluoro-	p-F	42c
1c	Amides								

Each cluster can be characterised by a number of metrics. First of all, *FactoMineR* applies a test to determine which variables most characterise each cluster (see Table 5.5). The test considers the mean and the standard deviation of a given variable in a cluster (e.g. the ion $m/z = 82$ in cluster 1a) and checks how likely it is that this average would arise if values were drawn at random from the whole population. The test centers and normalises the dataset so that its mean is 0 and its standard-deviation is 1 (standard normal distribution), then produces a test value. With such a standard normal distribution, the probability that the test value is comprised in the interval $[-1.96 : 1.96]$ is 95%. Thus, at a confidence interval of 95%, a variable with an absolute test value greater than 1.96 does not follow the normal distribution and significantly contributes to the cluster. The higher the absolute test value, the more strongly a variable characterises a given cluster. Negative test values arise if a certain ion has a consistently lower intensity in individuals of a given cluster than in the total population. Only ions with positive test values are reported in Table 5.5, in order to characterise clusters by their common fragments.

Most characteristic ions tend not to include the amide chain, but rather portions of the molecule which are common to all derivatives in a class. For instance, cluster 1a includes *N*-benzyl derivatives (**58-64**) and is characterised mostly by $m/z = 82$, 91 and 173, ions which have previously been reported to arise strongly in this class of compounds, and not in traditional *N*-phenethyl analogues. Cluster 1b includes ions methylated on the aniline ring ($m/z = 160$, 203) or the phenethyl chain ($m/z = 119$). As noted before, cluster 1b includes “inconclusive” compounds; it is situated close to the center of the PCA space and is the most heterogeneous cluster. Ions characteristic of cluster 1b also deviate less strongly from the normal distribution than other clusters: the *p*-

value of the most characteristic cluster 1b ion ($m/z = 160$, p -value = 9.1×10^{-3}) is many orders of magnitude lower than most other clusters.

Cluster 1c includes fentanyl (**2b**) and similar amide-chain derivatives. None of the ions strongly characteristic of this cluster have previously been reported. The typical ions of $m/z = 146$ and 189 , are common to analogues of clusters 1b, 1c and 1d, and thus cluster 1c is differentiated by the more specific ions reported in Table 5.5. The most notable ion associated with cluster 1d is the fluorinated tropylium ion at $m/z = 109$. Some of the other ions, although they have not been characterised, must include the propionyl amide chain, to explain why non-propionyl 4'-fluorinated derivatives fall within cluster 1b, not 1d.

Two of the most important cluster 1e ions, $m/z = 136$ and 150 , have not been characterised, but likely structures, which arise from fragmentation of the piperidine ring, are suggested in Table 5.5. Ions analogous to $m/z = 150$ were observed in other clusters, with a mass difference consistent with the substituent on the aromatic ring ($m/z = 132$ for cluster 1c; $m/z = 166$ for cluster 1h, $m/z = 162$ for cluster 1h). The $m/z = 275$ ion and its 276 isotope are unique to *para*-fluoro cyclopropylfentanyl (**86**). This seems to be a rare occurrence where an ion from a single compound contributes to defining a cluster, and may be a limitation of cluster 1e.

Cluster 1f, which includes 3-fluorinated derivatives (**48**, **87-88**), is characterised mostly by unknown ions. Most common ions of 3-fluorinated compounds also arise in fluoroaniline derivatives (clusters 1e and 1i), because of the position of the fluorine atom, which is retained in major EI-MS fragments. Therefore, the distinction between these clusters is based on differences detected in minor

fragments. The ion at $m/z = 207$ is an exception: it characterises cluster 1f because its intensity in 3-fluorinated derivatives is stronger than other fluorinated compounds.

Cluster 1g is most strongly characterised by the chlorinated $m/z = 223$ ion and its 224 and 225 isotopes. As previously discussed, the $m/z = 166$ ion is suggested to arise from a fragmentation of the piperidine ring. Cluster 1h includes methoxylated derivatives (**92-96**). It is strongly characterised by $m/z = 162$, as well as $m/z = 134$ which is consistent with further fragmentation of the piperidine ring. $m/z = 108$ corresponds to a methoxyphenyl cation, while $m/z = 176$ and its 177 isotope are the methoxyl equivalent of a known fentanyl ion. Finally, individuals in cluster 1i are differentiated from other fluorinated compounds in clusters 1e and 1f mostly by $m/z = 263$, which includes the propionyl amide chain. Cluster 1i is also characterised by common fluorinated fragment $m/z = 164$.

The characterisation of unidentified ions could be the object of further research and would require more advanced, high-resolution mass spectrometry techniques. This would help better understand the present model.

Table 5.5. Description of clusters by the five most significant *m/z* values.

Cluster	<i>m/z</i>	Test value ^a	Mean in cluster	Overall mean ^b	p-value ^c	Suspected fragment
1a	82	7.12	0.816	0.133	1.1E-12	
	91	6.88	1.000	0.302	6.0E-12	
	173	6.83	0.168	0.026	8.6E-12	
	174	6.83	0.070	0.011	8.6E-12	m/z = 173 isotope
	92	5.38	0.089	0.039	7.5E-08	m/z = 91 isotope
1b	160	2.61	0.179	0.077	9.1E-03	
	203	2.51	0.086	0.033	1.2E-02	
	204	2.38	0.018	0.009	1.8E-02	m/z = 203 isotope
	119	2.14	0.035	0.025	3.3E-02	
	117	2.07	0.037	0.030	3.8E-02	—
1c	104	4.59	0.177	0.081	4.5E-06	—
	159	4.59	0.027	0.009	4.5E-06	—
	132	4.47	0.167	0.076	7.7E-06	¹³ C ₃ H ₄ -NH
	147	4.45	0.087	0.031	8.6E-06	m/z = 146 isotope
	98	4.40	0.067	0.023	1.1E-05	—
1d	109	6.54	0.197	0.022	6.0E-11	
	101	6.05	0.043	0.005	1.5E-09	—
	93	5.37	0.529	0.096	7.8E-08	—
	66	4.95	0.040	0.011	7.4E-07	—
	103	4.71	0.216	0.078	2.4E-06	—

Table 5.5 Description of clusters by the five most significant *m/z* values. (cont.)

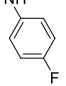
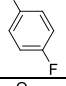
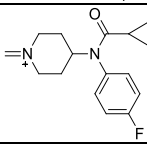
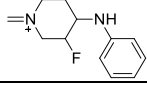
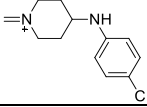
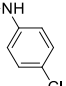
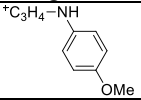
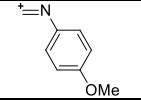
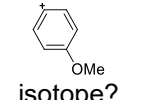
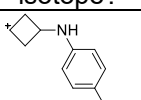
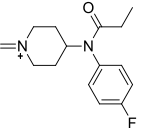
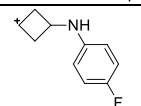
Cluster	<i>m/z</i>	Test value ^a	Mean in cluster	Overall mean ^b	p-value ^c	Suspected fragment
1e	150	3.78	0.069	0.018	1.5E-04	⁺ C ₃ H ₄ -NH 
	206	3.47	0.070	0.009	5.2E-04	—
	136	3.18	0.048	0.015	1.5E-03	⁺ C ₂ H ₂ -NH 
	275	3.12	0.200	0.019	1.8E-03	
	276	3.11	0.036	0.004	1.8E-03	<i>m/z</i> = 275 isotope
1f	114	7.27	0.060	0.004	3.7E-13	—
	186	6.88	0.248	0.034	5.8E-12	—
	207	4.82	0.498	0.081	1.5E-06	
	185	4.41	0.035	0.010	1.0E-05	—
	71	4.32	0.395	0.044	1.6E-05	—
1g	225	7.26	0.122	0.007	4.0E-13	<i>m/z</i> = 223 isotope
	223	7.25	0.381	0.022	4.1E-13	
	224	7.21	0.056	0.003	5.4E-13	<i>m/z</i> = 223 isotope
	127	7.08	0.121	0.007	1.5E-12	—
	166	6.94	0.065	0.004	3.9E-12	⁺ C ₃ H ₄ -NH 

Table 5.5. Description of clusters by the five most significant m/z values. (cont.)

Cluster	m/z	Test value ^a	Mean in cluster	Overall mean ^b	p-value ^c	Suspected fragment
1h	162	6.66	0.078	0.010	2.8E-11	
	134	6.52	0.094	0.020	7.2E-11	
	108	6.43	0.100	0.011	1.3E-10	 isotope?
	176	6.29	0.676	0.073	3.2E-10	
	177	6.13	0.106	0.014	8.6E-10	m/z = 176 isotope
1i	111	6.97	0.567	0.046	3.1E-12	—
	167	6.91	0.066	0.005	5.0E-12	—
	263	6.24	1.000	0.075	4.3E-10	
	164	6.19	0.668	0.071	6.2E-10	
	112	6.14	0.039	0.004	8.0E-10	—

^a Test value determining the likelihood that values of variable q can be drawn from the total population at random (if $|\text{test value}| \geq 1.96$, the hypothesis that they were drawn at random is rejected at 95% confidence interval); ^b Average value for the total population; ^c Probability that a variable follows a standard normal distribution.

The quality of clusters can be evaluated based on their silhouette coefficient S_i , which is defined in Equation 6: [179, 181]

$$S_i = \frac{(b_i - a_i)}{\max(a_i, b_i)} \quad \text{Eqn. 6}$$

For each individual i , the average dissimilarity a_i between it and other members of its cluster is calculated. Then, the average dissimilarity between i and every other cluster is calculated; the smallest of these, *i.e.* the dissimilarity between i and its neighbour cluster, is noted b_i . This coefficient can take values between -1 and 1 and measures the quality of clustering for each object. A coefficient near 1 means an object clusters almost perfectly, 0 means it lies between two clusters and a negative value indicates that an individual is likely in the wrong cluster. The silhouette plot is shown in Figure 5.11. All individuals have a coefficient above 0 and cluster relatively well. Unsurprisingly, the least cohesive cluster appears to be cluster 1b.

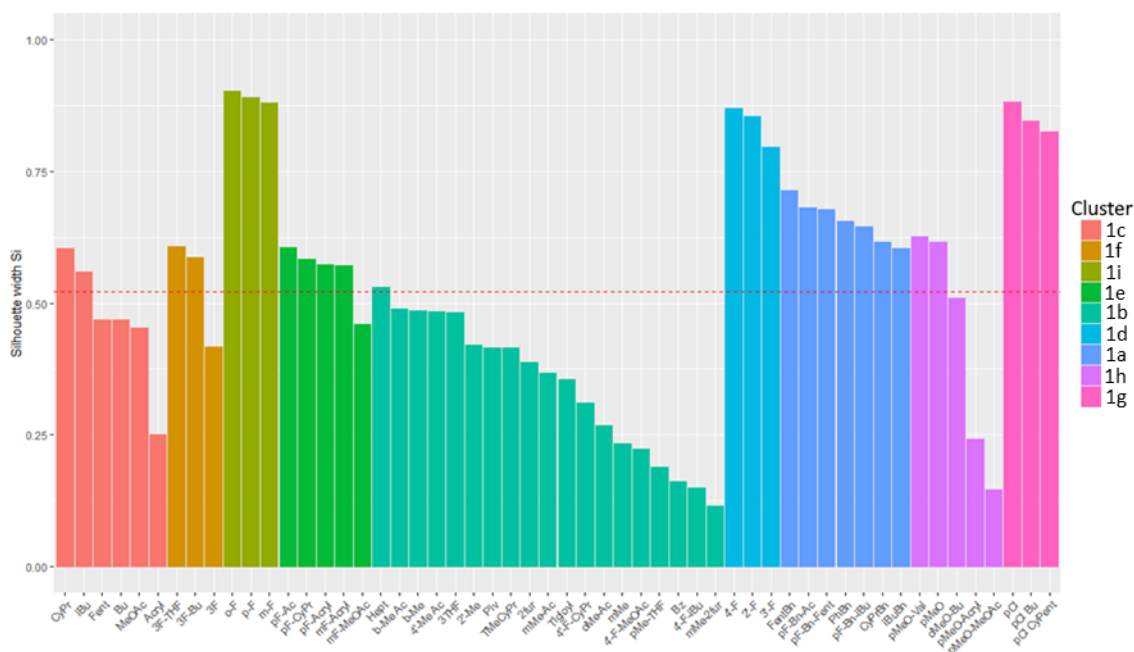


Figure 5.11. Silhouette coefficients of individuals in classifier 1. *Note:* The dotted line represents the average silhouette coefficient.

However, as discussed previously, there is a danger of overfitting the model by dividing it into too many clusters. By doing so, the model would be able to completely discriminate compounds from this dataset, but it will do poorly when classifying new, unknown data. Hence, overfitting can be detected indirectly when testing the model on new data.

To get around this, and because cluster 1b is not currently very useful for prediction purposes, a second classifier was designed. This included only individuals from cluster 1b, in the hopes that the differences between these compounds could be extracted more efficiently in a restrained dataset. Thus, during the evaluation phase, test samples will first be compared with Classifier 1 to see which cluster they belong to, then any sample falling within cluster 2

will be compared with Classifier 2. This iterative classification process can be automated, so that the use of two classifiers (or more) is not more complex for the end-user.

The 17 compounds used to build Classifier 2 are detailed in Table 5.6. A PCA was performed and, with the same criteria previously described, PCs 1-4 were retained (51.2% of total variance). Four clusters clearly arose from hierarchical clustering, resulting in the dendrogram shown in Figure 5.12. As opposed to the first classifier, this one allows the proper grouping of fluorophenethyl- (cluster 2a) and methylaniline (cluster 2d) analogues. Cluster 2c groups compounds with aromatic amides which, because of the increased stability of their amide and acylium ions, produce significantly different mass spectra from other amides. Cluster 2b groups two types of compounds. Firstly, “*unconventional*” aliphatic amides which are uncaptured by classifier 1 [*i.e.* 3-tetrahydrofuranyl- (**72**); heptanoyl- (**74**) and 2,2-dimethylpropanoylfentanyl (pivaloylfentanyl, **79**)]. Cluster 2b also includes compounds bearing methyl substituents on their phenethyl- tails, either on the aromatic ring or on the ethyl linker, which are difficult to identify because the resulting fragment ions are not significantly different, in mass or intensity, from those of other analogues. [141] However, although these two groups cluster together on the PC1-PC2 plane (Figure 5.13), they could potentially be differentiated by PC4 (Figure 5.14).

Table 5.6. Individuals in each cluster of Classifier 2.

Cluster		Fentanyl analogue	Abbreviation	N°
2a	Fluorophenethyl-	4'-Fluoro-methoxyacetyl-	4'-F-MeOAc	81
		4'-Fluoro-cyclopropyl-	4'-F-CyPr	77
		4'-Fluoro-butyryl-	4'-F-Bu	80
2b	Methylphenethyl- & Amides	4'-Methyl-acetyl-	4'-Me Ac	68
		Heptanoyl-	Hept	74
		β -Methyl-acetyl-	b-Me Ac	69
		Tetrahydrofuranyl- (3-isomer)	3THF	72
		2'-Methyl-	2'-Me	70
		2,2-dimethylpropanoyl-	Piv	79
		β -Methyl-	b-Me	73
2c	Aromatic amides	Benzoyl- (Phenyl)	Bz	2r
		Furanyl-	2-fur	2o
		<i>meta</i> -Methyl-furanyl-	mMe-2fur	75
2d	Methylanilines	<i>meta</i> -Methyl-acetyl-	mMe-Ac	67
		<i>para</i> -Methyl-tetrahydrofuranyl-	pMe-THF	71
		<i>ortho</i> -Methyl-acetyl-	oMe-Ac	66
		<i>meta</i> -Methyl-	mMe	65

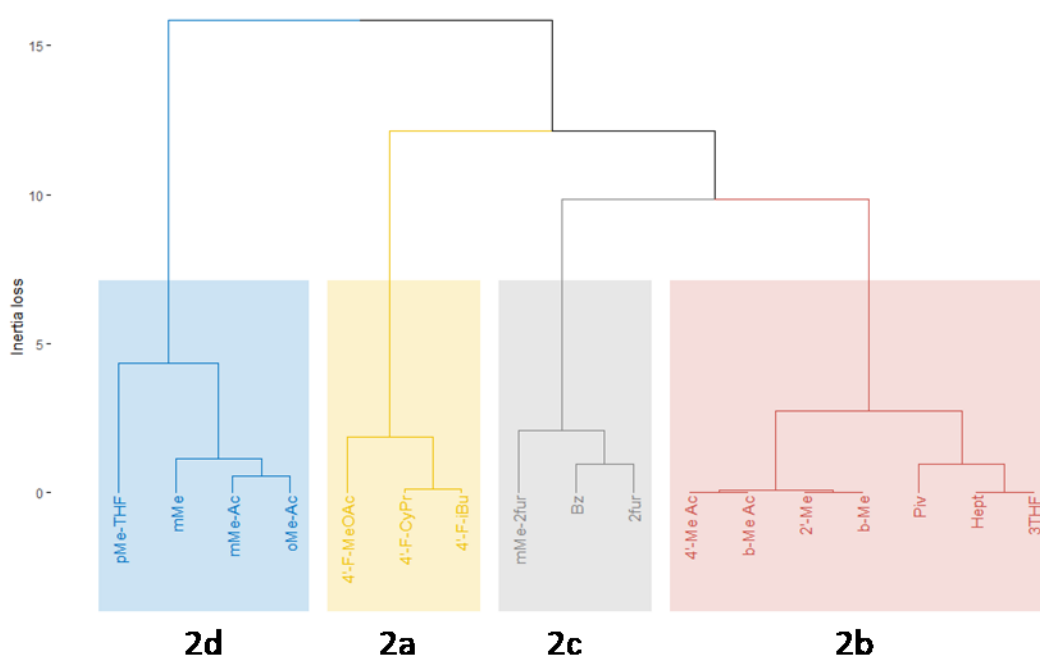


Figure 5.12. Dendrogram created from the hierarchical clustering of fentanyl analogues (Classifier 2). *Note:* The vertical axis represents the loss of inertia caused by each grouping.

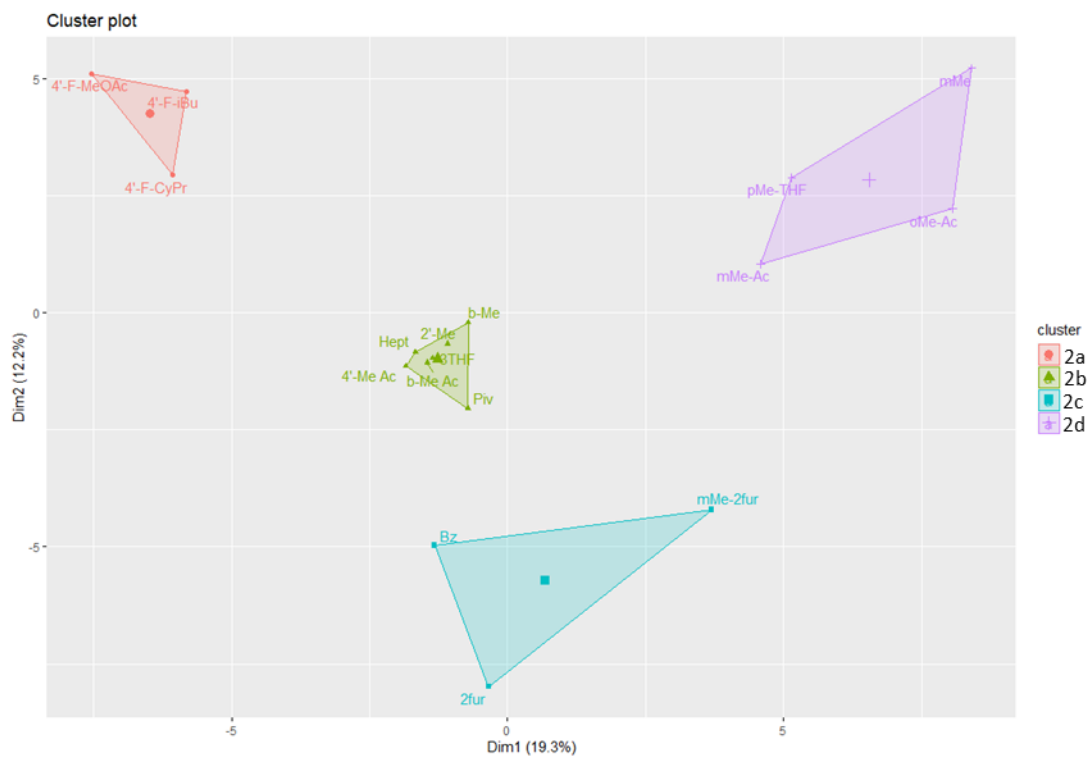


Figure 5.13. Classifier 2 hierarchical clustering shown on the PC1-PC2 plane.

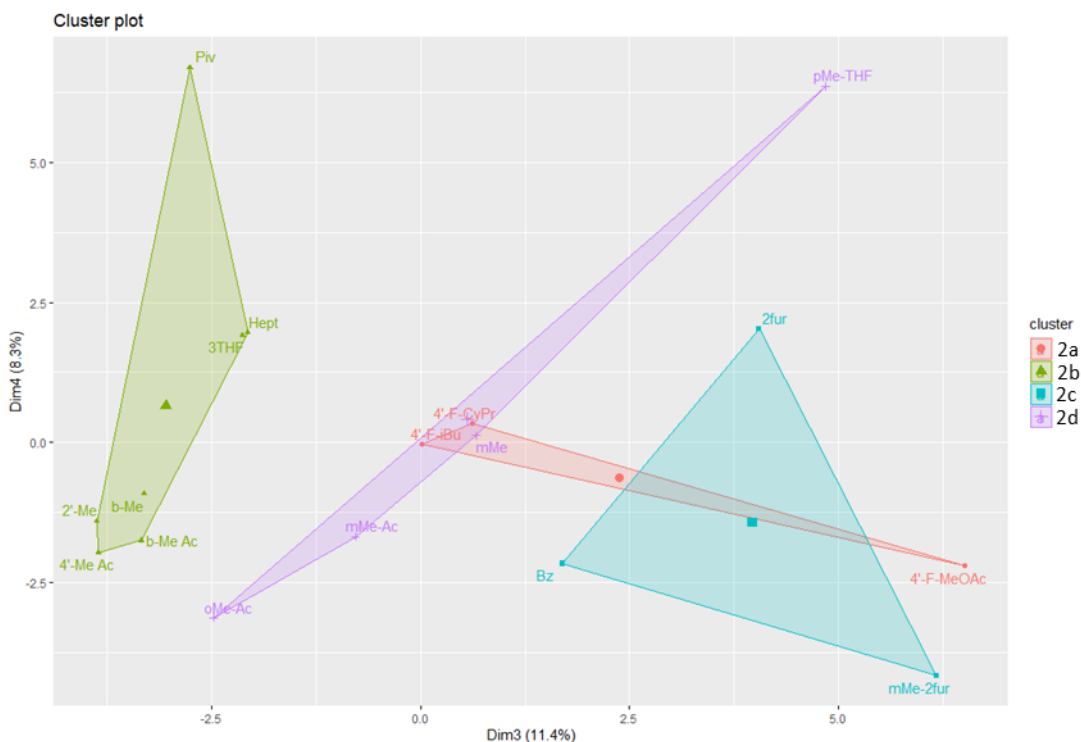


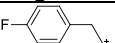
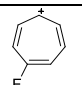
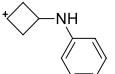
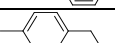
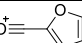
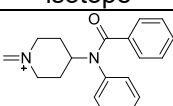
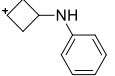
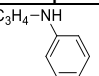
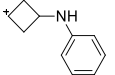
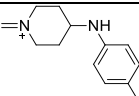
Figure 5.14. Classifier 2 hierarchical clustering shown on the PC3-PC4 plane.

The fragments most characteristic of each cluster are reported in Table 5.7. Cluster 2a is characterised by a fluorophenethyl cation ($m/z = 123$) and a fluorinated tropylium fragment ($m/z = 109$), both characteristic of fentanyl analogues bearing a fluorine on their phenethyl chain. Cluster 2b includes $m/z = 146$, a typical fentanyl fragment, as well as a methylphenethyl cation ($m/z = 119$).

The ions reported for cluster 2c in Table 5.7 do not readily appear to be common to all three compounds. In this case, it may be more relevant to examine ions with a negative test value. All compounds have an acylium ion

as their base peak due to the increased stability of their aromatic amide chain ($m/z = 95$ for 2-furanylfentanyl (**2o**) and *meta*-methyلفuranylfentanyl (**75**); $m/z = 105$ for benzoylfentanyl (**2r**)). This decreases the relative intensity of common fragment ions when compared to other analogues. As shown in Table 5.7, $m/z = 146$ and its 147 isotope, one of the major fragments of fentanyl (**2b**), is lower in cluster 2c than in the whole dataset. This explains how aromatic compounds with different fragment ions can cluster together. Finally, cluster 2d is characterised by $m/z = 160$ and 203 fragments, expected for methylaniline compounds.

Table 5.7. Description of Classifier 2 clusters by the five most significant *m/z* values.

Cluster	<i>m/z</i>	Test value	Mean in cluster	Overall mean	p-value	Suspected fragment
2a	123	3.98	0.174	0.031	6.8E-05	
	122	3.93	0.073	0.013	8.7E-05	—
	121	3.89	0.032	0.007	1.0E-04	—
	109	3.87	0.079	0.015	1.1E-04	
	101	3.81	0.026	0.006	1.4E-04	—
2b	131	2.98	0.049	0.040	2.9E-03	—
	146	2.63	0.481	0.298	8.5E-03	
	119	2.17	0.059	0.037	3.0E-02	
	188	2.08	0.124	0.061	3.8E-02	—
	147	2.06	0.054	0.038	3.9E-02	m/z = 146 isotope
2c	95	3.13	0.669	0.138	1.8E-03	
	98	2.91	0.056	0.018	3.6E-03	—
	184	2.38	0.034	0.012	1.7E-02	—
	294	2.26	0.022	0.004	2.4E-02	m/z = 293 isotope
	293	2.25	0.103	0.019	2.4E-02	
	146	-2.14	0.028	0.298	3.2E-02	
	131	-2.19	0.028	0.040	2.8E-02	—
	147	-2.32	0.005	0.038	2.0E-02	m/z = 146 isotope
	132	-3.34	0.039	0.087	8.3E-04	
2d	160	3.85	0.791	0.197	1.2E-04	
	161	3.75	0.103	0.027	1.8E-04	m/z = 160 isotope
	145	3.69	0.074	0.026	2.2E-04	—
	144	3.49	0.082	0.032	4.9E-04	—
	203	3.43	0.387	0.096	6.0E-04	

5.4 Model evaluation

Classifiers 1 and 2 proved that most fentanyl analogues could successfully be grouped, using mass spectral data, into clusters consistent with their structural classes. Sixty-seven new compounds were compared against these classifiers, to test whether the model was able to successfully attribute unknown compounds to the right class.

Each given test analogue was projected as a point in the PCA space and assigned to the nearest cluster. Two distance measurement methods were evaluated: a sample could be matched to the cluster with the nearest centroid, or to the cluster of its nearest neighbour. Test analogues which were classed in cluster 1b were then fed into Classifier 2, where the process was repeated. Finally, analogues classed in cluster 2b, which includes methylphenethyl compounds and “unconventional” aliphatic amides, were attributed to one of these two groups based on their nearest neighbour in this cluster, regardless of the distance measurement used. The classification result is then compared to the analogue’s actual class to determine accuracy.

A comparison of these two match criteria is reported in Table 5.8. The nearest neighbour method, which correctly classified 61 of the 67 test compounds, was more accurate overall (91.0% accuracy).

Table 5.8. Comparison of the centroid and nearest neighbour classification criteria.

	Centroid method	Nearest neighbour method
Classifier 1 matches ^a	37 / 43	37 / 39
Classifier 2 matches	19 / 24	24 / 28
Total matches	56 / 67	61 / 67
Overall accuracy	83.6%	91.0%

^a Compounds classed in cluster 2 excluded.

Table 5.9. Detailed model evaluation results obtained with the nearest neighbour method.

Fentanyl analogue	N°	Classifier 1		Classifier 2		Match?
		Nearest neighbour	Cluster	Nearest neighbour	Cluster	
<i>meta</i> -Fluoro- <i>N</i> -benzyl-	97	pF-Bn-Ac	1a	—	—	Y
<i>para</i> -Fluoro- <i>N</i> -benzylfuranlyl-	98	pF-Bn-Ac	1a	—	—	Y
Acetyl- <i>N</i> -benzyl-	99	CyPrBn	1a	—	—	Y
Furanlyl- <i>N</i> -benzyl-	100	PhBn	1a	—	—	Y
Methoxyacetyl- <i>N</i> -benzyl-	101	FentBn	1a	—	—	Y
Butyryl- <i>N</i> -benzyl-	102	iBuBn	1a	—	—	Y
Acryl- <i>N</i> -benzyl-	103	FentBn	1a	—	—	Y
<i>para</i> -Fluoro- <i>N</i> -benzyl-cyclopropyl-	104	pF-Bn-Ac	1a	—	—	Y
Tetrahydrofuranlyl- <i>N</i> -benzyl-	105	pF-Bn-Fent	1a	—	—	Y
4-ANPP	4	2'-Me	1b	b-Me	2b	N
Crotonyl- ((<i>E</i>)-But-2-enoyl)	106	2'-Me	1b	Hept	2b	Y
(2-Methyl)butyryl-	107	Piv	1b	Piv	2b	Y
Ethoxyacetyl-	108	Piv	1b	3THF	2b	Y
Cyclopropylacetyl-	109	3THF	1b	Piv	2b	Y
<i>ortho</i> -Methyl-acryl-	110	Hept	1b	Hept	2b	N
<i>para</i> -Methyl-acetyl-	111	oMe-Ac	1b	oMe-Ac	2d	Y
<i>ortho</i> -Methyl-	10	mMe	1b	mMe-Ac	2d	Y
<i>meta</i> -Methyl-cyclopropyl-	112	b-Me Ac	1b	mMe-Ac	2d	Y
<i>ortho</i> -Methyl-furanlyl-	113	mMe-2fur	1b	mMe-2fur	2c	Y
<i>para</i> -Methyl-furanlyl-	114	mMe-2fur	1b	mMe-2fur	2c	Y
<i>meta</i> -Methyl-methoxyacetyl-	115	mMe-Ac	1b	mMe-Ac	2d	Y
<i>ortho</i> -Methyl-cyclopropyl-	116	mMe-Ac	1b	mMe-Ac	2d	Y
4'-Fluoro-furanlyl-	117	TMeCyPr	1b	2fur	2c	Y
<i>meta</i> -Methoxy-furanlyl-	118	Bz	1b	Bz	2c	Y
<i>ortho</i> -Methoxy-furanlyl-	119	Piv	1b	Bz	2c	Y
<i>para</i> -Methoxy-furanlyl-	120	TMeCyPr	1b	Bz	2c	Y
<i>para</i> -Chloro-furanlyl- (3-isomer)	121	Bz	1b	Bz	2c	Y
3'-Methyl-acetyl-	122	2'-Me	1b	2'-Me	2b	Y
4'-Methyl-	123	2'-Me	1b	2'-Me	2b	Y
α -Methyl-acetyl-	124	Tigloyl	1b	b-Me Ac	2b	Y
α -Methyl-butyryl-	125	Tigloyl	1b	3THF	2b	N
α -Methyl-	126	4'-F-iBu	1b	3THF	2b	N
4'-Fluoro-acetyl-	127	4'-F-MeOAc	1b	4'-F-CyPr	2a	Y
2'-Methyl-acetyl-	128	2'-Me	1b	2'-Me	2b	Y

Table 5.9. Detailed model evaluation results obtained with the nearest neighbour method. (cont.)

Fentanyl analogue	N°	Classifier 1		Classifier 2		Match?
		Nearest neighbour	Cluster	Nearest neighbour	Cluster	
Thiophenyl- (3-isomer)	129	Bz	1b	Bz	2c	Y
3'-Methyl-	130	2'-Me	1b	2'-Me	2b	Y
<i>ortho</i> -Fluoro-furanyl-	131	Bz	1b	Bz	2c	Y
Acetyl-	2a	Acryl	1c	—	—	Y
<i>iso</i> -Valeryl-	2k	Bu	1c	—	—	Y
Valeryl-	2d	MeOAc	1c	—	—	Y
Hexanoyl-	2e	CyPr	1c	—	—	Y
Cyclobutyryl-	2g	MeOAc	1c	—	—	Y
2'-fluoro- <i>ortho</i> -fluoro-	47	pF-Ac	1e	—	—	Y
<i>para</i> -Fluoro-butyryl-	132	pF-CyPr	1e	—	—	Y
<i>para</i> -Fluoro-isobutyryl-	133	pF-CyPr	1e	—	—	Y
<i>para</i> -Fluoro-cyclopentyl-	134	mF-MeOAc	1e	—	—	Y
<i>para</i> -Fluoro-tetrahydrofuranyl-	135	pF-CyPr	1e	—	—	Y
<i>para</i> -Fluoro-crotonyl-	136	mF-Acryl	1e	—	—	Y
<i>meta</i> -Fluoro isobutyryl	137	pF-CyPr	1e	—	—	Y
<i>ortho</i> -Fluoro-butyryl-	138	pF-CyPr	1e	—	—	Y
<i>ortho</i> -Fluoro-isobutyryl-	139	pF-CyPr	1e	—	—	Y
<i>para</i> -Fluoro-valeryl-	140	pF-CyPr	1e	—	—	Y
<i>para</i> -Fluoro-furanyl- (3-isomer)	141	mF-Acryl	1e	—	—	Y
2,3-Benzodioxolyl-	142	pF-Acryl	1e	—	—	N
<i>para</i> -Chloro-furanyl-	143	mF-MeOAc	1e	—	—	N
<i>meta</i> -Fluoro-butyryl-	144	pF-CyPr	1e	—	—	Y
<i>para</i> -Fluoro-furanyl-	145	mF-Acryl	1e	—	—	Y
<i>meta</i> -Fluoro-furanyl-	146	mF-Acryl	1e	—	—	Y
<i>meta</i> -Fluoro-isobutyryl-	147	pF-CyPr	1e	—	—	Y
3-Fluoro-isoburytyl-	148	3F-THF	1f	—	—	Y
<i>para</i> -Chloro-cyclobutyryl-	149	pCl Bu	1g	—	—	Y
<i>para</i> -Chloro-isobutyryl-	150	pCl Bu	1g	—	—	Y
<i>para</i> -Chloro-methoxyacetyl-	151	pCl CyPent	1g	—	—	Y
<i>para</i> -Chloro-valeryl-	152	pCl CyPent	1g	—	—	Y
<i>para</i> -Chloro-acryl-	153	pCl CyPent	1g	—	—	Y
<i>para</i> -Methoxy-butyryl-	154	pMeO-Acryl	1h	—	—	Y
<i>para</i> -Methoxy-methoxyacetyl-	155	p-F	1i	—	—	Y

The detailed results obtained using the nearest neighbour method are reported in Table 5.9. Overall, Classifier 1 reliably identified a variety of *N*-benzyl derivatives (cluster 1a), most aliphatic amides (cluster 1c), fluoroaniline derivatives (cluster 1e) and chloroaniline derivatives (cluster 1g). It also properly classified 3-fluoro-isobutyrylfentanyl (**148**) in cluster 1f and *para*-methoxy-butyrylfentanyl (**154**) in cluster 1h, though only had a limited number of compounds were available to test these classes. Misclassifications made by Classifier 1 involved aromatic amides 2,3-benzodioxolefentanyl (**142**) and *para*-chloro-3-furanylfentanyl (**143**), wrongly classed in cluster 1e.

Compounds in cluster 1b were screened against Classifier 2, which properly identified methylaniline (cluster 2d) and 4'-fluoro (cluster 2a) derivatives. As cluster 2b also includes methylphenethyl- and non-aromatic amide derivatives, test individuals in cluster 2b were tentatively classified into one of these two classes based on their nearest neighbour. Although Classifier 2 had limitations, this could be solved by including more derivatives from each class in the model, which was not possible with the current dataset.

As noted previously, aromatic amides tend to cluster together in the Classifier 2 model because the presence of an aromatic amide significantly modifies the observed *m/z* ions. Aromatic amides tested were thus classified in cluster 2c, regardless of other modifications to their structure (fluorinated (**117**, **131**), chlorinated (**121**), methoxylated (**118-120**) and methylated (**113-114**) analogues). It is worth noting one exception, in that Classifier 1 correctly classed *meta*- and *para*-fluoro-furanylfentanyl (**141**, **145-146**) into the fluorinated analogues cluster. Again, this could be remediated by adding aromatic compounds representative of each class of derivatives to the model. In fact, an initial exploration using all aromatic compounds available in the full

dataset shows that they can cluster based on their secondary modification (see Figure 5.15). The partition was not perfect, with furanylfentanyl (**2o**) clustering on its own, but could be improved by including more examples of this class of derivatives.

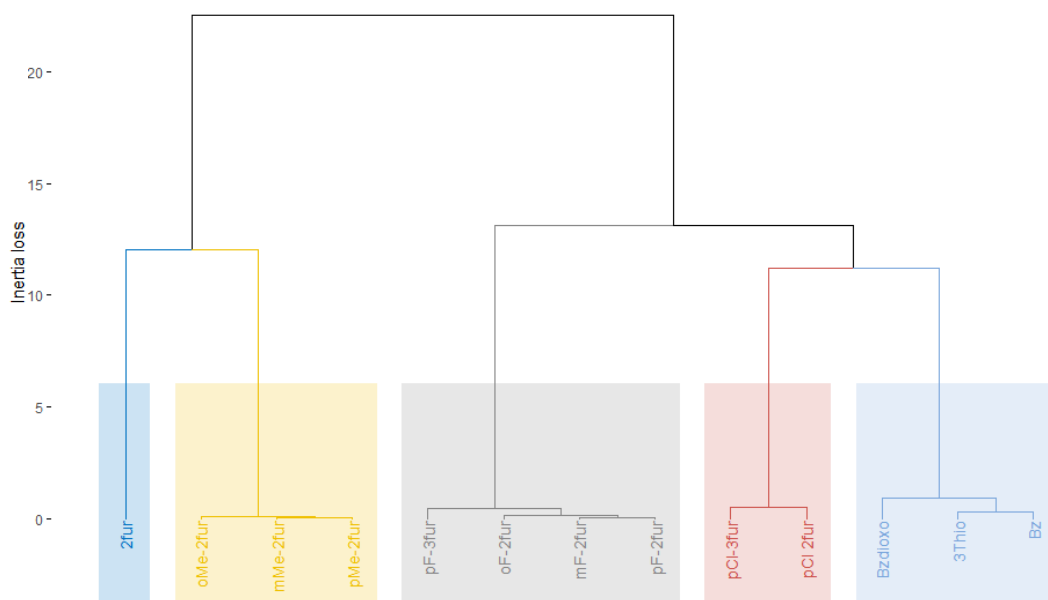


Figure 5.15. Dendrogram created from the hierarchical clustering of aromatic amide analogues. Note: The vertical axis represents the loss of inertia caused by each grouping.

Although this model allows the classification of fentanyl analogues, it does not allow the discrimination of closely related regioisomers which produce the same mass ions (*e.g.* *ortho*-, *meta*- and *para*-fluorofentanyl (**42a-c**)). However, separation of fluorofentanyl regioisomers has been achieved by Bonetti *et al* using PCA followed by linear discriminant analysis on multiple injections of the

same compounds. [115] The model presented in this chapter and Bonetti's model could be used in conjunction to first identify the class of an unknown substituted fentologue, then determine the position of its substituent.

5.5 Conclusion

In conclusion, a principal component analysis (PCA) and hierarchical clustering model was used to classify fentanyl analogues with high accuracy. The model is more precise than previously described spectral mapping models, because the PCA forms clusters based on the intensity of specific fragments rather than shifts in spectral peaks. [116] For instance, all *ortho*-, *meta*- and *para*-fluorinated compounds project close to each other in the PCA space, because fluorination of the aniline ring of fentanyl leads to very specific fragments shared by these analogues. Rather than only detect a modification of the aniline ring, the classifier was able to detect what modification was introduced. This model works reliably with compounds that are two modifications away from fentanyl, because it has been constructed using many examples of these types of compounds. The proposed model can be adapted to other classes of compounds with some optimisation. One drawback is that the model relies on the availability of enough spectra of representative analogues for classes to arise.

CHAPTER VI

CONCLUSION AND FUTURE WORK

In conclusion, each chapter of this thesis focused on a different aspect of fentanyl detection in a forensic context. In Chapter II, analytical methods were tested for the detection and quantification of 18 amide derivatives of fentanyl, using reference material synthesised in-house. A combination of the Marquis and Eosin Y colour tests allowed presumptive discrimination of fentalogues from common controlled drugs and adulterants. Thin-layer chromatography allowed partial separation of fentalogues from each other, and full separation from heroin. Formal separation and identification of fentanyls, however, requires more advanced techniques and was achieved using GC-EI-MS. Fragmentation patterns common to all fentalogues and fragments specific to certain compounds were described. A GC-MS separation method was optimised and fully validated for quantification at low concentrations (LOD: 0.008 – 0.125 µg/mL and LOQ: 0.025 – 0.415 µg/mL). The analytical methods described were applied to seven seized heroin samples. The Eosin Y colour test and TLC analysis allowed the presumptive detection of fentanyl in one sample (SS-1). FTIR analysis only allowed the clear identification of heroin in samples containing no caffeine or paracetamol. It did not allow the detection of fentanyl in SS-1. An initial GC-MS screening confirmed the presence of fentanyl in only one sample (SS-1). The optimised SIM method showed greatly improved sensitivity and allowed the detection of fentanyl in a second, lower-concentration sample (SS-2). Using the optimised quantification method,

fentanyl concentration was determined in both SS-1 and SS-2 at $6.29 \pm 0.01\%$ w/w and $0.288 \pm 0.008\%$ w/w, respectively.

In Chapter III, it was shown that fluorinated regioisomers of fentanyl, which are increasingly common on drug markets, could not be fully discriminated using methods previously explored (*i.e.* colour tests, TLC, infrared spectroscopy or GC-MS). GC-MS afforded partial discrimination, but the co-elution of compounds with the same major *m/z* fragments prevented a conclusive identification. A GC-MS quantification method was developed, as it could still be useful for single-component samples or samples containing non co-eluting compounds. ^{19}F benchtop NMR was proposed as an orthogonal method for the identification and quantification of fluorinated regioisomers of fentanyl. Most fentalogues investigated produced distinct signals in low-field ^{19}F NMR and a quantification method was developed using this technique. Despite its lower sensitivity than GC-MS, benchtop ^{19}F NMR showed sufficiently low LODs and LOQs, and it was shown that it could detect *ortho*-fluorofentanyl in a 2.4 %w/w heroin mixture.

In Chapter IV, the reaction between the eosin Y dye and illicit drugs, including heroin and fentanyl, was investigated. It was determined that eosin Y caused the precipitation of fentanyl free-base through an acid-base reaction. It was suggested that the characteristic deep pink colour observed with fentanyl was due to the co-precipitation of eosin Y. The test could not successfully be applied to the quantification of fentanyl in mixtures, but it could still be used for qualitative detection. This was especially reliable when using UV-Vis spectrophotometry, because the fentanyl – eosin Y mixture absorbs at a specific wavelength. Solgel detection coupled with RGB measurement, on the other hand, lacked selectivity and proved susceptible to interference from other

components found in mixtures (e.g. heroin, caffeine, paracetamol). Nevertheless, the developed methodology proved useful for the standardisation of colorimetric tests.

In Chapter V, a principal component analysis (PCA) and hierarchical clustering model was used to classify fentanyl analogues with high accuracy. The model formed clusters based on the intensity of specific EI-MS fragments representative of the structural classes of analogues. It was able to classify test analogues with 91% accuracy. The model can be used to help the structural elucidation of novel analogues seized in forensic casework, based solely on their mass spectrum.

Future work will involve the development of a PCA classification model that will include different types of illicit drugs, for instance natural opiates, members of new synthetic opiate families (e.g. MT-45 or U-49900), or others. When confronted with an unidentified seized sample, this model would allow an initial triage by drug family. Different classification models, such as the one presented in Chapter V, can then be developed for each family, to determine structural modifications. Efforts should also go towards the identification, by high-resolution mass spectrometry, of the unknown m/z fragments of fentanyl and its analogues shown in Table 5.5. This would give greater insight into the developed model and the fragmentation patterns of fentanyl analogues in general. Finally, a PCA classification model could be built using ^1H NMR data. This would allow the discrimination of substituted regioisomers: as shown in Chapter III, for instance, fluorofentanyl isomers can be differentiated by the appearance of their aromatic region. An NMR model including fluoro-, chloro-, methoxy- and methyl-aniline compounds, could be used to automatically

determine the position of a substituent and be used in conjunction with the GC-MS model from Chapter V.

CHAPTER VII

EXPERIMENTAL SECTION

7.1 Presumptive colour tests

Presumptive tests were carried out according to the United Nations recommended guidelines. [77, 140] Each test sample (1 – 2 mg) was placed into a separate dimple well of a white spotting tile and 2 drops of the test reagent added. Additionally, for Scott's test, 2 drops of methanol were added to solubilize analytes. Any colour change or other noticeable effect were noted on addition of the reagent and after 5 min. The preparation of the reagents and the test procedure is detailed below.

Marquis Test: 1% Formaldehyde (37% aqueous solution) in concentrated sulfuric acid (10 mL, $d = 1.86$ g/mL).

Scott Test: 1% Cobalt(II)thiocyanate in glycerol-deionized water (1:1, 10 mL).

Nitric acid Test: Concentrated nitric acid ($d = 1.51$ g/mL).

Eosin Y Test: 150 μ M Eosin Y (2', 4', 5', 7'-tetrabromofluorescein) in aqueous potassium phosphate buffer (pH 7).

7.2 Thin-layer chromatography

Thin layer chromatography (TLC) was carried out on aluminium-backed SiO₂ plates (Merck, Germany). The mobile phase used was dichloromethane-methanol (9:1 v/v) containing 1% triethylamine. The developed plate was viewed under UV light (254 nm) and any spots noted. The plate was sprayed with modified Dragendorff-Ludy-Tenger reagent. [182]

7.3 Infrared spectroscopy

Infrared spectra were obtained in the range 4000 – 400 cm⁻¹ using a Thermo Scientific Nicolet iS10ATR-FTIR instrument (Thermo Scientific, Rochester, USA).

7.4 GC-MS analysis

GC-MS analysis was performed using an Agilent 7890B GC and a MS5977B mass selective detector (Agilent Technologies, Wokingham, UK). The mass spectrometer was operated in the electron ionization mode at 70 eV. Separation was achieved with a capillary column (HP-5MS, 30 m length, 0.25 mm i.d., 0.25 µm film thickness) with helium as the carrier gas at a constant flow rate of 1.2 mL/min. A 2 µL aliquot of the samples was injected with a split ratio of 50:1. The injector and the GC interface temperatures were both maintained at 280°C and 290 C respectively. The MS source and quadrupole temperatures were set at 230 C and 150 C. Scan spectra were obtained between 50-550 amu. Samples were dissolved in methanol, with no derivatization.

7.4.1 GC-MS calibration standards

10.0 mg of each analyte was weighed accurately into a 10.0 mL clear glass class A volumetric flask and diluted to volume with methanol to give a solution containing components at 1 mg/mL. This solution was then further diluted with methanol and 100 µL of eicosane (50 µg/mL in methanol) added (in each case) to give calibration standards containing 2.5 µg/mL, 5.0 µg/mL, 10.0 µg/mL, 20.0 µg/mL and 25.0 µg/mL of each analyte and the internal standard at 5.0 µg/mL.

7.4.2 GC-MS method validation

Mass spectra were obtained in selected ion monitoring (SIM) mode, using three specific fragment ions for each analyte (see Table 2.13 and Table 3.5 for a list of ions). The GC-MS method was validated in accordance with the ICH guidelines [143] using the following parameters: linearity, accuracy, precision (repeatability), limit of detection (LOD) and limit of quantification (LOQ). Linearity, precision: six replicate injections of the calibration standards were performed and the data analyzed under the same conditions. The %RSD was calculated for each replicate test sample. Accuracy (percentage recovery study): determined from spiked samples prepared in triplicate at three levels over a range of 80-120% of the target concentration (15 µg/mL). The percentage recovery and %RSD were calculated for each of the replicate samples. Repeatability (intraday precision) and intermediate precision (interday precision): determined from six replicate injections of a spiked sample (10 µg/mL), analysed on two consecutive days. The percentage purity and %RSD were calculated for each of the replicate samples. Limits of detection and quantification: six replicate injections of the calibration standards were performed and the data analyzed under the same conditions. The limits of detection and quantification were determined based on the signal-to-noise

(S/N) ratio, where a signal-to-noise ratio of 3:1 and 10:1 was used to calculate the LOD and LOQ respectively. [143] Signal-to-noise ratios were measured over six injections in the lower end of the concentration range (2.5 µg/mL for most analytes; 5.0 µg/mL for morphine) using the auto-root-mean-squared (Auto-RMS) algorithm from the Agilent MassHunter Qualitative Analysis software.

7.4.3 GC-MS quantitative analysis of seized heroin samples

The seven seized samples of heroin were provided by Greater Manchester Police, in accordance with Manchester Metropolitan University's Home Office license (Ref. No. 423023) requirements and agreed procedures.

Each test substance (SS-1 – SS-7) was weighed accurately (12.5 mg) into a 5.0 mL clear glass class A volumetric flask, diluted to volume with methanol and then filtered. This solution was then further diluted (8:2, 1.0 mL) with 100 µL methanol and 100 µL eicosane (50 µg/mL in methanol) added (in each case) to give the test solution containing ca. 15 µg/mL of the sample and the internal standard at 5.0 µg/mL. The test solutions were injected in triplicate. Quantification of the primary components, caffeine (**25**), paracetamol (**26**) and heroin (**1c**), was determined in full scan mode (50-550 amu), whereas fentanyl (**2b**) or its analogues (**2a**, **2c** – **2r**) was determined using selected ion monitoring (SIM) mode, using three specific fragment ions for each analyte (see Table 2.13 for a list of ions).

7.5 Benchtop NMR analysis

Low resolution NMR spectra were acquired on an Oxford Instruments Pulsar benchtop NMR Spectrometer (Oxford Instruments, Oxford, UK) operating at a proton resonance frequency of 60 MHz and referenced to the residual solvent peak (^1H NMR) or TFA (^{19}F NMR).

7.5.1 Benchtop ^{19}F NMR validation

Each analyte was weighed accurately (75.0 mg) into a 5.0 mL class A volumetric flask. Concentrated TFA was added (0.5 μL) before diluting to volume with $\text{d}_6\text{-DMSO}$ to produce a 15 mg/mL solution containing TFA at 0.01%. This solution was then further diluted with $\text{d}_6\text{-DMSO}$ (containing 0.01% TFA) to produce calibration standards containing 5.0 mg/mL, 8.0 mg/mL, 10.0 mg/mL, 12.0 mg/mL and 15.0 mg/mL of the analyte and the internal standard at 0.01%.

^{19}F experiments were run using 16 scans, a relaxation delay of 15 s and a filter of 5000 Hz for a total runtime of 5.7 min. A 10000 Hz filter is required to analyze 3-fluorofentanyl (**48**) for a 4.9 min runtime. Signal-to-noise ratios were measured using the MestReNova software algorithm.

7.5.2 Heroin sample benchtop NMR analysis

Heroin (**1c**) was weighed accurately (22.5 mg) and dissolved in 0.5 mL $\text{d}_6\text{-DMSO}$ (containing 0.01% TFA) to produce a solution containing heroin at 45 mg/mL. A 420 μL aliquot of this solution was mixed with 30 μL of a solution containing *ortho*-fluorofentanyl **42a** at 15 mg/mL and TFA at 0.01%. The resulting 450 μL solution contained 42 mg mL^{-1} heroin **1c** and 1 mg/mL **42a**,

corresponding to a **42a/1c** ratio of 2.4% w/w. The solution was analyzed by ^1H and ^{19}F NMR using the Pulsar benchtop NMR spectrometer.

7.6 UV-Vis Eosin Y fentanyl quantification

UV-Vis spectra were acquired on an Agilent 8453 spectrophotometer in the range 400-700 nm. For the fentanyl calibration graph, a 1 mg/mL stock solution of fentanyl in methanol was prepared. Volumes ranging between 0.1 – 1 mL (0.1 – 1 mg fentanyl) were transferred to vials and evaporated *in vacuo*. The dried solids were reconstituted in 5 mL eosin Y (750 μM) in aqueous pH = 7 phosphate buffer. Absorbance was measured at $\lambda = 590$ nm.

7.7 Solgel preparation and fentanyl detection

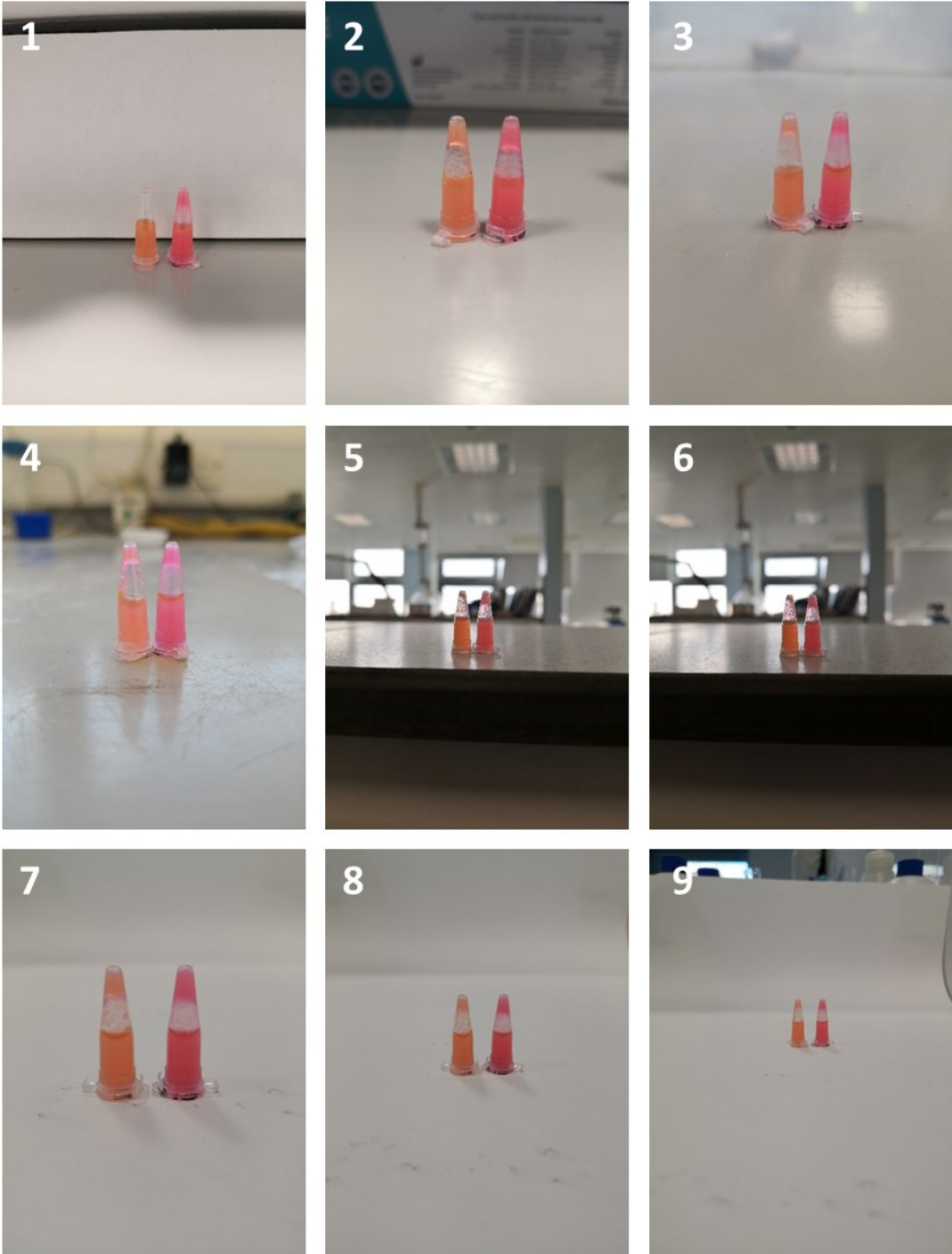
A 2:1:2 mixture of tetraethoxysilane, aqueous HCl (0.04 M) and ethanol was prepared (solution A) and mixed with eosin Y (1000 μM) in aqueous pH = 7 buffer (solution B). Solutions A and B were mixed in a 1:2 ratio and 75 μL of the resulting solgel was quickly transferred to a 200 μL Eppendorf tube before the polymerisation started. Solgel vials were kept in the freezer until use. For detection, 150 μL of a fentanyl solution was transferred to the solgel vial, and the resulting mixture was stirred with a pipette tip until homogeneous. Vials were then photographed (see Section 7.8).

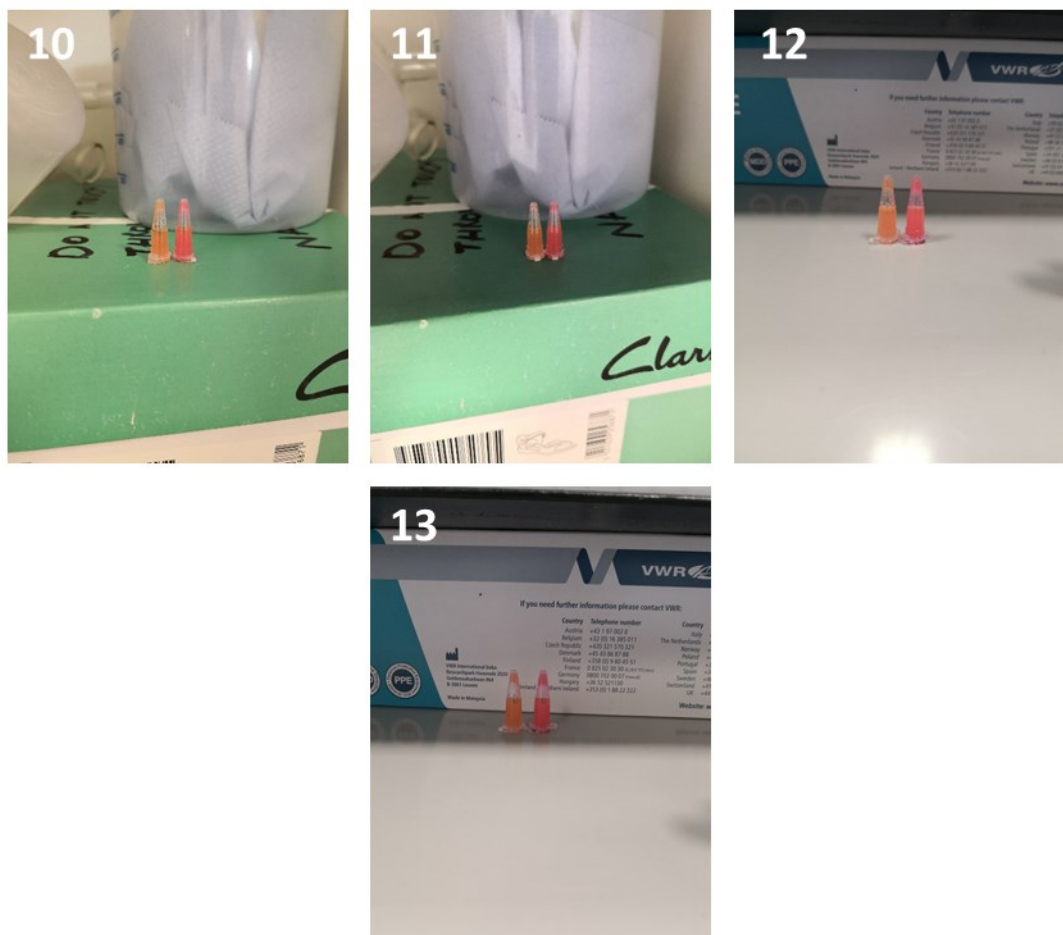
7.8 Solgel RGB detection

Fentanyl solgel vials were photographed next to a blank solgel vial (to which 150 μL methanol was added). Photographs were taken with a Huawei Mate 10 Pro smartphone and RGB values were measured with the paint.net free software (version 4.2.12), using the average from a 51 x 51 pixels grid in the

center of the vial. RGB values for both the fentanyl and the blank vials were measured. To standardise the result, the G/R ratio of the fentanyl vial was divided by the G/R ratio of the blank.

7.9 Lighting conditions for RGB evaluation (reference for Table 4.7)





7.10 PCA and clustering analysis

All mass spectra were extracted in .csv format. Only peaks between $m/z = 41$ and 352 were retained, rounded to the nearest mass unit, and the dataset was zero-filled. Relative intensities were calculated, with the base peak normalized to an intensity of 1. The resulting dataset was imported into *R* statistical computing software (version 3.6.3).

Compounds were separated into generic classes based on their structural modifications. Approximately half the compounds in each class (at least three)

were selected to build the model (54 analogues total). Variables (m/z ions) with a variance below 0.0001 were excluded as an initial clean-up, which reduced the dataset to 176 variables. Principal component analysis was performed with mean centering and data scaling, using the PCA function from the *FactoMineR* package (version 2.2). [172] Data visualisation was performed using the *factoextra* package (version 1.0.7). [173] Hierarchical clustering was performed using the *HCPC* function from the *FactoMineR* package. The following procedure details how to retrieve the *R* code, which is freely available on Github, build the models and classify test samples.

Model building and evaluation procedure:

Download the mass spectral data .csv files and the “Model Building and Evaluation” R script from Github (<https://github.com/Nicolas-Gilbert/Fentanyl-PCA-HC>)

Copy the .csv files to your R Studio working directory.

Open the “Model Building and Evaluation” script in R Studio.

Install and load the *factoextra*, *FactoMineR* and *fields* packages.

Execute the “MODEL 1 CREATION” and “MODEL 2 CREATION” sections of the script to generate the PCA models.

Note: These use the “Classifier_1.csv” and “Classifier_2.csv” files, which contain the MS data of analogues included in each classifier. The .csv files can be modified to add analogues to the model, if needed.

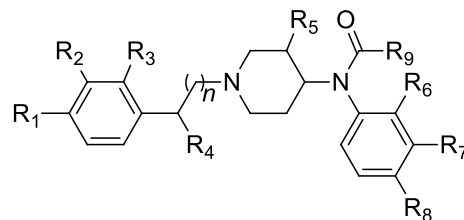
Export the MS data of suspected analogue(s) as a .csv file and copy it to your working directory.

Note: This file must be called “Test_data.csv”. Each analogue must be included on a separate row, each column must show the relative intensity of m/z ions from 41 to 352. See the “Test_data.csv” included in the Github repository as an example of the required format.

Execute the “EVALUATION”, “CLASSIFICATION 1” and “CLASSIFICATION 2” sections of the script. This will output the nearest neighbour results for each classifier, as separate tables.

7.11 Structures of compounds included in the PCA study

Table 7.1. Chemical structure of fentanyl analogues included in the PCA study (Chapter V).



Fentanyl analogue	N°	<i>n</i>	R ₁	R ₂	R ₃	R ₄	R ₅	R ₆	R ₇	R ₈	R ₉
Isobutyryl <i>N</i> -benzyl-	1	0	H	H	H	H	H	H	H	H	<i>i</i> Pr
<i>N</i> -Benzyl-	2	0	H	H	H	H	H	H	H	H	Et
Cyclopropyl- <i>N</i> -benzyl-	3	0	H	H	H	H	H	H	H	H	CyPr
<i>para</i> -Fluoro-isobutyryl- <i>N</i> -benzyl-	4	0	H	H	H	H	H	H	H	F	<i>i</i> Pr
<i>para</i> -Fluoro- <i>N</i> -benzyl-	5	0	H	H	H	H	H	H	H	F	Et
Phenyl- <i>N</i> -benzyl-	6	0	H	H	H	H	H	H	H	H	Ph
<i>para</i> -Fluoro-acetyl- <i>N</i> -benzyl-	7	0	H	H	H	H	H	H	H	F	Me
<i>meta</i> -Methyl-	8	1	H	H	H	H	H	H	Me	H	Et
<i>ortho</i> -Methyl-acetyl-	9	1	H	H	H	H	H	Me	H	H	Me
<i>meta</i> -Methyl-acetyl-	10	1	H	H	H	H	H	H	Me	H	Me
4'-Methyl-acetyl-	11	1	Me	H	H	H	H	H	H	H	Me
β-Methyl-acetyl-	12	1	H	H	H	Me	H	H	H	H	Me
2'-Methyl-	13	1	H	H	Me	H	H	H	H	H	Et
<i>para</i> -Methyl-tetrahydrofuranyl-	14	1	H	H	H	H	H	H	H	Me	THF

Tetrahydrofuranyl- (3-isomer)	15	1	H	H	H	H	H	H	H	H	H	3-THF
-------------------------------	----	---	---	---	---	---	---	---	---	---	---	-------

Table 7.1. Chemical structure of fentanyl analogues included in the PCA study (Chapter V). (cont.)

Fentanyl analogue	N ^o	<i>n</i>	R ₁	R ₂	R ₃	R ₄	R ₅	R ₆	R ₇	R ₈	R ₉
β-Methyl-	16	1	H	H	H	Me	H	H	H	H	Et
Heptanoyl-	17	1	H	H	H	H	H	H	H	H	Hex
<i>meta</i> -Methyl-furanyl-	18	1	H	H	H	H	H	H	Me	H	2-Fur
(<i>E</i>)-2-Methyl-2-butenoyl-	19	1	H	H	H	H	H	H	H	H	(<i>E</i>)-2-Methyl-2-butenoyl
4'-Fluoro-cyclopropyl-	20	1	F	H	H	H	H	H	H	H	CyPr
Benzoyl- (phenyl)	21	1	H	H	H	H	H	H	H	H	Ph
2,2,3,3-Tetramethylcyclopropyl-	22	1	H	H	H	H	H	H	H	H	2,2,3,3-Tetramethylcyclopropyl
2,2-Dimethylpropanoyl-	23	1	H	H	H	H	H	H	H	H	<i>t</i> Bu
4'-Fluoro-isobutyryl-	24	1	F	H	H	H	H	H	H	H	<i>i</i> Pr
Furanyl-	25	1	H	H	H	H	H	H	H	H	2-Fur
4'-Fluoro-methoxyacetyl-	26	1	F	H	H	H	H	H	H	H	-MeOMe
Methoxyacetyl-	27	1	H	H	H	H	H	H	H	H	-MeOMe
Acryl-	28	1	H	H	H	H	H	H	H	H	-CH=CH ₂
Butyryl-	29	1	H	H	H	H	H	H	H	H	Pr
Propionyl- [<i>aka.</i> Fentanyl]	30	1	H	H	H	H	H	H	H	H	Et
Cyclopropyl-	31	1	H	H	H	H	H	H	H	H	CyPr
Isobutyryl-	32	1	H	H	H	H	H	H	H	H	<i>i</i> Pr
3'-Fluoro-	33	1	H	F	H	H	H	H	H	H	Et
4'-Fluoro-	34	1	F	H	H	H	H	H	H	H	Et
2'-Fluoro-	35	1	H	H	F	H	H	H	H	H	Et
<i>meta</i> -Fluoro-acryl-	36	1	H	H	H	H	H	H	F	H	-CH=CH ₂
<i>meta</i> -Fluoro-methoxyacetyl-	37	1	H	H	H	H	H	H	F	H	-MeOMe

<i>para</i> -Fluoro-acryl-	38	1	H	H	H	H	H	H	H	H	F	-CH=CH ₂
----------------------------	-----------	---	---	---	---	---	---	---	---	---	---	---------------------

Table 7.1. Chemical structure of fentanyl analogues included in the PCA study (Chapter V). (cont.)

Fentanyl analogue	N°	<i>n</i>	R ₁	R ₂	R ₃	R ₄	R ₅	R ₆	R ₇	R ₈	R ₉
<i>para</i> -Fluoro-acetyl-	39	1	H	H	H	H	H	H	H	F	Me
<i>para</i> -Fluoro-cyclopropyl-	40	1	H	H	H	H	H	H	H	F	CyPr
3-Fluoro-butyryl-	41	1	H	H	H	H	F	H	H	H	Pr
3-Fluoro-tetrahydrofuran-yl-	42	1	H	H	H	H	F	H	H	H	THF
3-Fluoro-	43	1	H	H	H	H	F	H	H	H	Et
<i>para</i> -Chloro-butyryl-	44	1	H	H	H	H	H	H	H	Cl	Pr
<i>para</i> -Chloro-	45	1	H	H	H	H	H	H	H	Cl	Et
<i>para</i> -Chloro-cyclopentyl-	46	1	H	H	H	H	H	H	H	Cl	CyPent
<i>para</i> -Methoxy-acryl-	47	1	H	H	H	H	H	H	H	MeO	-CH=CH ₂
<i>para</i> -Methoxy-methoxyacetyl-	48	1	H	H	H	H	H	H	H	MeO	-MeOMe
<i>para</i> -Methoxy-	49	1	H	H	H	H	H	H	H	MeO	Et
<i>para</i> -Methoxy-valeryl-	50	1	H	H	H	H	H	H	H	MeO	Bu
<i>ortho</i> -Methoxy-butyryl-	51	1	H	H	H	H	H	MeO	H	H	Pr
<i>meta</i> -Fluoro-	52	1	H	H	H	H	H	H	F	H	Et
<i>ortho</i> -Fluoro-	53	1	H	H	H	H	H	F	H	H	Et
<i>para</i> -Fluoro-	54	1	H	H	H	H	H	H	H	F	Et
<i>meta</i> -Fluoro- <i>N</i> -benzyl-	55	0	H	H	H	H	H	H	F	H	Et
<i>para</i> -Fluoro- <i>N</i> -benzyl-furan-yl-	56	0	H	H	H	H	H	H	H	F	2-Fur
Acetyl- <i>N</i> -benzyl-	57	0	H	H	H	H	H	H	H	H	Me
Furan-yl- <i>N</i> -benzyl-	58	0	H	H	H	H	H	H	H	H	2-Fur
Methoxyacetyl- <i>N</i> -benzyl-	59	0	H	H	H	H	H	H	H	H	-MeOMe
Butyryl- <i>N</i> -benzyl-	60	0	H	H	H	H	H	H	H	H	Pr

Table 7.1. Chemical structure of fentanyl analogues included in the PCA study (Chapter V). (cont.)

Fentanyl analogue	N°	<i>n</i>	R ₁	R ₂	R ₃	R ₄	R ₅	R ₆	R ₇	R ₈	R ₉
Acryl- <i>N</i> -benzyl-	61	0	H	H	H	H	H	H	H	H	-CH=CH ₂
<i>para</i> -Fluoro- <i>N</i> -benzyl- cyclopropyl-	62	0	H	H	H	H	H	H	H	F	CyPr
Tetrahydrofuranyl- <i>N</i> -benzyl-	63	0	H	H	H	H	H	H	H	H	THF
4-ANPP	64	1	H	H	H	H	H	H	H	H	-
((<i>E</i>)-But-2-enoyl)-	65	1	H	H	H	H	H	H	H	H	(<i>E</i>)-But-2-enoyl
(2-Methyl)butyryl-	66	1	H	H	H	H	H	H	H	H	<i>sec</i> -Bu
Ethoxyacetyl-	67	1	H	H	H	H	H	H	H	H	-MeOEt
Cyclopropylacetyl-	68	1	H	H	H	H	H	H	H	H	-MeCyPr
<i>ortho</i> -Methyl-acryl-	69	1	H	H	H	H	H	Me	H	H	-CH=CH ₂
<i>para</i> -Methyl-acetyl-	70	1	H	H	H	H	H	H	H	Me	Me
<i>ortho</i> -Methyl-	71	1	H	H	H	H	H	Me	H	H	H
<i>meta</i> -Methyl-cyclopropyl-	72	1	H	H	H	H	H	H	Me	H	CyPr
<i>ortho</i> -Methyl-furanyl-	73	1	H	H	H	H	H	Me	H	H	2-Fur
<i>para</i> -Methyl-furanyl-	74	1	H	H	H	H	H	H	H	Me	2-Fur
<i>meta</i> -Methyl-methoxyacetyl-	75	1	H	H	H	H	H	H	Me	H	-MeOMe
<i>ortho</i> -Methyl-cyclopropyl-	76	1	H	H	H	H	H	Me	H	H	CyPr
4'-Fluoro-furanyl-	77	1	F	H	H	H	H	H	H	H	2-Fur
<i>meta</i> -Methoxy-furanyl-	78	1	H	H	H	H	H	H	MeO	H	2-Fur
<i>ortho</i> -Methoxy-furanyl-	79	1	H	H	H	H	H	MeO	H	H	2-Fur
<i>para</i> -Methoxy-furanyl-	80	1	H	H	H	H	H	H	H	MeO	2-Fur
<i>para</i> -Chloro-furanyl- (3-isomer)	81	1	H	H	H	H	H	H	H	Cl	3-Fur

3'-Methyl-acetyl-	82	1	H	Me	H	H	H	H	H	H	Me
4'-Methyl-	83	1	Me	H	H	H	H	H	H	H	Et

Table 7.1. Chemical structure of fentanyl analogues included in the PCA study (Chapter V). (cont.)

Fentanyl analogue	N°	<i>n</i>	R ₁	R ₂	R ₃	R ₄	R ₅	R ₆	R ₇	R ₈	R ₉
α-Methyl-acetyl-	84	1	H	H	H	H	H	H	H	H	Me
α-Methyl-butyryl-	85	1	H	H	H	H	H	H	H	H	Pr
α-Methyl-	86	1	H	H	H	H	H	H	H	H	Et
4'-Fluoro-acetyl-	87	1	F	H	H	H	H	H	H	H	Me
2'-Methyl-acetyl-	88	1	H	H	Me	H	H	H	H	H	Me
Thiophenyl- (3-isomer)	89	1	H	H	H	H	H	H	H	H	3-Thio
3'-Methyl-	90	1	H	Me	H	H	H	H	H	H	Et
<i>ortho</i> -Fluoro-furanyl-	91	1	H	H	H	H	H	F	H	H	2-Fur
Acetyl-	92	1	H	H	H	H	H	H	H	H	Me
<i>iso</i> -Valeryl-	93	1	H	H	H	H	H	H	H	H	<i>i</i> Bu
Valeryl-	94	1	H	H	H	H	H	H	H	H	Bu
Hexanoyl-	95	1	H	H	H	H	H	H	H	H	Pent
Cyclobutyryl-	96	1	H	H	H	H	H	H	H	H	CyBu
2'-fluoro- <i>ortho</i> -fluoro-	97	1	H	H	F	H	H	F	H	H	Et
<i>para</i> -Fluoro-butyryl-	98	1	H	H	H	H	H	H	H	F	Pr
<i>para</i> -Fluoro-isobutyryl-	99	1	H	H	H	H	H	H	H	F	<i>i</i> Pr
<i>para</i> -Fluoro-cyclopentyl-	100	1	H	H	H	H	H	H	H	F	CyPent
<i>para</i> -Fluoro-tetrahydrofuranyl-	101	1	H	H	H	H	H	H	H	F	THF
<i>para</i> -Fluoro-crotonyl-	102	1	H	H	H	H	H	H	H	F	(<i>E</i>)-But-2-enoyl
<i>meta</i> -Fluoro-isobutyryl-	103	1	H	H	H	H	H	H	F	H	<i>i</i> Pr
<i>ortho</i> -Fluoro-butyryl-	104	1	H	H	H	H	H	F	H	H	Pr

<i>ortho</i> -Fluoro-isobutyryl-	105	1	H	H	H	H	H	H	F	H	H	<i>i</i> Pr
<i>para</i> -Fluoro-valeryl-	106	1	H	H	H	H	H	H	H	H	F	Bu

Table 7.1. Chemical structure of fentanyl analogues included in the PCA study (Chapter V). (cont.)

Fentanyl analogue	N°	<i>n</i>	R ₁	R ₂	R ₃	R ₄	R ₅	R ₅	R ₆	R ₇	R ₈	R ₉
<i>para</i> -Fluoro-furanyl- (3-isomer)	107	1	H	H	H	H	H	H	H	H	F	3-Fur
2,3-Benzodioxoyl-	108	1	H	H	H	H	H	H	H	H	H	2,3-Benzodioxole
<i>para</i> -Chloro-furanyl-	109	1	H	H	H	H	H	H	H	H	Cl	2-Fur
<i>meta</i> -Fluoro-butyryl-	110	1	H	H	H	H	H	H	H	F	H	Pr
<i>para</i> -Fluoro-furanyl-	111	1	H	H	H	H	H	H	H	H	F	2-Fur
<i>meta</i> -Fluoro-furanyl-	112	1	H	H	H	H	H	H	H	F	H	2-Fur
<i>meta</i> -Fluoro-isobutyryl-	113	1	H	H	H	H	H	H	H	F	H	<i>i</i> Pr
3-Fluoro-isoburytyl-	114	1	H	H	H	H	H	F	H	H	H	<i>i</i> Pr
<i>para</i> -Chloro-cyclobutyryl-	115	1	H	H	H	H	H	H	H	H	Cl	CyBu
<i>para</i> -Chloro-isobutyryl-	116	1	H	H	H	H	H	H	H	H	Cl	<i>i</i> Pr
<i>para</i> -Chloro-methoxyacetyl-	117	1	H	H	H	H	H	H	H	H	Cl	-MeOMe
<i>para</i> -Chloro-valeryl-	118	1	H	H	H	H	H	H	H	H	Cl	Bu
<i>para</i> -Chloro-acryl-	119	1	H	H	H	H	H	H	H	H	Cl	-CH=CH ₂
<i>para</i> -Methoxy-butyryl-	120	1	H	H	H	H	H	H	H	H	MeO	Pr
<i>para</i> -Methoxy-methoxyacetyl-	121	1	H	H	H	H	H	H	H	H	MeO	-MeOMe

7.12 Synthesis and characterisation data

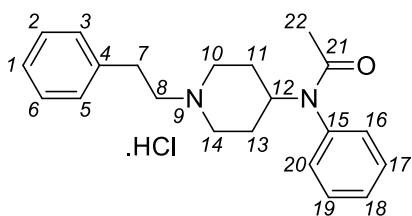
Reagents were of commercial quality (Sigma-Aldrich, Gillingham, UK or Fluorochem Limited, Hadfield, UK) and used without further purification unless specified. Aniline was distilled under reduced pressure prior to use. Solvents (Fisher Scientific, Loughborough, UK) were dried, where necessary, using standard procedures. [183] ^1H NMR and ^{13}C NMR spectra were acquired on a JEOL JMN-ECS-400 (JEOL, Tokyo, Japan) NMR spectrometer operating at a proton resonance frequency of 400 MHz and referenced to the residual solvent peak. ^{19}F -NMR spectra were acquired on the same instrument and referenced to trifluoroacetic acid (TFA). Infrared spectra were obtained in the range 4000 – 400 cm^{-1} using a Thermo Scientific Nicolet iS10ATR-FTIR instrument (Thermo Scientific, Rochester, USA). High-resolution mass spectrometry (HRMS) data were obtained on an Agilent 6540 LC-QToF spectrometer in positive electrospray ionization mode. ATR-FTIR and NMR (^1H , ^{13}C , ^{19}F) spectra are reported in the Appendix.

7.12.1 Synthesis of fentanyl analogues **2a-r**

Fentanyl analogues **2a-r** were prepared as reported by Valdez *et al.* [4] with the following modifications: *N*-[1-(2-phenylethyl)-4-piperidinyl]aniline (4-ANPP, **4**, 1.35 g, 4.8 mmol) was added to dichloromethane (40 mL) and was treated with diisopropylamine (1.68 mL, 9.6 mmol, 2 eq). The system was flushed with argon, the mixture cooled in an ice bath and the appropriate acyl chloride (9.6 mmol, 2 eq) added dropwise. The resulting solution was stirred at ambient temperature for 2h. The mixture was diluted with water (50 mL) and the organic phase washed sequentially with brine (1 x 50 mL) and saturated aqueous sodium bicarbonate solution (1 x 50 mL), dried with magnesium sulfate and concentrated *in vacuo*. The crude oils were purified by flash column

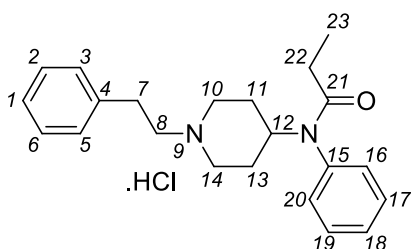
chromatography (SiO₂, 3:7 – 7:3 v/v EtOAc-hexane). The resulting free-base was dissolved in either diethyl ether or acetone, and an equimolar amount of hydrogen chloride (3 M in cyclopentyl methyl ether) added. The mixture was left to stand for 5-10 minutes and the salt isolated by filtration. The product(s) were dried in an oven (60 °C, 12h) to give white – off-white powders.

N-(1-Phenethylpiperidin-4-yl)-*N*-phenylacetamide hydrochloride
(Acetylfentanyl, **2a**)



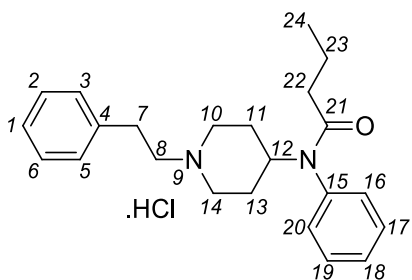
Acetyl fentanyl **2a** was obtained in 33% yield over two steps. ¹H NMR (400 MHz, DMSO-D₆) δ 10.56 (bs, 1H, H9), 7.58-7.40 (m, 3H, H17-19), 7.34-7.17 (m, 7H, H1-3/H5-6/H16/H20), 4.69 (tt, J = 3.2 Hz, 12.1 Hz, 1H, H12), 3.52 (d, J = 10.8 Hz, 2H, H10a/H14a), 3.37 (H₂O), 3.20-3.04 (m, 4H, H8/H10b/H14b), 3.02-2.93 (m, 2H, H7), 1.92 (d, J = 12.8 Hz, 2H, H11a/H13a), 1.70-1.55 (m, 5H, H11b/H13b/H22); ¹³C NMR (100 MHz, DMSO-D₆) δ 169.03 (C21), 138.65 (C15), 137.16 (C4), 130.21 (C17/C19), 129.53 (C18), 128.67 (C2-3/C5-6), 128.57 (C16/C20), 126.79 (C1), 56.41 (C8), 50.83 (C10/C14), 49.01 (C12), 29.39 (C7), 27.27 (C11/C13), 23.17 (C22); ATR-FTIR $\nu_{\text{max}}/\text{cm}^{-1}$: 3038, 2995 and 2938, 2458 and 2405, 1647, 1595; HRMS (C₂₁H₂₆N₂O) : predicted mass = 323.2118 [M+H]⁺; experimental mass = 323.2125 [M+H]⁺.

N-(1-Phenethylpiperidin-4-yl)-*N*-phenylpropionamide hydrochloride (Fentanyl, **2b**)



Fentanyl **2b** was obtained in 41% yield over two steps. ^1H NMR (400 MHz, DMSO- D_6) δ 10.43 (bs, 1H, H9), 7.50-7.42 (m, 3H, H17-19), 7.33-7.21 (m, 7H, H1-3/H5-6/H16/H20), 4.71 (t, J = 11.9 Hz, 1H, H12), 3.51 (d, J = 11.4 Hz, 2H, H10a/H14a), 3.36 (s, H_2O), 3.26-3.02 (m, 4H, H8/H10b/H14b), 2.99-2.95 (m, 2H, H7), 1.92 (d, J = 12.8 Hz, 2H, H11a/H13a), 1.82 (q, J = 7.3 Hz, 2H, H22), 1.62 (q, J = 11.9 Hz, 2H, H11b/H13b), 0.87 (t, J = 7.3 Hz, 3H, H23); ^{13}C NMR (100 MHz, DMSO- D_6) δ 172.15 (C21), 138.11 (C15), 137.11 (C4), 130.36 (C17/19), 129.49 (C18), 128.64 (C2-3/C5-6), 128.52 (C16/C20), 126.76 (C1), 56.40 (C8), 50.88 (C10/C14), 49.01 (C12), 29.41 (C7), 27.73 (C22), 27.28 (C11/C13), 9.39 (C23); ATR-FTIR $\nu_{\text{max}}/\text{cm}^{-1}$: 3042, 2993, 2962 and 2936, 2450 and 2403, 1644, 1596; HRMS ($\text{C}_{22}\text{H}_{28}\text{N}_2\text{O}$) : predicted mass = 337.2274 $[\text{M}+\text{H}]^+$; experimental mass = 337.2274 $[\text{M}+\text{H}]^+$.

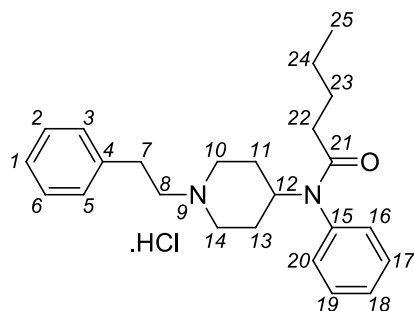
N-(1-Phenethylpiperidin-4-yl)-*N*-butyramide hydrochloride (Butyrfentanyl, **2c**)



Butyrfentanyl **2c** was obtained in 39% yield over two steps. ^1H NMR (400 MHz, DMSO- D_6) δ 10.42 (bs, 1H, H9), 7.51-7.44 (m, 3H, H17-19), 7.33-7.22 (m, 7H, H1-3/H5-6/H16/H20), 4.71 (t, J = 11.9 Hz, 1H, H12), 3.51 (d, J = 11.4 Hz, 2H, H10a/H14a), 3.36 (H_2O), 3.20-3.06 (m, 4H, H8/H10b/H14b), 2.99-2.95 (m, 2H, H7), 1.92 (d, J = 12.8 Hz, 2H, H11a/H13a), 1.79 (t, J = 7.1 Hz, 2H, H22), 1.62 (q, J = 11.9 Hz, 2H,

H11b/H13b), 1.42 (sext, $J = 12.0$ Hz, 2H, H23), 0.71 (t, $J = 7.3$ Hz, 3H, H24); ^{13}C NMR (100 MHz, DMSO- D_6) δ 171.28 (C21), 138.13 (C15), 137.11 (C4), 130.37 (C17/C19), 129.49 (C18), 128.64 (C2-3/C5-6), 128.53 (C16/C20), 126.76 (C1), 56.39 (C8), 50.87 (C10/C14), 49.01 (C12), 36.17 (C22), 29.39 (C7), 27.28 (C11/C13), 18.14 (C23), 13.62 (C24); ATR-FTIR $\nu_{\text{max}}/\text{cm}^{-1}$: 3045, 2963, 2933 and 2873, 2452 and 2402, 1641, 1596; HRMS ($\text{C}_{23}\text{H}_{30}\text{N}_2\text{O}$) : predicted mass = 351.2431 $[\text{M}+\text{H}]^+$; experimental mass = 351.2434 $[\text{M}+\text{H}]^+$.

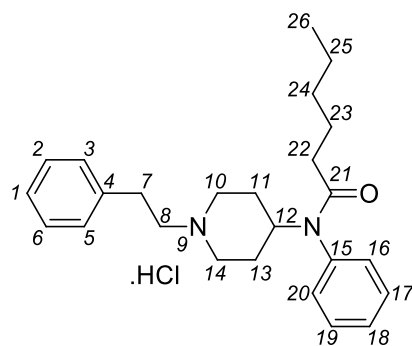
N-(1-Phenethylpiperidin-4-yl)-*N*-phenylpentanamide hydrochloride
(Valerylfehtanyl, **2d**)



Valerylfehtanyl **2d** was obtained in 30% yield over two steps. ^1H NMR (400 MHz, DMSO- D_6) δ 10.52 (bs, 1H, H9), 7.53-7.40 (m, 3H, H17-19), 7.35-7.17 (m, 7H, H1-3/H5-6/H16/H20), 4.71 (t, $J = 11.7$ Hz, 1H, H12), 3.51 (d, $J = 11.9$ Hz, 2H, H10a/H14a), 3.37 (H $_2\text{O}$), 3.20-3.04 (m, 4H, H8/H10b/H14b), 3.03-2.94 (m, 2H, H7), 1.91 (d, $J = 12.8$ Hz, 2H, H11a/H13a), 1.81 (t, $J = 7.1$ Hz, 2H, H22), 1.63 (q, $J = 12.1$ Hz, 2H, H11b/H13b), 1.39 (quint, $J = 7.1$ Hz, 2H, H23), 1.10 (sext, $J = 7.1$ Hz, 2H, H24), 0.71 (td, $J = 7.6, 1.4$ Hz, 3H, H25); ^{13}C NMR (100 MHz, DMSO- D_6) δ 171.24 (C21), 137.95 (C15), 136.94 (C4), 130.16 (C17/C19), 129.30 (C18), 128.45 (C2-3/C5-6), 128.36 (C16/C20), 126.58 (C1), 56.20 (C8), 50.65 (C10/C14), 48.84 (C12), 33.69 (C22), 29.20 (C7), 27.09 (C11/C13), 26.74 (C23), 21.48 (C24), 13.50 (C25); ATR-FTIR $\nu_{\text{max}}/\text{cm}^{-1}$: 3032, 2955, 2931 and 2871, 2459 and 2407, 1644, 1595; HRMS ($\text{C}_{24}\text{H}_{32}\text{N}_2\text{O}$) : predicted mass = 365.2587 $[\text{M}+\text{H}]^+$; experimental mass = 365.2592 $[\text{M}+\text{H}]^+$.

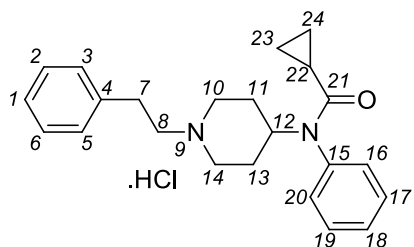
N-(1-Phenethylpiperidin-4-yl)-*N*-phenylhexanamide
(Hexanoylfentanyl, **2e**)

hydrochloride



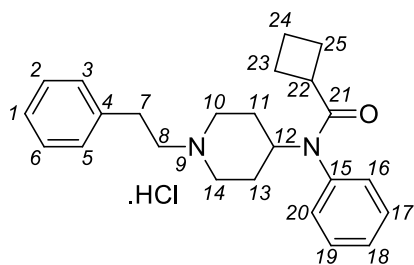
Hexanoylfentanyl **2e** was obtained in 43% yield over two steps. ^1H NMR (400 MHz, DMSO- D_6) δ 10.29 (bs, 1H, H9), 7.51-7.43 (m, 3H, H17-19), 7.33-7.22 (m, 7H, H1-3/H5-6/H16/H20), 4.71 (t, $J = 11.7$ Hz, 1H, H12), 3.52 (d, $J = 11.4$ Hz, 2H, H10a/H14a), 3.35 (H $_2$ O), 3.21-3.02 (m, 4H, H8/H10b/H14b), 3.02-2.87 (m, 2H, H7), 1.92 (d, $J = 12.8$ Hz, 2H, H11a/H13a), 1.81 (t, $J = 7.3$ Hz, 2H, H22), 1.61 (q, $J = 11.9$ Hz, 2H, H11b/H13b), 1.41 (quint, $J = 7.3$ Hz, 2H, H23), 1.14-1.02 (m, 4H, H24-25), 0.77 (t, $J = 7.1$ Hz, 3H, H26); ^{13}C NMR (100 MHz, DMSO- D_6) δ 171.47 (C21), 138.16 (C15), 137.10 (C4), 130.38 (C17/C19), 129.52 (C18), 128.67 (C2-3/C5-6), 128.58 (C16/C20), 126.81 (C1), 56.42 (C8), 50.93 (C10/C14), 49.00 (C12), 34.18 (C22), 30.77 (C23), 29.45 (C7), 27.31 (C11/C13), 24.45 (C24), 21.81 (C25), 13.79 (C26); ATR-FTIR $\nu_{\text{max}}/\text{cm}^{-1}$: 3039, 2954, 2931 and 2860, 2501, 2461 and 2403, 1651, 1593; HRMS (C $_{25}$ H $_{34}$ N $_2$ O) : predicted mass = 379.2744 [M+H] $^+$; experimental mass = 379.2744 [M+H] $^+$.

N-(1-Phenethylpiperidin-4-yl)-*N*-phenylcyclopropanecarboxamide hydrochloride (Cyclopropylfentanyl, **2f**)



Cyclopropylfentanyl **2f** was obtained in 64% yield over two steps. ¹H NMR (400 MHz, DMSO-D₆) δ 10.51 (bs, 1H, H9), 7.53-7.43 (m, 3H, H17-19), 7.33-7.21 (m, 7H, H1-3/H5-6/H16/H20), 4.69 (tt, J = 12.1 Hz, 3.2 Hz, 1H, H12), 3.51 (d, J = 11.4 Hz, 2H, H10a/H14a), 3.36 (H₂O), 3.25-3.05 (m, 4H, H8/H10b/H14b), 3.00-2.96 (m, 2H, H7), 1.93 (d, J = 12.4 Hz, 2H, H11a/H13a), 1.67 (q, J = 12.6 Hz, 2H, H11b/H13b), 1.00 (bs, 1H, H22), 0.75 (t, J = 3.2 Hz, 2H, H23a/H24a), 0.56-0.54 (m, 2H, H23b/H24b); ¹³C NMR (100 MHz, DMSO-D₆) δ 172.00 (C21), 138.13 (C15), 137.13 (C4), 130.52 (C17/C19), 129.55 (C18), 128.64 (C2-3/C5-6), 128.52 (C16/C20), 126.76 (C1), 56.39 (C8), 50.86 (C10/C14), 49.44 (C12), 29.39 (C7), 27.27 (C11/C13), 12.81 (C22), 7.99 (C23-24); ATR-FTIR $\nu_{\max}/\text{cm}^{-1}$: 3012, 2932, 2470 and 2394, 1646, 1597; HRMS (C₂₃H₂₈N₂O) : predicted mass = 349.2234 [M+H]⁺; experimental mass = 349.2275 [M+H]⁺.

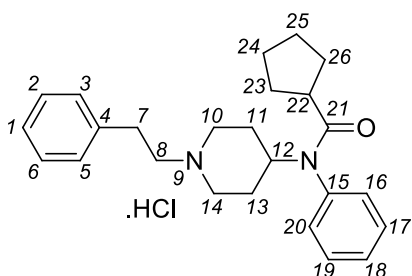
N-(1-Phenethylpiperidin-4-yl)-*N*-phenylcyclobutanecarboxamide hydrochloride (Cyclobutylfentanyl, **2g**)



Cyclobutylfentanyl **2g** was obtained in 64% yield over two steps. ¹H NMR (400 MHz, DMSO-D₆) δ 10.41 (bs, 1H, H9), 7.49-7.41 (m, 3H, H17-19), 7.32-7.29 (m, 2H, H2/H6), 7.24-7.16 (m, 5H, H1/H3/H5/H16/H20), 4.67 (tt, J = 12.1 Hz, 3.7 Hz, 1H, H12), 3.51 (d, J = 11.4 Hz, 2H, H10a/H14a), 3.35 (H₂O),

3.19-3.05 (m, 4H, H8/H10b/H14b), 2.99-2.95 (m, 2H, H7), 2.73 (quint, 1H, H22), 2.15-2.06 (m, 2H, H23a/H25a), 1.91 (d, $J = 12.8$ Hz, 2H, H11a/H13a), 1.66-1.51 (m, 6H, H11b/H13b/H23b/H25b/H24); ^{13}C NMR (100 MHz, DMSO- D_6) δ 172.96 (C21), 137.52 (C15), 137.14 (C4), 130.53 (C17/C19), 129.25 (C18), 128.65 (C2-3/C5-6), 128.53 (C16/C20), 126.78 (C1), 56.40 (C8), 50.86 (C10/C14), 49.22 (C12), 38.08 (C22), 29.41 (C7), 27.22 (C11/C13), 25.05 (C23/C25), 17.15 (C24); ATR-FTIR $\nu_{\text{max}}/\text{cm}^{-1}$: 3060 and 3037, 2940 and 2866, 2460, 1654, 1596; HRMS ($\text{C}_{24}\text{H}_{30}\text{N}_2\text{O}$) : predicted mass = 363.2431 $[\text{M}+\text{H}]^+$; experimental mass = 363.2431 $[\text{M}+\text{H}]^+$.

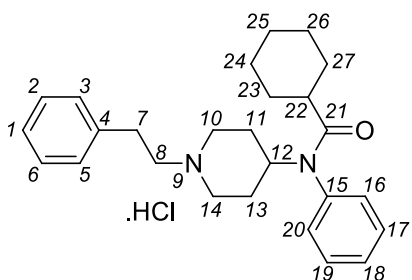
N-(1-Phenethylpiperidin-4-yl)-*N*-phenylcyclopentanecarboxamide hydrochloride (Cyclopentylfentanyl, **2h**)



Cyclopentylfentanyl **2h** was obtained in 37% yield over two steps. ^1H NMR (400 MHz, DMSO- D_6) δ 10.62 (bs, 1H, H9), 7.48-7.44 (m, 3H, H17-19), 7.32-7.21 (m, 7H, H1-3/H5-6/H16/H20), 4.69 (t, $J = 11.9$ Hz, 1H, H12), 3.51 (d, $J = 11.4$ Hz, 2H, H10a/H14a), 3.37 (H $_2\text{O}$),

3.20-3.03 (m, 4H, H8/H10b/H14b), 3.02-2.94 (m, 2H, H7), 2.23 (quint, $J = 8.0$ Hz, 1H, H22), 1.91 (d, $J = 12.4$ Hz, 2H, H11a/H13a), 1.70-1.39 (m, 8H, H11b/H13b/H23/H24a/H25a/H26), 1.29 (bs, 2H, H24b/H25b); ^{13}C NMR (100 MHz, DMSO- D_6) δ 174.96 (C21), 138.04 (C15), 137.12 (C4), 130.55 (C17/C19), 129.40 (C18), 128.66 (C2-3/C5-6/C16/C20), 126.78 (C1), 56.39 (C8), 50.89 (C10/C14), 49.17 (C12), 42.05 (C22), 30.51 (C23/C26), 29.42 (C7), 27.29 (C11/C13), 25.77 (C24/C25); ATR-FTIR $\nu_{\text{max}}/\text{cm}^{-1}$: 3056 and 3035, 2961 and 2868, 2397, 1651, 1597; HRMS ($\text{C}_{25}\text{H}_{32}\text{N}_2\text{O}$) : predicted mass = 377.2587 $[\text{M}+\text{H}]^+$; experimental mass = 377.2585 $[\text{M}+\text{H}]^+$.

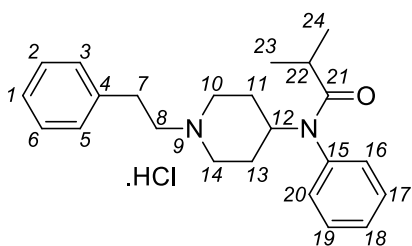
N-(1-Phenethylpiperidin-4-yl)-*N*-phenylcyclohexanecarboxamide hydrochloride (Cyclohexylfentanyl, **2i**)



Cyclohexylfentanyl **2i** was obtained in 36% yield over two steps. ^1H NMR (400 MHz, DMSO- D_6) δ 10.47 (bs, 1H, H9), 7.52-7.44 (m, 3H, H17-19), 7.33-7.21 (m, 7H, H1-3/H5-6/H16/H20), 4.67 (t, J = 11.9 Hz, 1H, H12), 3.51 (d, J = 11.4 Hz, 2H, H10a/H14a), 3.36 (H $_2\text{O}$),

3.20-3.02 (m, 4H, H8/H10b/H14b), 3.01-2.93 (m, 2H, H7), 1.94-1.76 (m, 3H, H11a/H13a/H22), 1.67-1.51 (m, 6H, H11b/H13b/H23/H27), 1.46 (d, J = 12.4 Hz, 1H, H25a), 1.32 (q, J = 11.9 Hz, 2H, H24a/H26a), 1.06 (q, J = 12.8 Hz, 1H, H25b), 0.78 (q, J = 12.8 Hz, 2H, H24b/H26b); ^{13}C NMR (100 MHz, DMSO- D_6) δ 174.44 (C21), 138.00 (C15), 137.14 (C4), 130.18 (C17/C19), 129.50 (C18), 128.66 (C2-3/C5-6/C16/C20), 126.79 (C1), 56.40 (C8), 50.88 (C10/C14), 48.90 (C12), 41.55 (C22), 29.42 (C7), 28.95 (C23/C27), 27.31 (C11/C13), 25.25 (C25), 25.07 (C24/C26); ATR-FTIR $\nu_{\text{max}}/\text{cm}^{-1}$: 3060, 2933 and 2854, 2647 and 2563, 1642, 1594; HRMS (C $_{26}\text{H}_{34}\text{N}_2\text{O}$) : predicted mass = 391.2744 [M+H] $^+$; experimental mass = 391.2740 [M+H] $^+$.

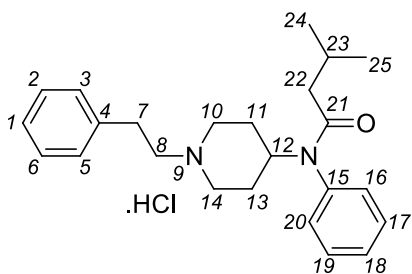
N-(1-Phenethylpiperidin-4-yl)-*N*-phenylisobutyramide hydrochloride (Isobutyrfentanyl, **2j**)



Isobutyrfentanyl **2j** was obtained in 60% yield over two steps. ^1H NMR (400 MHz, DMSO- D_6) δ 10.51 (bs, 1H, H9), 7.52-7.43 (m, 3H, H17-19), 7.33-7.21 (m, 7H, H1-3/H5-6/H16/H20), 4.68 (t, J = 12.1 Hz, 1H, H12), 3.51 (d, J = 11.0

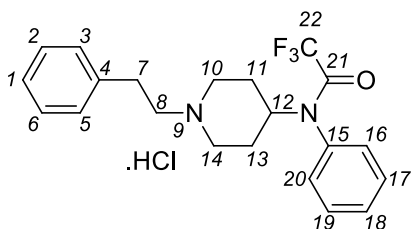
Hz, 2H, H10a/H14a), 3.36 (H₂O), 3.20-3.03 (m, 4H, H8/H10b/H14b), 3.02-2.94 (m, 2H, H7), 2.11 (sep, J = 6.8 Hz, 1H, H22), 1.91 (d, J = 12.4 Hz, 2H, H11a/H13a), 1.62 (q, J = 11.8 Hz, 2H, H11b/H13b), 0.88 (d, J = 6.4 Hz, 6H, H23-24); ¹³C NMR (100 MHz, DMSO-D₆) δ 175.54 (C21), 138.06 (C15), 137.14 (C4), 130.16 (C17/C19), 129.50 (C18), 128.64 (C2-3/C5-6), 128.62 (C16/C20), 126.74 (C1), 56.40 (C8), 50.86 (C10/C14), 49.04 (C12), 31.16 (C22), 29.40 (C7), 27.27 (C11/C13), 19.42 (C23-24); ATR-FTIR $\nu_{\text{max}}/\text{cm}^{-1}$: 3066 and 3037, 2962, 2931 and 2870, 2453 and 2400, 1654, 1596; HRMS (C₂₃H₃₀N₂O) : predicted mass = 351.2431 [M+H]⁺; experimental mass = 351.2432 [M+H]⁺.

3-Methyl-*N*-(1-phenethylpiperidin-4-yl)-*N*-phenylbutanamide hydrochloride
(Isovaleryl-fentanyl, **2k**)



Isovaleryl-fentanyl **2k** was obtained in 33% yield over two steps. ¹H NMR (400 MHz, DMSO-D₆) δ 10.46 (bs, 1H, H9), 7.52-7.41 (m, 3H, H17-19), 7.31 (t, J = 7.6 Hz, 2H, H2/H6), 7.26-7.17 (m, 5H, H1/H3/H5/H16/H20), 4.72 (tt, J = 3.2 Hz, 12.1 Hz, 1H, H12), 3.51 (d, J = 11.9 Hz, 2H, H10a/H14a), 3.37 (H₂O), 3.20-3.03 (m, 4H, H8/H10b/H14b), 3.01-2.93 (m, 2H, H7), 2.01-1.87 (m, 3H, H11a/H13a/H23), 1.71 (d, J = 7.3 Hz, 2H, H22), 1.63 (q, J = 12.8 Hz, 2H, H11b/H13b), 0.73 (d, J = 6.4 Hz, 6H, H24-25); ¹³C NMR (100 MHz, DMSO-D₆) δ 170.81 (C21), 138.16 (C15), 137.15 (C4), 130.44 (C17/C19), 129.54 (C18), 128.69 (C2-3/C5-6), 128.58 (C16/C20), 126.80 (C1), 56.41 (C8), 50.89 (C10/C14), 49.11 (C12), 43.07 (C22), 29.43 (C7), 27.32 (C11/C13), 25.10 (C23), 22.37 (C24-25); ATR-FTIR $\nu_{\text{max}}/\text{cm}^{-1}$: 3061 and 3037, 2954 and 2870, 2443 and 2387, 1648, 1596; HRMS (C₂₄H₃₂N₂O) : predicted mass = 365.2587 [M+H]⁺; experimental mass = 365.2592 [M+H]⁺.

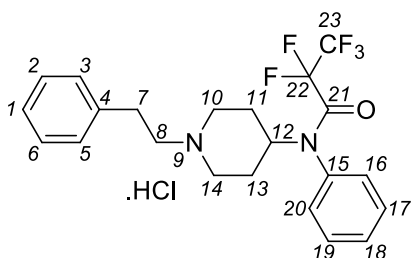
2,2,2-Trifluoro-*N*-(1-phenethylpiperidin-4-yl)-*N*-phenylacetamide hydrochloride (Trifluoroacetylfentanyl, **2l**)



Trifluoroacetylfentanyl **2l** was obtained in 38% yield over two steps. ¹H NMR (400 MHz, DMSO-*D*₆) δ 10.61 (bs, 1H, H9), 7.53-7.47 (m, 3H, H17-19), 7.37 (t, *J* = 3.9 Hz, 2H, H2/H6), 7.31 (t, *J* = 7.8 Hz, 2H, H3/H5), 7.26-7.18 (m,

3H, H1/H16/H20), 4.67 (tt, *J* = 3.2 Hz, 12.1 Hz, 1H, H12), 3.55 (d, *J* = 11.9 Hz, 2H, H10a/H14a), 3.41 (H₂O), 3.20-3.09 (m, 4H, H8/H10b/H14b), 3.01-2.94 (m, 2H, H7), 2.05 (d, *J* = 13.3 Hz, 2H, H11a/H13a), 1.69 (q, *J* = 11.8 Hz, 2H, H11b/H13b); ¹³C NMR (100 MHz, DMSO-*D*₆) δ 155.36 (d, *J* = 34.5 Hz, C21), 137.11 (C15), 134.01 (C4), 130.48 (C17/C19), 129.76 (C18), 129.02 (C16/C20), 128.68 (C2-3/C5-6), 126.81 (C1), 116.10 (d, *J* = 289.5 Hz, C22), 56.37 (C8), 52.09 (C10/C14), 50.42 (C12), 29.37 (C7), 26.34 (C11/C13); ¹⁹F NMR (376 MHz, CDCl₃) δ -68.30 (s); ATR-FTIR $\nu_{\text{max}}/\text{cm}^{-1}$: 3035 and 3010, 2941, 2447 and 2393, 1681, 1597, 1204-1156 (C-F); HRMS (C₂₁H₂₃N₂OF₃) : predicted mass = 377.1835 [M+H]⁺; experimental mass = 377.1840 [M+H]⁺.

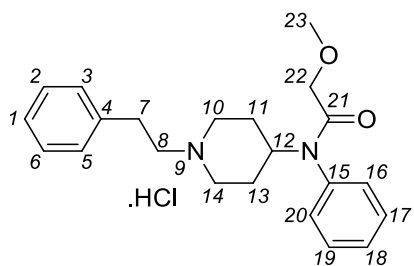
2,2,3,3,3-Pentafluoro-*N*-(1-phenethylpiperidin-4-yl)-*N*-phenylpropanamide hydrochloride (Pentafluoropropionylfentanyl, **2m**)



Pentafluoropropionylfentanyl **2m** was obtained in 52% yield over two steps. ¹H NMR (400 MHz, DMSO-*D*₆) δ 10.61 (s, 1H, H9), 7.61-7.46 (m, 3H, H17-19), 7.43-7.36 (m, 2H, H2/H6), 7.35-7.28 (m, 2H, H3/H5), 7.26-7.20 (m, 3H, H1/H16/H20), 4.68 (tt, *J* = 12.1 Hz, 3.7 Hz, 1H, H12), 3.55 (d, *J* = 11.9 Hz, 2H,

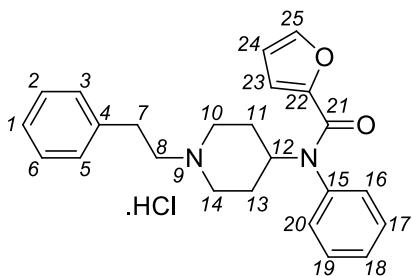
H10a/H14a), 3.37 (H₂O), 3.24-3.07 (m, 4H, H8/H10b/H14b), 3.03-2.93 (m, 2H, H7), 2.10-2.00 (m, 2H, H11a/H13a and acetone), 1.89-1.54 (q, J = 11.8 Hz, 2H, H11b/H13b); ¹³C NMR (100 MHz, DMSO-D₆) δ 156.11 (t, J = 24.0 Hz, C21), 137.10 (C15), 133.67 (C4), 130.34 (C17/C19), 129.75 (C18), 128.99 (C16/C20), 128.67 (C2-3/C5-6), 126.81 (C1), 56.35 (C8), 52.14(C10/C14), 50.42 (C12), 29.39 (C7), 26.26 (C11/C13); ¹⁹F NMR (376 MHz, CDCl₃) δ -83.36 (s), -114.29 (s); ATR-FTIR ν_{max}/cm⁻¹: 2941, 2438 and 2371, 1685, 1597; HRMS (C₂₂H₂₃N₂O_F₅) : predicted mass = 427.1803 [M+H]⁺; experimental mass = 427.1806 [M+H]⁺.

2-Methoxy-*N*-(1-phenethylpiperidin-4-yl)-*N*-phenylacetamide hydrochloride (Methoxyacetylfentanyl, **2n**)



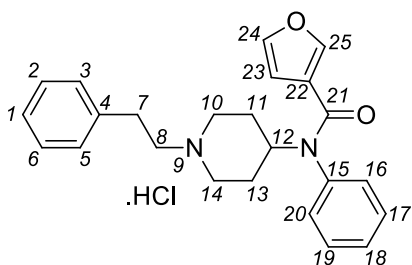
Methoxyacetylfentanyl **2n** was obtained in 29% yield over two steps. ¹H NMR (400 MHz, DMSO-D₆) δ 10.53 (bs, 1H, H9), 7.52-7.43 (m, 3H, H17-19), 7.35-7.19 (m, 7H, H1-3/H5-6/H16/H20), 4.69 (t, J = 11.9 Hz, 1H, H12), 3.56-3.49 (m, 4H, H10a/H14a/H22), 3.36 (H₂O), 3.20-3.04 (m, 7H, H8/H10b/H14b/H23), 3.01-2.94 (m, 2H, H7), 1.93 (d, J = 12.8 Hz, 2H, H11a/H13a), 1.64 (q, J = 11.9 Hz, 2H, H11b/H13b); ¹³C NMR (100 MHz, DMSO-D₆) δ 167.97 (C21), 137.14 (C15), 136.34 (C4), 130.33 (C17/C19), 129.55 (C18), 128.94 (C16/C20), 128.66 (C2-3/C5-6), 126.79 (C1), 70.15 (C22), 58.28 (C23), 56.41 (C8), 50.77 (C10/C14), 49.17 (C12), 29.39 (C7), 27.03 (C11/C13); ATR-FTIR ν_{max}/cm⁻¹: 3042, 2928 and 2820, 2464 and 2410, 1674, 1597, 1134 (C-O ether); HRMS (C₂₂H₂₈N₂O₂) : predicted mass = 353.2224 [M+H]⁺; experimental mass = 353.2220 [M+H]⁺.

N-(1-Phenethylpiperidin-4-yl)-*N*-phenylfuran-2-carboxamide hydrochloride (2-Furanylfentanyl, **2o**)



2-Furanylfentanyl **2o** was obtained in 26% yield over two steps. ^1H NMR (400 MHz, DMSO- D_6) δ 10.56 (s, 1H, H9), 7.66 (s, 1H, H25), 7.53-7.46 (m, 3H, H17-19), 7.35-7.19 (m, 7H, H1-3/H5-6/H16/H20), 6.32 (dd, $J = 3.2$ Hz, 1.4 Hz, 1H, H24), 5.38 (s, 1H, H23), 4.83 (tt, $J = 3.7$ Hz, 12.1 Hz, 1H, H12), 3.56 (d, $J = 11.4$ Hz, 2H, H10a/H14a), 3.37 (H₂O), 3.24-3.09 (m, 4H, H8/H10b/H14b), 3.05-2.95 (m, 2H, H7), 2.04 (d, $J = 12.4$ Hz, 2H, H11a/H13a), 1.76 (q, $J = 12.4$ Hz, 2H, H11b/H13b); ^{13}C NMR (400 MHz, DMSO- D_6) δ 157.98 (C21), 146.50 (C22), 145.23 (C25), 137.80 (C15), 137.15 (C4), 130.78 (C17/C19), 129.49 (C18), 129.13 (C16/C20), 128.69 (C2-3/C5-6), 126.81 (C1), 115.87 (C23), 111.28 (C24), 56.43 (C8), 50.82 (C10/C14), 50.22 (C12), 29.42 (C7), 27.01 (C11/C13); ATR-FTIR $\nu_{\text{max}}/\text{cm}^{-1}$: 3143, 3121, 3047 and 3001, 2934, 2455 and 2406, 1636, 1594 and 1558; HRMS ($\text{C}_{24}\text{H}_{26}\text{N}_2\text{O}_2$): predicted mass = 375.2067 [M+H] $^+$, 397.1892 [M+Na] $^+$; experimental mass = 375.2070 [M+H] $^+$ and 397.1890 [M+Na] $^+$.

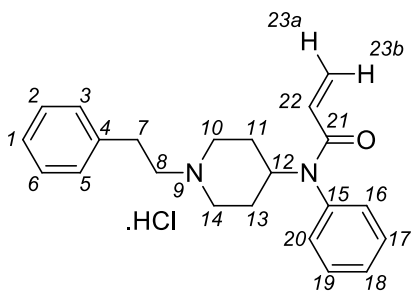
N-(1-Phenethylpiperidin-4-yl)-*N*-phenylfuran-3-carboxamide hydrochloride (3-furanylfentanyl, **2p**)



3-Furanylfentanyl **2p** was obtained in 42% yield over two steps. ^1H NMR (400 MHz, DMSO- D_6) δ 10.64 (bs, 1H, H9), 7.55-7.46 (m, 4H, H17-19/H25), 7.43-7.14 (m, 7H, H1-3/H5-6/H16/H20), 6.75 (s, 1H, H24), 5.98 (s, 1H,

H23), 4.83 (t, J = 11.9 Hz, 1H, H12), 3.55 (d, J = 11.4 Hz, 2H, H10a/H14a), 3.37 (H₂O), 3.25-3.09 (m, 4H, H8/H10b/H14b), 3.05-2.96 (m, 2H, H7), 2.07 (acetone), 2.02 (d, J = 12.4 Hz, 2H, H11a/H13a), 1.76 (q, J = 11.8 Hz, 2H, H11b/H13b); ¹³C NMR (100 MHz, DMSO-D₆) δ 161.94 (C21), 145.04 (C25), 142.87 (C24), 137.92 (C15), 137.19 (C4), 131.01 (C17/C19), 129.55 (C18), 129.19 (C16/C20), 128.69 (C2-3/C5-6), 126.79 (C1), 122.15 (C22), 110.82 (C23), 56.43 (C8), 50.83 (C10/C14), 50.10 (C12), 29.43 (C7), 27.09 (C11/C13); ATR-FTIR $\nu_{\max}/\text{cm}^{-1}$: 3044 and 3003, 2933, 2452 and 2404, 1620, 1595 and 1557; HRMS (C₂₄H₂₆N₂O₂) : predicted mass = 375.2067 [M+H]⁺; experimental mass = 375.2071 [M+H]⁺.

N-(1-Phenethylpiperidin-4-yl)-*N*-phenylacrylamide hydrochloride
(Acrylfentanyl, **2q**)

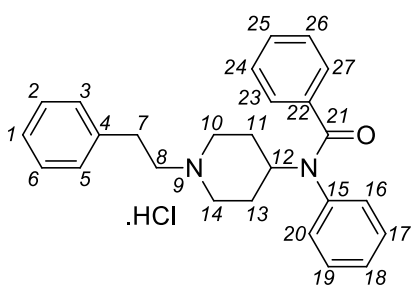


Acrylfentanyl **2q** was obtained in 32% yield over two steps. ¹H NMR (400 MHz, DMSO-D₆) δ 10.52 (bs, 1H, H9), 7.53-7.44 (m, 3H, H17-19), 7.34-7.19 (m, 7H, H1-3/H5-6/H16/H20), 6.15 (dd, J = 16.9, 2.3 Hz, 1H, H23b), 5.71 (dd, J = 16.5, 10.5 Hz, 1H, H22), 5.53 (dd, J = 10.5,

2.3 Hz, 1H, H23a), 4.75 (t, J = 12.1 Hz, 1H, H12), 3.53 (d, J = 11.4 Hz, 2H, H10a/H14a), 3.36 (H₂O), 3.21-3.06 (m, 4H, H8/H10b/H14b), 3.02-2.93 (m, 2H, H7), 1.97 (d, J = 12.8 Hz, 2H, H11a/H13a), 1.69 (dd, J = 22.9, 12.4 Hz, 2H, H11b/H13b); ¹³C NMR (100 MHz, DMSO-D₆) δ 164.17 (C21), 137.41 (C15), 137.14 (C4), 130.47 (C17/C19), 129.59 (C18), 128.98 (C22), 128.78 (C16/C20), 128.67 (C2-3/C5-6), 127.70 (C23), 126.79 (C1), 56.41 (C8), 50.81 (C10/C14), 49.51 (C12), 29.41 (C7), 27.17 (C11/C13); ATR-FTIR $\nu_{\max}/\text{cm}^{-1}$:

3044, 2936, 2453 and 2404, 1649, 1614 and 1593; HRMS (C₂₂H₂₆N₂O) : predicted mass = 335.2118 [M+H]⁺; experimental mass = 335.2124 [M+H]⁺.

N-(1-Phenethylpiperidin-4-yl)-*N*-phenylbenzamide hydrochloride
(Benzoylfentanyl, **2r**)



Benzoylfentanyl **2r** was obtained in 15% yield over two steps. ¹H NMR (400 MHz, DMSO-D₆) δ 10.01 (bs, 1H, H9), 7.35-7.11 (m, 15H, H1-3/H5-6/H16-20/H23-27), 4.82 (bs, 1H, H12), 3.58 (d, J = 11.9 Hz, 2H, H10a/H14a), 3.36 (H₂O), 3.24-3.11 (m, 4H, H8/H10b/H14b), 3.04-

2.97 (m, 2H, H7), 2.11 (d, J = 13.3 Hz, 2H, H11a/H13a), 1.80 (dq, J = 2.7 Hz, 12.8 Hz, 2H, H11b/H13b); ¹³C NMR (100 MHz, DMSO-D₆) δ 169.04 (C21), 138.66 (C15), 137.14 (C4), 136.89 (C22), 130.89 (C17/C19), 129.00 (C18), 128.84 (C16/C20), 128.69 (C2-3/C5-6), 127.86 (C25), 127.73 (C24/C26), 127.61 (C23/C27), 126.82 (C1), 56.44 (C8), 50.93 (C10/C14), 50.52 (C12), 29.45 (C7), 27.24 (C11/C13); ATR-FTIR ν_{max}/cm⁻¹: 3059 and 3026, 2999 and 2938, 2434 and 2389, 1630, 1594; HRMS (C₂₆H₂₈N₂O) : predicted mass = 385.2274 [M+H]⁺; experimental mass = 385.2276 [M+H]⁺.

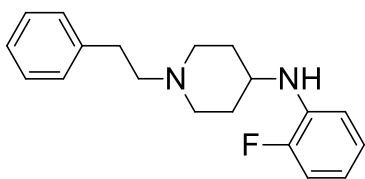
7.12.2 Synthesis of fluorinated fentalogues

General procedure for the synthesis of 49a-c [1]

1-Phenethyl-4-piperidone (**5**, 4.9 mmol) and fluoroaniline (5.4 mmol) were added to dichloromethane (16 mL) and treated with acetic acid (4.9 mmol). Sodium triacetoxyborohydride was added slowly to the mixture (4.9 mmol). The system was flushed with argon and the resulting solution was stirred at room

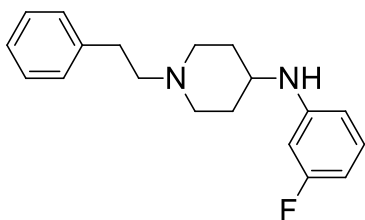
temperature for 24 h. At this point a second portion of sodium triacetoxyborohydride was added to the mixture (4.9 mmol), which was then stirred for another 24 h. The reaction mixture was transferred to a separation funnel with saturated aqueous sodium bicarbonate (50 mL) and extracted twice with ethyl acetate (2 x 50 mL). The combined organic layers were dried over magnesium sulfate and concentrated *in vacuo*. The crude oil was purified using a Biotage Isolera One Flash Purification System (eluent: 0-10% MeOH in DCM).

N-(2-Fluorophenyl)-1-phenethylpiperidin-4-amine (**49a**)



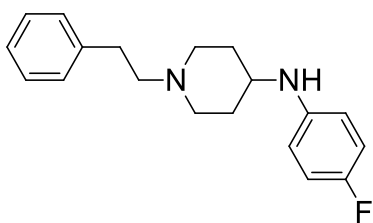
Compound **49a** was obtained as a yellow oil in 68% yield. $^1\text{H NMR}$ (400 MHz, CDCl_3) δ 7.38 – 7.20 (m, 5H), 7.05 – 6.95 (m, 2H), 6.76 – 6.60 (m, 2H), 5.78 (s(br), 1H), 3.50 – 3.36 (m, 1H), 3.34 – 3.13 (m, 2H), 3.01 – 2.82 (m, 4H), 2.54 (t, $J = 10.6$ Hz, 2H), 2.27 – 2.09 (m, 2H), 1.87 – 1.68 (m, 2H); $^{13}\text{C NMR}$ (100 MHz, CDCl_3) δ 152.91, 150.55, 139.23, 135.41, 135.29, 128.85, 128.84, 128.83, 128.71, 128.70, 128.68, 128.67, 128.66, 126.51, 124.68, 124.64, 116.92, 116.85, 114.94, 114.76, 112.70, 112.67, 59.66, 51.62, 48.97, 32.62, 31.17; $^{19}\text{F NMR}$ (376 MHz, CDCl_3) δ -131.95; ATR-FTIR $\nu_{\text{max}}/\text{cm}^{-1}$: 3357, 2939, 2516, 1707, 1628, 1514; HRMS ($\text{C}_{19}\text{H}_{23}\text{N}_2\text{F}$) : predicted mass = 299.1924 $[\text{M}+\text{H}]^+$; experimental mass = 299.1921 $[\text{M}+\text{H}]^+$.

N-(3-Fluorophenyl)-1-phenethylpiperidin-4-amine (**49b**)



Compound **49b** was obtained as a yellow solid in 65% yield. ^1H NMR (400 MHz, CDCl_3) δ 7.40 – 7.18 (m, 5H), 7.16 – 7.05 (m, $J = 8.1, 6.9$ Hz, 1H), 6.43 – 6.26 (m, 3H), 3.71 (d, 1H), 3.45 – 3.16 (m, 1H), 3.00 (d, $J = 11.9$ Hz, 2H), 2.91 – 2.80 (m, 3H), 2.70 – 2.61 (m, 2H), 2.33 – 2.18 (m, 2H), 2.18 – 2.03 (m, 2H), 1.90 (s(br), 1H), 1.55 (qd, $J = 11.0, 3.6$ Hz, 2H); ^{13}C NMR (100 MHz, CDCl_3) δ 164.22 (d, $J = 242.6$ Hz), 148.88 (d, $J = 10.7$ Hz), 140.28, 130.35 (d, $J = 10.3$ Hz), 128.71, 128.48, 128.44, 126.11, 109.08 (d, $J = 2.4$ Hz), 103.54 (d, $J = 21.5$ Hz), 99.64 (d, $J = 25.4$ Hz), 60.58, 53.11, 52.39, 49.94, 41.26, 33.84, 32.36; ^{19}F NMR (376 MHz, CDCl_3) δ -113.49; ATR-FTIR $\nu_{\text{max}}/\text{cm}^{-1}$: 3268, 3029, 2933, 2807, 2768, 1716, 1620, 1588, 1533; HRMS ($\text{C}_{19}\text{H}_{23}\text{N}_2\text{F}$) : predicted mass = 299.1924 $[\text{M}+\text{H}]^+$; experimental mass = 299.1919 $[\text{M}+\text{H}]^+$.

N-(4-Fluorophenyl)-1-phenethylpiperidin-4-amine (**49c**)



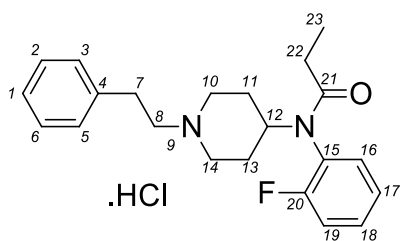
Compound **49c** was obtained as an off-white solid in 65% yield. ^1H NMR (400 MHz, CDCl_3) δ 7.26 – 7.08 (m, 5H), 6.85 – 6.76 (m, 2H), 6.51 – 6.42 (m, 2H), 3.23 – 3.13 (m, 1H), 2.92 (d, $J = 11.9$ Hz, 2H), 2.82 – 2.71 (m, 2H), 2.61 – 2.51 (m, 2H), 2.14 (t, $J = 11.2$ Hz, 2H), 2.06 – 1.90 (m, 2H), 1.54 – 1.34 (m, 2H); ^{13}C NMR (100 MHz, CDCl_3) δ 155.74 (d, $J = 235.0$ Hz), 154.57, 143.36 (d, $J = 1.9$ Hz), 140.21, 128.57 (d, $J = 25.9$ Hz), 126.13, 121.77, 115.74 (d, $J = 22.2$ Hz), 114.28 (d, $J = 7.3$ Hz), 60.55, 52.44, 50.63, 33.77, 32.44; ^{19}F NMR (376 MHz, CDCl_3) δ -128.14; ATR-FTIR $\nu_{\text{max}}/\text{cm}^{-1}$: 3405, 3273, 3026, 2927, 2843, 2810, 2773, 1665,

1617, 1559, 1506; HRMS (C₁₉H₂₃N₂F) : predicted mass = 299.1924 [M+H]⁺; experimental mass = 299.1922 [M+H]⁺.

General procedure for the synthesis of 42a-c [4]

The starting amine (**49a-c**, 1.0 mmol) was added to dichloromethane (10 mL) and was treated with diisopropylethylamine (2.0 mmol). The system was flushed with argon, the mixture cooled in an ice bath and propionyl chloride (2.0 mmol) added dropwise. The resulting solution was stirred at room temperature for 2 h. The mixture was diluted with water (30 mL) and the organic layer washed sequentially with brine (30 mL) and saturated aqueous sodium bicarbonate (30 mL). The organic layer was dried with magnesium sulfate and concentrated *in vacuo*. The crude oil was purified using a Biotage Isolera One Flash Purification System (eluent: 0-10% MeOH in DCM). The free-base was dissolved in acetone, and an equimolar amount of hydrogen chloride (3 M in cyclopentyl methyl ether (CPME)) added. The mixture was left to stand for 5-10 minutes and the salt isolated by filtration. The products were dried in an oven (60 °C, 12h).

N-(2-Fluorophenyl)-*N*-(1-phenethylpiperidin-4-yl)propionamide (*ortho*-Fluoro fentanyl, **42a**)

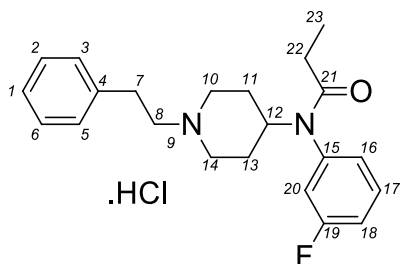


ortho-Fluoro fentanyl **42a** was obtained as a white solid in 25% yield. ¹H NMR (400 MHz, DMSO-D₆): 10.35 (s(br), 1H, H9), 7.57-7.48 (m, 1H, H18), 7.48-7.27 (m, 5H, H2/H6/H16-17/H19), 7.26-7.18 (m, 3H, H1/H3/H5), 4.75 (tt,

J = 12.1 Hz, 3.4 Hz, 1H, H12), 3.52 (t, *J* = 10.8 Hz, 2H, H10a/H14a), 3.34 (s, H₂O), 3.21-3.04 (m, 4H, H8/H10b/H14b), 3.01-2.92 (m, 2H, H7), 1.98 (d, *J* =

13.3 Hz, 1H, H13a), 1.93-1.49 (m, 5H, H13b/H11/H22), 0.89 (t, J = 7.3 Hz, 3H, H23); ^{13}C NMR (100 MHz, DMSO- D_6) δ 172.38 (C21), 158.64 (d, J = 246.3 Hz, C20), 137.10 (C4), 132.78 (C16), 131.19 (d, J = 7.7 Hz, C18), 128.66 (C2-3/C5-6), 126.80 (C1), 125.60 and 125.47 (overlap of C15 (d) and C17(s)), 116.74 (d, J = 21.1 Hz, C19), 56.36 (C8), 50.80 (C10/C14), 49.55 (C12), 29.41 (C7), 27.30 and 27.20 (C13/C22), 26.41 (C11), 9.21 (C23); ^{19}F NMR (376 MHz, DMSO- D_6) δ -122.048 (s); ATR-FTIR $\nu_{\text{max}}/\text{cm}^{-1}$: 3062 and 3029, 2978 and 2930, 2628, 2588, 2526 and 2471, 1661 (C=O amide), 1607 and 1588; HRMS (C₂₂H₂₇N₂OF): predicted mass = 355.218 [M+H]⁺, experimental mass = 355.2187 [M+H]⁺.

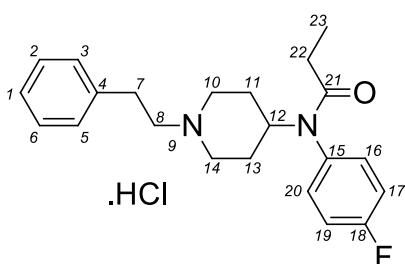
N-(3-Fluorophenyl)-*N*-(1-phenethylpiperidin-4-yl)propionamide (*meta*-Fluoro fentanyl, **42b**)



meta-Fluoro fentanyl **42b** was obtained as a white solid in 36% yield. ^1H NMR (400 MHz, DMSO- D_6): 10.34 (s(br), 1H, H9), 7.53 (q, J = 7.6 Hz, 1H, H17), 7.45-7.18 (m, 8H, H1-3/H5-6/H18/H20), 7.12 (d, J = 7.8 Hz, 1H, H16), 4.70 (t, J = 11.4 Hz, 1H, H12), 3.52 (d, J = 11.4 Hz, 2H, H10a/H14a), 3.35 (s, H₂O), 3.22-3.04 (m, 4H, H8/H10b/H14b), 3.04-2.92 (m, 2H, H7), 2.04-1.80 (m, 4H, H11a/H13a/H22), 1.63 (qd, J = 11.2 Hz, 3.2 Hz, 2H, H11b/H13b), 0.89 (t, J = 7.3 Hz, 3H, H23); ^{13}C NMR (100 MHz, DMSO- D_6) δ 171.97 (C21), 162.15 (d, J = 245.4 Hz, C19), 139.82 (d, J = 9.6 Hz, C15), 137.11 (C4), 130.96 (d, J = 8.6 Hz, C17), 128.68 (C2-3/C5-6), 126.86 and 126.80 (overlap of C1(s) and C16(d)), 117.79 (d, J = 21.1 Hz, C20), 115.71 (d, J = 20.1 Hz, C18), 56.39 (C8), 50.87 (C10/C14), 49.09 (C12), 29.43 (C7), 27.73 (C22), 27.17 (C11/C13), 9.32 (C23); ^{19}F NMR (376 MHz, DMSO- D_6) δ -114.064 (s); ATR-FTIR $\nu_{\text{max}}/\text{cm}^{-1}$:

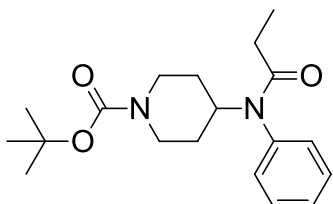
3042 and 3013, 2994, 2964 and 2937, 2457 and 2410, 1647 (C=O amide), 1606 and 1590; HRMS (C₂₂H₂₇N₂OF): predicted mass = 355.218 [M+H]⁺, experimental mass = 355.2179 [M+H]⁺.

N-(4-Fluorophenyl)-*N*-(1-phenethylpiperidin-4-yl)propionamide (*para*-Fluoro fentanyl, **42c**)



para-Fluoro fentanyl **42c** was obtained as a white solid in 43% yield. ¹H NMR (400 MHz, DMSO-D₆): 10.36 (s(br), 1H, H9), 7.38-7.28 (m, 6H, H2/H6/H16-17/H19-20), 7.27-7.18 (m, 3H, H1/H3/H5), 4.71 (t, J = 12.1 Hz, 1H, H12), 3.52 (d, J = 11.4 Hz, 2H, H10a/H14a), 3.34 (s, H₂O), 3.24-3.03 (m, 4H, H8/H10b/H14b), 3.03-2.91 (m, 2H, H7), 1.92 (d, J = 12.8 Hz, 2H, H11a/H13a), 1.83 (q, J = 7.3 Hz, 2H, H22), 1.60 (q, J = 11.9 Hz, 2H, H11b/H13b), 0.88 (t, J = 7.6 Hz, 3H, H23); ¹³C NMR (100 MHz, DMSO-D₆) δ 172.25 (C21), 161.69 (d, J = 246.3 Hz, C18), 137.12 (C4), 134.38 (d, J = 2.9 Hz, C15), 132.55 (d, J = 9.6 Hz, C16/C20), 128.66 (C2-3/C5-6), 126.80 (C1), 116.28 (d, J = 22.0 Hz, C17/C19), 56.38 (C8), 50.85 (C10/C14), 48.90 (C12), 29.41 (C7), 27.74 (C22), 27.13 (C11/C13), 9.35 (C23); ¹⁹F NMR (376 MHz, DMSO-D₆) δ -115.977 (s); ATR-FTIR ν_{max}/cm⁻¹: 3062, 3029 and 3006, 2975 and 2936, 2627, 2587, 2526 and 2471, 1651 (C=O amide), 1602 and 1507; HRMS (C₂₂H₂₇N₂OF): predicted mass = 355.218 [M+H]⁺, experimental mass = 355.2181

Synthesis of tert-Butyl-4-(N-phenylpropionamido)piperidine-1-carboxylate (51)
[4, 184]



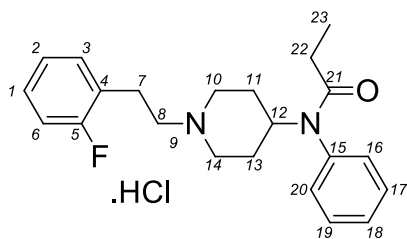
tert-Butyl 4-anilinopiperidine-1-carboxylate (**50**, 1.7 mmol) was added to dichloromethane (17 mL) and was treated with diisopropylethylamine (3.4 mmol). The system was flushed with argon, the mixture cooled in an ice bath and propionyl chloride (3.4 mmol) added dropwise. The resulting solution was stirred at room temperature for 2 h. The mixture was diluted with water (50 mL) and the organic layer washed sequentially with brine (50 mL) and saturated aqueous sodium bicarbonate (50 mL). The organic layer was dried with magnesium sulfate and concentrated *in vacuo*. The crude oil was purified using a Biotage Isolera One Flash Purification System (eluent: 10-40% ethyl acetate in hexanes). *tert*-Butyl 4-(*N*-phenylpropionamido)piperidine-1-carboxylate (**51**) was obtained as an off-white solid (95%). ¹H NMR (400 MHz, CDCl₃): 7.44-7.28 (m, 3H), 7.09-6.98 (m, 2H), 4.77 (tt, J = 12.1, 3.7 Hz, 1H), 4.10 (s(br), 2H), 2.87-2.65 (m, 2H), 1.90 (q, J = 7.5 Hz, 2H), 1.80 -1.68 (m, 2H), 1.41-1.11 (m, 11H), 1.00 (t, J = 7.6 Hz, 3H); ¹³C NMR (100 MHz, CDCl₃): 173.48, 154.50, 138.63, 130.20, 129.34, 128.39, 79.46, 52.09, 43.35, 30.42, 28.42, 28.29, 9.52; ATR-FTIR $\nu_{\max}/\text{cm}^{-1}$: 2982, 2940, 2864, 1681, 1656, 1597; HRMS (C₁₉H₂₈N₂O₃) : predicted mass = 333.2178 [M+H]⁺ and 277.1552 [M - *t*Bu]⁺; experimental mass = 333.2177 [M+H]⁺ (low abundance), 277.1551 [M - *t*Bu]⁺

General procedure for the synthesis of 46a-c [4, 185]

tert-Butyl 4-(*N*-phenylpropionamido)piperidine-1-carboxylate (**51**, 2.95 mmol) was dissolved in a 1:2 mixture of trifluoroacetic acid and dichloromethane

(9 mL). The resulting solution was stirred for an hour at room temperature. The reaction mixture was then cooled to 0°C, quenched with 1 M aqueous NaOH (10 mL) and transferred to a separatory funnel. The aqueous layer was removed, and the organic layer was washed successively with 1 M aqueous NaOH (20 mL), saturated aqueous sodium bicarbonate (20 mL) and brine (20 mL). The organic layer was dried over magnesium sulfate, filtered and concentrated *in vacuo*. The resulting oil was dissolved in acetonitrile (12 mL) and fluorophenethyl bromide (3.63 mmol) and cesium carbonate (6.67 mmol) were added. The reaction mixture was heated to reflux for 5 h. The mixture was then cooled to room temperature and transferred to a separation funnel with 50 mL water. The aqueous layer was extracted three times with dichloromethane (2 x 50 mL). The combined organic layers were washed sequentially with brine (3 x 50 mL) and saturated aqueous sodium bicarbonate (2 x 50 mL). The combined organic layers were dried with magnesium sulfate and concentrated *in vacuo*. The resulting oil was dissolved in acetone, and an equimolar amount of hydrogen chloride (3 M in cyclopentyl methyl ether) added. The mixture was left to stand for 5-10 minutes and the salt isolated by filtration. The products were dried in an oven (60 °C, 12h).

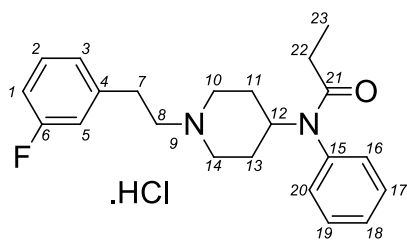
N-(1-(2-Fluorophenethyl)piperidin-4-yl)-*N*-phenylpropionamide (2'-Fluorofentanyl, **46a**)



Compound **46a** was obtained as a white solid in 60% yield. ¹H NMR (400 MHz, DMSO-D₆): 10.30 (s (br), 1H, H9), 7.52-7.40 (m, 3H, H17-19), 7.36-7.27 (m, 2H, H1/H3), 7.24 (d, J = 6.9 Hz, 2H, H16/H20), 7.21-7.12 (m, 2H, H2/H6), 4.72(tt, J = 12.1 Hz, 3.7 Hz, 1H, H12), 3.53 (d, J = 11.4 Hz, 2H, H10a/H14a),

3.19-3.06 (m, 4H, H8/H10b/H14b), 3.05-2.97 (m, 2H, H7), 1.93 (d, J = 12.8 Hz, 2H, H11a/H13a), 1.81 (q, J = 7.5 Hz, 2H, H22), 1.60 (qd, J = 12.8 Hz, 2.3 Hz, 2H, H11b/H13b), 0.87 (t, J = 7.6 Hz, 3H, H23); ^{13}C NMR (100 MHz, DMSO- D_6) δ 172.16 (C21), 160.42 (d, J = 244.4 Hz, C5), 138.12 (C15), 131.07 (d, J = 4.8 Hz, C3), 130.39 (C17/C19), 129.52 (C18), 129.16 (d, J = 8.6 Hz, C1), 128.55 (C16/C20), 124.75 (d, J = 3.8 Hz, C2), 123.71 (d, J = 16.3 Hz, C4), 115.42 (d, J = 22.0 Hz, C6), 54.88 (C8), 50.87 (C10/C14), 48.93 (C12), 27.74 (C22), 27.27 (C11/C13), 23.00 (C7), 9.42 (C23); ^{19}F NMR (376 MHz, DMSO- D_6) δ -120.762 (s); ATR-FTIR $\nu_{\text{max}}/\text{cm}^{-1}$: 3058, 3029 and 3011, 2971 and 2932, 2629, 2587, 2522 and 2471, 1660 (C=O amide), 1594; HRMS ($\text{C}_{22}\text{H}_{27}\text{N}_2\text{OF}$): predicted mass = 355.218 $[\text{M}+\text{H}]^+$, experimental mass = 355.2187

N-(1-(3-Fluorophenethyl)piperidin-4-yl)-*N*-phenylpropionamide (3'-Fluorofentanyl, **46b**)

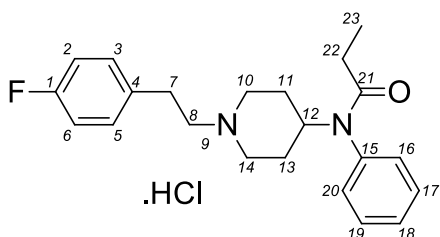


Compound **46b** was obtained as a white solid in 62% yield. ^1H NMR (400 MHz, DMSO- D_6): 10.29 (s(br), 1H, H9), 7.50-7.37 (m, 3H, H17-19), 7.37-7.28 (m, 1H, H2), 7.21 (d, J = 7.6 Hz, 2H, H16/H20), 7.12-6.99 (m, 3H, H1/H3/H5),

4.69 (tt, J = 12.1 Hz, 3.66 Hz, 1H, H12), 3.48 (d, J = 11.4 Hz, 2H, H10a/H14a), 3.21-3.01 (m, 4H, H8/H10b/H14b), 3.01-2.92 (m, 2H, H7), 1.90 (d, J = 12.8 Hz, 2H, H11a/H13a), 1.79 (q, J = 7.3 Hz, 2H, H22), 1.58 (qd, J = 13.1 Hz, 2.7 Hz, 2H, H11b/H13b), 0.84 (t, J = 7.3 Hz, 3H, H23); ^{13}C NMR (100 MHz, DMSO- D_6) δ 172.17 (C21), 162.22 (d, J = 243.5 Hz, C6), 140.01 (d, J = 7.7 Hz, C4), 138.12 (C15), 130.58 (d, J = 8.6 Hz, C2), 130.39 (C17/C19), 129.52 (C18), 128.55 (C16/C20), 124.90 (C3), 115.48 (d, J = 21.1 Hz, C5), 113.64 (d, J = 21.1 Hz, C1), 55.98 (C8), 50.94 (C10/C14), 48.96 (C12), 29.04 (C7), 27.74 (C22), 27.28

(C11/C13), 9.42 (C23); ^{19}F NMR (376 MHz, DMSO- D_6) δ -115.698 (s); ATR-FTIR $\nu_{\text{max}}/\text{cm}^{-1}$: 3014, 2991, 2966 and 2937, 2453 and 2404, 1640 (C=O amide), 1615, 1598 and 1588; HRMS ($\text{C}_{22}\text{H}_{27}\text{N}_2\text{OF}$): predicted mass = 355.218 $[\text{M}+\text{H}]^+$, experimental mass = 355.2186

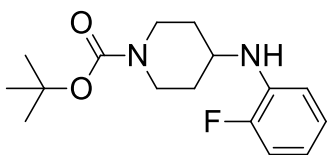
N-(1-(4-Fluorophenethyl)piperidin-4-yl)-*N*-phenylpropionamide (4'-Fluorofentanyl, **46c**)



Compound **46c** was obtained as a white solid in 70% yield. ^1H NMR (400 MHz, DMSO- D_6): 10.04 (s(br), 1H, H9), 7.53-7.41 (m, 3H, H17-19), 7.31-7.22 (m, 4H (H3/H5/H16/H20)), 7.19-7.10 (m, 2H,

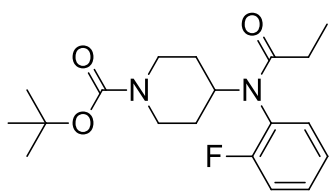
H2/H6), 4.72 (tt, $J = 12.1$ Hz, 3.7 Hz, 1H, H12), 3.51 (d, $J = 11.4$ Hz, 2H, H10a/H14a), 3.34 (s, H_2O), 3.21-3.03 (m, 4H, H8/H10b/H14b), 2.99-2.90 (m, 2H, H7), 1.93 (d, $J = 12.8$ Hz, 2H, H11a/H13a), 1.82 (q, $J = 7.3$ Hz, 2H, H22), 1.58 (qd, $J = 12.8$ Hz, 2.7 Hz, 2H, H11b/H13b), 0.87 (t, $J = 7.3$ Hz, 3H, H23); ^{13}C NMR (100 MHz, DMSO- D_6) δ 172.17 (C21), 161.15 (d, $J = 242.5$ Hz, C1), 138.13 (C15), 133.21 (C4), 130.60 (d, $J = 7.7$ Hz, C3/C5), 130.43 (C17/C19), 129.54 (C18), 128.57 (C16/C20), 115.41 (d, $J = 21.1$ Hz, C2/C6), 56.40 (C8), 50.97 (C10/14), 48.90 (C12), 28.60 (C7), 27.75 (C22), 27.29 (C11/13), 9.42 (C23); ^{19}F NMR (376 MHz, DMSO- D_6) δ -118.556 (s); ATR-FTIR $\nu_{\text{max}}/\text{cm}^{-1}$: 3006, 2984 and 2931, 2627, 2589, 2533, 2492 and 2475, 1657 (C=O amide), 1594 and 1514; HRMS ($\text{C}_{22}\text{H}_{27}\text{N}_2\text{OF}$): predicted mass = 355.218 $[\text{M}+\text{H}]^+$, experimental mass = 355.2190

Synthesis of *tert*-butyl-4-((2-fluorophenyl)amino)piperidine-1-carboxylate (**53**)
[1, 4]



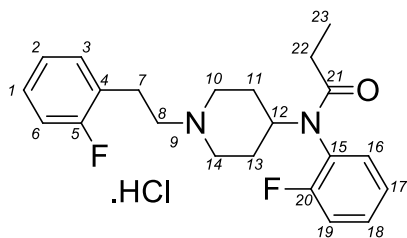
tert-Butyl 4-oxopiperidine-1-carboxylate (**52**, 2.52 mmol) and 2-fluoroaniline (2.8 mmol) were added to dichloromethane (8 mL) and treated with acetic acid (2.5 mmol). Sodium triacetoxyborohydride was added slowly to the mixture (2.5 mmol). The system was flushed with argon and the resulting solution was stirred at room temperature for 24 h. At this point a second portion of sodium triacetoxyborohydride was added to the mixture (2.5 mmol), which was then stirred for another 24 h. The reaction mixture was transferred to a separation funnel with saturated aqueous sodium bicarbonate (50 mL) and extracted twice with ethyl acetate (2 x 50 mL). The combined organic layers were dried over magnesium sulfate and concentrated *in vacuo*. The crude oil was purified using a Biotage Isolera One Flash Purification System (eluent: 0-10% MeOH in DCM). Compound **53** was obtained as an off-white solid (73%). ¹H NMR (400 MHz, CDCl₃) δ 7.19 (s, 1H), 6.96 – 6.85 (m, 2H), 6.65 (t, *J* = 8.0 Hz, 1H), 6.61 – 6.50 (m, 1H), 4.27 – 3.65 (m, 2H), 3.44 – 3.29 (m, 1H), 2.87 (t, *J* = 11.8 Hz, 2H), 2.07 – 1.91 (m, 2H), 1.55 (s (br), 1H), 1.40 (s, 9H), 1.37 – 1.20 (m, 2H); ¹³C NMR (100 MHz, CDCl₃) δ 154.82, 151.67 (d, *J* = 237.9 Hz), 135.31 (d, *J* = 11.5 Hz), 124.64 (d, *J* = 2.9 Hz), 116.77 (d, *J* = 6.9 Hz), 114.78 (d, *J* = 18.8 Hz), 112.68 (d, *J* = 2.6 Hz), 79.70, 49.96, 42.85, 32.35, 28.52; ¹⁹F NMR (376 MHz, CDCl₃) δ -126.69; ATR-FTIR $\nu_{\max}/\text{cm}^{-1}$: 3351, 2968, 2933, 2846, 1674, 1617, 1528; HRMS (C₁₆H₂₃N₂O₂F) : predicted mass = 295.1822 [M+H]⁺ and 239.1196 [M - *t*Bu]⁺; experimental mass = 295.1810 [M+H]⁺ (low abundance), 239.1195 [M - *t*Bu]⁺.

Synthesis of *tert*-butyl 4-((*N*-(2-fluorophenyl)propionamido)piperidine-1-carboxylate (**54**) [4]



tert-Butyl 4-((*N*-(2-fluorophenyl)amino)piperidine-1-carboxylate (**53**, 1.83 mmol) was added to dichloromethane (15 mL) and was treated with diisopropylethylamine (3.7 mmol). The system was flushed with argon, the mixture cooled in an ice bath and propionyl chloride (3.7 mmol) added dropwise. The resulting solution was stirred at room temperature for 2 h. The mixture was diluted with water (50 mL) and the organic layer washed sequentially with brine (50 mL) and saturated aqueous sodium bicarbonate (50 mL). The organic layer was dried with magnesium sulfate and concentrated *in vacuo*. The crude oil was purified using a Biotage Isolera One Flash Purification System (eluent: 0-10% MeOH in DCM). Compound **54** was obtained as a yellow solid (48%). ¹H NMR (400 MHz, CDCl₃) δ 7.45 – 7.35 (m, 1H), 7.25 – 7.06 (m, 3H), 4.79 (tt, *J* = 12.2, 3.7 Hz, 1H), 4.46 – 3.79 (m, 2H), 3.01 – 2.57 (m, 2H), 1.98 (m, 2H), 1.89 – 1.72 (m, 2H), 1.39 (s, 9H), 1.35 – 1.22 (m, 1H), 1.21 – 1.07 (m, 1H), 1.03 (t, *J* = 7.4 Hz, 3H); ¹³C NMR (100 MHz, CDCl₃) δ 173.61, 159.26 (d, *J* = 249.0 Hz), 154.58, 132.19, 130.49 (d, *J* = 7.9 Hz), 126.60 (d, *J* = 13.6 Hz), 124.80 (d, *J* = 3.9 Hz), 116.84 (d, *J* = 21.0 Hz), 79.54, 52.85, 43.24, 30.90, 30.71, 29.35, 28.34, 27.85, 9.25; ¹⁹F NMR (376 MHz, CDCl₃) δ -118.63; ATR-FTIR $\nu_{\text{max}}/\text{cm}^{-1}$: 2976, 2938, 2859, 1688, 1663, 1498; HRMS (C₁₉H₂₇N₂O₃F) : predicted mass = 373.1903 [M+Na]⁺; 295.1458 [M - *t*Bu]⁺; experimental mass = 373.1897 [M+Na]⁺ 295.1456 [M - *t*Bu]⁺.

Synthesis of *N*-(1-(2-fluorophenethyl)piperidin-4-yl)-*N*-(2-fluorophenyl)propionamide (2'-fluoro-ortho-fluorofentanyl, **47**)

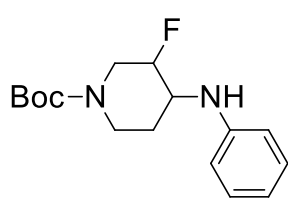


tert-Butyl 4-(*N*-(2-Fluorophenyl)propionamido) piperidine-1-carboxylate (**54**, 0.60 mmol) was dissolved in a 1:2 mixture of trifluoroacetic acid and dichloromethane (2 mL). The resulting solution was stirred for an hour at room

temperature. The reaction mixture was then concentrated *in vacuo*, and the oil transferred to a separation funnel with methanol (20 mL). Water (20 mL), 5 M aqueous NaOH (4 mL) and brine (15 mL) were added and the resulting mixture was extracted twice with ethyl acetate (2 x 25 mL). The combined organic layers were dried over magnesium sulfate, filtered and concentrated *in vacuo*. The resulting oil was dissolved in acetonitrile (2.5 mL) and 2-fluorophenethyl bromide (0.72 mmol) and cesium carbonate (1.32 mmol) were added. The reaction mixture was heated to reflux for 5 h. The mixture was then cooled to room temperature and transferred to a separation funnel with 30 mL water. The aqueous layer was extracted three times with dichloromethane (2 x 30 mL). The combined organic layers were washed sequentially with brine (3 x 30 mL) and saturated aqueous sodium bicarbonate (2 x 30 mL). The combined organic layers were dried with magnesium sulfate and concentrated *in vacuo*. The resulting oil was dissolved in acetone, and an equimolar amount of hydrogen chloride (3 M in CPME) added. The mixture was left to stand for 5-10 minutes and the salt isolated by filtration. The product was dried in an oven (60 °C, 12h) to give 2'-fluoro *ortho*-fluorofentanyl (**47**) as a white powder (53% yield). ¹H NMR (400 MHz, DMSO-D₆) δ 10.56-10.37 (s(br), 1H, H9), 7.58-7.48 (m, 1H, H18), 7.47-7.26 (m, 5H, H1/H3/16/H17/H19), 7.23-7.11 (m, 2H, H2/H6), 4.74 (tt, J = 12.1 Hz, 3.7 Hz, 1H, H12), 3.54 (t, J = 10.3 Hz, 2H, H10a/H14a), 3.35

(s, H₂O), 3.23-3.08 (m, 4H, H8/H10b/H14b), 3.08-2.95 (m, 2H, H7), 2.00 (d, J = 13.2 Hz, 1H, H13a), 1.95-1.49 (m, 4H, H13b/H11/H22), 0.89 (t, J = 7.3 Hz, 3H, H23); ¹³C NMR (100 MHz, DMSO-D₆) δ 172.39 (C21), 160.42 (d, J = 244.4 Hz, C5), 158.64 (d, J = 246.3 Hz, C20), 132.79 (C16), 131.20 (d, J = 8.6 Hz, C18), 131.07 (d, J = 3.8 Hz, C3), 129.16 (d, J = 7.7 Hz, C1), 125.60 and 125.47 (overlap of C15(d) and C17(s)), 124.75 (d, J = 3.8 Hz, C2), 123.68 (d, J = 15.3 Hz, C4), 116.74 (d, J = 21.1 Hz, C19), 115.41 (d, J = 21.1 Hz, C6), 54.85 (C8), 50.81 (C10/C14), 49.49 (C12), 27.29 and 27.20 (C13/C22), 26.40 (C11), 22.98 (C7), 9.20 (C23); ¹⁹F NMR (376 MHz, DMSO-D₆) δ -120.657 (s, 2'), -122.047 (s, *ortho*); ATR-FTIR $\nu_{\text{max}}/\text{cm}^{-1}$: 3014, 2976 and 2939, 2630, 2587, 2520, 2471 and 2415, 1662 (C=O amide), 1607 and 1588; HRMS (C₂₂H₂₆N₂OF₂): predicted mass = 373.2086 [M+H]⁺, experimental mass = 373.2085

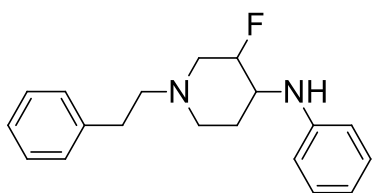
Synthesis of tert-butyl 3-fluoro-4-(phenylamino)piperidine-1-carboxylate (56)
[1, 4, 184]



tert-Butyl 3-fluoro-4-oxopiperidine-1-carboxylate (**55**, 23.1 mmol) and aniline (25.4 mmol) were added to dichloromethane (70 mL) and treated with acetic acid (23.1 mmol). Sodium triacetoxyborohydride (23.1 mmol) was added slowly to the mixture. The system was flushed with argon and the resulting solution was stirred at room temperature for 24 h. At this point a second portion of sodium triacetoxyborohydride (23.1 mmol) was added to the mixture, which was then stirred for another 24 h. The reaction mixture was transferred to a separation funnel with saturated aqueous sodium bicarbonate (250 mL). The aqueous layer was extracted twice with ethyl acetate (2 x 250 mL). The combined organic layers were dried with magnesium

sulfate and concentrated *in vacuo*. The resulting oil was filtered on silica using an eluent of 50% ethyl acetate in hexanes. The resulting crude solid was recrystallized from an ethyl acetate / hexanes mixture to obtain compound **56** as an orange solid (39%). ^1H NMR (400 MHz, CDCl_3) δ 7.25 – 7.14 (m, 2H), 6.78 (t, $J = 7.3$ Hz, 1H), 6.67 (d, 2H), 4.79 (d, $J = 48.5$ Hz, 1H), 4.64 – 4.06 (m, 2H), 3.65 – 3.43 (m, 1H), 3.20 – 2.65 (m, 2H), 1.93 (dd, $J = 13.1, 2.8$ Hz, 1H), 1.84 – 1.58 (m, 2H), 1.54-1.24 (m, 10H); ^{13}C NMR (100 MHz, CDCl_3) δ 155.20, 146.12, 129.57, 118.35, 113.91, 87.12 (d, $J = 177.2$ Hz), 80.18, 77.48, 77.17, 76.85, 52.55 (d, $J = 19.5$ Hz), 47.72, 46.54, 43.15, 42.33, 28.45, 26.43; ^{19}F NMR (376 MHz, CDCl_3) δ -205.71; ATR-FTIR $\nu_{\text{max}}/\text{cm}^{-1}$: 3361, 2979, 2931, 1677, 1600, 1593; HRMS ($\text{C}_{16}\text{H}_{23}\text{N}_2\text{O}_2\text{F}$) : predicted mass = 295.1822 $[\text{M}+\text{H}]^+$ and 239.1196 $[\text{M} - \text{tBu}]^+$; experimental mass = 295.1819 $[\text{M}+\text{H}]^+$ (low abundance), 239.1198 $[\text{M} - \text{tBu}]^+$.

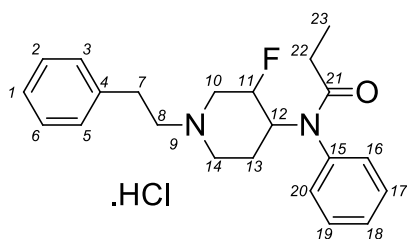
Synthesis of 3-fluoro-1-phenethyl-N-phenylpiperidin-4-amine (**57**)



Compound **56** (9.09 mmol) was dissolved in a 1:2 mixture of trifluoroacetic acid and dichloromethane (30 mL). The resulting solution was stirred for an hour at room temperature. The reaction mixture was then concentrated *in vacuo*, and the oil transferred to a separation funnel with methanol (80 mL). Water (80 mL), 5 M aqueous NaOH (16 mL) and brine (60 mL) were added and the resulting mixture was extracted twice with ethyl acetate (2 x 200 mL). The combined organic layers were dried over magnesium sulfate, filtered and concentrated *in vacuo*. The resulting oil was dissolved in THF (90 mL) and 2-fluorophenethyl bromide (27.1 mmol) and triethylamine (18.0 mmol) were added. The reaction mixture was heated to reflux for 5 h. The mixture was then cooled to room temperature and transferred

to a separation funnel with 200 mL ethyl acetate. The organic layer was washed with saturated aqueous sodium bicarbonate (2 x 100 mL). The organic layer was dried with magnesium sulfate and concentrated *in vacuo*. The crude product was purified using a Biotage Isolera One Flash Purification System. Compound **57** was obtained as an orange solid in 31% yield. ¹H NMR (400 MHz, CDCl₃) δ 7.37 – 7.06 (m, 7H), 6.78 – 6.56 (m, 3H), 4.81 (d, *J* = 49.0 Hz, 1H), 3.92 (d, *J* = 7.7 Hz, 1H), 3.38 (m, 2H), 3.05 (d, *J* = 11.5 Hz, 1H), 2.89 – 2.74 (m, 2H), 2.71 – 2.49 (m, 2H), 2.43-2.15 (m, 2H), 2.05 – 1.91 (m, 1H), 1.84 (qd, *J* = 12.3, 2.8 Hz, 1H), 1.72 (s (br), 1H); ¹³C NMR (100 MHz, CDCl₃) δ 146.42, 140.16, 129.45, 129.32, 128.73, 128.47, 126.16, 118.06, 113.82, 113.52, 88.09 (d, *J* = 176.2 Hz), 60.09, 56.22 (d, *J* = 19.0 Hz), 52.26 (d, *J* = 18.9 Hz), 51.98, 33.54, 27.03 (d, *J* = 2.1 Hz); ¹⁹F NMR (376 MHz, CDCl₃) δ -203.52; ATR-FTIR $\nu_{\text{max}}/\text{cm}^{-1}$: 3413, 3050, 2949, 2784, 1670, 1601, 1509; HRMS (C₁₉H₂₃N₂F) : predicted mass = 299.1924 [M+H]⁺; experimental mass = 299.1918 [M+H]⁺.

Synthesis of N-(3-fluoro-1-phenethylpiperidin-4-yl)-N-phenylpropionamide (3-Fluorofentanyl, 48)



Compound **57** was dissolved in dichloromethane (0.1 M) and treated with diisopropylamine (2 eq). The system was flushed with argon, the mixture cooled in an ice bath and propionyl chloride (2 eq) was added

dropwise. The resulting solution was stirred at ambient temperature for 2h. The mixture was diluted with water (50 mL) and the organic phase washed sequentially with brine (1 x 50 mL) and saturated aqueous sodium bicarbonate solution (1 x 50 mL), dried with magnesium sulfate and concentrated *in vacuo*.

The crude oils were purified by flash column chromatography (SiO₂, 3:7 – 7:3 v/v EtOAc-hexane) to obtain 3-fluorofentanyl free-base as an off-white solid (55%). 3-Fluorofentanyl free-base (0.36 mmol) was dissolved in acetone and an equimolar amount of hydrogen chloride (3 M in CPME) was added. The mixture was left to stand for 5-10 minutes and the salt isolated by filtration. The product was dried in an oven (60 °C, 12h) to give 3-fluorofentanyl (**48**) as a white powder (82% yield). ¹H NMR (400 MHz, DMSO-D₆) δ 10.05 (s(br), 1H, H9), 7.52-7.38 (m, 3H, H17-19), 7.38-7.15 (m, 7H, H1-3/H5-6/H16/H20), 5.35 (d, J = 47.6 Hz, 1H, H11), 4.81 (dd, J = 33.43 Hz, 10.1 Hz, 1H, H12), 3.83 (t, J = 11.4 Hz, 1H, H10a), 3.72-3.43 (m, 2H, H10b/H14a), 3.40 (s, H₂O), 3.35-3.13 (m, 3H, H8/H14b), 3.08-2.87 (m, 2H, H7), 1.94-1.75 (m, 3H, H22/H13a), 1.59 (qd, J = 12.8 Hz, 2.7 Hz, 1H, H13b), 0.90 (t, J = 7.3 Hz, 3H, H23); ¹³C NMR (100 MHz, DMSO-D₆) δ 173.00 (C21), 138.76 (C15), 136.97 (C4), 130.80, 130.75, 130.58, 129.32, 129.02, 128.72, 128.67 and 128.50 (C2-3/C5-6/C16-20), 126.83 (C1), 86.93 (d, J = 176.36 Hz, C11), 56.70 (C8), 53.18 (d, J = 20.1 Hz, C10), 51.55 (d, J = 17.3 Hz, C12), 50.53 (C14), 48.58, 29.22 (C7), 27.73 (C22), 22.31 (C13), 9.34 (C23); ¹⁹F NMR (376 MHz, DMSO-D₆) δ -199.434 (s); ATR-FTIR $\nu_{\text{max}}/\text{cm}^{-1}$: 3059 and 3044, 2989 and 2945, 2441, 1653 (C=O amide), 1569; HRMS (C₂₂H₂₇N₂OF): predicted mass = 355.218 [M+H]⁺, experimental mass = 355.2187.

7.12.3 Synthesis of additional compounds for the PCA model

General procedures for the synthesis of PCA model compounds

Method A – Reductive Amination [1]

The starting piperidone (4.9 mmol, 1.0 eq.) and aniline (5.4 mmol, 1.1 eq.) were added to dichloromethane (16 mL) and treated with acetic acid (4.9 mmol, 1.0 eq.). Sodium triacetoxyborohydride was added slowly to the mixture (4.9 mmol, 1.0 eq.). The system was flushed with argon and the resulting solution was stirred at room temperature for 24 h. At this point a second portion of sodium triacetoxyborohydride was added to the mixture (4.9 mmol, 1.0 eq.), which was then stirred for another 24 h. The reaction mixture was transferred to a separation funnel with saturated aqueous sodium bicarbonate (50 mL) and extracted twice with ethyl acetate (2 x 50 mL). The combined organic layers were dried over magnesium sulfate and concentrated *in vacuo*. The crude oil was purified using a Biotage Isolera One Flash Purification System

Method B – Boc-Deprotection and Alkylation [4, 185]

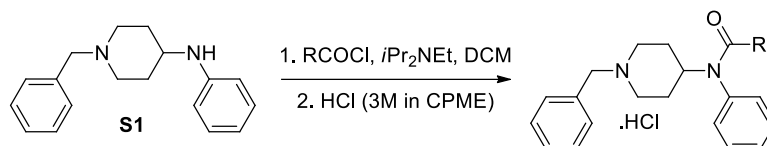
The starting Boc-protected piperidine (0.96 mmol, 1.0 eq.) was dissolved in a 1:2 mixture of trifluoroacetic acid and dichloromethane (3.2 mL). The resulting solution was stirred for an hour at room temperature. The reaction mixture was then cooled to 0 °C, quenched with 1M aqueous NaOH (5 mL) and transferred to a separatory funnel. The aqueous layer was removed, and the organic layer was washed successively with 1M aqueous NaOH (10 mL), saturated aqueous sodium bicarbonate (10 mL) and brine (10 mL). The organic layer was dried over magnesium sulfate, filtered and concentrated *in vacuo*. The resulting oil was dissolved in acetonitrile (4 mL) and phenethyl bromide (0.96 mmol, 1.0 eq.) and cesium carbonate (2.11 mmol, 2.2 eq.) were added. The reaction

mixture was heated to reflux for 5 h. The mixture was then cooled to room temperature and transferred to a separation funnel with 30 mL water. The aqueous layer was extracted three times with dichloromethane (2 x 30 mL). The combined organic layers were washed sequentially with brine (3 x 30 mL) and saturated aqueous sodium bicarbonate (2 x 30 mL). The combined organic layers were dried with magnesium sulfate and concentrated *in vacuo*. The crude product was purified using a Biotage Isolera One Flash Purification System

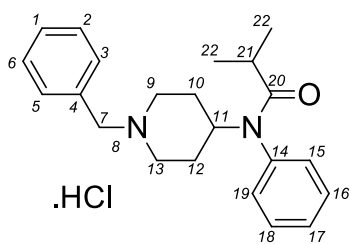
Method C – Acylation and HCl Salt Formation [4]

The starting amine (1.0 mmol, 1.0 eq.) was added to dichloromethane (10 mL) and was treated with diisopropylethylamine (2.0 mmol, 2.0 eq.). The system was flushed with argon, the mixture cooled in an ice bath and propionyl chloride (2.0 mmol, 2.0 eq.) added dropwise. The resulting solution was stirred at room temperature for 2 h. The mixture was diluted with water (30 mL) and the organic layer washed sequentially with brine (30 mL) and saturated aqueous sodium bicarbonate (30 mL). The organic layer was dried with magnesium sulfate and concentrated *in vacuo*. The free base was dissolved in acetone, and an equimolar amount of hydrogen chloride (3 M in cyclopentyl methyl ether (CPME)) added. The mixture was left to stand for 5-10 minutes and the salt isolated by filtration. The product was dried in an oven (60°C, 12 h) to give white – off-white powders.

Synthesis of *N*-benzyl fentanyl analogues **58-60**, **63**, **99**, **100-102**, **105**



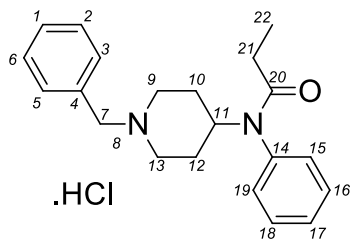
N-(1-Benzylpiperidin-4-yl)-*N*-phenylisobutyramide (Isobutyryl-*N*-benzylfentanyl, **58**)



Compound **58** was synthesised from **S1** using Method C (white solid, 83% yield). ¹H NMR (400 MHz, DMSO) δ 10.33 (s, 1H, H8), 7.61 – 7.33 (m, 8H, H1-2/6/15-19), 7.22 (d, *J* = 6.9 Hz, 2H, H3/5), 4.66 (tt, *J* = 16.5, 7.7 Hz, 1H, H11), 4.21 (d, *J* = 5.2

Hz, 2H, H7), 3.35 (s, H₂O), 3.27 (d, *J* = 11.6 Hz, 2H, H9a/H13a), 3.09 (q, *J* = 10.8 Hz, 2H, H9b/H13b), 2.21 – 2.03 (m, 1H, H21), 1.88 (d, *J* = 12.8 Hz, 2H, H10a/H12a), 1.61 (q, *J* = 12.0 Hz, 2H, H10b/H12b), 0.88 (d, *J* = 6.7 Hz, 6H, H22); ¹³C NMR (100 MHz, DMSO) δ 176.00 (C20), 138.49 (C14), 131.74, 130.63, 130.35, 129.95, 129.86, 129.17 and 129.02 (C1-6/15-19), 59.29 (C7), 51.12 and 49.46 (C9/11/13), 31.61 (C21), 27.47 (C10/12), 19.88 (C22); ATR-FTIR $\nu_{\text{max}}/\text{cm}^{-1}$: 3066, 2972, 2946, 2474, 2401, 1650, 1597, 1496; HRMS (C₂₂H₂₈N₂O) : predicted mass = 337.2280 [M+H]⁺; experimental mass = 337.2279 [M+H]⁺.

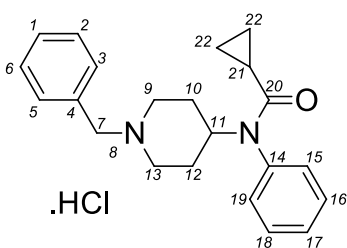
N-(1-Benzylpiperidin-4-yl)-*N*-phenylpropionamide (*N*-Benzylfentanyl, **59**)



Compound **59** was synthesised from **S1** using Method C (white solid, 55% yield). ¹H NMR (400 MHz, DMSO) δ 10.31 (s, 1H, H8), 7.60 – 7.32 (m, 8H, H1-2/6/15-19), 7.21 (d, *J* = 6.9 Hz, 2H, H3/5), 4.69 (t, *J* = 12.0 Hz, 1H, H11), 4.20 (d, *J* = 5.2 Hz, 1H, H7), 3.27 (d, *J* = 11.6 Hz, 2H, H9a/H13a),

3.10 (q, *J* = 10.6 Hz, 2H, H9b/H13b), 1.90 (d, *J* = 12.7 Hz, H10a/H12a), 1.82 (q, *J* = 7.3 Hz, 2H, H21), 1.62 (qd, *J* = 12.7, 2.7 Hz, 2H, H10b/H12b), 0.87 (t, *J* = 7.4 Hz, 2H, H22); ¹³C NMR (100 MHz, DMSO) δ 172.61 (C20), 138.57 (C14), 131.76, 130.80, 130.33, 129.93, 129.87, 129.17 and 128.95 (C1-6/15-19), 59.29 (C7), 51.11 and 49.50 (C9/11/13), 28.16, (C21), 27.49 (C10/12), 9.85 (C22); ATR-FTIR $\nu_{\text{max}}/\text{cm}^{-1}$: 3066, 2972, 2942, 2475, 2398, 1658, 1597. Spectral data are consistent with the literature. [185]

N-(1-Benzylpiperidin-4-yl)-*N*-phenylcyclopropanecarboxamide (Cyclopropyl-*N*-benzylfentanyl, **60**)

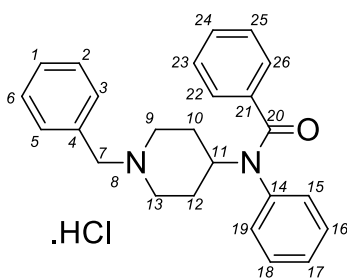


Compound **60** was synthesised from **S1** using Method C (white solid, 76% yield). ¹H NMR (400 MHz, DMSO) δ 10.47 (s, 1H, H8), 7.63 – 7.36 (m, 8H, H1-2/6/15-19), 7.25 (d, *J* = 7.2 Hz, 2H, H3/5), 4.67 (tt, *J* = 12.2, 8.7, 3.6 Hz, 1H, H11), 4.21 (d, *J* =

4.9 Hz, 2H, H7), 3.35 (s, H₂O), 3.26 (d, *J* = 11.7 Hz, 2H, H9a/H13a), 3.09 (q, *J* = 22.4, 10.8 Hz, 2H, H9b/H13b), 1.90 (d, *J* = 12.5 Hz, 2H, H10a/12a), 1.68 (qd, *J* = 12.6, 2.4 Hz, 2H, H10b/12b), 1.00 (s (br), 1H, H21), 0.82 – 0.69 (m, 2H, H22a), 0.66 – 0.46 (m, 2H, H22b); ¹³C NMR (100 MHz, DMSO) δ 172.47 (C20),

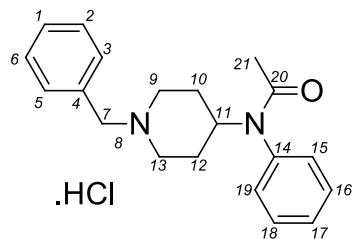
138.60 (C14), 131.77, 130.94, 130.36, 129.99, 129.84, 129.15 and 128.94 (C1-6/15-19), 59.24 (C7), 51.09 and 49.95 (C9/11/13), 27.49 (C10/12), 13.26 (C21), 8.44 (C22); ATR-FTIR $\nu_{\max}/\text{cm}^{-1}$: 3067, 3012, 2972, 2948, 2478, 1648, 1596, 1497; HRMS (C₂₂H₂₆N₂O) : predicted mass = 335.2123 [M+H]⁺; experimental mass = 335.2123 [M+H]⁺

N-(1-Benzylpiperidin-4-yl)-*N*-phenylbenzamide (Phenyl-*N*-benzylfentanyl, **63**)



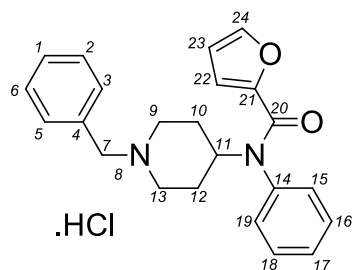
Compound **63** was synthesised from **S1** using Method C (white solid, 94% yield). ¹H NMR (400 MHz, DMSO) δ 10.37 (s, 1H, H8), 7.63 – 7.49 (m, 2H, H15/19), 7.49 – 7.36 (m, 3H, H16-18), 7.32 – 7.09 (m, 10H, H1-3/5-6/22-26), 4.78 (t, *J* = 11.5 Hz, 1H, H11), 4.24 (d, *J* = 5.2 Hz, 2H, H7), 3.38 – 3.21 (m, H₂O and H9a/13a), 3.16 (q, *J* = 11.4 Hz, 2H, H9b/13b), 2.08 (d, *J* = 12.7 Hz, 2H, H10a/12a), 1.81 (qd, *J* = 12.8, 9.7 Hz, 2H, H10b/12b); ¹³C NMR (100 MHz, DMSO) δ 170.32 (C20), 139.13 (C14), 137.29 (C21), 131.78, 131.27, 130.33, 129.90, 129.45, 129.26, 129.20, 128.25, 128.17 and 128.05 (C1-6/15-19/22-26), 59.35 (C7), 51.17 and 51.02 (C9/11/13), 27.44 (C10/12); ATR-FTIR $\nu_{\max}/\text{cm}^{-1}$: 3037, 2927, 2451, 2393, 1646, 1594. Spectral data are consistent with the literature. [186]

N-(1-Benzylpiperidin-4-yl)-*N*-phenylacetamide (Acetyl-*N*-benzylfentanyl, **99**)



Compound **99** was synthesised from **S1** using Method C (white solid, 66% yield). ¹H NMR (400 MHz, DMSO) δ 10.36 (s, 1H, H8), 7.60 – 7.33 (m, 8H, H1-2/6/15-19), 7.22 (d, J = 6.9 Hz, 2H, H3/5), 4.66 (tt, J = 12.1, 3.5 Hz, 1H, H11), 4.20 (d, J = 5.1 Hz, 2H, H7), 3.35 (H₂O), 3.27 (d, J = 11.7 Hz, 2H, H9a/13a), 3.09 (q, J = 10.6 Hz, 2H, H9b/13b), 1.90 (d, J = 12.7 Hz, 2H, H10a/12a), 1.78 – 1.45 (m, 5H, H10b/12b/21); ¹³C NMR (100 MHz, DMSO) δ 169.45 (C20), 139.10 (C14), 131.77, 130.63, 130.31, 129.94, 129.86, 129.16 and 128.97 (C1-6/15-19), 59.30 (C7), 51.08 and 49.49 (C9/11/13), 27.47 (C10/12), 23.56 (C22); ATR-FTIR $\nu_{\text{max}}/\text{cm}^{-1}$: 2989, 2969, 2945, 2627, 2476, 1657, 1509; HRMS (C₂₀H₂₄N₂O) : predicted mass = 309.1967 [M+H]⁺; experimental mass = 309.1964 [M+H]⁺.

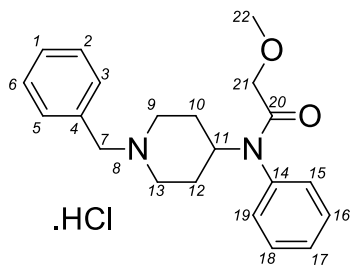
N-(1-Benzylpiperidin-4-yl)-*N*-phenylfuran-2-carboxamide (Furanyl-*N*-benzylfentanyl, **100**)



Compound **100** was synthesised from **S1** using Method C (white solid, 80% yield). ¹H NMR (400 MHz, DMSO) δ 10.56 (s, 1H, H8), 7.65 (d, J = 1.0 Hz, 1H, H24), 7.63 – 7.35 (m, 8H, H1-2/6/15-19), 7.26 (m, 2H, H3/5), 6.32 (dd, J = 3.5, 1.7 Hz, 1H, H23), 5.41 (d, J = 2.8 Hz, 1H, H22), 4.79 (tt, J = 12.1, 3.6 Hz, 1H, H11), 4.23 (d, J = 5.1 Hz, 2H, H7), 3.38 – 3.21 (m, H₂O and H9a/13a), 3.15 (q, J = 10.6 Hz, 2H, H9b/13b), 2.01 (d, J = 12.7 Hz, 2H, H10a/12a), 1.78 (q, J = 12.6 Hz, 2H, H10b/12b); ¹³C NMR (100 MHz, DMSO)

δ 158.44 (C20), 146.96 (C21), 145.64 (C24), 138.27 (C14), 131.80, 131.16, 130.33, 129.88, 129.49 and 129.17 (C1-6/15-19), 116.29 (C22), 111.69 (C23), 59.28 (C7), 51.01 and 50.75 (C9/11/13), 27.20 (C10/12); ATR-FTIR $\nu_{\max}/\text{cm}^{-1}$: 3138, 3119, 3042, 2974, 2949, 2468, 2397, 1634, 1595, 1558, 1497; HRMS ($\text{C}_{23}\text{H}_{24}\text{N}_2\text{O}_2$) : predicted mass = 361.1916 $[\text{M}+\text{H}]^+$; experimental mass = 361.1913 $[\text{M}+\text{H}]^+$.

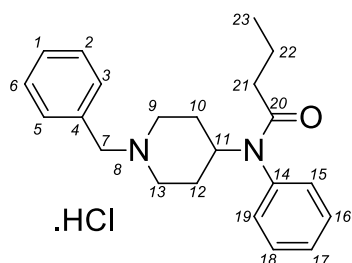
N-(1-Benzylpiperidin-4-yl)-2-methoxy-*N*-phenylacetamide (Methoxyacetyl-*N*-benzylfentanyl, **101**)



Compound **101** was synthesised from **S1** using Method C (white solid, 55% yield). ^1H NMR (400 MHz, DMSO) δ 10.27 (s, 1H, H8), 7.55 – 7.27 (m, 8H, H1-2/6/15-19), 7.21 (d, $J = 7.1$ Hz, 2H, H3/5), 4.63 (t, $J = 11.9$ Hz, 1H, H11), 4.16 (d, $J = 5.1$ Hz, 2H, H7), 3.51 (d, $J = 15.0$ Hz, 2H, H21), 3.33

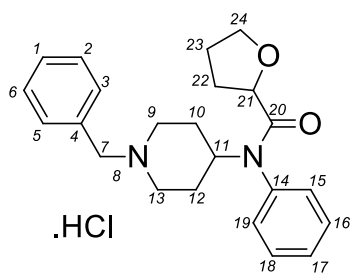
(H_2O), 3.23 (d, $J = 11.6$ Hz, 2H, H9a/13a), 3.15 – 2.91 (m, 5H, H9b/13b,22), 1.87 (d, $J = 12.9$ Hz, 2H, H10a/12a), 1.58 (q, $J = 12.5$ Hz, 2H, H10b/12b); ^{13}C NMR (100 MHz, DMSO) δ 168.47 (C20), 136.83 (C14), 131.82, 130.82, 130.36, 130.04, 129.93, 129.42 and 129.23 (C1-6/15-19), 70.65 (C21), 59.34 (C7), 58.79 (C22), 51.06 and 49.65 (C9/11/13), 27.29 (C10/12); ATR-FTIR $\nu_{\max}/\text{cm}^{-1}$: 3064, 2949, 2821, 2475, 1668, 1595; HRMS ($\text{C}_{21}\text{H}_{25}\text{N}_2\text{O}_2$) : predicted mass = 339.2073 $[\text{M}+\text{H}]^+$; experimental mass = 339.2068 $[\text{M}+\text{H}]^+$.

N-(1-Benzylpiperidin-4-yl)-*N*-phenylbutyramide (Butyryl-*N*-benzylfentanyl, **102**)



Compound **102** was synthesised from **S1** using Method C (white solid, 71% yield). ^1H NMR (400 MHz, DMSO) δ 10.40 (s, 1H, H8), 7.61 – 7.33 (m, 8H, H1-2/6/15-19), 7.19 (d, J = 6.9 Hz, 2H, H3/5), 4.68 (t, J = 12.1 Hz, 1H), 4.20 (d, J = 5.2 Hz, 2H, H7), 3.35 (H₂O), 3.26 (d, J = 11.6 Hz, H9a/13a), 3.09 (q, J = 10.6 Hz, 2H, H9b/13b), 1.89 (d, J = 12.8 Hz, 2H, H10a/12a), 1.79 (t, J = 7.3 Hz, 2H, H21), 1.63 (qd, J = 12.6, 2.7 Hz, 2H, H10b/12b), 1.42 (sext, J = 7.2 Hz, 2H, H22), 0.72 (t, J = 7.4 Hz, 3H, H23); ^{13}C NMR (100 MHz, DMSO) δ 171.74 (C20), 138.59 (C14), 131.76, 130.81, 130.35, 129.93, 129.85, 129.16 and 128.96 (C1-6/15-19), 59.27 (C7), 51.10 and 49.52 (C9/11/13), 36.62 (C21), 27.49 (C10/12), 18.60 (C22), 14.08 (C23); ATR-FTIR $\nu_{\text{max}}/\text{cm}^{-1}$: 3065, 2969, 2935, 2474, 1651, 1597; HRMS (C₂₂H₂₈N₂O) : predicted mass = 337.2280 [M+H]⁺; experimental mass = 337.2279 [M+H]⁺

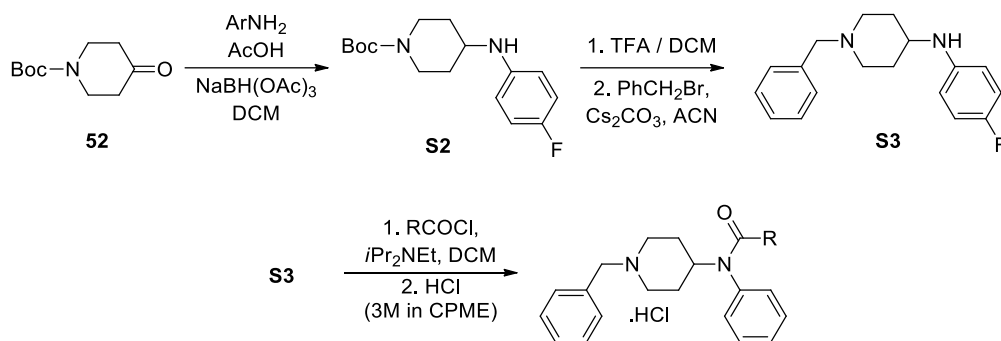
N-(1-Benzylpiperidin-4-yl)-*N*-phenyltetrahydrofuran-2-carboxamide (Tetrahydrofuranyl-*N*-benzylfentanyl, **105**)



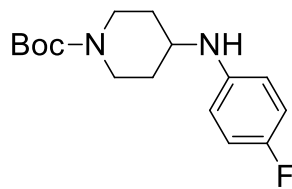
Compound **105** was synthesised from **S1** using Method C (white solid, 69% yield). ^1H NMR (400 MHz, DMSO) δ 10.30 (s, 1H, H8), 7.61 – 7.33 (m, 8H, H1-2/6/15-19), 7.23 (d, J = 6.4 Hz, 2H, H3/5), 4.64 (t, 1H, J = 12.2, 3.6 Hz, H11), 4.21 (d, J = 4.9 Hz, 2H, H7), 3.89 (m, 1H, H21), 3.78 (q, J = 7.6 Hz, 1H, H24a), 3.68 – 3.54 (m, 1H, H24b), 3.36 (H₂O), 3.27 (d, J = 10.9 Hz, 2H,

H9a/13a), 3.10 (q, $J = 22.2, 11.7$ Hz, 2H, H9b/13b), 2.04 – 1.70 (m, 4H, H10a/12a/22a/23b), 1.70 – 1.49 (m, $J = 11.7, 7.6$ Hz, 4H, H10b/12b/22b/23b); ^{13}C NMR (100 MHz, DMSO) δ 171.91 (C20), 137.41 (C14), 131.75, 131.03, 130.31, 129.88 and 129.18 (C1-6/15-19), 75.16 (C21), 69.08 (C24), 59.30 (C7), 51.08 and 49.85 (C9/11/13), 30.14 (C22), 27.33 (C10/12), 27.16 (C23), 25.87 (C23); ATR-FTIR $\nu_{\text{max}}/\text{cm}^{-1}$: 3063, 2946, 2878, 2478, 2399, 1661, 1596, 1497; HRMS ($\text{C}_{23}\text{H}_{28}\text{N}_2\text{O}_2$): predicted mass = 365.2229 $[\text{M}+\text{H}]^+$; experimental mass = 365.2225 $[\text{M}+\text{H}]^+$

Synthesis of *para*-Fluoro-*N*-benzyl fentanyl analogues **61-62, **64**, **98**, **104****



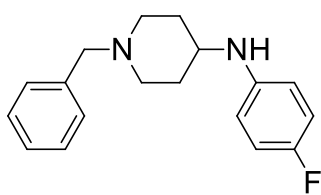
***tert*-Butyl 4-((4-fluorophenyl)amino)piperidine-1-carboxylate (**S2**)**



Compound **S2** was synthesised from **52** using Method A (off-white solid, 50% yield). ^1H NMR (400 MHz, CDCl_3) δ 7.01 – 6.81 (m, 2H), 6.66 – 6.46 (m, 2H), 4.04 (d, $J = 7.9$ Hz, 2H), 3.79 – 3.14 (m, 2H), 2.91 (t, $J = 11.9$ Hz, 2H), 2.13 – 1.90 (m, 2H), 1.67 (s (br), 1H), 1.46 (s, 9H), 1.44 – 1.17 (m, 2H); ^{13}C NMR (100 MHz, CDCl_3) δ 155.84 (d, $J = 235.3$ Hz), 154.80, 143.07 (d, $J = 1.9$ Hz), 115.79 (d, $J = 22.3$ Hz), 114.37 (d, $J = 7.4$ Hz), 79.65, 50.92, 42.59,

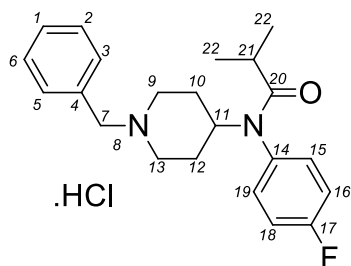
32.40, 28.44; ^{19}F NMR (376 MHz, CDCl_3) δ -114.43; ATR-FTIR $\nu_{\text{max}}/\text{cm}^{-1}$: 3358, 3043, 2981, 2944, 2922, 2885, 2847, 1672, 1611, 1529, 1505; HRMS ($\text{C}_{16}\text{H}_{23}\text{N}_2\text{O}_2\text{F}$) : predicted mass = 295.1822 $[\text{M}+\text{H}]^+$ and 239.1196 $[\text{M} - t\text{Bu}]^+$; experimental mass = 295.1816 $[\text{M}+\text{H}]^+$ (low abundance), 239.1192 $[\text{M} - t\text{Bu}]^+$.

1-Benzyl-*N*-(4-fluorophenyl)piperidin-4-amine (**S3**)



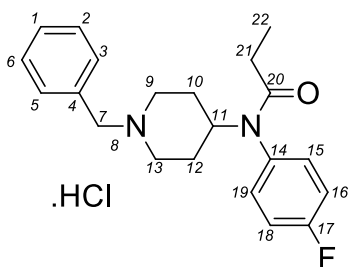
Compound **S3** was synthesised from **S2** using Method B (off-white solid, 42% yield). ^1H NMR (400 MHz, CDCl_3) δ 7.39 – 7.18 (m, 5H), 6.94 – 6.84 (m, 2H), 6.59 – 6.50 (m, 2H), 3.58 (s, 2H), 3.30 – 3.20 (m, 1H), 3.17-2.55 (s(br) and d, $J = 11.9$ Hz, 3H), 2.29 – 2.09 (m, 2H), 2.05 (d, $J = 12.4$ Hz, 2H), 1.51 (qd, $J = 13.7, 3.5$ Hz, 2H); ^{13}C NMR (100 MHz, CDCl_3) δ 155.70 (d, $J = 234.8$ Hz), 143.40 (d, $J = 1.8$ Hz), 137.81, 129.28, 128.29, 127.23, 121.75 (d, $J = 7.9$ Hz), 115.72 (d, $J = 22.4$ Hz), 114.26 (d, $J = 7.3$ Hz), 77.36, 77.04, 76.73, 63.02, 52.27, 50.62, 32.37, 24.45; ^{19}F NMR (376 MHz, CDCl_3) δ -128.3; ATR-FTIR $\nu_{\text{max}}/\text{cm}^{-1}$: 3373, 3291, 3028, 2938, 2815, 2773, 1662, 1612, 1557, 1506; HRMS ($\text{C}_{18}\text{H}_{21}\text{N}_2\text{F}$) : predicted mass = 285.1767 $[\text{M}+\text{H}]^+$; experimental mass = 285.1764 $[\text{M}+\text{H}]^+$.

N-(1-Benzylpiperidin-4-yl)-*N*-(4-fluorophenyl)isobutyramide (*para*-Fluoro-isobutyryl-*N*-benzylfentanyl, **61**)



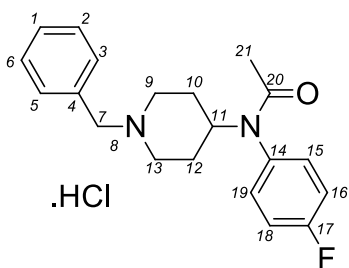
Compound **61** was synthesised from **S3** using Method C (white solid, 12% yield). ¹H NMR (400 MHz, DMSO) δ 9.90 (s, 1H, H8), 7.59 – 7.37 (m, 5H, H1-3/5-6), 7.38 – 7.20 (m, 4H, H15-16/18-19), 4.67 (t, *J* = 12.1 Hz, 1H, H11), 4.21 (d, *J* = 5.3 Hz, 2H, H7), 3.37 – 3.17 (m, H₂O and H9a/13a), 3.10 (q, *J* = 10.9 Hz, 2H, H9b/13b), 2.12 (sept, *J* = 6.2 Hz, 1H, H21), 1.89 (d, *J* = 13.3 Hz, 2H, H10a/12a), 1.71 – 1.39 (m, 2H, H10b/12b), 0.89 (d, *J* = 6.7 Hz, 6H, H22); ¹³C NMR (100 MHz, DMSO) δ 176.10 (C20), 162.18 (d, *J* = 245.8 Hz, C17), 134.77 (C14), 132.80 (d, *J* = 8.8 Hz, C15/19), 131.83, 130.48, 129.84 and 129.19 (C1-6), 116.77 (d, *J* = 22.6 Hz, C16/18), 59.17 (C7), 51.01 and 49.51 (C9/11/13), 31.64 (C21), 27.33 (C10/12), 19.89 (C22); ¹⁹F NMR (376 MHz, DMSO) δ -114.76; ATR-FTIR $\nu_{\text{max}}/\text{cm}^{-1}$: 2972, 2936, 2874, 2460, 1650, 1508; HRMS (C₂₂H₂₇N₂OF) : predicted mass = 355.2186 [M+H]⁺; experimental mass = 355.2186 [M+H]⁺.

N-(1-Benzylpiperidin-4-yl)-*N*-(4-fluorophenyl)propionamide (*para*-Fluoro-*N*-benzylfentanyl, **62**)



Compound **62** was synthesised from **S3** using Method C (white solid, 9% yield). ¹H NMR (400 MHz, DMSO) δ 9.75 (s, 1H, H8), 7.57 – 7.39 (m, 5H, H1-3/5-6), 7.39 – 7.17 (m, *J* = 9.0 Hz, 4H, H15-16/18-19), 4.69 (t, *J* = 12.2 Hz, 1H, H11), 4.21 (d, *J* = 5.3 Hz, 2H, H7), 3.35 – 3.24 (m, H₂O and H9a/13a), 3.11 (q, *J* = 10.5 Hz, 2H, H9b/13b), 1.90 (d, *J* = 12.6 Hz, 2H, H10a/12a), 1.83 (q, *J* = 7.4 Hz, 2H, H21), 1.54 (qd, *J* = 12.4, 2.8 Hz, 2H, H10b/12b), 0.88 (t, *J* = 7.4 Hz, 3H, H22); ¹³C NMR (100 MHz, DMSO) δ 172.21 (C20), 161.65 (d, *J* = 245.4 Hz, C17), 134.35 (d, *J* = 2.9 Hz, C14), 132.49 (d, *J* = 8.6 Hz, C15/19), 131.30, 129.89, 129.38 and 128.70 (C1-6), 116.22 (d, *J* = 23.0 Hz, C16/18), 58.75 (C7), 50.56 and 48.93 (C9/11/13), 27.71 (C10/12), 26.85 (C21), 9.32 (C22); ¹⁹F NMR (376 MHz, DMSO) δ -115.13; ATR-FTIR $\nu_{\text{max}}/\text{cm}^{-1}$: 3072, 2992, 2946, 2476, 2399, 1661, 1509; HRMS (C₂₁H₂₅N₂OF) : predicted mass = 341.2029 [M+H]⁺; experimental mass = 341.2024 [M+H]⁺.

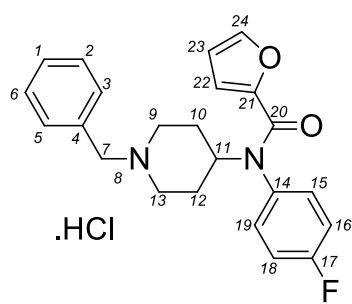
N-(1-Benzylpiperidin-4-yl)-*N*-(4-fluorophenyl)acetamide (*para*-Fluoro-acetyl-*N*-benzylfentanyl, **64**)



Compound **64** was synthesised from **S3** using Method C (white solid, 5% yield). ¹H NMR (400 MHz, DMSO) δ 10.46 (s, 1H, H8), 7.61 – 7.49 (m, 2H, H2/6), 7.49 – 7.41 (m, *J* = 3.8 Hz, 3H, H1/3/5), 7.41 – 7.19 (m, 4H, H15-16/18-19), 4.66 (tt, *J* = 12.2, 3.6 Hz, 1H, H11), 4.20 (d, *J* = 5.3 Hz, 2H,

H7), 3.36 (H₂O), 3.27 (d, $J = 11.5$ Hz, 2H, H_{9a}/13a), 3.10 (q, 2H, $J = 11.8$ Hz, H_{9b}/13b), 1.90 (d, 2H, H_{10a}/12a), 1.78 – 1.49 (m, 5H, H_{10b}/12b/21); ¹³C NMR (100 MHz, DMSO) δ 169.64 (C₂₀), 162.17 (d, $J = 245.3$ Hz, C₁₇), 135.39 (d, $J = 2.9$ Hz, C₁₄), 132.9 (d, $J = 8.8$ Hz, C₁₅/19), 131.80, 130.34, 129.95 and 129.25 (C₁₋₆), 116.77 (d, $J = 22.9$ Hz, C₁₆/18), 59.35 (C₇), 51.11 and 49.36 (C₉/11/13), 27.37 (C₁₀/12), 23.66 (C₂₁); ¹⁹F NMR (376 MHz, DMSO) δ - 115.01; ATR-FTIR $\nu_{\max}/\text{cm}^{-1}$: 3437, 2967, 2945, 2628, 2484, 1626, 1596; HRMS (C₂₀H₂₃N₂OF) : predicted mass = 327.1873 [M+H]⁺; experimental mass = 327.1869 [M+H]⁺.

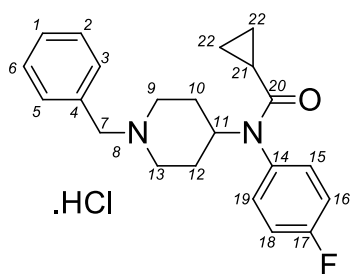
N-(1-Benzylpiperidin-4-yl)-*N*-(4-fluorophenyl)furan-2-carboxamide (*para*-Fluoro-*N*-benzylfuranlylfentanyl, **98**)



Compound **98** was synthesised from **S3** using Method C (white solid, 22% yield). ¹H NMR (400 MHz, DMSO) δ 10.16 (s, 1H, H₈), 7.65 (d, $J = 1.1$ Hz, 1H, H₂₄), 7.56-7.36 (m, 5H, H₁₋₃/5-6), 7.37 – 7.25 (m, 4H, H₁₅₋₁₆/18-19), 6.37 (dd, $J = 3.5, 1.7$ Hz, 1H, H₂₃), 5.65 (s, 1H, H₂₂), 4.78 (tt, $J = 12.1, 3.5$ Hz, 1H, H₁₁), 4.22 (d, $J = 5.0$ Hz, 2H, H₇), 3.33 (H₂O), 3.15 (q, $J = 11.7$ Hz, 2H, H_{9b}/H_{13b}), 2.01 (d, $J = 12.9$ Hz, 2H, H_{10a}/12a), 1.73 (q, $J = 12.6$ Hz, 2H, H_{10b}/12b); ¹³C NMR (100 MHz, DMSO) δ 162.46 (d, $J = 246.0$ Hz, C₁₇), 158.51 (C₂₀), 147.00 (C₂₁), 145.81 (C₂₄), 134.58 (d, $J = 2.3$ Hz, C₁₄), 133.33 (d, $J = 8.8$ Hz, C₁₅/19), 131.89, 130.44, 129.86 and 129.19 (C₁₋₆), 116.75 (d, $J = 21.5$ Hz, C₁₆/18), 116.64 (C₂₂), 111.86 (C₂₃), 59.18 (C₇), 53.66, 50.92 and 50.77 (C₉/11/13), 41.96, 27.08 (C₁₀/12), 18.43, 17.20, 12.60; ¹⁹F NMR (376 MHz, DMSO) δ -113.99; ATR-FTIR $\nu_{\max}/\text{cm}^{-1}$: 3127, 2972, 2949, 2475,

2398, 1634, 1559, 1508; HRMS (C₂₃H₂₃N₂O₂F) : predicted mass = 379.1822 [M+H]⁺; experimental mass = 379.1819 [M+H]⁺.

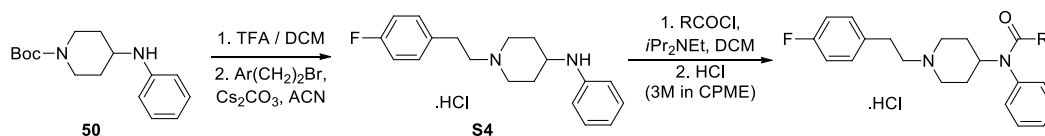
N-(1-Benzylpiperidin-4-yl)-*N*-(4-fluorophenyl)cyclopropanecarboxamide (*para*-Fluoro-*N*-benzylcyclopropylfentanyl, **104**)



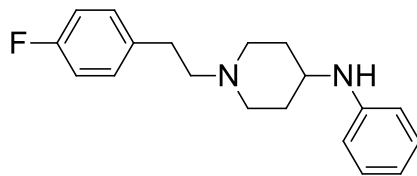
Compound **104** was synthesised from **S3** using Method C (white solid, 33% yield). ¹H NMR (400 MHz, DMSO) δ 10.24 (s, 1H, H8), 7.60 – 7.39 (m, *J* = 5H, H1-3/5-6), 7.39 – 7.24 (m, 4H, H15-16/18-19), 4.66 (tt, *J* = 12.2, 3.5 Hz, 1H, H11), 4.20 (d, *J* = 5.1 Hz, 2H, H7), 3.34 (H₂O), 3.27 (d, *J* = 11.6 Hz, 2H,

H9a/13a), 3.08 (q, *J* = 10.8 Hz, 2H, H9b/13b), 1.90 (d, *J* = 12.5 Hz, 2H, H10a/12a), 1.64 (q, *J* = 12.4 Hz, 2H, H10b/12b), 1.19 – 0.83 (m, *J* = 3.9 Hz, 1H, H21), 0.83 – 0.69 (m, 2H, H22a), 0.57 (m, 2H, H22b); ¹³C NMR (100 MHz, DMSO) δ 172.58 (C20), 162.15 (d, *J* = 245.3 Hz, C17), 134.90 (C14), 133.11 (d, *J* = 8.8 Hz, C15/19), 131.86, 130.47, 129.85 and 129.18 (C1-6), 116.83 (d, *J* = 22.6 Hz, C16/18), 59.14 (C7), 53.66, 50.99 and 49.92 (C9/11/13)), 41.96, 27.33 (C10/12), 18.43, 17.20, 13.32 (C21), 12.61, 8.55 (C22); ¹⁹F NMR (376 MHz, DMSO) δ -115.13; ATR-FTIR ν_{max}/cm⁻¹: 3070, 2947, 2624, 2478, 1652, 1508; HRMS (C₂₂H₂₅N₂O₂F) : predicted mass = 353.2029 [M+H]⁺; experimental mass = 353.2026 [M+H]⁺.

Synthesis of 4'-fluoro fentanyl analogues 77, 80-81, 117, 127



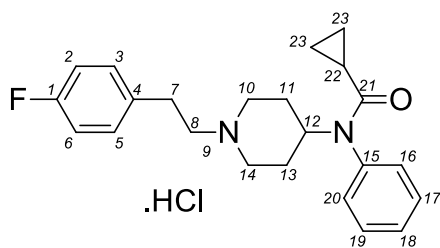
1-(4-Fluorophenethyl)-*N*-phenylpiperidin-4-amine (**S4**)



Compound **S4** was synthesised from **50** using Method B (grey solid, 74% yield). ¹H NMR (400 MHz, CDCl₃) δ 7.26 – 7.11 (m, 4H), 7.11 – 6.93 (m, 2H), 6.71 (t, *J* = 7.3 Hz, 1H), 6.63 (m, 2H),

3.55 (s(br), 1H), 3.35 (m, 1H), 2.98 (m, 2H), 2.90 – 2.71 (m, 2H), 2.67 – 2.57 (m, 2H), 2.34 – 2.19 (t, *J* = 11.3 Hz, 2H), 2.19 – 2.01 (m, 2H), 1.55 (qd, *J* = 12.5, 2.5 Hz, 2H); ¹³C NMR (100 MHz, CDCl₃) δ 161.43 (d, *J* = 243.7 Hz), 147.05, 130.04 (d, *J* = 7.8 Hz), 129.35, 117.30, 115.17 (d, *J* = 21.1 Hz), 113.28, 60.58, 52.47, 49.85, 33.00, 32.48; ¹⁹F NMR (376 MHz, CDCl₃) δ -116.03; ATR-FTIR $\nu_{\text{max}}/\text{cm}^{-1}$: 3399, 3048, 2944, 2922, 2856, 2802, 2767, 1687, 1600, 1507; HRMS (C₁₉H₂₃N₂F) : predicted mass = 299.1924 [M+H]⁺; experimental mass = 299.1920 [M+H]⁺

N-(1-(4-Fluorophenethyl)piperidin-4-yl)-*N*-phenylcyclopropanecarboxamide (4'-Fluorocyclopropylfentanyl, **77**)

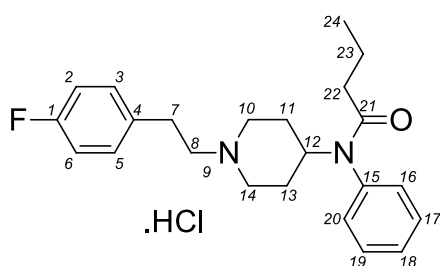


Compound **77** was synthesised from **S4** using Method C (white solid, 28% yield). ¹H NMR (400 MHz, DMSO) δ 10.18 (s, 1H, H9), 7.59 – 7.42 (m, 3H, H17-19), 7.36 – 7.23 (m, 4H, H3/5/16/20), 7.22 – 7.06 (m, 2H, H2/6),

4.71 (tt, *J* = 12.2, 3.6 Hz, 1H, H12), 3.52 (d, *J* = 11.6 Hz, 2H, H10a/14a), 3.33 (H₂O), 3.28 – 3.03 (m, H8/10b/14b), 3.03 – 2.88 (m, 2H, H7) 1.95 (d, *J* = 13.0 Hz, 2H, H11a/13a), 1.66 (qd, *J* = 12.8, 2.9 Hz, 2H, H11b/13b), 1.02 (s, 1H, H22), 0.82 – 0.70 (m, 2H, H23a), 0.64 – 0.47 (m, 2H, H23b); ¹³C NMR (100 MHz, DMSO) δ 172.56 (C21), 161.65 (d, *J* = 242.6 Hz, C1), 138.66 (C15),

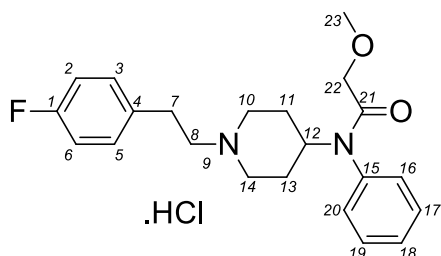
133.76 (C4), 131.11 (d, $J = 6.5$ Hz, C3/5), 131.08, 130.11 and 129.07 (C16-20), 115.91 (d, $J = 21.1$ Hz, C2/6), 56.89 (C8), 51.47 (C10/14), 49.85 (C12), 29.09 (C7), 27.79 (C11/13), 13.35 (C22), 8.54 (C23); ^{19}F NMR (376 MHz, DMSO) δ -117.50; ATR-FTIR $\nu_{\text{max}}/\text{cm}^{-1}$: 3016, 2930, 2627, 2589, 2532, 2474, 1651, 1594, 1514, 1494; HRMS ($\text{C}_{23}\text{H}_{27}\text{N}_2\text{OF}$) : predicted mass = 367.2186 $[\text{M}+\text{H}]^+$; experimental mass = 367.2184 $[\text{M}+\text{H}]^+$.

N-(1-(4-Fluorophenethyl)piperidin-4-yl)-*N*-phenylbutyramide (4'-Fluorobutyrylfentanyl, **80**)



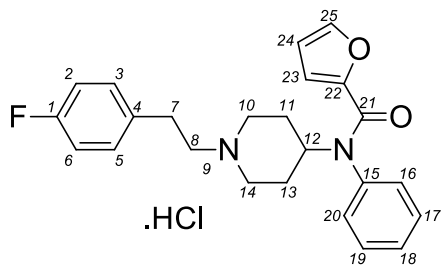
Compound **80** was synthesised from **S4** using Method C (white solid, 24% yield). ^1H NMR (400 MHz, DMSO) δ 10.23 (s, 1H, H9), 7.57 – 7.38 (m, 3H, H17-19), 7.33 – 7.19 (m, 4H, H3/5/16/20), 7.19 – 7.05 (m, 2H, H2/6), 4.73 (tt, 1H, H12), 3.52 (d, $J = 11.6$ Hz, 2H, H10a/14a), 3.34 (H_2O), 3.28 – 3.04 (m, 4H, H8/10b/14b), 3.04 – 2.90 (m, 2H, H7), 1.94 (d, $J = 13.0$ Hz, 2H, H11a/13a), 1.81 (t, $J = 7.3$ Hz, 2H, H22), 1.62 (qd, $J = 12.7, 10.1$ Hz, 2H, H11b/13b), 1.44 (sext, 2H, H23), 0.73 (t, $J = 7.4$ Hz, 3H, H24); ^{13}C NMR (100 MHz, DMSO) δ 171.82 (C21), 161.65 (d, $J = 242.7$ Hz, C1), 138.65 (C15), 133.74 (C4), 131.10 (d, $J = 8.1$ Hz, C3-5), 130.93, 130.04 and 129.08 (C16-20), 115.91 (d, $J = 21.2$ Hz, C2-6), 56.90 (C8), 51.47 (C10/14), 49.44 (C12), 36.71 (C22), 29.10 (C7), 27.80 (C11/13), 18.67 (C23), 14.15 (C24); ^{19}F NMR (376 MHz, DMSO) δ -117.49; ATR-FTIR $\nu_{\text{max}}/\text{cm}^{-1}$: 2965, 2933, 2877, 2627, 2590, 2534, 2474, 1657, 1594, 1514; HRMS ($\text{C}_{23}\text{H}_{29}\text{N}_2\text{OF}$) : predicted mass = 369.2342 $[\text{M}+\text{H}]^+$; experimental mass = 369.2341 $[\text{M}+\text{H}]^+$.

N-(1-(4-Fluorophenethyl)piperidin-4-yl)-2-methoxy-*N*-phenylacetamide (4'-Fluoromethoxyacetylfentanyl, **81**)



Compound **81** was synthesised from **S4** using Method C (white solid, 28% yield). ¹H NMR (400 MHz, DMSO) δ 10.02 (s, 1H, H₉), 7.58 – 7.37 (m, 3H, H₁₇₋₁₉), 7.28 (m, 4H, H_{3/H5/H16/H20}), 7.15 (t, *J* = 8.8 Hz, 2H, H_{2/6}), 4.70 (t, *J* = 11.2 Hz, 1H, H₁₂), 3.62 – 3.45 (m, *J* = 15.9 Hz, 4H H_{10a/14a/22}), 3.31 (H₂O), 3.23 – 3.03 (m, 7H, H_{8/10b/14b/23}), 3.03 – 2.81 (m, *J* = 8.1 Hz, 2H, H₇), 1.96 (d, *J* = 12.1 Hz, 2H, H_{11a/13a}), 1.61 (q, *J* = 11.9 Hz, 2H, H_{11b/13b}); ¹³C NMR (100 MHz, DMSO) δ 168.49 (C₂₁), 161.66 (d, *J* = 242.7 Hz, C₁), 136.87 (C₁₅), 133.70 (C₄), 131.11 (d, *J* = 8.0 Hz, C_{3/5}), 130.89, 130.09 and 129.48 (C₁₆₋₂₀), 115.92 (d, *J* = 21.1 Hz, C₂₋₆), 70.67 (C₂₂), 58.80 (C₂₃), 56.91 (C₈), 51.42 (C_{10/14}), 49.54 (C₁₂), 29.11 (C₇), 27.55 (C_{11/13}); ATR-FTIR $\nu_{\text{max}}/\text{cm}^{-1}$: 2930, 2823, 2466, 1669, 1598, 1508, 1494; HRMS (C₂₂H₂₇N₂O₂F) : predicted mass = 371.2135 [M+H]⁺; experimental mass = 371.2133 [M+H]⁺.

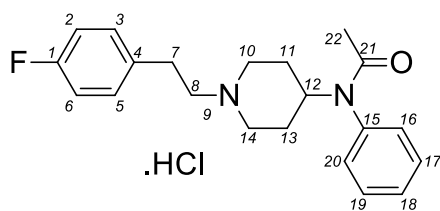
N-(1-(4-Fluorophenethyl)piperidin-4-yl)-*N*-phenylfuran-2-carboxamide (4'-Fluorofuranylfentanyl, **117**)



Compound **117** was synthesised from **S4** using Method C (white solid, 6% yield). ¹H NMR (400 MHz, DMSO) δ 10.09 (s, 1H, H₉), 7.66 (d, *J* = 1.1 Hz, 1H, H₂₅), 7.56 – 7.43 (m, 3H, H₁₇₋₁₉), 7.39 – 7.23 (m, 4H, H_{3/H5/H16/H20}), 7.16 (t, *J* = 8.8 Hz, 2H,

H2/6), 6.33 (dd, $J = 3.5, 1.7$ Hz, 1H, H24), 5.44 (d, $J = 3.0$ Hz, 1H, H23), 4.83 (t, $J = 11.4$ Hz, 1H, H12), 3.56 (d, $J = 10.0$ Hz, 2H, H10a/14a), 3.34 (H₂O), 3.26 – 3.07 (m, 4H, H8/H10b/H14b), 3.07 – 2.81 (m, 2H, H7), 2.07 (d, 2H, $J = 13.0$ Hz, H11a/H13a), 1.74 (q, $J = 12.2$ Hz, 2H, H11b/13b); ¹³C NMR (100 MHz, DMSO) δ 161.67 (d, $J = 242.6$ Hz, C1), 158.48 (C21), 146.99 (C22), 145.76 (C25), 138.35 (C15), 133.67 (C4), 131.35 (C16-20), 131.13 (d, $J = 8.2$ Hz, C3-5), 130.01 and 129.63 (C16-20), 116.41 (C23), 115.93 (d, $J = 21.2$ Hz, C2/6), 111.79 (C23), 56.94 (C8), 51.49 (C10/14), 50.57 (C12), 29.14 (C7), 27.50 (C11/13); ¹⁹F NMR (376 MHz, DMSO) δ -117.47; ATR-FTIR $\nu_{\text{max}}/\text{cm}^{-1}$: 3064, 2932, 2628, 2590, 2535, 2472, 1646, 1595, 1559, 1512, 1496; HRMS (C₂₄H₂₅N₂O₂F) : predicted mass = 393.1978 [M+H]⁺; experimental mass = 393.1976 [M+H]⁺.

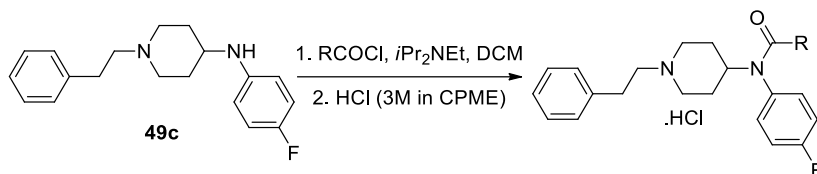
N-(1-(4-Fluorophenethyl)piperidin-4-yl)-*N*-phenylacetamide (4'-Fluoroacetyl)fentanyl, **127**)



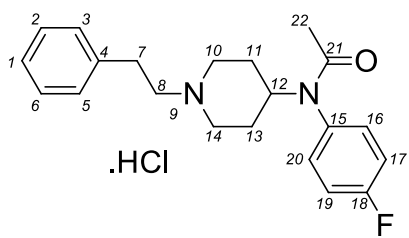
Compound **127** was synthesised from **S4** using Method C (white solid, 49% yield). ¹H NMR (400 MHz, DMSO) δ 10.14 (s, 1H, H9), 7.57 – 7.37 (m, 3H, H17-19), 7.34 – 7.20 (m, 4H, H3/5/16/20), 7.20 – 7.10 (m, 2H, H2/6), 4.71 (t, $J = 12.1$ Hz, 1H, H12), 3.52 (d, $J = 11.7$ Hz, 2H, H10a/14a), 3.33 (H₂O), 3.24 – 3.02 (m, 4H, H8/10b/14b), 3.03 – 2.87 (m, 2H, H7), 1.95 (d, $J = 12.8$ Hz, 2H, H11a/13a), 1.73 – 1.44 (m, 5H, H11b/13b/22); ¹³C NMR (100 MHz, DMSO) δ 169.55 (C21), 161.65 (d, $J = 242.3$ Hz, C1), 139.17 (C15), 133.72 (C4), 131.11 (d, $J = 7.9$ Hz, C3/5), 130.76, 130.05 and 129.09 (C16-20), 115.91 (d, $J = 21.1$ Hz, C2-6), 56.92 (C8), 51.47 (C10/14), 49.39 (C12), 29.10 (C7), 27.78 (C11/13), 23.66 (C22); ¹⁹F NMR (376 MHz, DMSO) δ -117.58; ATR-FTIR

$\nu_{\max}/\text{cm}^{-1}$: 3005, 2984, 2931, 2628, 2591, 2534, 2477, 1654, 1592, 1514, 1493;
 HRMS ($\text{C}_{21}\text{H}_{25}\text{N}_2\text{OF}$): predicted mass = 341.2029 $[\text{M}+\text{H}]^+$; experimental mass
 = 341.2026 $[\text{M}+\text{H}]^+$.

Synthesis of *para*-fluoro fentanyl analogues **85-86, **132-133**, **145****

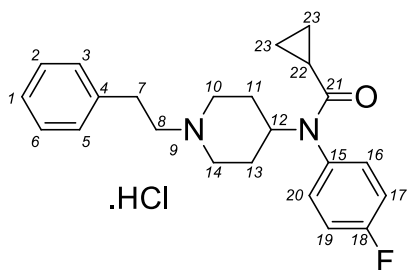


N-(4-Fluorophenyl)-*N*-(1-phenethylpiperidin-4-yl)acetamide (*para*-
 Fluoroacetylfentanyl, **85**)



Compound **85** was synthesised from **49c** using Method C (white solid, 44% yield). ^1H NMR (400 MHz, DMSO) δ 10.34 (s, 1H, H9), 7.46 – 7.28 (m, 6H, H2/6/16-17/18-19), 7.28 – 7.18 (m, 3H, H1/3/5), 4.69 (tt, J = 12.1, 3.5 Hz, 1H, H12), 3.53 (d, J = 11.6 Hz, 2H, H10a/14a), 3.34 (H₂O), 3.33 – 3.05 (m, 4H, H8/10b/14b), 3.05 – 2.89 (m, 2H, H7), 1.93 (d, J = 12.8 Hz, 2H, H11a/13a), 1.69 – 1.47 (m, 5H, H11b/13b/22); ^{13}C NMR (100 MHz, DMSO) δ 169.65 (C21), 162.19 (d, J = 247.0 Hz, C18), 137.66 (C4), 135.45 (C15), 132.89 (d, J = 8.5 Hz, C16/20), 129.17 and 127.29 (C1-3/5-6), 116.79 (d, J = 22.5 Hz, C17/19), 56.90 (C8), 51.32 (C10/14), 49.43 (C12), 29.90 (C7), 27.63 (C11/13), 23.68 (C22); ^{19}F NMR (376 MHz, DMSO) δ -114.92; ATR-FTIR $\nu_{\max}/\text{cm}^{-1}$: 3062, 3030, 3004, 2930, 2628, 2589, 2538, 2475, 1653, 1598, 1506; HRMS ($\text{C}_{21}\text{H}_{25}\text{N}_2\text{OF}$): predicted mass = 341.2029 $[\text{M}+\text{H}]^+$; experimental mass = 341.2026 $[\text{M}+\text{H}]^+$.

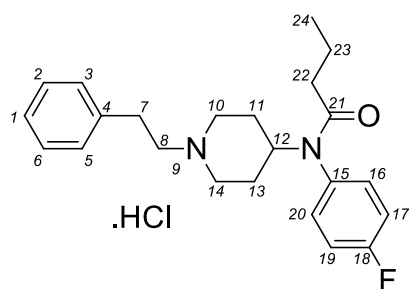
N-(4-Fluorophenyl)-*N*-(1-phenethylpiperidin-4-yl)cyclopropanecarboxamide
(*para*-Fluorocyclopropylfentanyl, **86**)



Compound **86** was synthesised from **49c** using Method C (white solid, 19% yield). ^1H NMR (400 MHz, DMSO) δ 10.27 (s, 1H, H9), 7.42 – 7.28 (m, 6H, H2/6/16-17/18-19), 7.28 – 7.18 (m, 3H, H1/3/5), 4.70 (tt, J = 12.2, 3.6 Hz, 1H, H12), 3.54 (d, J = 11.7 Hz, 2H, H10a/14a), 3.34 (H₂O), 3.27

– 3.04 (m, 4H, H8/10b/14b), 3.03-2.94 (m, 2H, H7), 1.95 (d, J = 12.6 Hz, 2H, H11a/13a), 1.66 (q, J = 12.6 Hz, 2H, H11b/13b), 1.21 – 0.85 (m, 1H, H22), 0.84 – 0.70 (m, 2H, H23a), 0.67 – 0.46 (m, J = 7.4, 3.3 Hz, 2H, H23b); ^{13}C NMR (100 MHz, DMSO) δ 172.63 (C21), 162.21 (d, J = 245.7 Hz, C18), 137.60 (C4), 134.94 (C15), 133.20 (d, J = 9.0 Hz, C3/5), 129.17 (C2-3/C5-6), 127.31 (C1), 116.89 (d, J = 22.3 Hz, C17/19), 56.88 (C8), 51.40 (C10/14), 49.79 (C12), 29.94 (C7), 27.64 (C11/13), 13.37 (C22), 8.57 (C23); ^{19}F NMR (376 MHz, DMSO) δ -115.01; ATR-FTIR $\nu_{\text{max}}/\text{cm}^{-1}$: 3063, 3029, 2929, 2627, 2587, 2527, 2488, 2470, 1649, 1601, 1507; HRMS (C₂₃H₂₇N₂OF) : predicted mass = 367.2186 [M+H]⁺; experimental mass = 367.2185 [M+H]⁺.

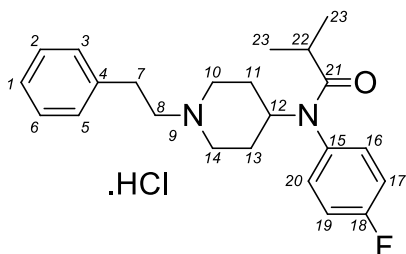
N-(4-Fluorophenyl)-*N*-(1-phenethylpiperidin-4-yl)butyramide
(*para*-Fluorobutyrylfentanyl, **132**)



Compound **132** was synthesised from **49c** using Method C (white solid, 25% yield). ^1H NMR (400 MHz, DMSO) δ 10.21 (s, 1H, H9), 7.43 – 7.28 (m, 6H, H2/6/16-17/18-19), 7.28 – 7.18 (m, 3H, H1/3/5), 4.71 (tt, J = 12.0, 3.5 Hz,

1H, H12), 3.53 (d, $J = 11.6$ Hz, 2H, H10a/14a), 3.33 (H₂O), 3.26 – 3.03 (m, 4H, H8/10b/14b), 3.03 – 2.80 (m, $J = 10.6, 6.1$ Hz, 2H, H7), 1.93 (d, $J = 12.8$ Hz, 2H, H11a/13a), 1.81 (t, $J = 7.4$ Hz, 2H, H22), 1.61 (q, $J = 12.0$ Hz, 2H, H11b/13b), 1.40 (sext, $J = 7.3$ Hz, 2H, H23), 0.75 (t, $J = 7.4$ Hz, 3H, H24); ¹³C NMR (100 MHz, DMSO) δ 171.91 (C21), 162.19 (d, $J = 246.7$ Hz, C18), 137.57 (C4), 134.93 (C15), 133.08 (d, $J = 8.0$ Hz, C16-20), 129.18 (C2-3/C5-6), 127.32 (C1), 116.81 (d, $J = 22.4$ Hz, C17-19), 56.90 (C8), 51.42 (C10/14), 49.36 (C12), 36.71 (C22), 29.95 (C7), 27.67 (C22), 18.61 (C23), 14.15 (C24); ¹⁹F NMR (376 MHz, DMSO) δ -115.04; ATR-FTIR $\nu_{\text{max}}/\text{cm}^{-1}$: 3057, 2974, 2931, 2886, 2626, 2587, 2524, 2487, 2468, 1653, 1601, 1509; HRMS (C₂₃H₂₉N₂OF) : predicted mass = 369.2342 [M+H]⁺; experimental mass = 369.2338 [M+H]⁺.

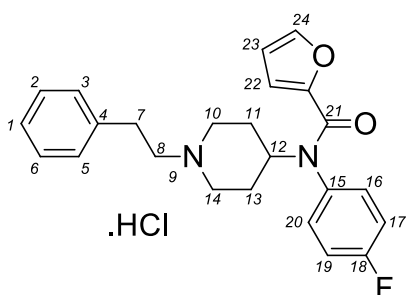
N-(4-Fluorophenyl)-*N*-(1-phenethylpiperidin-4-yl)isobutyramide (*para*-Fluoroisobutyrylfentanyl, **133**)



Compound **133** was synthesised from **49c** using Method C (white solid, 56% yield). ¹H NMR (400 MHz, DMSO) δ 10.20 (s, 1H, H9), 7.39 – 7.28 (m, 6H, H2/6/16-17/18-19), 7.28 – 7.18 (m, 3H, H1/3/5), 4.69 (t, $J = 12.1$ Hz, 1H, H12), 3.53 (d, $J = 11.6$ Hz, 2H, H10a/14a), 3.34 (H₂O), 3.26 – 3.03 (m, 4H, H8/10b/14b), 3.03 – 2.79 (m, $J = 10.6, 6.1$ Hz, 2H, H7), 2.13 (sept, $J = 13.4, 6.7$ Hz, 1H, H22), 1.93 (d, $J = 13.1$ Hz, 2H, H11a/13a), 1.60 (q, $J = 12.2$ Hz, 2H, H11b/13b), 0.90 (d, $J = 6.7$ Hz, 6H, H23); ¹³C NMR (100 MHz, DMSO) δ 176.15 (C21), 162.22 (d, $J = 246.2$ Hz, C18), 137.64 (C4), 134.84 (C15), 132.86 (d, $J = 8.7$ Hz, C16/20), 129.17 (C2-3/C5-6), 127.30 (C1), 116.82 (d, $J = 22.4$ Hz, C17/19), 56.88 (C8), 51.35 (C10/14), 49.45 (C12), 31.67 (C22), 29.92 (C7), 27.63 (C11/13), 19.91 (C23); ¹⁹F NMR (376 MHz, DMSO) δ -114.81; ATR-FTIR

$\nu_{\max}/\text{cm}^{-1}$: 2963, 2933, 2877, 2386, 1654, 1602, 1507; HRMS ($\text{C}_{23}\text{H}_{29}\text{N}_2\text{O}_2\text{F}$) : predicted mass = 369.2342 $[\text{M}+\text{H}]^+$; experimental mass = 369.2339 $[\text{M}+\text{H}]^+$.

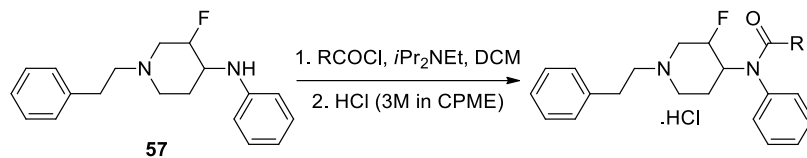
N-(4-Fluorophenyl)-*N*-(1-phenethylpiperidin-4-yl)furan-2-carboxamide (*para*-Fluorofuranylfentanyl, **145**)



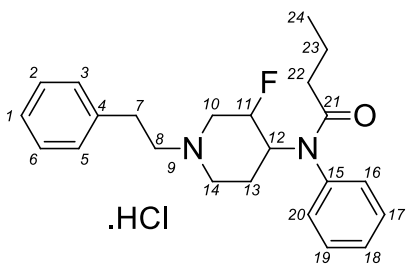
Compound **145** was synthesised from **49c** using Method C (white solid, 34% yield). ^1H NMR (400 MHz, DMSO) δ 10.34 (s, 1H, H9), 7.67 (d, J = 1.1 Hz, 1H, H24), 7.47 – 7.29 (m, 7H, H2/6/16-17/19-20), 7.29 – 7.20 (m, 3H, H1/3/5), 6.38 (dd, J = 3.5, 1.7 Hz, 1H, H23), 5.65 (s, 1H, H22), 4.82

(tt, J = 12.1, 3.6 Hz, 1H, H12), 3.58 (d, J = 11.8 Hz, 2H, H10a/14a), 3.35 (D_2O), 3.29 – 3.07 (m, 4H, H8/10b/14b), 3.06 – 2.91 (m, 2H, H7), 2.15 – 1.96 (m, 2H, H11a/13a), 1.75 (q, J = 12.5 Hz, 2H, H11b/13b); ^{13}C NMR (100 MHz, DMSO) δ 162.51 (d, J = 246.5 Hz, C18), 158.52 (C21), 147.01 (C22), 145.84 (C25), 137.62 (C4), 134.64 (C15), 133.43 (d, J = 8.7 Hz, C16/20), 129.19 (C2-3/C5-6), 127.32 (C1), 116.80 (d, J = 22.0 Hz, C17/19), 116.69 (C23), 111.89 (C24), 56.93 (C8), 51.34 (C10/14), 50.64 (C12), 29.95 (C7), 27.38 (C22); ^{19}F NMR (376 MHz, DMSO) δ -114.14; ATR-FTIR $\nu_{\max}/\text{cm}^{-1}$: 3056, 3028, 2930, 2628, 2584, 2540, 2468, 1644, 1600, 1561, 1574, 1508; HRMS ($\text{C}_{24}\text{H}_{25}\text{N}_2\text{O}_2\text{F}$) : predicted mass = 393.1978 $[\text{M}+\text{H}]^+$; experimental mass = 393.1973 $[\text{M}+\text{H}]^+$.

Synthesis of 3-fluoro fentanyl analogues **87-88**, **148**



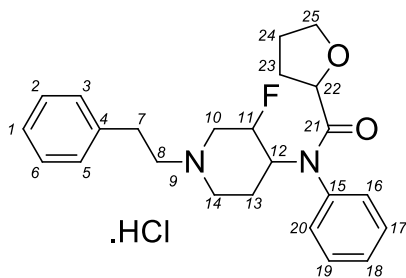
N-(3-Fluoro-1-phenethylpiperidin-4-yl)-*N*-phenylbutyramide
Fluorobutyrylfentanyl, **87**) (3-



Compound **87** was synthesised from **57** using Method C (white solid, 51% yield). ¹H NMR (400 MHz, DMSO) δ 10.18 (s, 1H, H9), 7.56 – 7.36 (m, 3H, H17-19), 7.36 – 7.17 (m, 7H, H1-3/H5-6/H16/H20), 5.35 (d, *J* = 47.8 Hz, 1H, H11), 4.81 (dd, *J* = 33.3, 10.4 Hz, 1H, H12), 3.84 (t, *J* = 11.3

Hz, 1H, H10a), 3.74 – 3.45 (m, 2H, H10b/14a), 3.35 (H₂O), 3.32 – 3.12 (m, 3H, H8/14a), 3.10 – 2.91 (m, 2H, H7), 1.86 (t, *J* = 7.3 Hz, 2H, H22), 1.80 (d, *J* = 12.1 Hz, 1H, H13a), 1.61 (qd, *J* = 12.1, 3.0 Hz, 1H, H13b), 1.45 (sext, *J* = 7.4 Hz, 2H, H23), 0.75 (t, *J* = 7.4 Hz, 3H, H24); ¹³C NMR (100 MHz, DMSO) δ 172.14 (C21), 138.76 (C15), 137.05 (C4), 130.70, 130.61, 129.325, 129.02, 128.71, 128.63 and 126.78 (C2-3/C5-6/C16-20), 86.72 (d, *J* = 178.28 Hz, C11), 56.71 (C8), 52.92 (d, *J* = 20.13 Hz, C10), 51.65 (d, *J* = 18.21 Hz, C12), 50.49 (C14), 36.10 (C22), 29.20 (C7), 22.25 (C13), 18.11 (C23), 13.57 (C24); ¹⁹F NMR (376 MHz, DMSO) δ -198.92; ATR-FTIR $\nu_{\text{max}}/\text{cm}^{-1}$: 3548, 3379, 2934, 2872, 2541, 1642, 1594, 1492; HRMS (C₂₃H₂₉N₂OF) : predicted mass = 369.2342 [M+H]⁺; experimental mass = 369.2337 [M+H]⁺.

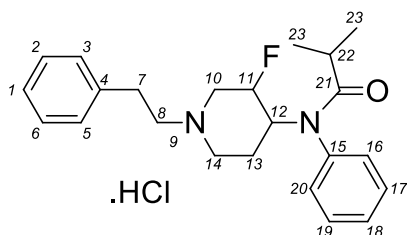
N-(3-Fluoro-1-phenethylpiperidin-4-yl)-*N*-phenyltetrahydrofuran-2-carboxamide (3-Fluorotetrahydrofuranylfentanyl, **88**)



Compound **88** was synthesised from **57** using Method C (white solid, 33% yield). ^1H NMR (400 MHz, DMSO) δ 10.16 (s, 1H, H9), 7.57 – 7.41 (m, 3H, H17-19), 7.41 – 7.14 (m, 7H, H1-3/H5-6/H16/H22), 5.37 (d, J = 47.8 Hz, 1H, H11), 4.90 – 4.65 (m, 1H, H12), 4.05 – 3.90 (m,

1H, H22), 3.90 – 3.74 (m, 2H, H10a/H25a), 3.74 – 3.37 (m, H₂O and H10b/14a/25b), 3.36 – 3.12 (m, 3H, H8/14b), 3.12 – 2.88 (m, 2H, H7), 2.04 – 1.76 (m, 3H, H13a/23a/24a), 1.76 – 1.43 (m, 3H, H13b/H23b/24b); Two rotamers are observed in carbon NMR, in an A/B ratio of ~3:1, certain signals are duplicated – ^{13}C NMR (100 MHz, DMSO- D_6) δ 172.84 (C21 A), 172.77 (C21 B), 138.09 (C15 B), 137.48 (C15 A), 131.54, 131.44, 131.38, 131.33, 129.87, 129.67, 129.6, 129.34, 129.23 and 129.18 (C16-20 A/B, C2-6), 127.34 (C1), 87.31 (d, J = 177.3 Hz, C11 A), 87.00 (d, J = 176.5 Hz, C11 B), 75.18 (C22 A), 75.05 (C22 B), 69.23 (C25), 57.20 (C8) 53.60 (d, J = 20.1 Hz, C10), 52.42 (d, J = 17.1 Hz, C12 A), 52.32 (d, J = 17.7 Hz, C12 B), 50.95 (C14), 30.41 (C23 B), 30.15 (C23 A), 29.72 (C7), 25.91 (C24), 22.68 (C13 A), 22.49 (C13 B); ^{19}F NMR (376 MHz, DMSO) δ -198.59; ATR-FTIR $\nu_{\text{max}}/\text{cm}^{-1}$: 2946, 2878, 2606, 1655, 1594, 1494; HRMS ($\text{C}_{24}\text{H}_{29}\text{N}_2\text{O}_2\text{F}$): predicted mass = 397.2291 [M+H] $^+$; experimental mass = 397.2288 [M+H] $^+$.

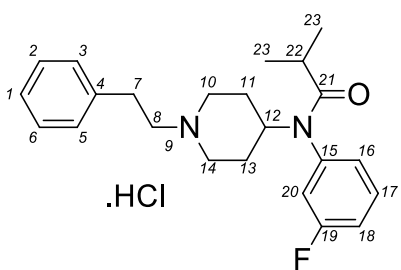
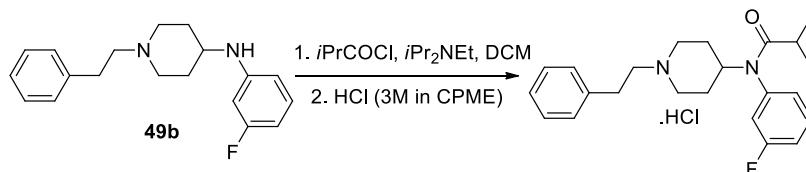
N-(3-Fluoro-1-phenethylpiperidin-4-yl)-*N*-phenylisobutyramide (3-Fluoroisobutyrylfentanyl, **148**)



Compound **148** was synthesised from **57** using Method C (white solid, 37% yield ^1H NMR (400 MHz, DMSO) δ 10.15 (s, 1H, H9), 7.57 – 7.41 (m, 3H, H17-19), 7.41 – 7.18 (m, 7H, H1-3/H5-6/H16/H20), 5.39 (d, $J = 47.8$ Hz,

1H, H11), 4.79 (dd, $J = 33.2, 10.0$ Hz, 1H, H12), 3.84 (t, $J = 11.2$ Hz, 1H, H10a), 3.74 – 3.43 (m, 2H, H10b/14a), 3.36 (H₂O), 3.32 – 3.11 (m, 3H, H8/14b), 2.93 (s, 2H, H7), 2.20 (sept, $J = 13.4, 6.7$ Hz, 1H, H22), 1.82 (d, 1H, H13a), 1.73 – 1.36 (m, $J = 13.3, 9.9$ Hz, 1H, H13b), 0.92 (dd, $J = 6.6, 4.6$ Hz, 6H, H23); ^{13}C NMR (100 MHz, DMSO) δ 176.89 (C21), 139.18 (C15), 137.50 (C4), 131.05, 130.96, 129.86, 129.57, 129.23, 129.17, 129.09 and 127.33 (C1-3/5-6/16-20), 87.30 (d, $J = 177.2$ Hz, C11), 57.20 (C8), 53.62 (d, $J = 19.7$ Hz, C10), 52.10 (d, $J = 17.5$ Hz, C12), 51.03 (C14), 31.60 (C22), 29.73 (C7), 22.85 (C13), 20.09 and 19.70 (C23); ^{19}F NMR (376 MHz, DMSO) δ -198.83; ATR-FTIR $\nu_{\text{max}}/\text{cm}^{-1}$: 2979, 2963, 2399, 1660, 1594, 1494; HRMS (C₂₃H₂₉N₂OF) : predicted mass = 369.2342 [M+H]⁺; experimental mass = 369.2338 [M+H]⁺.

Synthesis of *N*-(3-fluorophenyl)-*N*-(1-phenethylpiperidin-4-yl)isobutyramide (*meta*-Fluoroisobutyrylfentanyl, **137**)



Compound **137** was synthesised from **49b** using Method C (white solid, 37% yield ^1H NMR (400 MHz, DMSO) ^1H NMR (400 MHz, DMSO) δ 10.32 (s, 1H, H9), 7.56 (m, $J = 7.0$ Hz, 1H, H17), 7.42 – 7.21 (m, 8H, H1-3/H5-6/H18/H20), 7.15 (d, $J = 7.8$ Hz, 1H, H16), 4.69 (t, $J = 12.0$ Hz, 1H,

H12), 3.54 (d, $J = 11.6$ Hz, 2H, H10a/14a), 3.34 (H₂O), 3.29 – 3.04 (m, 4H, H8/10b/14b), 3.04 – 2.92 (m, 2H, H7), 2.16 (sept, $J = 6.6$ Hz, 1H, H22), 1.94 (m, 2H, H11a/13a), 1.64 (q, $J = 12.6$ Hz, 2H, H11b/13b), 0.92 (d, $J = 6.5$ Hz, 6H, H23); ^{13}C NMR (100 MHz, DMSO) δ 175.87 (C21), 162.66 (d, $J = 245.8$ Hz, C19), 140.29 (d, $J = 9.4$ Hz, C15), 137.59 (C4), 131.53 (d, $J = 9.1$ Hz, C17), 129.18 (C2-3/5-6), 127.32 and 123.23 (C1/16), 118.09 (d, $J = 21.7$ Hz, C20), 116.30 (d, $J = 20.9$ Hz, C18), 56.89 (C8), 51.41 (C10/14), 49.56 (C12), 31.85 (C22), 29.95 (C7), 27.66 (C11/13), 19.94 (C23); ^{19}F NMR (376 MHz, DMSO) - 112.90; ATR-FTIR $\nu_{\text{max}}/\text{cm}^{-1}$: 2963, 2933, 2871, 2459, 2400, 1858, 1607, 1593; HRMS (C₂₃H₂₉N₂OF) : predicted mass = 369.2342 [M+H]⁺; experimental mass = 369.2338 [M+H]⁺.

7.12.4 Purification of heroin from seized samples

Heroin (**1c**) was purified from seized samples using the method previously described by Guo *et al.* [187]

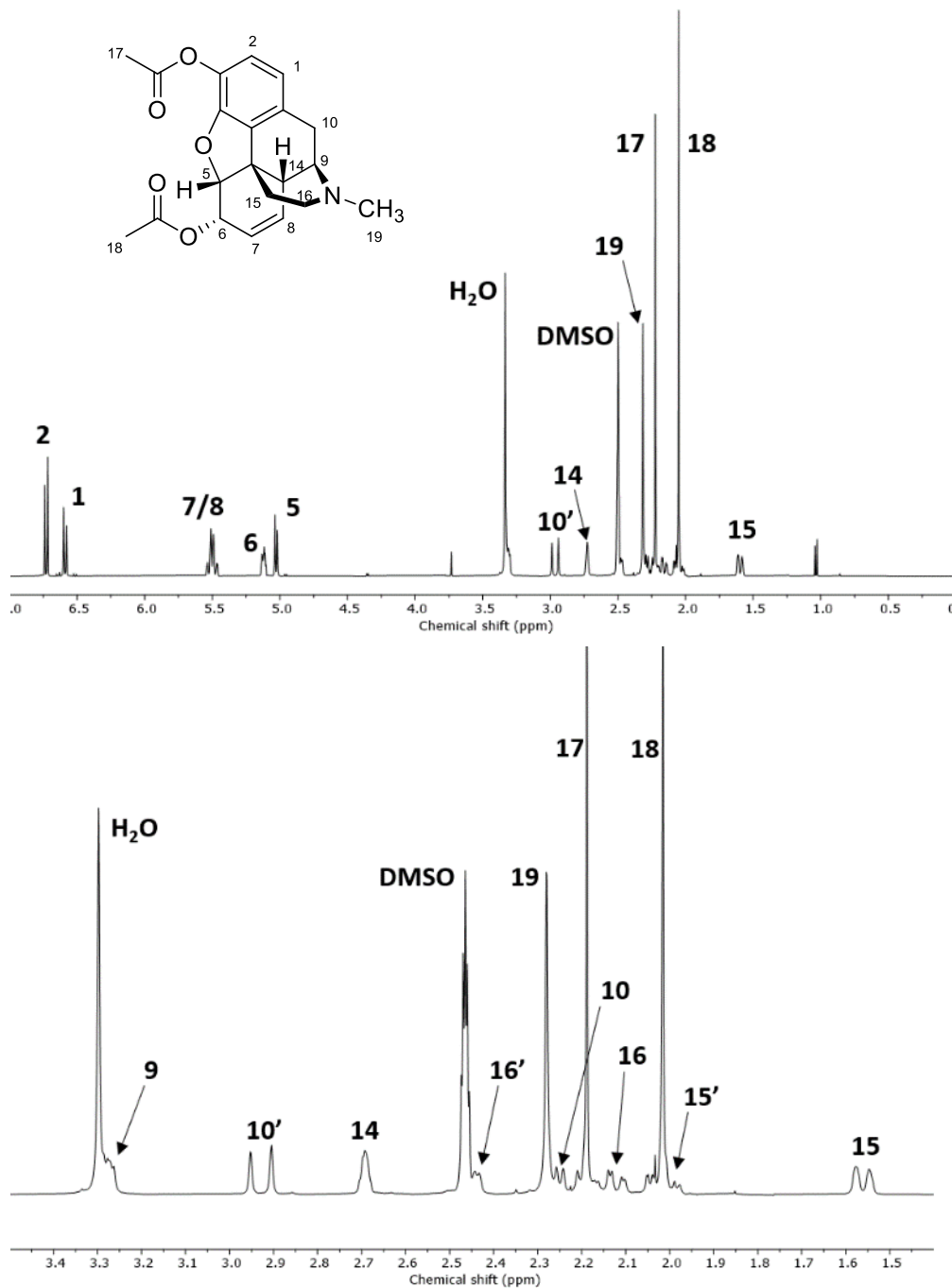


Figure 7.1. a) ¹H NMR spectrum of heroin (**1c**) free-base in DMSO-D₆; b) Detail of 7.1a, showing hidden proton signals.

Figure 7.2. ^1H - ^1H COSY NMR spectrum of heroin (**1c**) free base in DMSO- D_6 (0.8-4.0 ppm)

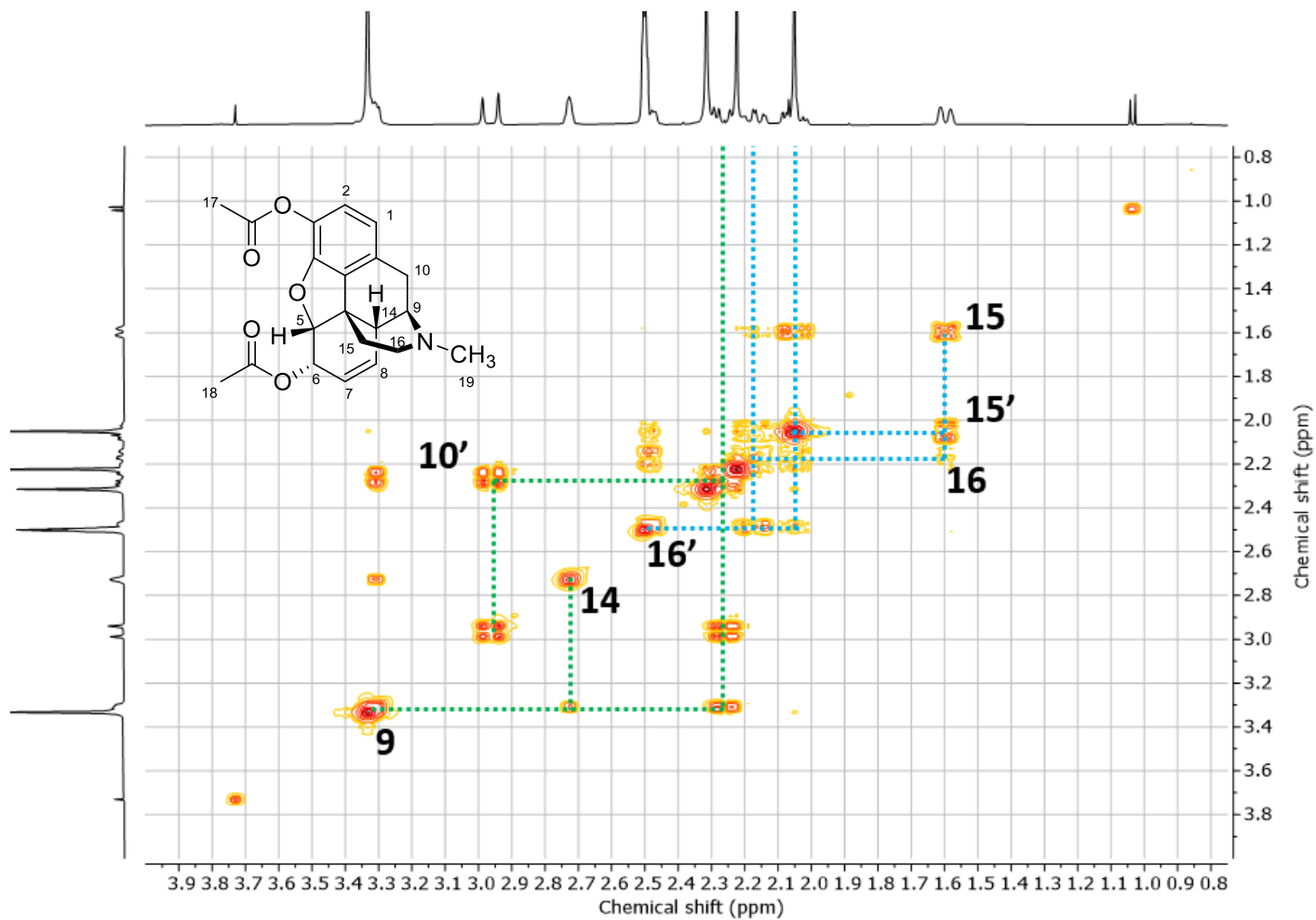


Figure 7.3. ^1H - ^1H COSY NMR spectrum of heroin (**1c**) free base in DMSO- D_6 (2.5-7.0 ppm)

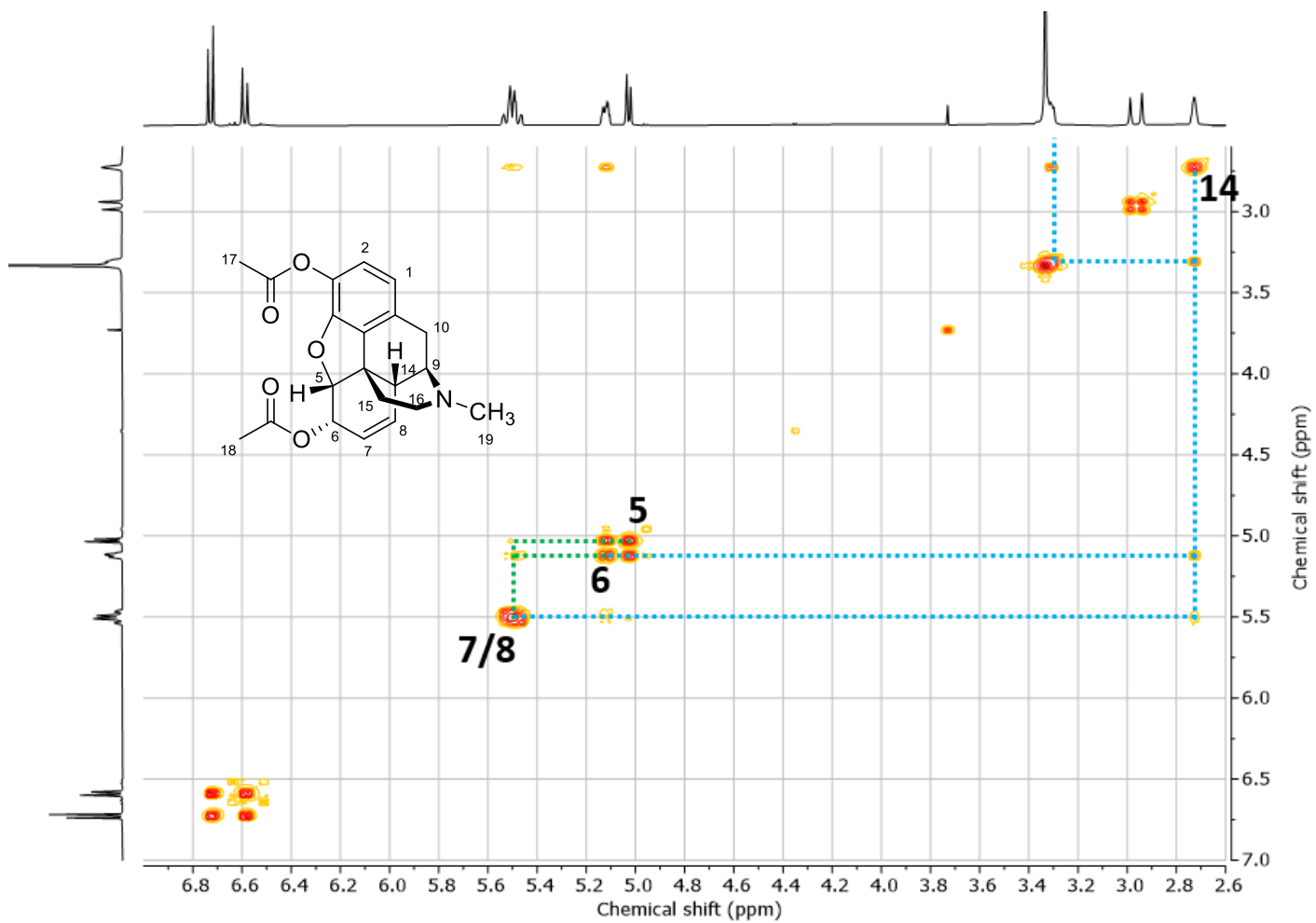


Figure 7.4. ^1H - ^{13}C HMQC NMR spectrum of heroin (**1c**) free base in DMSO- D_6 (0-100 ppm)

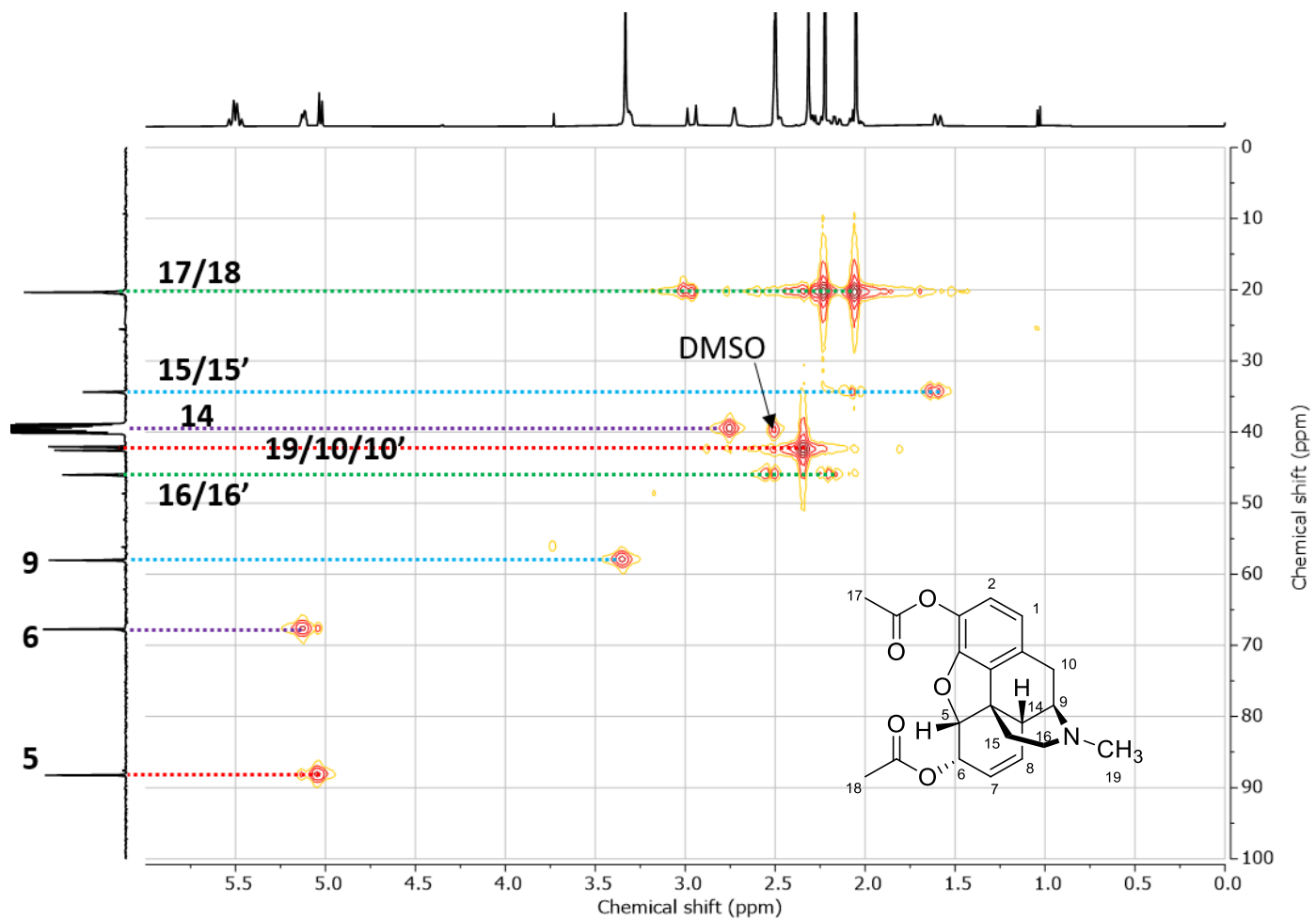


Figure 7.5. ^1H - ^{13}C HMQC NMR spectrum of heroin (**1c**) free base in DMSO- D_6 (105-150 ppm)

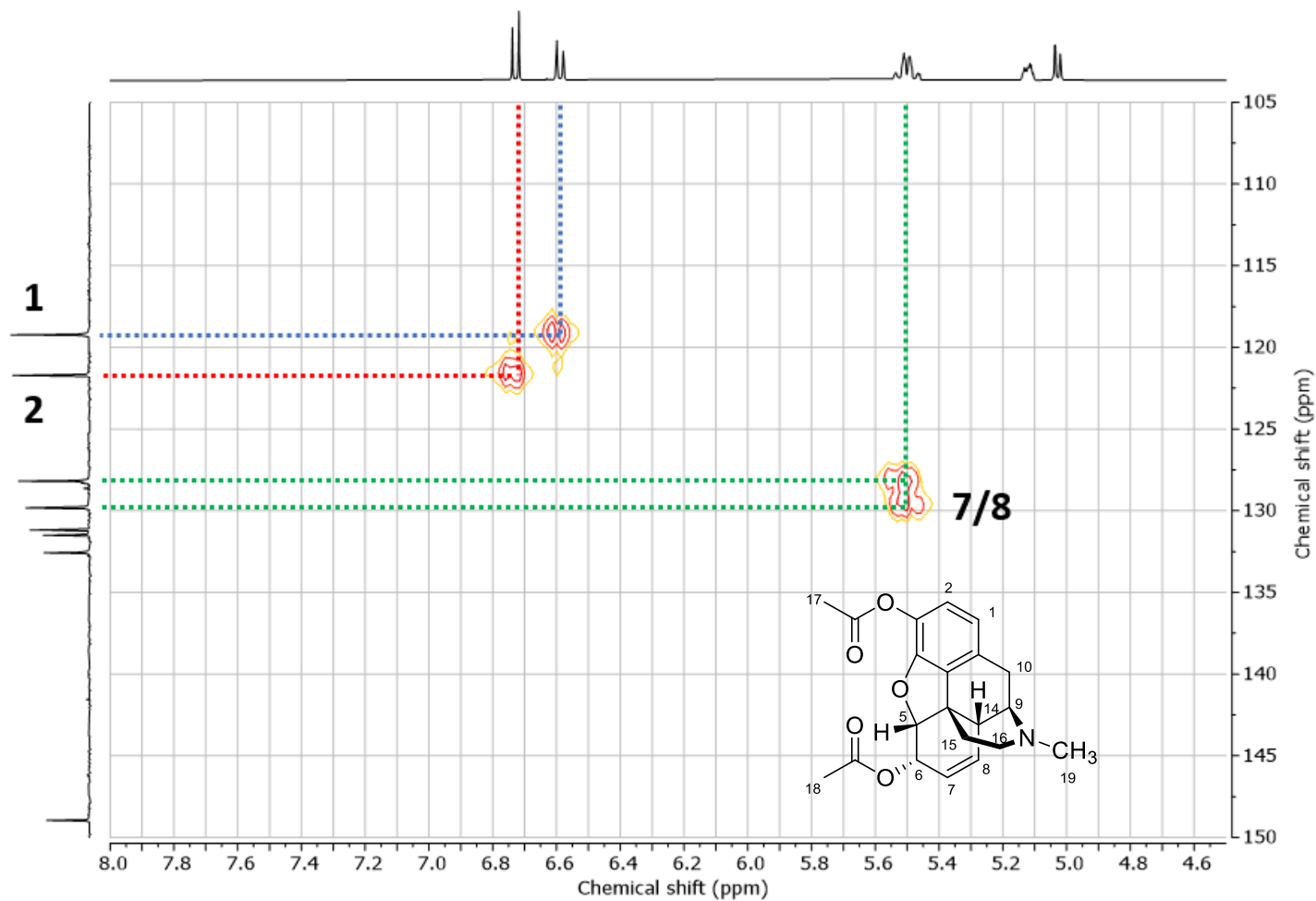
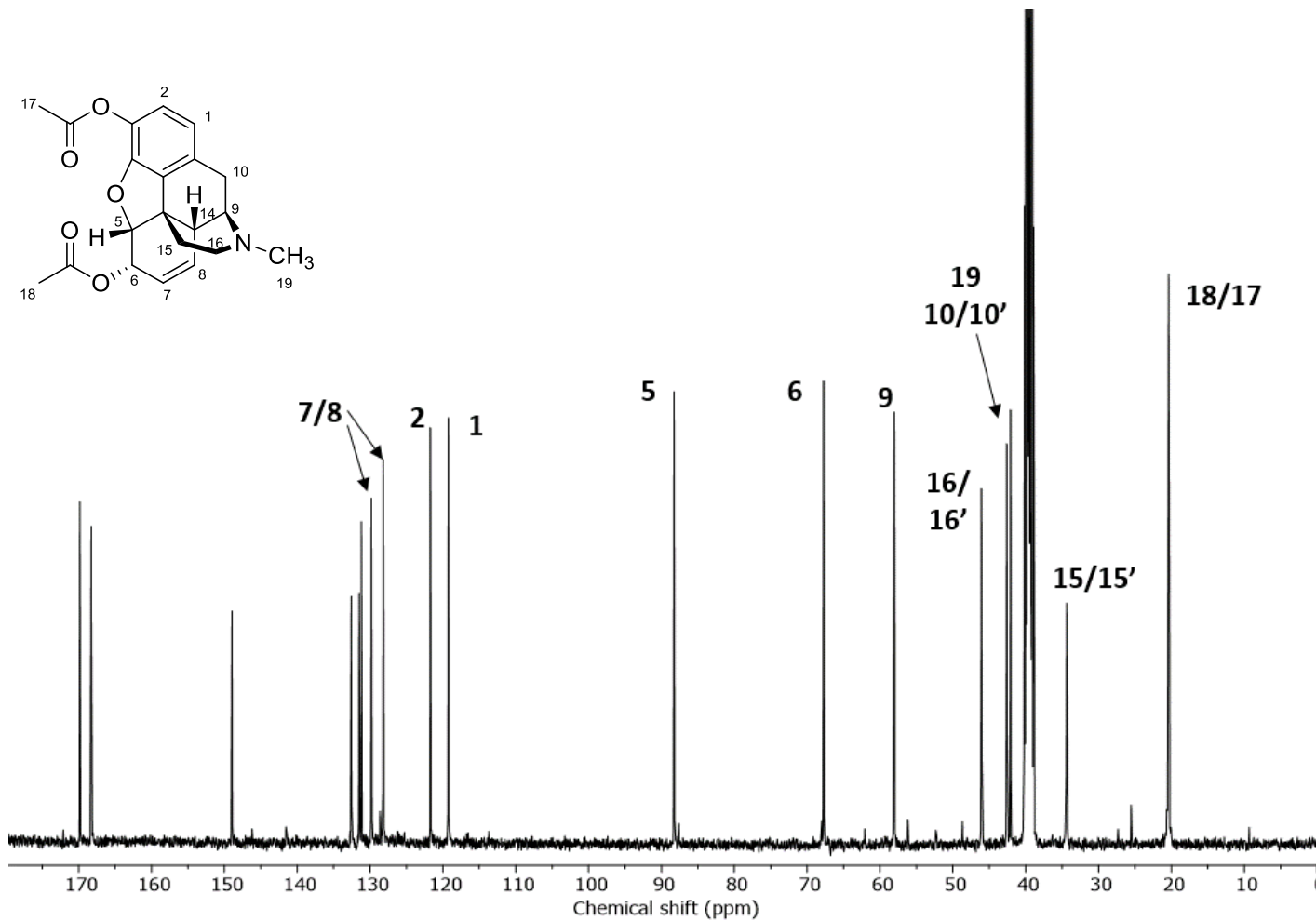


Figure 7.6. ^{13}C NMR spectrum of heroin (**1c**) free base in $\text{DMSO-}D_6$ (with partial attribution based on HMQC)



References

- [1] V. Spahn, G. Del Vecchio, D. Labuz, A. Rodriguez-Gaztelumendi, N. Massaly, J. Temp, V. Durmaz, P. Sabri, M. Reidelbach, H. Machelka, M. Weber, C. Stein. A nontoxic pain killer designed by modeling of pathological receptor conformations, *Science*. 355 (2017) 966-969. <http://doi.org/10.1126/science.aai8636>
- [2] P. G. Fline, R. K. Portenoy. (2004). Chapter 2: The Endogenous Opioid System *A Clinical Guide to Opioid Analgesia* (pp. 9-15): McGraw Hill.
- [3] P. A. J. Janssen. *1-Aralkyl-4-(N-aryl-carbonyl amino)-piperidines and related compounds*. 1965, United States Patent No. US3164600. U. S. P. Office.
- [4] C. A. Valdez, R. N. Leif, B. P. Mayer. An Efficient, Optimized Synthesis of Fentanyl and Related Analogs, *PLOS ONE*. 9 (2014) e108250. [10.1371/journal.pone.0108250](https://doi.org/10.1371/journal.pone.0108250)
- [5] R. Cookson, G. Towse. The search for new analgesics, *Clin. Res. Rev.*, 1,219. 225 (1981).
- [6] A. H. Beckett, A. F. Casy. Synthetic analgesics: Stereochemical considerations, *J. Pharm. Pharmacol.* 6 (1954) 986-1001. [10.1111/j.2042-7158.1954.tb11033.x](https://doi.org/10.1111/j.2042-7158.1954.tb11033.x)
- [7] A. H. Beckett, A. F. Casy, N. J. Harper. Analgesics and their antagonists: Some steric and chemical considerations, *J. Pharm. Pharmacol.* 8 (1956) 874-884. [10.1111/j.2042-7158.1956.tb12217.x](https://doi.org/10.1111/j.2042-7158.1956.tb12217.x)
- [8] E. J. M. Kuip, M. L. Zandvliet, S. L. W. Koolen, R. H. J. Mathijssen, C. C. D. van der Rijt. A review of factors explaining variability in fentanyl pharmacokinetics; focus on implications for cancer patients, *Br. J. Clin. Pharmacol.* 83 (2017) 294-313. [10.1111/bcp.13129](https://doi.org/10.1111/bcp.13129)
- [9] W. Jeal, P. Benfield. Transdermal fentanyl. A review of its pharmacological properties and therapeutic efficacy in pain control, *Drugs*. 53 (1997) 109-138. [10.2165/00003495-199753010-00011](https://doi.org/10.2165/00003495-199753010-00011)
- [10] E. J. M. Kuip, M. L. Zandvliet, R. H. J. Mathijssen, C. C. D. Van der Rijt. Pharmacological and clinical aspects of immediate release fentanyl

- preparations: criteria for selection, *Eur. J. Hosp. Pharm.* 19 (2012) 38-40. 10.1136/ejhpharm-2011-000040
- [11] Philip W. H. Peng, Alan N. Sandler. A Review of the Use of Fentanyl Analgesia in the Management of Acute Pain in Adults, *Anesthesiology*. 90 (1999) 576-599. 10.1097/00000542-199902000-00034
- [12] S. Friedrich, D. Raub, B. J. Teja, S. E. Neves, T. Thevathasan, T. T. Houle, M. Eikermann. Effects of low-dose intraoperative fentanyl on postoperative respiratory complication rate: a pre-specified, retrospective analysis, *Br. J. Anaesth.* 122 (2019) e180-e188. <https://doi.org/10.1016/j.bja.2019.03.017>
- [13] M. P. Davis. Fentanyl for breakthrough pain: a systematic review, *Expert Rev. Neurother.* 11 (2011) 1197-1216. 10.1586/ern.11.63
- [14] S. Mudd. Intranasal fentanyl for pain management in children: a systematic review of the literature, *J. Pediatr. Health Car.* 25 (2011) 316-322. 10.1016/j.pedhc.2010.04.011
- [15] P. Armenian, K. T. Vo, J. Barr-Walker, K. L. Lynch. Fentanyl, fentanyl analogs and novel synthetic opioids: A comprehensive review, *Neuropharmacology*. 134 (2018) 121-132. <https://doi.org/10.1016/j.neuropharm.2017.10.016>
- [16] R. M. Gladden, P. Martinez, P. Seth. Fentanyl Law Enforcement Submissions and Increases in Synthetic Opioid–Involved Overdose Deaths — 27 States, 2013–2014, *MMWR Morb. Mortal. Wkly Rep.* 65 (2016) 837-843. 10.2307/24858927
- [17] J. O'Donnell, R. Gladden, P. Seth. Trends in Deaths Involving Heroin and Synthetic Opioids Excluding Methadone, and Law Enforcement Drug Product Reports, by Census Region — United States, 2006–2015, *MMWR Morb. Mortal. Wkly Rep.* 66 (2017) 897-903. 10.15585/mmwr.mm6634a2
- [18] J. O'Donnell, J. Halpin, C. Mattson, B. Goldberger, R. Gladden. Deaths Involving Fentanyl, Fentanyl Analogs, and U-47700 — 10 States, July–December 2016, *MMWR Morb. Mortal. Wkly Rep.* 66 (2017). 10.15585/mmwr.mm6643e1
- [19] P. Armenian, K. T. Vo, J. Barr-Walker, K. L. Lynch. Fentanyl, fentanyl analogs and novel synthetic opioids: A comprehensive review, *Neuropharmacology* (2017). 10.1016/j.neuropharm.2017.10.016
- [20] L. Scholl, P. Seth, M. Kariisa, N. Wilson, G. Baldwin. Drug and opioid-involved overdose deaths — United States, 2013–2017, *MMWR Morb.*

- Mortal. Wkly Rep. 67 (2019) 1419–1427.
<http://dx.doi.org/10.15585/mmwr.mm675152e1>
- [21] M. A. Hedegaard H, Warner M, Drug overdose deaths in the United States, 1999–2018. NCHS Data Brief, no 356. Hyattsville, MD: National Center for Health Statistics. <https://www.cdc.gov/nchs/products/databriefs/db356.htm>, 2020 (accessed 4 September 2020).
- [22] J. Mounteney, I. Giraudon, G. Denissov, P. Griffiths. Fentanyl: Are we missing the signs? Highly potent and on the rise in Europe, *Int. J. Drug Policy*. 26 (2015) 626-631. <http://10.1016/j.drugpo.2015.04.003>
- [23] S. O'Connor, U.S.-China Economic and Security Review Commission - Fentanyl: China's Deadly Export to the United States. <https://www.uscc.gov/research/fentanyl-chinas-deadly-export-united-states>, 2017 (accessed 7 September 2020).
- [24] Drug Enforcement Administration, DEA Intelligence Report - Fentanyl Flow to the United States. <https://www.dea.gov/documents/2020/03/06/fentanyl-flow-united-states>, 2020 (accessed 7 September 2020).
- [25] D. A. Algren, C. P. Monteilh, M. Punja, J. G. Schier, M. Belson, B. R. Hepler, C. J. Schmidt, C. E. Miller, M. Patel, L. J. Paulozzi, M. Straetemans, C. Rubin. Fentanyl-associated Fatalities Among Illicit Drug Users in Wayne County, Michigan (July 2005–May 2006), *J. Med. Toxicol.* 9 (2013) 106-115. 10.1007/s13181-012-0285-4
- [26] L. J. Marinetti, B. J. Ehlers. A series of forensic toxicology and drug seizure cases involving illicit fentanyl alone and in combination with heroin, cocaine or heroin and cocaine, *J. Anal.Toxicol.* 38 (2014) 592-598. 10.1093/jat/bku086
- [27] National Crime Agency. *Recent Deaths Possibly Linked to Fentanyl*. 2017, Retrieved from <http://www.nationalcrimeagency.gov.uk/publications/795-recent-deaths-possibly-linked-to-fentanyl/file>
- [28] J. M. Stogner. The potential threat of acetyl fentanyl: legal issues, contaminated heroin, and acetyl fentanyl "disguised" as other opioids, *Ann. Emerg. Med.* 64 (2014) 637-639. <https://doi.org/10.1016/j.annemergmed.2014.07.017>
- [29] R. G. Frank, H. A. Pollack. Addressing the fentanyl threat to public health, *N. Engl. J. Med.* 376 (2017) 605-607. 10.1056/NEJMp1615145

- [30] Drug Enforcement Administration, Cocaine/fentanyl combination in Pennsylvania. <https://www.dea.gov/sites/default/files/2018-07/BUL-061-18%20Cocaine%20Fentanyl%20Combination%20in%20Pennsylvania%20--%20UNCLASSIFIED.PDF>, 2018 (accessed 06 July 2019).
- [31] D. Ciccarone. Fentanyl in the US heroin supply: A rapidly changing risk environment, *Int. J. Drug Policy.* 46 (2017) 107-111. 10.1016/j.drugpo.2017.06.010
- [32] S. A Klar, E. Brodtkin, E. Gibson, S. Padhi, C. Predy, C. Green, V. Lee. Notes from the field: Furanyl-fentanyl overdose events caused by smoking contaminated crack cocaine - British Columbia, Canada, July 15-18, 2016, *MMWR Morb. Mortal. Wkly. Rep.* 65 (2016) 1015-1016. 10.15585/mmwr.mm6537a6
- [33] L. N. Rodda, J. L. Pilgrim, M. Di Rago, K. Crump, D. Gerostamoulos, O. H. Drummer. A Cluster of Fentanyl-Laced Heroin Deaths in 2015 in Melbourne, Australia, *J. Anal. Toxicol.* 41 (2017) 318-324. 10.1093/jat/bkx013
- [34] R. T. DeRienz, D. D. Baker, N. E. Kelly, A. M. Mullins, R. Y. Barnett, J. M. Hobbs, J. A. Daniels, K. E. Harshbarger, A. M. Ortiz. Child fatalities due to heroin/fentanyl exposure: What the case history missed, *J. Anal. Toxicol.* 42 (2018) 581-585. 10.1093/jat/bky052
- [35] N. Baldwin, R. Gray, A. Goel, E. Wood, J. A. Buxton, L. M. Rieb. Fentanyl and heroin contained in seized illicit drugs and overdose-related deaths in British Columbia, Canada: An observational analysis, *Drug Alcohol Depend.* 185 (2018) 322-327. 10.1016/j.drugalcdep.2017.12.032
- [36] United Nations Office on Drugs and Crime. *Global Smart Update - Fentanyl and its analogues - 50 years on.* 2017, Retrieved from https://www.unodc.org/documents/scientific/Global_SMART_Update_17_web.pdf
- [37] C. F. Ramos-Matos, K. G. Bistas, W. Lopez-Ojeda. (2020). *Fentanyl StatPearls*. Treasure Island (FL): StatPearls Publishing Copyright © 2020, StatPearls Publishing LLC.
- [38] J. B. Streisand, J. R. Varvel, D. R. Stanski, L. Le Maire, M. A. Ashburn, B. I. Hague, S. D. Tarver, T. H. Stanley. Absorption and bioavailability of oral transmucosal fentanyl citrate, *Anesthesiology.* 75 (1991) 223-229. 10.1097/00000542-199108000-00009

- [39] I. Solassol, F. Bressolle, L. Caumette, F. Garcia, S. Poujol, S. Culine, F. Pinguet. Inter- and intraindividual variabilities in pharmacokinetics of fentanyl after repeated 72-hour transdermal applications in cancer pain patients, *Ther. Drug Monit.* 27 (2005) 491-498. 10.1097/01.ftd.0000160717.50704.42
- [40] P. S. Glass, S. Shafer, J. Reves. Intravenous drug delivery systems, *Miller's anesthesia*. 1 (2005) 445-461.
- [41] D. A. McClain, C. C. Hug Jr. Intravenous fentanyl kinetics, *Clin. Pharmacol. Ther.* 28 (1980) 106-114. 10.1038/clpt.1980.138
- [42] C. C. Hug, Jr., M. R. Murphy. Tissue redistribution of fentanyl and termination of its effects in rats, *Anesthesiology*. 55 (1981) 369-375. 10.1097/00000542-198110000-00006
- [43] B. Coda. (1996). Opioids. In P. Barash, B. Cullen, & R. Stoelting (Eds.), *Clinical Anesthesia* (3rd ed., pp. 329-358). Philadelphia: Lippincott-Raven.
- [44] W. E. Meuldermans, R. M. Hurkmans, J. J. Heykants. Plasma protein binding and distribution of fentanyl, sufentanil, alfentanil and lofentanil in blood, *Arch. Int. Pharmacodyn. Ther.* 257 (1982) 4-19.
- [45] J. McPherson, G. Rivero, M. Baptist, J. Llorente, S. Al-Sabah, C. Krasel, W. L. Dewey, C. P. Bailey, E. M. Rosethorne, S. J. Charlton, G. Henderson, E. Kelly. μ -opioid receptors: correlation of agonist efficacy for signalling with ability to activate internalization, *Mol. Pharmacol.* 78 (2010) 756-766. 10.1124/mol.110.066613
- [46] R. B. Labroo, M. F. Paine, K. E. Thummel, E. D. Kharasch. Fentanyl metabolism by human hepatic and intestinal cytochrome P450 3A4: implications for interindividual variability in disposition, efficacy, and drug interactions, *Drug Metabolism and Disposition: The Biological Fate of Chemicals*. 25 (1997) 1072-1080.
- [47] T. Goromaru, H. Matsuura, N. Yoshimura, T. Miyawaki, T. Sameshima, J. Miyao, T. Furuta, S. Baba. Identification and Quantitative Determination of Fentanyl Metabolites in Patients by Gas Chromatography-Mass Spectrometry, *Anesthesiology*. 61 (1984) 73-77. 10.1097/00000542-198407000-00013
- [48] P. Maguire, N. Tsai, J. Kamal, C. Cometta-Morini, C. Upton, G. Loew. Pharmacological profiles of fentanyl analogs at mu, delta and kappa opiate receptors, *Eur. J. Pharmacol.* 213 (1992) 219-225. 10.1016/0014-2999(92)90685-w

- [49] P. F. J. Lipiński, M. Jarończyk, J. C. Dobrowolski, J. Sadlej. Molecular dynamics of fentanyl bound to μ -opioid receptor, *J. Mol. Model.* 25 (2019) 144. 10.1007/s00894-019-3999-2
- [50] J. C. Scott, K. V. Ponganis, D. R. Stanski. EEG quantitation of narcotic effect: the comparative pharmacodynamics of fentanyl and alfentanil, *Anesthesiology.* 62 (1985) 234-241. 10.1097/00000542-198503000-00005
- [51] H. F. Hill, C. R. Chapman, L. S. Saeger, R. Bjurstrom, M. H. Walter, R. B. Schoene, M. Kippes. Steady-state infusions of opioids in human. II. Concentration-effect relationships and therapeutic margins, *Pain.* 43 (1990) 69-79. 10.1016/0304-3959(90)90051-e
- [52] R. S. Vardanyan, V. J. Hruby. Fentanyl-related compounds and derivatives: current status and future prospects for pharmaceutical applications, *Future Med. Chem.* 6 (2014) 385-412. 10.4155/fmc.13.215
- [53] United Nations Office on Drugs and Crime, January 2020 – United Kingdom: ACMD report on the misuse of fentanyl and fentanyl analogues as global number of opioid NPS rises. <https://www.unodc.org/LSS/Announcement/Details/94dc6286-16bb-4e7a-9429-65d28918b332>, 2020 (accessed 15 July 2020).
- [54] S. N. Lucyk, L. S. Nelson. Novel Synthetic Opioids: An Opioid Epidemic Within an Opioid Epidemic, *Ann. Emerg. Med.* 69 (2017) 91-93. <http://doi.org/10.1016/j.annemergmed.2016.08.445>
- [55] P. Armenian, A. Olson, A. Anaya, A. Kurtz, R. Ruegner, R. R. Gerona. Fentanyl and a Novel Synthetic Opioid U-47700 Masquerading as Street "Norco" in Central California: A Case Report, *Ann. Emerg. Med.* 69 (2017) 87-90. <http://doi.org/10.1016/j.annemergmed.2016.06.014>
- [56] Scientific Working Group for the Analysis of Seized Drugs, ortho-Fluorofentanyl. <http://www.swgdrug.org/Monographs/ortho-Fluorofentanyl.pdf>, 2016 (accessed 21/03/2018).
- [57] A. Helland, W. R. Brede, L. S. Michelsen, P. O. M. Gundersen, H. Aarset, J. E. Skjølås, L. Slørdal. Two hospitalizations and one death after exposure to ortho-fluorofentanyl, *J. Anal.Toxicol.* 41 (2017) 708-709. 10.1093/jat/bkx050
- [58] Finnish Medicines Agency, 2-Fluorofentanyl (N-(2-fluorophenyl)-N-[1-(2-phenylethyl)piperidin-4-yl]-propanamide); 3-Fluorofentanyl (N-(3-fluorophenyl)-N-[1-(2-phenylethyl)piperidin-4-yl]-propanamide). <http://ec.europa.eu/growth/tools->

- databases/tris/es/index.cfm/search/?trisation=search.detail&year=2017&num=438&iLang=EN, 2017 (accessed 14 August 2019).
- [59] Réseau Européen d'Information sur les Drogues et les Toxicomanies, Harms and harm reduction workbook. <https://en.ofdt.fr/BDD/publications/docs/France2017-3-4-Hhr-EN.pdf>, 2017 (accessed 14 August 2019).
- [60] Advisory Council on the Misuse of Drugs, Misuse of fentanyl and fentanyl analogues. https://assets.publishing.service.gov.uk/government/uploads/system/uploads/attachment_data/file/855893/ACMD_Report_-_Misuse_of_fentanyl_and_fentanyl_analogues.pdf, 2020 (accessed 15 Jan 2020).
- [61] F. E. Dussy, S. Hangartner, C. Hamberg, C. Berchtold, U. Scherer, G. Schlotterbeck, D. Wyler, T. A. Briellmann. An acute ofentanil fatality: A case report with postmortem concentrations, *J. Anal. Toxicol.* 40 (2016) 761-766. 10.1093/jat/bkw096
- [62] M. Bäckberg, O. Beck, K.-H. Jönsson, A. Helander. Opioid intoxications involving butyrfentanyl, 4-fluorobutyrfentanyl, and fentanyl from the Swedish STRIDA project, *Clin. Toxicol. (Phila)*. 53 (2015) 609-617. 10.3109/15563650.2015.1054505
- [63] M. Rojkiewicz, M. Majchrzak, R. Celinski, P. Kus, M. Sajewicz. Identification and physicochemical characterization of 4-fluorobutyrfentanyl (1-((4-fluorophenyl)(1-phenethylpiperidin-4-yl)amino)butan-1-one, 4-FBF) in seized materials and post-mortem biological samples, *Drug Test. Anal.* 9 (2017) 405-414. 10.1002/dta.2135
- [64] A. Helander, M. Backberg, P. Signell, O. Beck. Intoxications involving acrylfentanyl and other novel designer fentanyls - results from the Swedish STRIDA project, *Clin. Toxicol. (Phila)*. 55 (2017) 589-599. 10.1080/15563650.2017.1303141
- [65] European Monitoring Centre for Drugs and Drug Addiction, Fentanyl drug profile. <http://www.emcdda.europa.eu/publications/drug-profiles/fentanyl>, 2015 (accessed 21 March 2018).
- [66] R. S. Vardanyan, V. J. Hruby. Fentanyl-related compounds and derivatives: current status and future prospects for pharmaceutical applications, *Future Med. Chem.* 6 (2014) 385-412. 10.4155/fmc.13.215

- [67] A. F. Casy, F. O. Ogungbamila. 3-Allyl analogues of fentanyl, *J. Pharm. Pharmacol.* 34 (1982) 210-210. doi:10.1111/j.2042-7158.1982.tb04229.x
- [68] Cayman Chemical, 4'-methyl Acetyl fentanyl (hydrochloride). <https://www.caymanchem.com/product/9002271>, 2018 (accessed
- [69] C. Liu, T. Li, Y. Han, Z. Hua, W. Jia, Z. Qian. The identification and analytical characterization of 2,2'-difluorofentanyl, *Drug Test. Anal.* 10 (2018) 774-780. 10.1002/dta.2264
- [70] G. Henderson. Designer Drugs: Past History and Future Prospects, *J. Forensic Sci.* 33 (1988) 569-575.
- [71] J. R. Bagley, R. L. Wynn, F. G. Rudo, B. M. Doorley, H. K. Spencer, T. Spaulding. New 4-(heteroanilido)piperidines, structurally related to the pure opioidagonist fentanyl, with agonist and/or antagonist properties, *J. Med. Chem.* 32 (1989) 663-671. 10.1021/jm00123a028
- [72] Wildlife Pharmaceuticals Inc., Thianil (thiafentanil oxalate) injectable solution 10 mg/mL. <https://www.fda.gov/downloads/AnimalVeterinary/DevelopmentApprovalProcess/MinorUseMinorSpecies/UCM530322.pdf>, (accessed 21/03/2018).
- [73] P. M. Wax, C. E. Becker, S. C. Curry. Unexpected "gas" casualties in Moscow: A medical toxicology perspective, *Ann. Emerg. Med.* 41 (2003) 700-705. <https://doi.org/10.1067/mem.2003.148>
- [74] J. F. Casale, J. R. Mallette, E. M. Guest. Analysis of illicit carfentanil: Emergence of the death dragon, *Forensic Chem.* 3 (2017) 74-80. <https://doi.org/10.1016/j.forc.2017.02.003>
- [75] Y. Tsumura, T. Mitome, S. Kimoto. False positives and false negatives with a cocaine-specific field test and modification of test protocol to reduce false decision, *Forensic Sci. Int.* 155 (2005) 158-164. 10.1016/j.forsciint.2004.11.011
- [76] K. Oguri, S. Wada, S. Eto, H. Yamada. Specificity and Mechanism of the Color Reaction of Cocaine with Cobaltous Thiocyanate, *Eisei kagaku.* 41 (1995) 274-279. 10.1248/jhs1956.41.274
- [77] K.-A. Kovar, M. Laudszun, Chemistry and reaction mechanisms of rapid tests for drugs of abuse and precursors chemicals. <https://www.unodc.org/pdf/scientific/SCITEC6.pdf>, 1989 (accessed 06 July 2019).

- [78] H. Johnke, G. Batres, M. Wilson, A. E. Holmes, S. Sikich. Detecting Concentration of Analytes with DETECHIP: A Molecular Sensing Array, *J. Sens. Technol.* 3 (2013). 10.4236/jst.2013.33015
- [79] M. J. Kangas, D. Symonsbergen, A. E. Holmes. A New Possible Alternative Colorimetric Drug Detection Test for Fentanyl, *Organic & Medicinal Chem. I. J.* 4 (2017) 555645.
- [80] J. K. Brown, L. Shapazian, G. D. Griffin. A rapid screening procedure for some "street drugs" by thin-layer chromatography, *J. Chromatogr. A.* 64 (1972) 129-133. [https://doi.org/10.1016/S0021-9673\(00\)92956-X](https://doi.org/10.1016/S0021-9673(00)92956-X)
- [81] B. A. O'Brien, J. M. Bonicamp, D. W. Jones. Differentiation of Amphetamine and Its Major Hallucinogenic Derivatives Using Thin-Layer Chromatography, *J. Anal. Toxicol.* 6 (1982) 143-147. 10.1093/jat/6.3.143
- [82] H. I. Finkle. Phencyclidine Identification by Thin-layer Chromatography: A Rapid Screening Procedure for Emergency Toxicology, *Am. J. Clin. Pathol.* 70 (1978) 287-290. 10.1093/ajcp/70.2.287
- [83] H. Ohta, S. Suzuki, K. Ogasawara. Studies on fentanyl and related compounds IV. Chromatographic and spectrometric discrimination of fentanyl and its derivatives, *J. Anal. Toxicol.* 23 (1999) 280-285. 10.1093/jat/23.4.280
- [84] E. Gerace, F. Seganti, C. Luciano, T. Lombardo, D. Di Corcia, H. Teifel, M. Vincenti, A. Salomone. On-site identification of psychoactive drugs by portable Raman spectroscopy during drug-checking service in electronic music events, *Drug Alcohol Rev.* 38 (2019) 50-56. 10.1111/dar.12887
- [85] A. Haddad, M. A. Comanescu, O. Green, T. A. Kubic, J. R. Lombardi. Detection and Quantitation of Trace Fentanyl in Heroin by Surface-Enhanced Raman Spectroscopy, *Anal. Chem.* 90 (2018) 12678-12685. 10.1021/acs.analchem.8b02909
- [86] R. Salemmilani, M. Moskovits, C. D. Meinhart. Microfluidic analysis of fentanyl-laced heroin samples by surface-enhanced Raman spectroscopy in a hydrophobic medium, *Analyst.* 144 (2019) 3080-3087. 10.1039/C9AN00168A
- [87] R. Mirsafavi, M. Moskovits, C. Meinhart. Detection and classification of fentanyl and its precursors by surface-enhanced Raman spectroscopy, *Analyst.* 145 (2020) 3440-3446. 10.1039/C9AN02568E

- [88] J. Omar, B. Slowikowski, C. Guillou, F. Reniero, M. Holland, A. Boix. Identification of new psychoactive substances (NPS) by Raman spectroscopy, *J. Raman Spectrosc.* 50 (2019) 41-51. <https://doi.org/10.1002/jrs.5496>
- [89] L. Wang, C. Deriu, W. Wu, A. M. Mebel, B. McCord. Surface-enhanced Raman spectroscopy, Raman, and density functional theoretical analyses of fentanyl and six analogs, *J. Raman Spectrosc.* 50 (2019) 1405-1415. 10.1002/jrs.5656
- [90] F. Measham. City checking: Piloting the UK's first community-based drug safety testing (drug checking) service in 2 city centres, *British J. Clin. Pharmacol.* 86 (2020) 420-428. 10.1111/bcp.14231
- [91] K. McCrae, S. Tobias, C. Grant, M. Lysyshyn, R. Laing, E. Wood, L. Ti. Assessing the limit of detection of Fourier-transform infrared spectroscopy and immunoassay strips for fentanyl in a real-world setting, *Drug Alcohol Rev.* 39 (2020) 98-102. 10.1111/dar.13004
- [92] A. Lanzarotta. Analysis of Forensic Casework Utilizing Infrared Spectroscopic Imaging, *Sensors (Basel, Switzerland)*. 16 (2016) 278-278. 10.3390/s16030278
- [93] L. H. Antonides, R. M. Brignall, A. Costello, J. Ellison, S. E. Firth, N. Gilbert, B. J. Groom, S. J. Hudson, M. C. Hulme, J. Marron, Z. A. Pullen, T. B. R. Robertson, C. J. Schofield, D. C. Williamson, E. K. Kemsley, O. B. Sutcliffe, R. E. Mewis. Rapid Identification of Novel Psychoactive and Other Controlled Substances Using Low-Field (1)H NMR Spectroscopy, *ACS Omega*. 4 (2019) 7103-7112. 10.1021/acsomega.9b00302
- [94] Y. Zhong, K. Huang, Q. Luo, S. Yao, X. Liu, N. Yang, C. Lin, X. Luo. The Application of a Desktop NMR Spectrometer in Drug Analysis, *Int. J. Anal. Chem.* 2018 (2018) 3104569. 10.1155/2018/3104569
- [95] J. Duffy, A. Urbas, M. Niemitz, K. Lippa, I. Marginean. Differentiation of fentanyl analogues by low-field NMR spectroscopy, *Anal. Chim. Acta.* 1049 (2019) 161-169. 10.1016/j.aca.2018.12.014
- [96] E. Sisco, J. Verkouteren, J. Staymates, J. Lawrence. Rapid detection of fentanyl, fentanyl analogues, and opioids for on-site or laboratory based drug seizure screening using thermal desorption DART-MS and ion mobility spectrometry, *Forensic Chem.* 4 (2017) 108-115. 10.1016/j.forc.2017.04.001
- [97] I. S. Lurie, A. C. Allen. Reversed-phase high-performance liquid chromatographic separation of fentanyl homologues and analogues: II.

- Variables affecting hydrophobic group contribution, *J. Chromatogr. A.* 292 (1984) 283-294. [https://doi.org/10.1016/S0021-9673\(01\)83609-8](https://doi.org/10.1016/S0021-9673(01)83609-8)
- [98] Hadil M. Elbardisy, C. W. Foster, L. Cumba, L. H. Antonides, N. Gilbert, C. J. Schofield, T. S. Belal, W. Talaat, O. B. Sutcliffe, H. G. Daabees, C. E. Banks. Analytical determination of heroin, fentanyl and fentalogues using high-performance liquid chromatography with diode array and amperometric detection, *Anal. Methods.* 11 (2019) 1053-1063. 10.1039/C9AY00009G
- [99] C. M. Selavka, I. S. Krull, I. S. Lurie. Photolytic derivatization for improved LCEC determinations of pharmaceuticals in biological fluids, *J. Chromatogr. Sci.* 23 (1985) 499-508. 10.1093/chromsci/23.11.499
- [100] A. Skulska, M. Kala, A. Parczewski. Fentanyl and its analogues in clinical and forensic toxicology, *Przegl. Lek.* 62 (2005) 581-584.
- [101] M. Gergov, P. Nokua, E. Vuori, I. Ojanpera. Simultaneous screening and quantification of 25 opioid drugs in post-mortem blood and urine by liquid chromatography-tandem mass spectrometry, *Forensic Sci. Int.* 186 (2009) 36-43. 10.1016/j.forsciint.2009.01.013
- [102] K. E. Strayer, H. M. Antonides, M. P. Juhascik, R. Daniulaityte, I. E. Sizemore. LC-MS/MS-Based Method for the Multiplex Detection of 24 Fentanyl Analogues and Metabolites in Whole Blood at Sub ng mL⁻¹ Concentrations, *ACS Omega.* 3 (2018) 514-523. 10.1021/acsomega.7b01536
- [103] S. Sofalvi, H. E. Schueler, E. S. Lavins, C. K. Kaspar, I. T. Brooker, C. D. Mazzola, D. Dolinak, T. P. Gilson, S. Perch. An LC-MS-MS method for the analysis of carfentanil, 3-methylfentanyl, 2-furanyl fentanyl, acetyl fentanyl, fentanyl and norfentanyl in postmortem and impaired-driving cases, *J. Anal.Toxicol.* 41 (2017) 473-483. 10.1093/jat/bkx052
- [104] M. R. Boleda, M. T. Galceran, F. Ventura. Trace determination of cannabinoids and opiates in wastewater and surface waters by ultra-performance liquid chromatography-tandem mass spectrometry, *J. Chromatogr. A.* 1175 (2007) 38-48. 10.1016/j.chroma.2007.10.029
- [105] S. K. Grebe, R. J. Singh. LC-MS/MS in the Clinical Laboratory - Where to From Here?, *Clin. Biochem.* 32 (2011) 5-31.
- [106] N. R. C. Committee on Identifying the Needs of the Forensic Sciences Community, Strengthening forensic science in the United States: A path forward <https://www.ncjrs.gov/pdffiles1/nij/grants/228091.pdf>, 2009 (accessed 12 November 2019).

- [107] United Nations Office on Drugs and Crime, Recommended methods for the identification and analysis of fentanyl and its analogues in biological specimens. https://www.unodc.org/documents/scientific/Recommended_methods_for_the_identification_and_analysis_of_Fentanyl.pdf, 2017 (accessed 06 July 2019).
- [108] S. Strano-Rossi, I. Alvarez, M. J. Taberner, P. Cabarcos, P. Fernandez, A. M. Bermejo. Determination of fentanyl, metabolite and analogs in urine by GC/MS, *J. Appl. Toxicol.* 31 (2011) 649-654. 10.1002/jat.1613
- [109] N. Misailidi, S. Athanaselis, P. Nikolaou, M. Katselou, Y. Dotsikas, C. Spiliopoulou, I. Papoutsis. A GC–MS method for the determination of furanylfentanyl and ocfentanil in whole blood with full validation, *Forensic Toxicol.* 37 (2019) 238-244. <http://doi.org/10.1007/s11419-018-0449-2>
- [110] J. V. Abonamah, B. A. Eckenrode, M. Moini. On-site detection of fentanyl and its derivatives by field portable nano-liquid chromatography-electron ionization-mass spectrometry (nLC-EI-MS), *Forensic Chem.* 16 (2019) 100180. <https://doi.org/10.1016/j.forc.2019.100180>
- [111] F. Bravo, D. Gonzalez, J. Benites. Development and validation of a solid-phase extraction gas chromatography-mass spectrometry method for the simultaneous quantification of opioid drugs in human whole blood and plasma, *J. Chil. Chem. Soc.* 56 (2011) 799-802.
- [112] B. P. Mayer, A. J. DeHope, D. A. Mew, P. E. Spackman, A. M. Williams. Chemical Attribution of Fentanyl Using Multivariate Statistical Analysis of Orthogonal Mass Spectral Data, *Anal. Chem.* 88 (2016) 4303-4310. <https://doi.org/10.1021/acs.analchem.5b04434>
- [113] R. F. Kranenburg, D. Peroni, S. Affourtit, J. A. Westerhuis, A. K. Smilde, A. C. van Asten. Revealing hidden information in GC–MS spectra from isomeric drugs: Chemometrics based identification from 15 eV and 70 eV EI mass spectra, *Forensic Chem.* 18 (2020) 100225. <https://doi.org/10.1016/j.forc.2020.100225>
- [114] M. P. Levitas, E. Andrews, I. Lurie, I. Marginean. Discrimination of synthetic cathinones by GC–MS and GC–MS/MS using cold electron ionization, *Forensic Sci. Int.* 288 (2018) 107-114. <https://doi.org/10.1016/j.forsciint.2018.04.026>

- [115] J. Bonetti. Mass spectral differentiation of positional isomers using multivariate statistics, *Forensic Chem.* 9 (2018) 50-61. <https://doi.org/10.1016/j.forc.2018.06.001>
- [116] A. S. Moorthy, A. J. Kearsley, W. G. Mallard, W. E. Wallace. Mass spectral similarity mapping applied to fentanyl analogs, *Forensic Chem.* 19 (2020) 100237. <https://doi.org/10.1016/j.forc.2020.100237>
- [117] D. E. Nichols, S. Frescas, D. Marona-Lewicka, X. Huang, B. L. Roth, G. A. Gudelsky, J. F. Nash. 1-(2,5-Dimethoxy-4-(trifluoromethyl)phenyl)-2-aminopropane: A Potent Serotonin 5-HT_{2A/2C} Agonist, *J. Med. Chem.* 37 (1994) 4346-4351. 10.1021/jm00051a011
- [118] P. M. Geyer, M. C. Hulme, J. P. B. Irving, P. D. Thompson, R. N. Ashton, R. J. Lee, L. Johnson, J. Marron, C. E. Banks, O. B. Sutcliffe. Guilty by dissociation—development of gas chromatography–mass spectrometry (GC-MS) and other rapid screening methods for the analysis of 13 diphenidine-derived new psychoactive substances (NPSs), *Anal. Bioanal. Chem.* 408 (2016) 8467-8481. 10.1007/s00216-016-9969-y
- [119] T. Kumazawa, K. Hara, C. Hasegawa, S. Uchigasaki, X.-P. Lee, H. Seno, O. Suzuki, K. Sato. Fragmentation Pathways of Trifluoroacetyl Derivatives of Methamphetamine, Amphetamine, and Methylenedioxyphenylalkylamine Designer Drugs by Gas Chromatography/Mass Spectrometry, *Int. J. Spectrosc.* 2011 (2011) 318148. 10.1155/2011/318148
- [120] Y. Higashikawa, S. Suzuki. Studies on 1-(2-Phenethyl)-4-(N-Propionylanilino)Piperidine (Fentanyl) and Its Related Compounds: Novel Metabolites in Rat Urine Following Injection of α -Methylfentanyl, One of the Most Abused Typical Designer Drugs, *J. HEALTH Sci.* 54 (2008) 629-637. 10.1248/jhs.54.629
- [121] I. M. McIntyre, A. Trochta, R. D. Gary, M. Malamatos, J. R. Lucas. An acute acetyl fentanyl fatality: A case report with postmortem concentrations, *J. Anal. Toxicol.* 39 (2015) 490-494. 10.1093/jat/bkv043
- [122] J. Suzuki, S. El-Haddad. A review: Fentanyl and non-pharmaceutical fentanyls, *Drug Alcohol Depend.* 171 (2017) 107-116. [Http://doi.org/10.1016/j.drugalcdep.2016.11.033](http://doi.org/10.1016/j.drugalcdep.2016.11.033)
- [123] P. J. Jannetto, A. Helander, U. Garg, G. C. Janis, B. Goldberger, H. Ketha. The Fentanyl Epidemic and Evolution of Fentanyl Analogs in the United States and the European Union, *Clin. Chem.* 65 (2019) 242-253. <http://doi.org/10.1373/clinchem.2017.281626>

- [124] R. Daniulaityte, M. P. Juhascik, K. E. Strayer, I. E. Sizemore, M. Zatreh, R. W. Nahhas, K. E. Harshbarger, H. M. Antonides, S. S. Martins, R. G. Carlson. Trends in fentanyl and fentanyl analogue-related overdose deaths – Montgomery County, Ohio, 2015–2017, *Drug Alcohol Depend.* 198 (2019) 116-120. <https://doi.org/10.1016/j.drugalcdep.2019.01.045>
- [125] J. H. Kahl, J. Gonyea, S. M. Humphrey, G. W. Hime, D. M. Boland. Quantitative analysis of fentanyl and six fentanyl analogs in postmortem specimens by UHPLC–MS–MS†, *J. Anal. Toxicol.* 42 (2018) 570-580. 10.1093/jat/bky054
- [126] S. Pichini, R. Solimini, P. Berretta, R. Pacifici, F. P. Busardò. Acute intoxications and fatalities from illicit fentanyl and analogues: An update, *Ther. Drug Monit.* 40 (2018) 38-51. 10.1097/ftd.0000000000000465
- [127] L. Hikin, P. R. Smith, E. Ringland, S. Hudson, S. R. Morley. Multiple fatalities in the North of England associated with synthetic fentanyl analogue exposure: Detection and quantitation a case series from early 2017, *Forensic Sci. Int.* 282 (2018) 179-183. <http://doi.org/10.1016/j.forsciint.2017.11.036>
- [128] M. H. Sorg, Expanded Maine Drug Death Report for 2017. <https://htv-prod-media.s3.amazonaws.com/files/me-2018-annual-dd-report-finalr-1555603539.pdf>, 2018 (accessed 12 November 2019).
- [129] U.S. Department of Homeland Security, Testimony of Robert E. Perez for a hearing before U.S. House of Representatives Judiciary Committee on "Stop the Importation and Trafficking of Synthetic Analogues Act". <https://republicans-judiciary.house.gov/wp-content/uploads/2017/06/CBP-Perez-Testimony-Synthetic-Drugs-Hearing.pdf>, June 27, 2017 (accessed 12 November 2019).
- [130] Drug Enforcement Administration. Schedules of controlled substances: Temporary placement of seven fentanyl-related substances in Schedule I. Temporary amendment; temporary scheduling order, *Federal Register*. 83 (2018) 4580-4585.
- [131] Scientific Working Group for the Analysis of Seized Drugs, Hexanoyl fentanyl. <http://www.swgdrug.org/Monographs/Hexanoyl%20fentanyl.pdf>, 2017 (accessed 12 November 2019).
- [132] U.S. Department of Homeland Security, Testimony of Todd C. Owen for a hearing before United States Senate Committee on Appropriations on "The role of DHS in stopping the flow of opioids & other dangerous drugs".

<https://www.appropriations.senate.gov/imo/media/doc/051618%20-%20CBP%20Owen%20Testimony.pdf>, May 16, 2018 (accessed 12 November 2019).

- [133] J. Palaty, D. Konforte, T. Karakosta, E. Wong, C. Stefan. Rapid identification of cyclopropyl fentanyl/crotonyl fentanyl in clinical urine specimens: A case study of clinical laboratory collaboration in Canada, *Clin. Biochem.* 53 (2018) 164-167. 10.1016/j.clinbiochem.2018.01.013
- [134] Drug Enforcement Administration. Schedules of controlled substances: Temporary placement of cyclopropyl fentanyl in Schedule I. Temporary amendment; temporary scheduling order, *Federal Register*. 83 (2018) 469-472.
- [135] A. E. Steuer, E. Williner, S. N. Staeheli, T. Kraemer. Studies on the metabolism of the fentanyl-derived designer drug butyrfentanyl in human in vitro liver preparations and authentic human samples using liquid chromatography-high resolution mass spectrometry (LC-HRMS), *Drug Test. Anal.* 9 (2017) 1085-1092. 10.1002/dta.2111
- [136] Drug Enforcement Administration. Schedules of controlled substances: Temporary placement of ortho-fluorofentanyl, tetrahydrofuranyl fentanyl, and methoxyacetyl fentanyl into Schedule I. Temporary amendment; temporary scheduling order, *Federal Register*. 82 (2017) 49504-49508.
- [137] D. M. Swanson, L. S. Hair, S. R. Strauch Rivers, B. C. Smyth, S. C. Brogan, A. D. Ventoso, S. L. Vaccaro, J. M. Pearson. Fatalities involving carfentanil and furanyl fentanyl: Two case reports, *J. Anal. Toxicol.* 41 (2017) 498-502. 10.1093/jat/bkx037
- [138] Scientific Working Group for the Analysis of Seized Drugs, 3-Furanyl fentanyl. <http://www.swgdrug.org/Monographs/3-Furanyl%20fentanyl.pdf>, 2016 (accessed 12 November 2019).
- [139] D. C. Butler, K. Shanks, G. S. Behonick, D. Smith, S. E. Presnell, L. M. Tormos. Three Cases of Fatal Acrylfentanyl Toxicity in the United States and a Review of Literature, *J. Anal. Toxicol.* 42 (2018) e6-e11. 10.1093/jat/bkx083
- [140] United Nations Office on Drugs and Crime, Rapid testing methods of drugs of abuse. https://www.unodc.org/documents/scientific/Rapid_Testing_Methods_of_Drugs_of_Abuse_E.pdf, 1995 (accessed 06 July 2019).
- [141] H. Ohta, S. Suzuki, K. Ogasawara. Studies on Fentanyl and Related Compounds IV. Chromatographic and Spectrometric Discrimination of

Fentanyl and its Derivatives, *J. Anal. Toxicol.* 23 (1999) 280-285.
<https://doi.org/10.1093/jat/23.4.280>

- [142] World Anti-Doping Agency Laboratory Committee, Identification criteria for qualitative assays incorporating column chromatography and mass spectrometry. https://www.wada-ama.org/sites/default/files/resources/files/WADA_TD2010IDCRv1.0_Identification%20Criteria%20for%20Qualitative%20Assays_May%2008%202010_EN.doc.pdf, 2010 (accessed 12 November 2019).
- [143] International Council for Harmonisation of Technical Requirements for Pharmaceuticals for Human Use, Validation of analytical procedures: Text and methodology. <http://www.ich.org/products/guidelines/quality/quality-single/article/validation-of-analytical-procedures-text-and-methodology.html>, 2005 (accessed 06 July 2019).
- [144] R. Thomis, E. Roets, J. Hoogmartens. Analysis of tablets containing aspirin, acetaminophen, and ascorbic acid by high-performance liquid chromatography, *J. Pharm. Sci.* 73 (1984) 1830-1833. 10.1002/jps.2600731246
- [145] L. A. King. (2009). Generic and analogue control - International comparisons *Forensic chemistry of substance misuse: A guide to drug control* (pp. 185). Cambridge, UK: RSC Publishing.
- [146] C. R. Hind. Pulmonary complications of intravenous drug misuse. 1. Epidemiology and non-infective complications, *Thorax.* 45 (1990) 891-898. 10.1136/thx.45.11.891
- [147] C. Liu, T. Li, Y. Han, Z. Hua, W. Jia, Z. Qian. The identification and analytical characterization of 2,2'-difluorofentanyl, *Drug Test. Anal.* 10 (2018) 774-780. 10.1002/dta.2264
- [148] E. Kohyama, T. Chikumoto, H. Tada, K. Kitaichi, T. Ito. Analytical differentiation of quinolinyl- and isoquinolinyl-substituted 1-(5-fluoropentyl)-1H-indole-3-carboxylates: 5F-PB-22 and its ten isomers, *Forensic Toxicol.* 35 (2017) 56-65. 10.1007/s11419-016-0334-9
- [149] T. Chikumoto, R. Furukawa, E. Kohyama, K. Suenami, H. Nagai, H. Tada, H. Kawashima, N. Kadomura, M. Soda, K. Kitaichi, T. Ito. Liquid chromatography–mass spectrometry studies on the isomeric 1-fluorobenzyl-3-naphthoyl-indoles: FUB-JWH-018 and five isomers, *Forensic Toxicol.* 37 (2019) 113-120. 10.1007/s11419-018-0442-9
- [150] M. Kusano, K. Zaitso, H. Nakayama, J. Nakajima, K. Hisatsune, T. Moriyasu, S. Matsuta, M. Katagi, H. Tsuchihashi, A. Ishii. Positional

- isomer differentiation of synthetic cannabinoid JWH-081 by GC-MS/MS, *J. Mass Spectrom.* 50 (2015) 586-591. 10.1002/jms.3565
- [151] Y. Nakazono, K. Tsujikawa, K. Kuwayama, T. Kanamori, Y. T. Iwata, K. Miyamoto, F. Kasuya, H. Inoue. Differentiation of regioisomeric fluoroamphetamine analogs by gas chromatography–mass spectrometry and liquid chromatography–tandem mass spectrometry, *Forensic Toxicol.* 31 (2013) 241-250. 10.1007/s11419-013-0184-7
- [152] S. Negishi, Y. Nakazono, Y. T. Iwata, T. Kanamori, K. Tsujikawa, K. Kuwayama, T. Yamamuro, K. Miyamoto, T. Yamashita, F. Kasuya, H. Inoue. Differentiation of regioisomeric chloroamphetamine analogs using gas chromatography–chemical ionization-tandem mass spectrometry, *Forensic Toxicol.* 33 (2015) 338-347. 10.1007/s11419-015-0280-y
- [153] A. Takeda, T. Tagami, A. Asada, T. Doi, M. Kawaguchi, Y. Satsuki, Y. Sawabe. Regioisomeric separation of ring-substituted cathinones by liquid chromatography–mass spectrometry with a naphthylethyl column, *Forensic Toxicol.* 35 (2017) 399-407. 10.1007/s11419-016-0351-8
- [154] F. X. W. Robert M. Silverstein, David J. Kiemle, David L. Bryce, *Spectrometric Identification of Organic Compounds* (8th ed.), Wiley, 2014.
- [155] D. C. Butler, K. Shanks, G. S. Behonick, D. Smith, S. E. Presnell, L. M. Tormos. Three Cases of Fatal Acrylfentanyl Toxicity in the United States and a Review of Literature, *J. Anal. Toxicol.* 42 (2017) e6-e11. 10.1093/jat/bkx083
- [156] M. Bäckberg, O. Beck, K.-H. Jönsson, A. Helander. Opioid intoxications involving butyrfentanyl, 4-fluorobutyrfentanyl, and fentanyl from the Swedish STRIDA project, *J. Clin. Toxicol.* 53 (2015) 609-617. 10.3109/15563650.2015.1054505
- [157] R. Daniulaityte, M. P. Juhascik, K. E. Strayer, I. E. Sizemore, K. E. Harshbarger, H. M. Antonides, R. R. Carlson. Overdose Deaths Related to Fentanyl and Its Analogs - Ohio, January-February 2017, *MMWR Morb. Mortal. Wkly Rep.* 66 (2017) 904-908. 10.15585/mmwr.mm6634a3
- [158] M. Kangas. A New Possible Alternative Colorimetric Drug Detection Test for Fentanyl, *Organic & Medicinal Chem. I. J.* 4 (2017). 10.19080/OMCIJ.2017.05.555645

- [159] M. O. Okuom, M. V. W. A. J. A. E. Holmes. Intermolecular Interactions between Eosin Y and Caffeine Using ¹H-NMR Spectroscopy, *Int. J. Spectrosc.* 2013 (2013). 10.1155/2013/245376
- [160] F. G. Bordwell. Equilibrium acidities in dimethyl sulfoxide solution, *Acc. Chem. Res.* 21 (1988) 456-463. 10.1021/ar00156a004
- [161] National Center for Biotechnology Information, PubChem Annotation Record for Caffeine, Source: Hazardous Substances Data Bank (HSDB). <https://pubchem.ncbi.nlm.nih.gov/source/hsdb/36>, 2020 (accessed 20 Sep 2020).
- [162] V. R. Batistela, D. S. Pellosi, F. D. de Souza, W. F. da Costa, S. M. de Oliveira Santin, V. R. de Souza, W. Caetano, H. P. M. de Oliveira, I. S. Scarminio, N. Hioka. pKa determinations of xanthene derivatives in aqueous solutions by multivariate analysis applied to UV-Vis spectrophotometric data, *Spectrochim. Acta A.* 79 (2011) 889-897. <https://doi.org/10.1016/j.saa.2011.03.027>
- [163] A. Avdeef, D. A. Barrett, P. N. Shaw, R. D. Knaggs, S. S. Davis. Octanol-, Chloroform-, and Propylene Glycol Dipelargonat-Water Partitioning of Morphine-6-glucuronide and Other Related Opiates, *J. Med. Chem.* 39 (1996) 4377-4381. 10.1021/jm960073m
- [164] L. M. Jackman, S. Sternhell. (1969). Chapter 2-1 - Time-dependent effects in nuclear magnetic resonance spectroscopy. In L. M. Jackman & S. Sternhell (Eds.), *Application of Nuclear Magnetic Resonance Spectroscopy in Organic Chemistry (Second Edition)* (pp. 55-60): Pergamon.
- [165] A. Bain. Chapter 2 - Chemical Exchange, *Annual Reports on NMR Spectroscopy.* 63 (2008) 23-48. 10.1016/S0066-4103(07)63002-6
- [166] R. A. Y. Jones, A. R. Katritzky, A. C. Richards, R. J. Wyatt. The conformational analysis of saturated heterocycles. Part XXI. Dipole moment studies of 1-ethyl- and 1-isopropyl-piperidines and further studies of 1-methylpiperidines, *J. Chem. Soc. B Phys. Org.* (1970) 122-127. 10.1039/J29700000122
- [167] R. L. Thurlkill, D. A. Cross, J. M. Scholtz, C. N. Pace. pKa of fentanyl varies with temperature: implications for acid-base management during extremes of body temperature, *J. Cardiothorac. Vasc. Anesth.* 19 (2005) 759-762. 10.1053/j.jvca.2004.11.039
- [168] A. Choodum, P. Kanatharana, W. Wongniramaikul, N. Daéid. A sol-gel colorimetric sensor for methamphetamine detection, *Sensor Actuat. B-Chem.* 215 (2015). 10.1016/j.snb.2015.03.089

- [169] N. Gilbert, L. H. Antonides, C. J. Schofield, A. Costello, B. Kilkelly, A. R. Cain, P. R. V. Dalziel, K. Horner, R. E. Mewis, O. B. Sutcliffe. Hitting the Jackpot – development of gas chromatography–mass spectrometry (GC–MS) and other rapid screening methods for the analysis of 18 fentanyl-derived synthetic opioids, *Drug Test. Anal.* 12 (2020) 798-811. <http://doi.org/10.1002/dta.2771>
- [170] H. Abdi, L. J. Williams. Principal component analysis, *WIREs Comp. Stats.* 2 (2010) 433-459. <https://10.1002/wics.101>
- [171] Scientific Working Group for the Analysis of Seized Drugs, SWGDRUG MS Library Version 3.7. <http://www.swgdrug.org/ms.htm>, 2020 (accessed 17 June 2020).
- [172] F. Husson, J. Josse, S. Lê. FactoMineR: An R Package for Multivariate Analysis, *J. Stat. Softw.* 25 (2008). <https://doi.org/10.18637/jss.v025.i01>
- [173] A. Kassambara, F. Mundt, factoextra: Extract and Visualize the Results of Multivariate Data Analyses. R package version 1.0.6. <https://CRAN.R-project.org/package=factoextra>, 2019 (accessed 17 June 2020).
- [174] A. Kassambara, ggcorrplot: Visualization of a Correlation Matrix using 'ggplot2'. R package version 0.1.3. <https://CRAN.R-project.org/package=ggcorrplot>, 2019 (accessed 28 August 2020).
- [175] L. YiLan, Z. RuTong, clustertend: Check the Clustering Tendency. R package version 1.4. <https://CRAN.R-project.org/package=clustertend>, 2015 (accessed 28 August 2020).
- [176] H. F. Kaiser. The Application of Electronic Computers to Factor Analysis, *Educ. Psychol. Meas.* 20 (1960) 141-151. 10.1177/001316446002000116
- [177] A. L. Setser, R. Waddell Smith. Comparison of variable selection methods prior to linear discriminant analysis classification of synthetic phenethylamines and tryptamines, *Forensic Chem.* 11 (2018) 77-86. <https://doi.org/10.1016/j.forc.2018.10.002>
- [178] H. G. Pierzynski, L. Neubauer, C. Choi, R. Franckowski, S. D. Augustin, D. M. Iula. Tips for interpreting GC-MS fragmentation of unknown substituted fentanyls, *Cayman Currents.* 28 (2017) 1-3.
- [179] A. Kassambara, Practical guide to cluster analysis in R: Unsupervised machine learning, STHDA, 2017.
- [180] R. Tibshirani, G. Walther, T. Hastie. Estimating the number of clusters in a data set via the gap statistic, *J. R. Stat. Soc. Series B.* 63 (2001) 411-423. 10.1111/1467-9868.00293

- [181] L. Kaufman, P. Rousseeuw, *Finding Groups in Data: An Introduction to Cluster Analysis*, 2009.
- [182] G. McLaughlin, N. Morris, P. V. Kavanagh, J. D. Power, J. O'Brien, B. Talbot, S. P. Elliott, J. Wallach, K. Hoang, H. Morris, S. D. Brandt. Test purchase, synthesis, and characterization of 2-methoxydiphenidine (MXP) and differentiation from its meta- and para-substituted isomers, *Drug Test. Anal.* 8 (2016) 98-109. 10.1002/dta.1800
- [183] D. B. G. Williams, M. Lawton. Drying of organic solvents: Quantitative evaluation of the efficiency of several desiccants, *J. Org. Chem.* 75 (2010) 8351-8354. 10.1021/jo101589h
- [184] M. Schönberger, D. Trauner. A photochromic agonist for μ -opioid receptors, *Angew. Chem. Int. Ed.* 53 (2014) 3264-3267. doi:10.1002/anie.201309633
- [185] M. Schönberger, D. Trauner. A Photochromic Agonist for μ -Opioid Receptors, *Angew. Chem. Int. Ed.* 53 (2014) 3264-3267. <http://doi.org/10.1002/anie.201309633>
- [186] J. F. Casale, J. R. Mallette, G. Claro, P. A. Hays, M. Frisch, K. T. Chan. Synthesis and Characterization of Benzoylfentanyl and Benzoylbenzylfentanyl, *Microgram.* 15 (2018) 1-8.
- [187] Z. Guo, H. Zheng, Y. Lu, Y. Wei. Isolation and purification of heroin from heroin street samples by preparative high performance liquid chromatography, *Forensic Sci. Int.* 221 (2012) 120-124. <https://doi.org/10.1016/j.forsciint.2012.04.016>